ELECTRICAL TRACKING OVER SOLID INSULATING MATERIALS FOR AEROSPACE APPLICATIONS

A thesis submitted to The University of Manchester for the degree of Doctor of Philosophy in the Faculty of Engineering and Physical Sciences

2011

Lei Zhang

School of Electrical and Electronic Engineering

LIST OF CONTENTS

LIST OF FIGURES

LIST OF TABLES

LIST OF MAIN ABBREVIATIONS

AEA	**All Electric Airport**
CF	**Constant Frequency**
CSD	**Constant Speed Drive**
EHA	**Electric-hydraulic Actuator**
EMA	**Electromechanical Actuator**
IDG	**Integrated Drive Generator**
MEA	**More Electric Aircraft**
MEE	**More Electric Engine**
MOET	**More Open Electrical Technologies (Project)**
PMG	**Permanent Magnet Generator**
POA	**Power Optimized Aircraft**
VF	**Variable Frequency**
VSCF	**Variable Speed Constant Frequency**
WAI	**Wing Anti-Icing**

ABSTRACT

The concept of More Electric Aircraft, where is to utilize the electrical power to drive more or all aircraft subsystem instead of conventional combination of pneumatic, hydraulic, mechanical and electrical power, can be recalled to World War II. It has been proven to have more advantages for decades in terms of energy efficiency, environmental issues, logistics and operational maintenance. It can also enhance aircraft weight, volume and battle damage reconfigurability.

Thanks to the new electronics technologies and the emergence of new materials, It becomes feasible for high power density electrical power components to drive the majority of aircraft subsystem. However, sustaining the transmission of hundreds of kilowatts of electrical power at low voltages is not feasible owing to the penalties incurred due to high cable weights and voltage drop may become critical. It is very easy to come up with the solution of the increase of voltage. However, higher voltage will introduce other problems such as the reliability of insulation coordination on the aircraft due to the increased probability of electrical discharge.

For aircraft designers, it is very important to understand the rules of insulation coordination on the aircraft including determining clearance and creepage distances, and also have a clear investigation of the phenomena and mechanism of electrical discharges. Past research has identified a number of the concerns of operating electrical systems at higher voltages in an aerospace environment, especially for dimensioning of clearances. However, there is little study on dimensioning of creepage distances and relevantly flashover and electrical tracking on solid insulating material surfaces.

This thesis firstly discusses the rules for determining clearances and creepage distances. The experimental validation work was done for breakdown in air gap and on the solid insulating material surfaces under dry condition so that some standard recommended values can be evaluated not only with theoretical values such Paschen'law. Suggestions of application of those standards were provided.

Secondly, the complex electrical discharge under wet condition on solid insulating material surfaces was discussed. A mathematical model to predict this type of electrical failure -electrical tracking (the electrical discharges on solid insulation materials which will lead to physical damage in the materials) with the consideration of different environmental conditions including air pressure, ambient temperature, and pollution degrees was developed. A series of electrical tracking tests were carried out on organic materials to find out the mechanism of electrical tracking and validate the finding by the mathematic model. Finite element analysis simulations were also conducted to find out the background thermal transfer mechanism to support our explanation of those phenomena of electrical tracking. Different test techniques have ben developed for specific impact factors. Finally, the suggestions for utilization of the standards and feasible test techniques for electrical tracking under wet conditions were provided.

DECLARATION

No portion of the work referred to in this thesis has been submitted in support of an application for another degree or qualification of this or any other university, or institution of learning

COPYRIGHT

ACKNOWLEDGEMENTS

Initially, I wish to express my sincere gratitude to my supervisor, Prof. Ian Cotton who gives me an opportunity to do this research, and make this thesis possible. I also would like to sincerely thank him for his valuable guidance and continuous encouragement, which were essential to the completion of this PhD research study.

I am also very grateful to Mr. Frank Hogan in the high voltage laboratory for his warm and selfless advice, help and patience. Many thanks also to my other colleagues in the laboratory, particularly Dr. Ningyan Wang, Dr. Sanjay Bahadoorsingh, Xiaolei Cai,Vidyadhar Peesapati, Ilias Christou, Riccardo Giussani for providing such a stimulating and relaxed research environment and fun stuffs in Manchester.

Many thanks to Mr Steve and mechanical workshop stuff for their kindly smiles and instant response whenever I asked for supporting my research in the department.

Finally , very special thanks are also due to my dad and mum in Baotou, China, Jing Wang, Dan Wang, Qianqian, Judith, James and all of my friends in the UK for their great support and encouragement in whole remarkable days.

Many thanks to everybody who ever gave me help and support.

Chapter 1 Introduction

1.1. Overview

The concept of “all-electric aircraft”/”more electric aircraft” aircraft (AEA/MEA) is far from new. Since World War II, military aircraft designers have been aware of this concept [1-3]. MEA means that more power off-takes from the aircraft are electrical in nature, which means the need for on-engine hydraulic power generation and bleed air off-takes is removed. By adopting the concept, advantages in terms of energy efficiency, environmental issues, logistics and operational maintenance can be achieved. It can also enhance aircraft weight, volume and battle damage reconfigurability.

Conventional aircraft architectures used for civil aircraft are comprised of a combination of systems dependent on mechanical, hydraulic, pneumatic and electrical sources. The resulting conventional equipment is the product of decades of development by system suppliers.

In a conventional architecture (Figure 1.1 is a basic schematic) fuel is converted into power by the engines. Most of this power is used as propulsive power to move the aircraft. The remainder is converted into four main forms of non-propulsive power [4]:

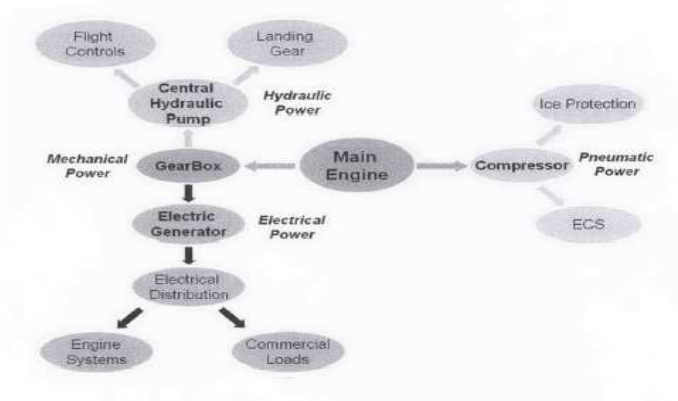

Figure 1. 1 Schematic of the conventional airplane power distribution [4]

- *Pneumatic power*, obtained from the engines' high-pressure compressors. This kind of energy is conventionally used to power the Environmental Control System (ECS) and supply hot air for Wing Anti-Icing (WAI) systems. Its drawbacks are low efficiency and a difficulty in detecting leaks.
- *Mechanical power*, which is transferred (by means of the mechanical gearboxes) from the engines to central hydraulic pumps, to local pumps for engine equipment and other mechanically driven subsystems, and to the main electrical generator.
- *Hydraulic power*, which is transferred from the central hydraulic pumps,: to the actuation systems for primary and secondary flight control; to landing gear for deployment, retraction, and braking; to engine auction; and to numerous ancillary systems. Hydraulic systems have a high power density and are very robust. Their drawbacks are a heavy and inflexible infrastructure (piping) and the potential leakage of dangerous and corrosive fluids.
- *Electrical power*, which is obtained from the main generator in order to power the avionics cabin and aircraft lighting, galleys and other commercial loads (such as entertainment systems). Electrical power does not require a heavy infrastructure and is very flexible. Its main drawbacks are that conventionally it has a lower power density than hydraulic power, and results in a higher risk of fire (in the case of a short circuit) [4].

In a conventional aircraft, electrical subsystems are driven from electrical sources through point-to-point topology distribution systems. And the conventional aircraft electrical subsystems are shown in Figure 1.2. All the subsystems are driven from the main bus

through relays and switches. This kind of distribution network leads to expensive complicated and heavy wiring circuits.

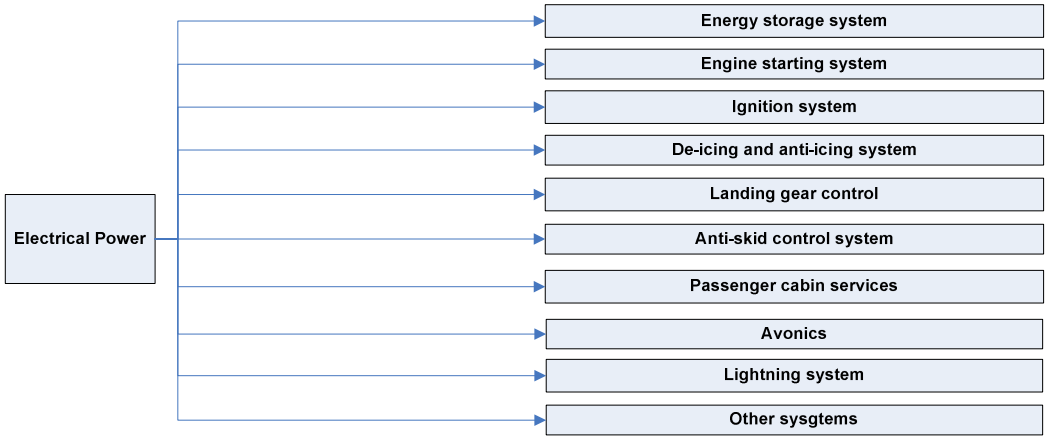

Figure 1.2 Conventional aircraft electrical subsystems

As time has gone by, each system has become more complex, and interactions between different pieces of equipments reduce the efficiency of the whole system. A simple leak in the pneumatic or hydraulic system may lead to the outage of every user of that network, resulting in a grounded aircraft and flight delays. The leak is generally difficult to locate and once located it cannot be addressed easily.

The trend is to move towards “all-electric aircraft”/”more electric aircraft” aircraft (AEA/MEA) as shown in Figure 1.3. The drives for civil aircraft and fast military jets to apply the concept of MEA are to maximize dynamic performance and its efficiency while minimizing equipment volume and mass. Meanwhile, due to the difficult economy environment, the affordability is key consideration in terms of cost of the development, manufacture, operation, maintenance, and personnel. Removal of pneumatic and hydraulic systems with electrical systems results in improvement in fuel efficiency. And electrical subsystems can be used only when needed. Figure 1.3 shows the manners to realize the concept of MEA [4]. And MEA electrical power subsystems are illustrated in Figure 1.4.

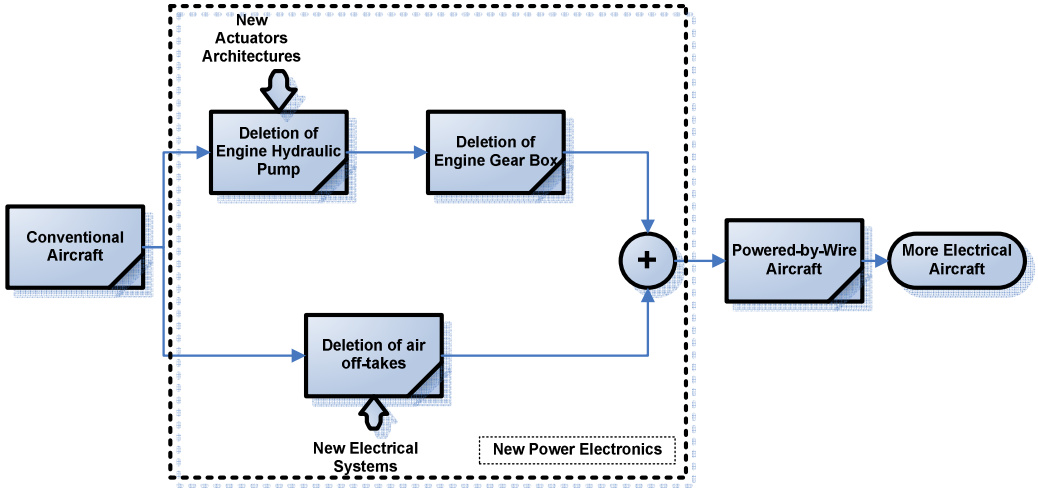

Figure 1. 3 Current trend of the MEA [4]

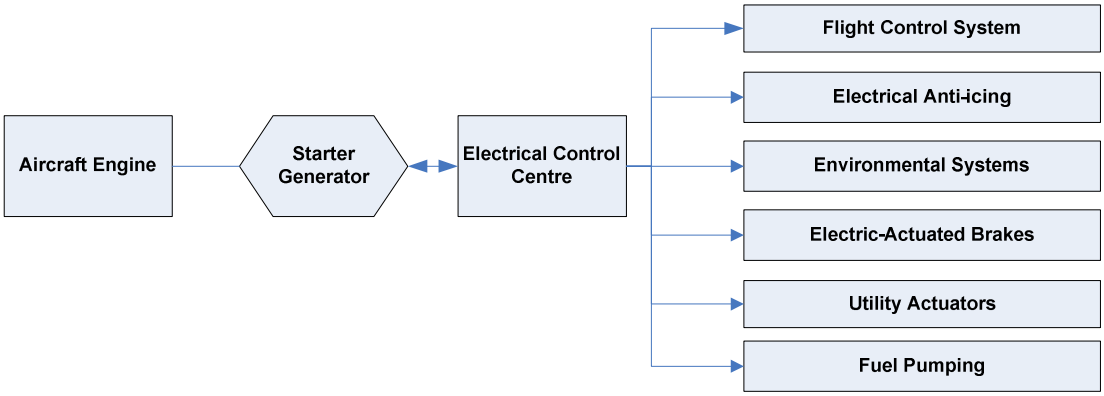

Figure 1.4 The MEA electrical power subsystems.

To achieve MEA, there are several very important key technologies including high power density starter-generator, high power density, high integrity electric actuation (such as electric-hydraulic actuators (EHAs) and electromechanical actuators (EMAs) and fault-tolerant electrical power distribution. The biggest challenges to achieve the advantages promised by application of MEA technologies are with the advances in power electronics. They are required for all the enabling technologies for the MEA.

The MEA requires a highly reliable, fault tolerant, autonomously controlled electrical power system to deliver high quality power and electrical levels to the aircraft's loads. Reliable high integration and safety of the electrical power system also leads to the use of distributed generation and control architecture. The first factor considered should therefore

be the large amount of power electronics for power conversions and power users that MEA will involve: at least 1.6MW for a next generation 300 pax aircraft [5]. Further, one major evolutionary technological advance which has contributed heavily to the feasibility of an electrically-cased aircraft non-propulsive power system has been the development of reliable, solid state, high power density, power related electronics, since the power transferred to the load is processed almost three times [5-8].

Much literature [9-12] has already proven that even without the advent of more electrical aircraft, the power level of the airplane has been increased. In order to provide a clearer view of contemporary electrical generation for the airplane, the different types of electrical power generation currently being considered and proposed civil and military aircraft platforms through the 1990s are shown in Figure 1.5.

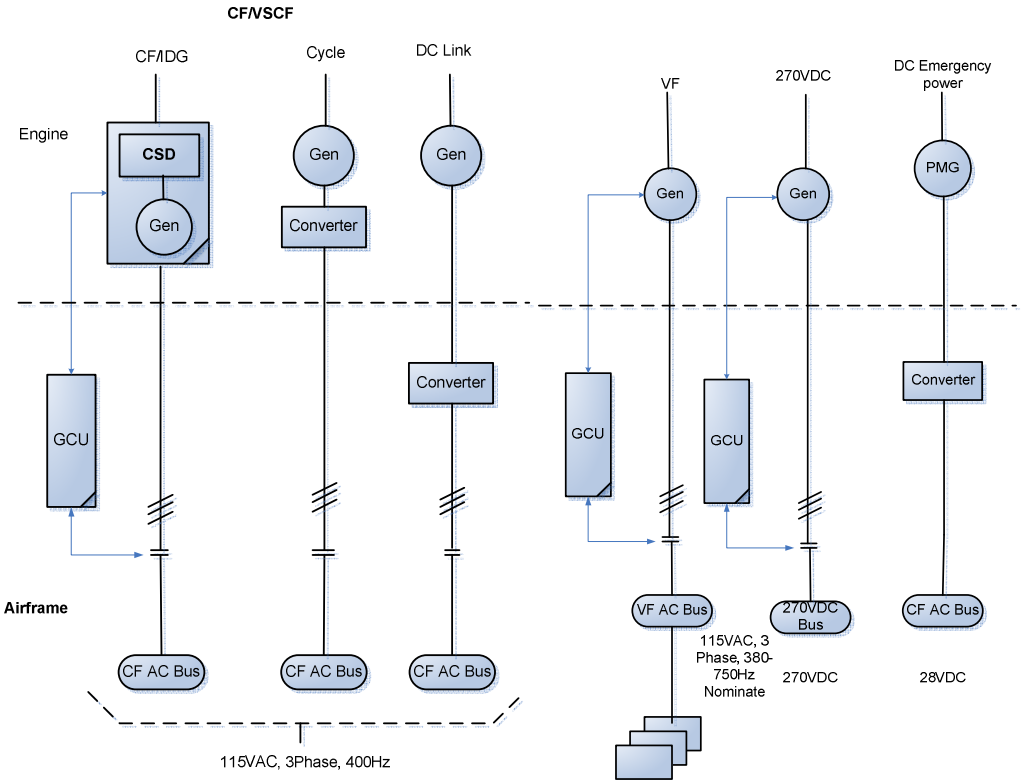

Figure 1.5 Candidate electrical power generation types

From Figure 1.5, we can see that the Constant Frequency (CF) 115 V AC, 3-phase, 400 Hz options consist of the Integrated Drive Generator (IDG), Variable Speed Constant Frequency (VSCF) cycle-converter and DC link options. Variable Frequency (VF) 115 V

AC, 3-phase power generation – sometimes termed ‘frequency wild’ [13] – is also a more recent competitor, and although a relatively inexpensive form of power generation, it has the disadvantage that some motor loads may require motor controllers. Military aircraft in the US are inclining toward 270 V DC systems. Permanent Magnet Generators (PMGs) are used to generate 28 V DC emergency power for high integrity systems. In such a 115 V AC, 3 phase system there is no possibility of electrical discharge across an air gap during normal operating condition based on Paschen’s law.

Although the above-stated Constant-Frequency power systems have been widely used for years, many aircraft manufacturers are thinking about how to develop variable frequency systems or even hybrid system configuration because of the complication of a CF/IDG system and its relatively low efficiency. In addition, constant frequency cannot be optimized to many AC loads, such as AC motors that need adjustable-frequency excitation to obtain the desirable speed or torque [8].

To solve the possible problems with the concept of MEA, there are several levels of approaches. At system level, hybrid or bleedless air conditioning systems, the “More Electric Engine (MEE)”, fuel cells, variable frequency generators and distributed system architectures are just a few of the technologies vying for space on the next aircraft [13]. Some of these have already been applied for use on the Airbus A380 and the Boeing B7E7. The system level approach can be used not only for aerospace but also other transport systems, such as marine propulsion [14]. Although at system level there are fundamental concerns with the Power-by-Wire systems development approach, these concerns are no longer sufficient for preventing its use. The effects of the new systems in terms of safety, cost, reliability, maintenance, power management and fuel usage at the total aircraft level have to be considered together rather than only considering the technical benefits of implementing these systems. At this level, projects, for example in 2002 the Power Optimized Aircraft project (POA) was conducted to validate the aircraft level both qualitatively and quantitatively, have been launched with the initial conclusion that this approach is not only feasible but also reliable within a surprisingly relatively short time

span compared to a system level approach. Although there is a trend for aircraft electrical systems being heavier it is possible for a MEA to provide a reduction in fuel usage at the aircraft level [15]. These results indicate that it is inevitable to have a high degree of integration of equipment systems in the MEA and points the way towards an intensively integrated approach to designing new aircraft.

A number of programs have been launched in this field [16]. For example, the US Air Force MEA Program aims to investigate providing more electrical capability for fighter aircrafts; in the late nineties, the Division of Militaries Aircrafts of Norhrop/Grumman developed the MADMEL project, related to the power distribution system and power management for more electric aircraft [17]. Power Optimized Aircraft (POA), the first important integration initiative in Europe, aims to optimize the management of electrical power on aircraft. One of the main research lines has been the introduction of electrical loads management, which permits the introduction of new technologies in onboard systems, power electronics [18].

Meanwhile, the European Commission of Community Research has initiated a dynamic program named European Technology/Research and Product Development in Aeronautics (EUR/TD in Aeronautics). From 1990 up to 2006, a total of six Framework programs had proceeded successfully. The seventh Framework program was launched in 2007 and is supposed to be accomplished in 2013. The recent program aims to develop an integrated “greener” and “smarter” pan-European transport system for the benefit of citizens and society, respecting the environment and natural resources so that the leading role attained by the European industries in the global market can be developed and extended. For aeronautics and air transport, the Aeronautic Joint Technology Initiative has been proposed with the aim of providing a step forward in the technological capability of environmentally friendly Air Transport Systems (ATS), improving overall ATS impact on the environment including noise, emission reduction and fuel consumption. Other minor projects performed in Europe are the TIMES and DEPMA programs [19, 20].

Recently, Boeing, in collaboration with the European Research Center located in Madrid,

has developed a totally electric propeller aircraft, promoted by a hybrid power system. The system is based on a fuel cell in combination with an Ion-Lithium battery which provides the energy to an electric engine, connected to a conventional propeller. The fuel cell is able to supply the overall energy during the cruise-flight stage. During takeoff or landing, the energy is provided by both the fuel cell and the ion-lithium battery [21].

In the aircraft, different kinds of load require different power supplies. Even in conventional examples there are different voltage types, normally commercial aircraft 115 V AC with some components requiring 28 V DC. In the advanced future aircraft, higher voltage levels will be employed such as 270 V DC and 230VAC, so far used in military aircraft, and to be used in commercial aircraft in the future [7, 17, 22, 24, 25]. Other approaches are focused on applications with higher voltage levels like 540 V DC [26]. Whereas 270 V DC is obtained from rectification of the traditional 115 V AC, 230 V AC could be easily obtained by doubling the existing voltage level provided by the generator, 115 VAC. Regarding 540 V DC, voltage level is a consequence of using the differential voltage provided by two buses of ± 270 V DC with a common reference on ground.. Therefore future aircraft electrical system will use a multi-voltage level hybrid DC and AC system. The electrical system is no longer only comprised of components which convert electrical power from one form to another, but also components which convert the supply to a higher or lower voltage level. As a result, the modern aircraft has all kinds of power electronics converters such as AC/DC rectifier, DC/AC inverters, and DC/DC choppers. In addition, in the variable speed constant frequency (VSCF) systems, solid-state bi-directional converters are used to condition variable-frequency power into a fixed frequency and voltage. Moreover, bi-directional DC/DC converters are used in battery charge/discharge units. Therefore MEA electrical distribution systems are mainly in the form of multi-converter power electronic systems. Due to extensive interconnection of components, a large variety of dynamic interactions is possible [28].

Increases in the operating voltage of an aircraft have been gradual. Aircraft electrical systems, from operating at 14.25 V DC in 1936, rose to 28 V DC in 1946 [3] and ultimately

became the common 115/200 V AC 400 Hz systems in use in the majority of civil aircraft today. 270 V DC was used by the military to provide further weight savings in the 1980s [29].

The current aircraft being designed with a more electric architecture include the Boeing 787, which will have 250 kVA of electrical generation capability in each engine. Along with the auxiliary power generation, the total available generation is in the order of 1500 kVA [27]. The Airbus A350 is expected to have a power generation capability in the order of 800 kVA. To support these generation levels, Boeing have moved from a 115V AC 400Hz system to a combined 230 V AC 360-800Hz and +/- 270 VDC (540 V DC) system. [27].

Since the concept of MEA involves the power level increasing, sustaining the transmission of hundreds of kilowatts of electrical power at low voltages is not feasible owing to the penalties incurred due to high cable weights [13] and voltage drop may become critical. It is very easy to come up with the solution of the increase of voltage. However, higher voltage will introduce other problems such as the reliability of insulation coordination on the aircraft due to the increased probability of electrical discharge.

Past research has identified a number of the concerns of operating electrical systems at higher voltages in an aerospace environment. Bilodeau, Dunbar and Sarjeant discussed the increased demand for higher voltage usage in space power systems owing to the need to reduce the weight that would result from the use of lower voltage systems and the necessary test regimes[30]. Many papers examine some of the basic issues relating to the operation / testing of higher voltage systems in a low pressure environment. Dunbar [31] stressed a wire with high voltage to determine the effect of high frequency at high altitudes. His results indicate a reduction in the partial discharge inception voltage of around 15% at frequencies above 40 kHz for an altitude of 33000 ft. Dunbar states in another paper [32] that partial discharge can cause significant numbers of failures in high voltage systems. Brockschmidt [33]also discusses the problems associated with the operation of higher voltage systems in a low pressure environment and states that the voltage required to sustain partial discharge

can be lower than that required to initiate it. Karady et al [34] examined the corona inception voltage of simple electrode geometries including ones that involved thin layers of electrical insulation. The authors show that for certain experimental arrangements, corona inception can take place at voltages lower than Paschen's minimum. Hammoud and Stavnes [35] conducted breakdown tests on different types of aerospace cable observing a reduction in the breakdown voltage of 20% occurred when using a testing frequency of 400 Hz at 200 ºC. A study was conducted on polypropylene cable by [36] at different frequencies, ranging from 50 to 400 Hz. The results of these tests correlated with [35] in that breakdown voltages of such insulation could fall as a function of frequency.

A key document, although dated, provides excellent information across many of the pertinent issues; this was produced by Dunbar [37]. This describes the operating environment of an aircraft, the types of electrical discharge that could take place and provides guidelines and precautions to be taken into consideration in the insulation design of electrical and electronic equipment. It also provides guidelines for monitoring and testing. Dunbar recognized that all types of discharges lead to the deterioration of the insulation of machines, drives and cabling – something that could lead to premature failure of the aircraft system. In designing insulation systems, factors such as out-gassing, and thermal and high voltage field stresses on materials have to be taken into account. In addition the effects of "temperature cycling, high density packaging, frequency and long mission durations" have to be investigated.

1.2. Aims and objectives of the research

In order to get deep understating of insulation coordination of electrical systems in More Electrical Aircraft, a considerable amount of research works has been done in my department such as the PhD research work of Dr. Andrew Nelms has dealt with the cabling systems, and Miss Rui Rui is now working on the machinery systems. My research concentrated on the electrical discharges on any surfaces that electrical fields cross, such as

the printed circuit boards, connectors or outside of power electronics modules. This inevitably comes down to dimensioning of clearances and creepage distances with regard to its application and in relation to its surroundings. The term clearance has come to be used to refer to the shortest distance in air between two conductive parts. Creepage distances can be defined as the shortest distance along the surface of the insulating material between two conductive parts.

First of all, the project will focus on studying the determination of clearances and creepage distances under dry condition. The rules of the dimensioning of clearances and creepage distances will be reviewed according to the understanding of the IEC 60664 and IPC 2221. And then experimental test results will be presented and compared with the values suggested in those standards to validate and explain the standards deeply. My work will provide science basis of allocation of those standard values for aircraft designers.

Secondly, the project will mainly concentrate on tracking phenomena under wet condition. To develop a mathematical model to predict this type of electrical failure -electrical tracking (the electrical discharges on solid insulation materials which will lead to physical damage in the materials) with the consideration of different environmental conditions including air pressure, ambient temperature, and pollution degrees. A series of electrical tracking tests will be carried out on organic materials to find out the mechanism of electrical tracking and validate the finding by the mathematic model. Finite element analysis simulations will also be conducted to find out the background thermal transfer mechanism to support my explanation of those phenomena of electrical tracking. Different test techniques will be developed for specific impact factors. Contribution will be made to:

- establishing the electrical tracking behavior of surfaces that exist in power switches and the power electronic cores used in aircraft,
- determining models describing it,
- providing guidelines for better electrical tracking testing methods for creepage distances,

and

- Generating design rules for the mitigation of electrical tracking for next-generation aircraft.

1.3. The AIMEA program

The research was sponsored by the project called More Open Electrical Technologies (MOET) which was launched successfully on July 2006. MOET aims to establish a new industrial standard for electrical system design in commercial aircraft. This will strengthen the competitiveness of the EU's aerospace industry. One of MOET's important design objectives is to improve operational aircraft capacity. Its Power-by-Wire (PbW) concept will enhance aircraft design and electrical power flexibility.

The main result of the three-year project will be the validation of scalable electrical networks up to 1 MW for future air, actuation and electrical systems, considering new voltage levels and advanced concepts. To achieve its goals, MOET will need to develop new design principles, technologies and standards. The entire project will run under the overall management of Airbus France.

The Electrical Energy and Power Systems group at the University of Manchester is a participant in this joint development project by 61 companies in the EU's Framework Programme 6. My contribution will be in work package 3.32, which aims to: establish the partial discharge behaviour of existing power switches and the power electronic core; determine models describing partial discharge in power switches and power electronic core; and also generate design rules for mitigation of partial discharge.

On 14th December 2004 AIMEA was formed by four UK Universities, including the University of Manchester, the University of Sheffield, the University of Nottingham, and the University of Bristol. It is the second largest partner in MOET in term of man-hours and

fifth in terms of costs.

1.4. Organization of the thesis

The thesis is subdivided into 8 chapters. In Chapter 1, the background of the project is outlined, including an introduction to More Electrical Aircraft, and the sponsoring organization. A brief literature review of More Electrical Aircraft and the challenges coming up with it is presented.

In Chapter 2, the literature survey is conducted on different types of electrical discharges and their characteristics. In addition, some test methods are also represented. Problems faced at present are further explained.

In Chapter 3, the design of insulation coordination in low-voltage equipment including dimensioning of clearances and creepage distances specified in both IEC 60664 and IPC 2221 is presented in detail. The requirements in the existing guidelines are evaluated and validated against the test results attained from breakdown of air gap tests under both uniform fields and non-uniform fields and dry breakdown tests on solid insulation materials. Paschen's curve is also used to compare these test results. Finally, recommendations of employing these standards are summarized.

In Chapter 4, the mathematical model of initiating electrical tracking on solid insulation material is developed. Different impact factors are discussed by applying the model and finite element analysis simulation is conducted to not only find out the static analysis of this model but also to look into the dynamic status of electrical progressing.

In Chapter 5, standardized comparative tracking index test techniques are employed to investigate the mechanism of electrical tracking under aqueous contamination environment, and a comparison is done between the test results and theoretical calculation results by using

the model developed in Chapter 4. Thermal images are recorded and discussed to correlate the initial electrical discharges and electrical tracking under wet conditions.

Chapter 6 focuses on the test results under lower air pressure environmental condition. The same aqueous contamination and similar test methods are used, and the environment chamber is used to change the ambient air pressure. The influence of air pressure, which is a unique factor to be considered for aerospace application, is also discussed.

To generate a guideline of clearance and creepage distances, the standardized comparative tracking test technique is not applicable due to its gap distance limitation of 4mm. Chapter 7 shows the development of test techniques on electrical tracking to varying gap distance on solid insulation. The repeatability of the test results is compared with the previous test results from standardized tests. Test results provide a guideline of creepage distances under atmospheric pressure. The comparison is also conducted against those in IEC 60664 and IPC 2221.

Finally, some conclusions based on the test results are given, and last but not least areas of future work are discussed.

Chapter 2 Review Electrical Discharge, Characteristics, and Relevant Test Techniques

2.1. Introduction

The aim of our research was to firstly examine and validate existing guidelines for dimensioning clearances and creepage distances for aerospace applications, especially for advanced More Electrical Aircraft electrical systems operating at higher voltages. These clearances and creepage distances must be specified to avoid all kinds of electrical discharge. A brief review of IEC 60664: 2003 “Insulation Coordination For Equipments Within Low-voltage Systems” and IPC 2221 “Generic Standard on Printed Board Design” will be presented in this chapter. By doing this, we can show that it is necessary to re-validate those rules so that more precise ones with more detailed environmental conditions will help in future electrical system design for large More Electrical Aircraft.

Generally speaking, electrical discharges can be classified into three major types: disruptive discharges, partial discharges and tracking. As shown in the following detailed information, we can see that all of them are directly or indirectly agree to Paschen’s law to some extent. To understand Paschen’s law, it is important to review the fundamental principle of breakdown in the air under uniform and non-uniform fields, following this, each discharge type will be discussed. The approach employed in “High Voltage Engineering Fundamentals” written by E. Kuffel, W. S. Zaengl and J. Kuffel is followed in this section[38]. For partial discharge, we only give a very brief review since it will not be my research focus. Electrical tracking will be explained in detail.

Relevant test techniques will also be discussed. The electrical breakdown test method, specified in IEC 60: 1989”High-voltage Testing Techniques” has been widely accepted by

most researchers as the method to study breakdown. In this thesis it will not emphatically state. However, for electrical tracking tests, to date various methods have been developed to measure inception voltage for tracking or just to observe the behaviour of it. The standardized test methods including A.S.T.M D 495"High voltage low current arc resistance of solid electrical insulating materials", IEC 60112 "comparative tracking index test", IEC 60587 inclined plane test will be discussed in detail and further method ,such as dust-fog test, developed by different organizations also presented.

2.2. Electrical breakdown in gases

This section will elaborate the mechanism of ionization and decay processes which are critical to promote conduction in gases, and then a complete breakdown and spark formation. Before proceeding to discuss electrical breakdown in gases it is appropriate to introduce some import fundamental definitions relevant to kinetic theory of gases.

At ambient pressure and temperature, most gases have very good insulation properties. E. Kuffel claimed in the book [38] the conduction in air at low field is between 10^{-16} -10^{-17} A/cm^2 (on page 294). This minor conductive effect is from cosmic radiation and radioactive substances present in the earth and the atmosphere.

Historically the electron collision ionization was first explained by Townsend [39]. It is the most important ionization processes leading to breakdown of gases under high electric field. As explained electrons always exist in atmospheric space. Under higher electrical fields, those free electrons could gain sufficient kinetic energy ($\Delta W = eE\overline{\lambda_e}$) which must be at least equal to the ionization energy of the molecule (eV_i) between collisions to cause ionization on impact with neutral molecules. Hence, the amount of energy gained by an electron depends on the distances through which the electron is accelerated by the electrical force between collisions and determines the effectiveness of ionizations. The average distance can be defined as the free path (λ). For an electron, this parameter is a stochastic

quantity and the mean free path ($\bar{\lambda}$) depends on the nature of the gases and their density. The impact of attachments and recombination and the cathode effect to the ionization processes is also illustrated in this section to give a whole picture.

The derivation of theoretical ionization equations for initiating discharge is also provided by considering the Townsend first ionization coefficient α, the attachment coefficient η and Townsend second ionization coefficient γ, where $\bar{\alpha} = \alpha - \eta$ represents the effective ionization coefficient. This is called the Townsend criterion for spark formation or Townsend breakdown criterion. The criteria of conductive current between two electrodes to become self-sustaining discharge indicate the initial one electron through electron avalanche and secondary electron emission by photo impact at cathode can produce at least one electron which can consequently cause a repetition of the avalanche. The expression for breakdown voltage for uniform field gaps as a function of gap length and gas pressure can be derived based on the Townsend breakdown criteria, which is named Paschen's law.

Finally the mechanism of breakdown under non-uniform field and partial discharges were illustrated.

2.2.1. Useful definitions in gas kinetic theory

There are two types of collision between gas particles. One is called elastic or simple mechanical collisions in which the energy exchange is always kinetic. The other is inelastic, in which some of the kinetic energy of the collision particles is transferred into the potential energy of the struck particle or vice versa. The latter includes excitation, ionization, attachments, etc, closely connected to electrical breakdown in gases.

The Mean Free Path λ of molecules and electrons

The free path (λ) is defined as the distance molecules or particles travel between collisions.

The free path is a random quantity, and it will be shown that the mean free path depends upon the concentration of particles or the density of the gas.

The relation between the effective diameter of a molecule and the concentration of particles can be expressed that at room temperature and air pressure (27 $^{\circ}C$, 10^5 Pa), the larger the diameter of molecule, the more likely collision is, and the smaller the average free path. Further, the relationship with temperature T and pressure p is that, when temperature is kept constant, an increase in pressure results in the mean free path decreasing. Additionally, with constant pressure, the mean free path is directly proportional to the temperature.

Numerically speaking, to derive the mean free path, we can assume an assembly of stationary molecules of radius r_1, and a moving layer of smaller particles of radius r_2 as particles move. As the smaller particles move, their density will decrease due to scatting caused by collision with gas molecules. We can therefore deduce the expression of the mean free path based on the probability of the free path of length x being equal to the probability of collisions between x to $x+dx$. For mean free path, therefore:

$$\bar{x} = \bar{\lambda} = \int_{x=0}^{\infty} xf(x)dx$$

$$= N\pi(r_1 + r_2)^2 \int_{x=0}^{\infty} xe^{-N\pi(r_1+r_2)^2 x}dx$$

$$= \frac{1}{N\pi(r_1 + r_2)^2} \text{ …… (2.1)}$$

The denominator in eqn. 2.1 has represents the dimensions of area and the value $\pi(r_1 + r_2)^2$ is usually called the cross-section for interception or simply collision cross-section, and is defined by σ

$$\sigma = \frac{1}{N\bar{\lambda}} \text{ ……(2.2)}$$

As we know that $N = p/kT$, it follows that the mean free path is directly proportional to temperature and inversely proportional to the gap pressure.

$$\lambda(p,T) = \lambda_0 \frac{p_0}{p} \frac{T}{T_0} \text{ ……. (2.3)}$$

2.2.2. The appearance and disappearance of the charged particles in gases

Ionization by collision

The state of equilibrium of a gas can be upset by the application of a sufficiently high field. At higher fields charged particles are accelerated by electrical field force. However, they cannot keep building up their kinetic energy, due to collisions. On one hand, during elastic collisions, they lose little energy and kinetic energy can still accumulate. On the other hand, however, some of the particles that have already gained enough energy will have inelastic collisions. As a result, a large fraction of their kinetic energy is transferred into potential energy, causing, for example, ionization of the struck molecule. Electrons in gases are always at a much high velocity than those very big molecular. They can more easily collect kinetic energy and cause ionization, which is the most important process leading to breakdown of gases. The effectiveness of ionization by electron impact depends upon the energy that an electron can gain along the mean free path in the direction of the field.

If $\overline{\lambda_e}$ is the mean free path in the field direction of strength E then the average energy gained over a distance $\overline{\lambda}$ is $\Delta W = eE\overline{\lambda_e}$. This quantity is proportional to E/p since $\overline{\lambda_e} \propto 1/p$. To cause ionization on impact the energy ΔW must be at least equal to the ionization energy of the molecule (eV_i) which may excite the particle; the excited particles on collision with electrons of low energy may become ionized. Furthermore, not all electrons having gained energy $\Delta W \geq eV_i$ upon collision will cause ionization. This

simple model is not applicable for quantitative calculations, because ionization by collision, as with all other processes in gas discharges, is a probability phenomenon, and is generally expressed in terms of cross-section for ionization defined as the product $P_i\sigma = \sigma_i$ where P_i the probability of ionization on impact is and σ is the molecular or atomic cross-sectional area for interception defined. The cross-section σ_i is measured using monoenergetic electron beams of different energies. The variation of ionization cross-section for H_2, O_2 and N_2 with electron energy is shown in Fig 2.1[38]. It is seen that the cross-section is strongly dependent upon the electron energy. At energies below ionization potential the collision may lead to excitation of electron to become ionized. This process becomes significant only when densities of electrons are high. Very fast moving electrons may pass near an atom without ejecting an electron from it. For varying gases there exists an optimum electron energy range which gives a maximum ionization probability.

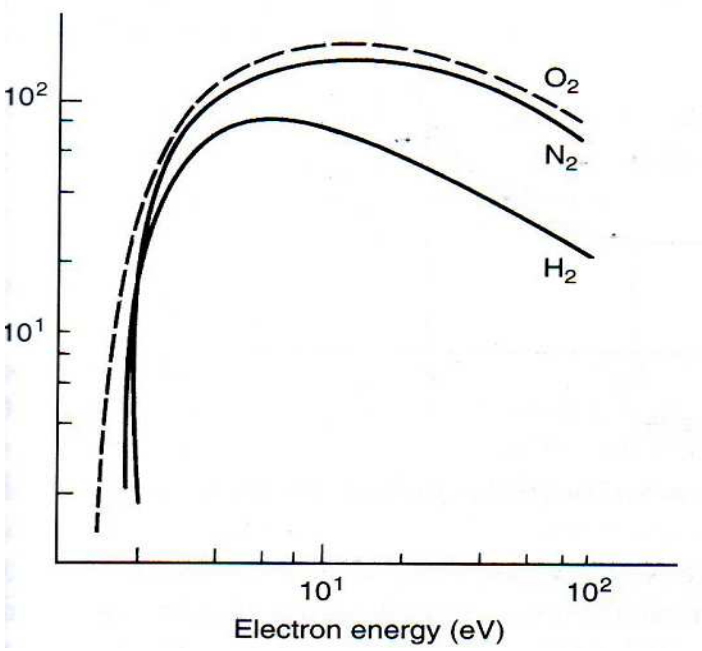

Figure 2. 1 Variation of ionization cross-sections for, and with electron energy [38]

Photoionization

Electrons of lower energy than the ionization energy eV_i may on collision excite the gas atoms to higher states. The reaction may be symbolically represented as $A+e+K$ energy $\longrightarrow A^*+e$; $A^* \longrightarrow A+h\upsilon$; A^* represents the atom in an excited state. On recovering from the excited state in some $10^{-7}-10^{-10}$ sec, the atom radiates a quantum of energy of photon ($h\upsilon$) which in turn may ionize another atom whose ionization potential energy is equal to or less than the photon energy. The process is known as photoionization and may be represented as $A+h\upsilon \longrightarrow A^+ + e$, where A represents a neutral atom or molecule in the gas and $h\upsilon$ the photon energy. For ionization to occur $h\upsilon \geq eV_i$ or the photon wavelength $\lambda \leq c_0 h / eV_i$, c_0 being the velocity of light and h being Planck's constant. Therefore, only very short wavelength light quanta can cause photoionization of gas. For example, the shortest wavelength radiated from a UV light with quartz envelope is 145nm, which corresponds to $eV_i = 8.5eV$, lower than the ionization potential of most gases.

The probability of photon ionization of a gas or molecule is maximum when $(h\upsilon - eV_i)$ is small $(0.1-1eV)$. Photoionization is a secondary ionization process and may be acting in the Townsend breakdown mechanism, as explained in section 2.1.3.2, and is essential in the streamer breakdown mechanism in some corona discharges. If the photon energy is less than eV_i it may still be absorbed by the atom and raise the atom to a higher energy level. This process is known as photoexcitation.

Ionization by interaction of metastables with atoms

In certain elements the lifetime in some of the excited electronic states extends to seconds. These states are known as metastable states and the atoms in these states are simply referred to as metastables, represented by A^m. Metastables have relatively high potential energy and

are therefore able to ionize neutral particles. If V_m, the energy of a metastable A^m, exceeds V_i, the ionization of another atom B, then on collision ionization may result according to the reaction:

$$A^m + B \longrightarrow A + B^+ + e \text{ ..... (2.4)}$$

For V^m of atom $A^m \langle V_i$ of an atom B the reaction may lead to the exciting of the atom B which may be represented by

$$A^m + B \longrightarrow A + B^* \text{ ..... (2.5)}$$

Another possibility for ionization by metastables is when $2V^m$ for A^m is greater than V_i for A. The reaction may proceed as:

$$A^m + A^m \longrightarrow A^+ + A + e + K.E. \text{ ..... (2.6)}$$

The last reaction is important only when the density of metastables is high.

Another reaction may follow as:

$$A^m + 2A \longrightarrow A_2^* + A \text{ ..... (2.7)}$$

$$A_2^* \longrightarrow A + A + h\upsilon \text{ ..... (2.8)}$$

The photon released in the last reaction is of too low energy to cause ionization in pure gas, but it may release electrons from the cathode.

Ionization by metastable interactions comes into operation long after excitation, and it has been shown that these reactions are responsible for long time lags but within the region of 10^{-6}-10^{-7} observed in some gases. It is effective in gas mixtures.

Thermal ionization

The term thermal ionization, in general, applies to the ionizing actions of molecular collisions, radiation and electron collisions occurring in gases at high temperature. If a gas is heated to sufficiently high temperature many of the gas atoms or molecules acquire

sufficiently high velocity to cause ionization on collision with other atoms or molecules. Thermal ionization is the principal source of ionization in flames and high-pressure arcs.

Cathode process –secondary effect

Electrodes, in particular the cathode, play a very important role in gas discharge by supplying electrons for the initiation, for sustaining and for the completion of a discharge. Under normal conditions electrons are prevented from leaving the solid electrode by the electrostatic forces between the electrons and the ions in the lattice. The energy required to remove an electron from a Fermi level is known as the work function and is a characteristic of a given material. There are several ways in which the required energy may be supplied to release the electrons.

- **Photoelectric emission**

Photons incident upon the cathode surface whose energy exceeds the work function may eject electrons from the surface. For most metals the critical frequency υ_0 lies in the UV range. When the photon energy exceeds the work function, the excess energy may be transferred to electron kinetic energy according to the Einstein relation:

$$\frac{1}{2}mu_e^2 = h\upsilon = h\upsilon_0 \ldots\ldots\ldots \text{(2.9)}$$

where m is the electron mass, u_e its velocity and $h\upsilon_0 = W_a$ the work function.

- **Electron emission by collision of positive ions with the cathode**
- When positive ions collide with the cathode, electrons will be emitted from the metal material of the cathode. This phenomenon can occur when the transmitting energy, including the kinetic energy and potential energy of the positive ion, is at least twice as large as the work function of the cathode's metal material. The key mechanism of this kind of electron emission is that the impinging ion must release two electrons, one of which is used to combine with the positive ion thus becoming a

neutralized atom. In Townsend spark discharge, the principal secondary process is electron emission by positive ions.

- **Thermionic emission**

In normal conditions (room temperature), the possibility of the electrons leaving the surface of the cathode is supposed to be very low due to lack of sufficient thermal energy. When the cathode is heated to a high temperature, the electron can obtain enough energy to be greater than the work function. The electron emission then happens. Data from High Voltage Engineering by E. Kuffel[38] can show a clearer picture for us. At room temperature, the average thermal energy of the electron is considered to be $3\times10^{-2}eV$. This is lower than the work function of any material shown in Table 2.1. However, if the metal temperature is increased to around 1500-2500 K, the electrons receive sufficient energy from the violent thermal lattice vibrations to cross the surface barrier and leave the cathode. In some circumstances, the thermionic emission may be enhanced, such as in a very strong electric field, where there is the Schottky effect.

Table 2. 1 Work function for typical elements [42]

Element	Ag	Al	Cu	Fe	W
W_a (eV)	4.74	2.98-4.43	4.07-4.7	3.91-4.6	4.35-4.6

- **Field emission**

Electrons can also leave the surface of the metal of the cathode as long as the external electrostatic field is strong enough. A strong electric field at the surface of a metal may modify the potential barrier at the metal surface to such an extent that electrons in the upper level close to the Fermi level will have a definite probability of passing though the barrier. They also show that the fields required for producing emission currents of a few microampere are of the order of $10^7-10^8\ \ V/cm$. As we all know, this kind of field can be gained only at the surface of the electrode with a very high value of the curvature, such as a fine wire, sharp points and submicroscopic irregularities with an average applied voltage that is quite low (2-5 kV)[38]. These fields are much higher than the breakdown stress even

in concentrated gases.

Deionization by recombination

Wherever there are positively and negatively charged particles present, recombination takes place. The potential energy and relative kinetic energy of the recombination electron-ion is released as a quantum of radiation. Symbolically the reaction may be represented as:

or $\left.\begin{array}{l} A^+ + e \longrightarrow A + h\upsilon \\ A^+ + e \longrightarrow A^m + h\upsilon \end{array}\right\}$ radiation recombination

Alternatively a third body C may be involved and may absorb the excess energy released in the recombination. The third body C may be another heavy particle or electron. Symbolically:

$$A^+ + C + e \rightarrow A^* + C \rightarrow A + C + h\upsilon \text{ …….. (2.10)}$$

Or

$$A^+ + e + e \rightarrow A^* + e \rightarrow A + e + h\upsilon \text{ ……. (2.11)}$$

Deionization by attachment-electron affinity

Certain atoms or molecules in their gaseous state can readily acquire a free electron to form a stable negative ion. Gases, whether atomic or molecular, that have this tendency are those that are lacking one or two electrons in their outer shell and are known as electronegative gases. Examples include the halogens (F, Cl, Br, I and At) with one electron missing in their outer shell, and O, S, and Se, with two electrons deficient in the outer shell.

For a negative ion to remain stable for some time, total energy must be lower than that of an atom in the ground state. The change in energy that occurs when an electron is added to a gaseous atom or molecule is called the electron affinity of the atom and is designated by W_a.

This energy is released as a quantum or kinetic energy upon attachment. Table 2.2 shows the electron affinities of some elements.

Table 2.2 Electron affinities of some elements [42]

Element	Ion formed	$W_a\,(kJ/mole)$
H	H^-	-72
O	O^-	-135
F	F^-	-330
Cl	Cl^-	-350
Br	Br^-	-325
I	I^-	-295

There are several processes of negative ion formation:

(1) The simplest mechanism is one in which the excess energy upon attachment is released as a quantum known as radioactive attachment. This process is reversible; that is, the captured electron can be released by absorption of a photon known as photodetachement. Symbolically the process is represented as:

$$A + e \Leftrightarrow A^- + h\upsilon \quad (W_a = h\upsilon) \ldots\ldots\ldots\ldots\ldots (2.12)$$

(2) The excess energy upon attachment can be acquired as kinetic energy of a third body upon collision and is known as a third body collision attachment, represented symbolically as:

$$e + A + B \rightarrow A^- + (B + W_k) \quad (W_a = W_k) \ldots\ldots\ldots (2.13)$$

(3) A third process is known as dissociative attachment, which is predominant in molecular gases. Here the excess energy is used to separate the molecule into a neutral particle and an atomic negative ion, symbolically expressed as:

$$e + AB \Leftrightarrow (AB^-)^* \Leftrightarrow A^- + B \quad \ldots\ldots\ldots\ldots\ldots\ldots (2.14)$$

(4) In process (3) in the intermediate stage the molecular ion is at a higher potential level and upon collision with a different particle this excitation energy may be lost to the colliding particle as potential and/or kinetic energy. The two stages of the process here are:

$$e + AB \Leftrightarrow (AB^-)^* \ldots\ldots\ldots\ldots\ldots\ldots (2.15)$$

$$(AB^{-})^{*} + A \Leftrightarrow (AB)^{-} + A + W_k + W_p \text{ …….. (2.16)}$$

Other processes of negative ion formation include splitting of a molecule into positive and negative ions upon impact of an electron without attaching the electron:

$$e + AB \Leftrightarrow A^{+} + B^{-} + e \text{ ……. (2.17)}$$

And a charge transfer following heavy particle collision, yielding an ion pair according to:

$$A + B \rightarrow A^{+} + B^{-} \text{ …… (2.18)}$$

All the above electron attachment processes are reversible, leading to electron detachment.

2.2.3. Electron avalanche and Townsend's first ionization coefficient

The electron avalanche is essential to the dielectric breakdown. It starts with the first electron accelerated by an electric field, ionizing the medium's atoms by collision to produce the second generation electrons, which continuously undergo the same process in successive cycles. More and more generation free electrons can be produced, just like an avalanche. This process can culminate in corona discharges, streamers, or a continuous arc that completely bridges the gas. Most of the free electrons are collected at the head of the cone due to electrons' higher velocity than that of the positive ions, which always gather at the tail of the cone.

Townsend first studied the variation of gas current measured between two parallel plate electrodes as a function of applied voltage. He observed that at the beginning of an increase of the voltage between two electrodes the gas current increased nearly directly proportionally. It then remains constant i_0 until voltage reaches a higher value. The current then increased above the value i_0 at an exponential rate.

Te explain this phenomenon, Townsend introduced a quantity α, known as *Townsend's first ionization coefficient*, defined as the number of electrons produced by an electron per unit length of path in the direction of the field.

Assume that an electron can produce n free electrons of n within the distance of x from the cathode in the field direction. According to the specification of Townsend's first ionization coefficient, the increase in electrons dn in the additional distance dx is given by:

$$dn = n\alpha dx \text{ ……. (2.19)}$$

Integration over the distance (d) from the cathode to anode gives:

$$n = n_0 e^{\alpha d} \text{ …… (2.20)}$$

Where n_0 is the number of primary electrons generated at the cathode, in terms of current, with I_0 the current leaving the cathode, equation (2.20) becomes:

$$I = I_0 e^{\alpha d} \text{ ……. (2.21)}$$

The term $e^{\alpha d}$ in the equation is called the electron avalanche and it represents the number of electrons produced by one electron in traveling from the cathode to the anode.

2.2.4. Townsend's second ionization

When a beam of positive ions collides with the surface of a cathode, secondary electron emission is likely to occur. Townsend measured this effect of the secondary process in the same experiment that he measured α / p. In his experiment, he found that with the voltage applied between two parallel plates increasing, the rate of the increase of current was higher than given in equation (2.21). To explain this departure from linearity Townsend postulated that a second mechanism must be affecting the current, which was firstly considered to be the liberation of electrons in gas by the collision of positive ions, but later was attributed to the liberation of electrons from the cathode by positive ion bombardment according to the

mechanism discussed earlier. Townsend then introduced γ, called Townsend's second ionization coefficient, which describe the efficiency of production of secondary electrons per ion pair formed in the gas. So the expression of the current carried by the non-self-sustained discharges is given by the following equation:

$$I = I_0 \frac{e^{\alpha d}}{1-\gamma(e^{\alpha d}-1)} \text{ …… (2.22)}$$

To simplify the equation above, due to the fact that $e^{\alpha d} \gg 1$, it can expressed by:

$$I = I_0 \frac{e^{\alpha d}}{1-\gamma e^{\alpha d}} \text{ ……. (2.23)}$$

2.2.5. Townsend mechanism–transition from non-self-sustained discharges to breakdown

According to previous section, we know that Townsend developed the expression of the current carried by discharges after he introduced two coefficients, α and γ. However, it should be noted that this equation is applicable when the voltage between two parallel plates' electrodes is not as large as the point where there is a sudden transition from the dark current I_0 to self-sustaining discharge. As soon as the voltage reaches this point, the denominator of equation (2.22) approaches zero. The current then tends to infinity, independent of the external current I_0. We can then derive:

$$\gamma(e^{\alpha d}-1) = 1 \quad \text{…… (2.24)}$$

If the electron attachment is taken into account, this equation becomes:

$$\gamma e^{(\alpha-\eta)d} = \gamma e^{\bar{\alpha} d} = 1 \text{ ……. (2.25)}$$

since $e^{\bar{\alpha} d} \gg 1$ and $\alpha \gg \eta$

Where η the attachment coefficient of electrons is $\bar{\alpha}$ is the effective ionization coefficient. It can then be seen that the current at the anode equals the external current I_0 in

external circuit. The physical picture of breakdown is that a sufficient number of ion pairs are formed by the α mechanism so that through the γ process at least one electron is produced to maintain the current [38].

In summary, when $\gamma e^{\bar{\alpha}d} = 1$, the number of ion pairs produced in the gap by the passage of one electron avalanche is able to produce one secondary electron since the positive ions generated can collide with the cathode to generate secondary electron emission, which can consequently cause a repetition of the avalanche process. We can therefore say this is the Townsend breakdown criterion to define the sparking threshold. When $\gamma e^{\bar{\alpha}d} \rangle 1$, the ionization produce by successive avalanches is cumulative. The spark discharge grows more rapidly the more $\gamma e^{\bar{\alpha}d}$ exceeds unity. When $\gamma e^{\bar{\alpha}d} \langle 1$, the current I is not self-sustained.

2.2.6. Paschen's law

The Townsend criterion, equation (2.24), enables the breakdown voltage of the gap to be determined by using the appropriate values $\bar{\alpha}/p$ and γ corresponding to the values E/p without ever taking the gap currents to high values (that is, keeping them below 10^{-7} A) so that space charge distortions are kept to a minimum and more importantly so that no damage to electrodes occurs. Good agreement has been found between calculated and experimentally determined breakdown voltages for short or long gaps and relatively low pressures for which this criterion is applicable.

Further, analytical expression for breakdown voltage for uniform field gap as a function of gap length and gas pressure can be derived from the threshold equation (2.24) by expressing the ionization coefficient $\bar{\alpha}/p$ as a function of field strength and gas pressure. If we put $\bar{\alpha}/p = f(E/p)$ in criterion equation we obtain

$$f(E/p)pd = \ln(\frac{1}{\gamma}+1) = K \text{ ……. (2.26)}$$

For uniform field $V_b = Ed$, where V_b is the breakdown voltage.

$$e^{f(V_b/pd)pd} = e^k = K' \text{ ……. (2.27)}$$

Or

$$V_b = F(pd) \text{ …….. (2.28)}$$

which means that the breakdown voltage of a uniform field gap is a unique function of the product of pressure and the electrode separation for a particular gas and electrode material. Equation (2.27) is known as Paschen's law, and was established experimentally in 1889. The shape of Paschen's law is shown in Figure 2.2, which was produced by Andrew Nelms in his PhD thesis [40]. It can be seen that there is a minimum breakdown voltage/sparking potential in Paschen's curve. Table 2.3 shows us the typical values of the minimum sparking constants for various gases.

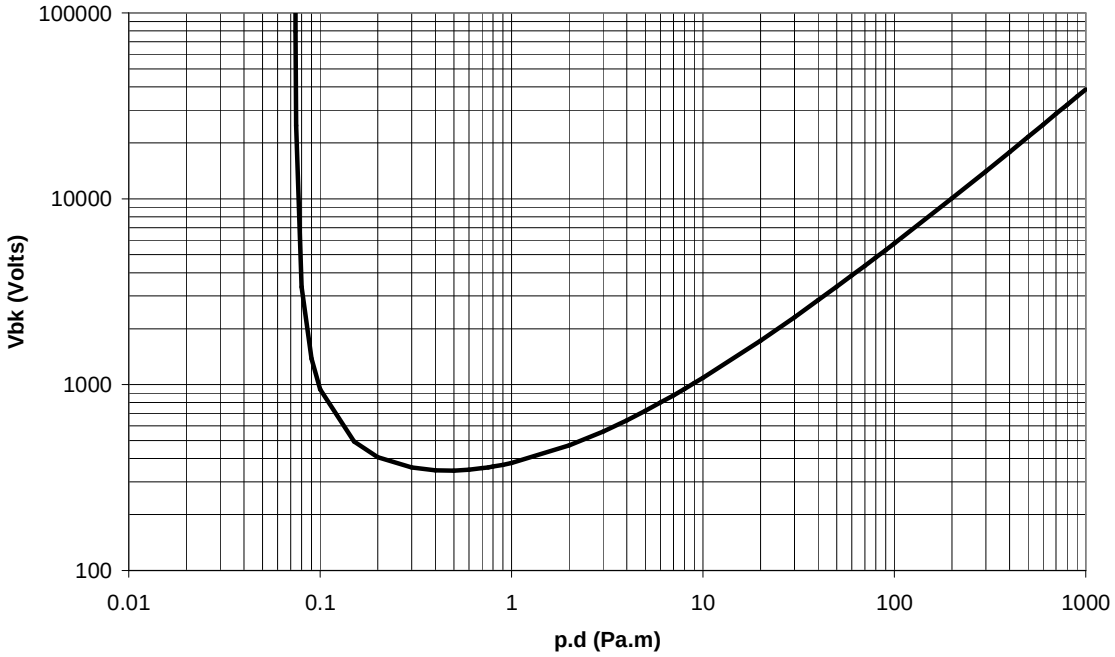

Figure 2. 2 Breakdown voltage in air for a given air pressure - distance product according to Paschen's law [40]

Table 2. 3 minimum sparking constants for various gases

Gas	$(pd)_{\min}$ ($Pa \cdot m$)	$V_{b\min}$ (volts)
Air	0.73	352
Nitrogen	0.84	240
Hydrogen	1.40	230
Oxygen	0.93	450
Sulphur hexafluoride	0.35	507
Carbon dioxide	0.76	420
Neon	5.33	245
Helium	5.33	155

It should be noted that it has been proven that the breakdown voltage is affected by the cathode material and cathode conditions due to the various real values of γ.

If we substitute $\overline{\alpha}$ by using the equation $\overline{\alpha} = Ap\exp(-\frac{Bp}{E})\left[= A\exp(-\frac{Bpd}{V})\right]$, we can obtain the expression of the breakdown voltage for uniform field gaps.

$$V_b = \frac{Bpd}{\ln\frac{Apd}{\ln(1+1/\gamma)}} \quad \text{.....} \quad (2.29)$$

where Constant A=12, B=365 and $\gamma = 0.02$ which is commonly quoted in the literature [41].

Paschen's law states that the breakdown characteristics of a gap are a function of the product of the gas pressure and the gap length. Strictly, Paschen's law is only valid for electrodes with uniform electric field (in compact systems where separation distances are relatively small, this will normally be the case). In any breakdown, a number of ionizing collisions must take place between electrons and other molecules. Raising the voltage across a gap or reducing the gap distance with a fixed voltage increases the electric field, which causes increased acceleration of electrons and therefore a higher likelihood of an ionizing collision. Variations of breakdown voltage as a function of pressure are in contrast due to the increase in the mean free path of electrons (the average distance that an electron travels before colliding with another molecule). Increasing this distance allows electrons to gain a

higher velocity before collision and therefore be more likely to cause an ionizing collision. Paschen's curve for air is shown in Figure 2.2. As the pressure is reduced breakdown voltage initially falls. It reaches a minimum and then, as pressure is further reduced, rises steeply again. This rise in strength of a gap is reached once the mean free path of an electron becomes comparable with the size of the gap (meaning the likelihood of ionizing collisions is very low).

The minimum point of this curve is Paschen's minimum. In air, this is 327V for a pressure distance product of 0.754 Pa.m [45]. Below this voltage, breakdowns cannot take place, hence the lack of consideration given to some forms of electrical discharges in previous designs of aircraft operating at lower levels of voltage.

In modern aircraft electrical systems, the voltages between two electrodes can be higher than Paschen's minimum and this means that air gaps between electrodes could breakdown should these not be kept a sufficient distance apart. Such a discharge would be classed as a disruptive discharge since it would result in a flow of fault current between the electrodes and would usually necessitate the operation of some form of power system protection to clear the fault.

2.2.7. Breakdown in non-uniform fields

Non-uniform fields usually can be produced between the gap of a point /sphere/stick and plane electrodes or coaxial cylinders. The characteristic of this kind of field is that the field strength and hence the effective ionization coefficient $\bar{\alpha}$ vary across the gap.

The characteristics of the breakdown in non-uniform fields

In general, breakdown in non-uniform fields presents a very significant polarity effect, which means that the different polarity applied to the electrodes influences the process of ionization and breakdown voltage very significantly. In the following table the difference is

illustrated in brief. Another characteristic is that usually it takes a longer time to break down the gap.

The electron multiplication is governed by the integral of $\bar{\alpha}$ over the path ($\int \bar{\alpha} dx$). At low pressure the Townsend criterion for spark takes the form:

$$\gamma\left[\exp(\int_0^d \bar{\alpha} dx) - 1\right] = 1 \quad \ldots\ldots\ldots (2.30)$$

where d is the gap length. The integration must be taken along the line of the highest fields' strength. The expression is valid also for higher pressure if the field is only slightly non-uniform. In the strongly divergent fields there will be at first a region of high values of E/p over which $\alpha/p \rangle 0$. When the field falls below a given strength E_c the integral $\int \bar{\alpha} dx$ ceases to exist. Townsend's mechanism then loses its validity when the criterion relies solely on the γ effect, especially when the field strength at the cathode is low.

In reality breakdown or inception discharge is still possible if taking the photoionization processes into account. The criterion can be written as:

$$\int_0^{x_c \langle d} \bar{\alpha} dx = \ln N_{cr} = 18 - 20 \ldots\ldots\ldots (2.31) \qquad ([38,40])$$

where N_{cr} is the critical electron concentration in an avalanche giving rise to initiation of a streamer. (It was shown to be approx.10^8). x_C is the path of avalanche to reach this size and *d* the gap length.

The process of the breakdown in short gaps

The process of the breakdown between short gaps is that at first there will be a corona discharge occurring around the region of high field strength, then streamer is produced until it reaches the opposite electrode and finally breakdown. It has a significant polarity effect due to the difference of field distortion for different polarity of the electrodes. We specify the positive polarity gap stands for the setting where the point electrode is positive, and a negative polarity gap means that the negative potential is applied on the point electrodes.

The conclusion can be reached that the inception voltage for the positive polarity gap is higher than the negative one, because it is easier for a negative polarity gap to have a streamer during the period of non-self-sustaining discharge. However, after self-sustaining discharge occurs between the gap, the positive polarity gap more readily has a streamer than the negative polarity gap. This will result in the breakdown voltage of the negative polarity gap being higher than the positive one.

2.2.8. Partial discharge (PD)

In a uniform field or approximate uniform field gap, as soon as the voltage between two electrodes reaches the threshold of the breakdown, there will be a complete breakdown of the gap. However, in non-uniform fields, partial discharge is observed long before the complete breakdown occurs since some discharges can happen at stages with a higher field than other parts.

Partial discharge in insulation systems comprises a large variety of physical phenomena ranging from low level surface emissions, over glow discharges, leakage currents along weakly conducting insulator surfaces, sub-critical avalanche activity, electrical tree inception and growth to streamers, leaders, sparks, and arcs. PD is very important in H.V. engineering where non-uniform fields are unavoidable. This phenomenon can lead to deterioration of insulation by the combined action of the discharge ions bombarding the surface and the action of chemical compounds that are formed by the discharge.

For most systems that would be found in the More Electric Aircraft, these will take the form of a discharge in air – these therefore also require a voltage exceeding Paschen’s minimum. As an example, a partial discharge would occur when an insufficient thickness of insulation around a wire allows sufficient electric field to build up in the gap between outside of that wire and another grounded electrode. Figure 2.3 shows an example of this where an aerospace cable is operated at a voltage such that partial discharges form in the air gap. Partial discharges can also take place across surfaces, around sharp electrodes (usually referred to as corona) and within insulation systems containing gas bubbles (voids). A key

characteristic of partial discharges is that they will usually not result in the flow of fault current (and therefore will not instigate the operation of power system protection). However, they have the ability to continually damage an insulation system until complete failure results. The second picture in Figure 2.3 shows an acrylic that has been subjected to partial discharges for one week and in which erosion can be observed – this has a depth of 0.3mm.

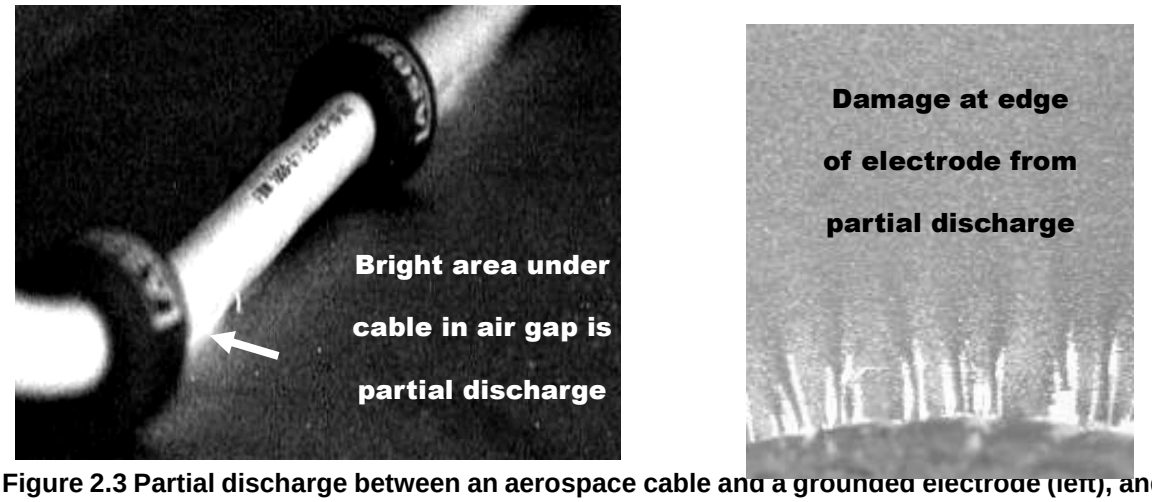

Figure 2.3 Partial discharge between an aerospace cable and a grounded electrode (left), and erosion of an insulating material due to partial discharge (right).

2.3. Electrical tracking

Organic insulation materials are used in a variety of electrical apparatus owing to their light weight and good electrical and mechanical properties. The degradation of organic materials can contribute to electrical discharges. One type of them is called electrical tracking. Electrical tracking can happened both under dry and wet condition, higher voltage is needed to trigger small electrical discharges for eventual electrical tracking on solid organic materials under dry condition though [43]. Where a surface path exists along insulation and when this is contaminated, electrical tracking can occur between two points with different potentials, much lower than those under dry condition. This is because damage caused during tracking over wet surfaces is due to current flow. This can eventually lead to electrical failure in the form of a short circuit. Those surface failures occur just above or underneath the surface where it is influenced by the surface. Otherwise it can also happen between two solid surfaces in contact by what is more properly called interfacial failure.

Many researches [44-46] have studied surface discharge and electrical tracking under dry condition with the influences of ambient environmental factors such as the ambient temperature, contamination such as both pure liquids and particular contaminants of many kinds deposited on the surface of electrical insulation to represent reality, and magnetic fields. And the limitation of this research is they do not consider air pressure effects. It is known that electrical systems on aircraft will always operate under extremely rapid airframe ascent/descent. Research [47] showed that the corona discharges on PCB occur more readily under low air pressure around the highest electrical stress area with a large effect on the degradation of solid insulation materials. B. X. Du with other researchers [47-51] also investigated the surface breakdown phenomenon of printed circuit boards with increasing temperature from $23^{o}C$ up to $150^{o}C$ and atmospheric pressure from 100 kPa to 1 kPa. It is found that smaller insulation distances are necessary to ensure the insulation reliability under lower pressure. The mechanism they were looked into was the electrical tracking under dry condition on PCBs but not wet conditions.

The research on the electrical tracking under wet condition showed that when the carbonized deposits bridge the electrodes, the dielectric breakdown phenomenon called tracking failure will occur, which can cause an abrupt reduction in the insulating resistace.[52]

All of the literatures stated above focused on the dielectric endurance. In other words, their researches was interested in finding out failure time and erosion left due to the electrical tracking either under dry or wet conditions. Even in a recent paper published in 2008 with the topic of effect of ambient pressure on the mechanism of electrical tracking failure written by X. Du. and Yong Liu [53] was to investigate the failure time rather than the behaviour of initiation of electrical tracking. In my PhD thesis, the focus will be on the initiation of discharges between two electrodes on solid insulation surfaces and hence the initiation of tracking. The ultimate long-term degradation due to initiation of discharges on

the surfaces has been studied in abovementioned research already.

The surfaces of insulation material are supposed to be ideal smooth and perfect. The process of tracking across a small gap contaminated with a conductive aqueous contaminant is illustrated in Figure 2.4. When a liquid layer is deposited between two electrodes, a current will flow in the liquid. Heating of this liquid layer will lead to evaporation. This will often take place in the middle of the gap away from the electrodes which stabilize the temperature of the nearby liquid. As the liquid evaporates, a spark will develop across the new dry band due to the interruption of current flow. In other words, at least one spark will occur when a liquid layer dries out. The spark, if energetic enough, can damage the underlying insulation. It should be noted that the insulation material type is not the key factor to influence the initiation of dry band spark but the evaporation rate. However, the severity of damages is dependent on the solid insulation itself. With continuous contaminant deposited on the surface, should carbonaceous deposits develop, this can accelerate further damage owing to the reduction in the 'healthy' insulation within the gap. The severity of the damage will depend on the voltage and current of the arc along with the characteristics of the material itself.

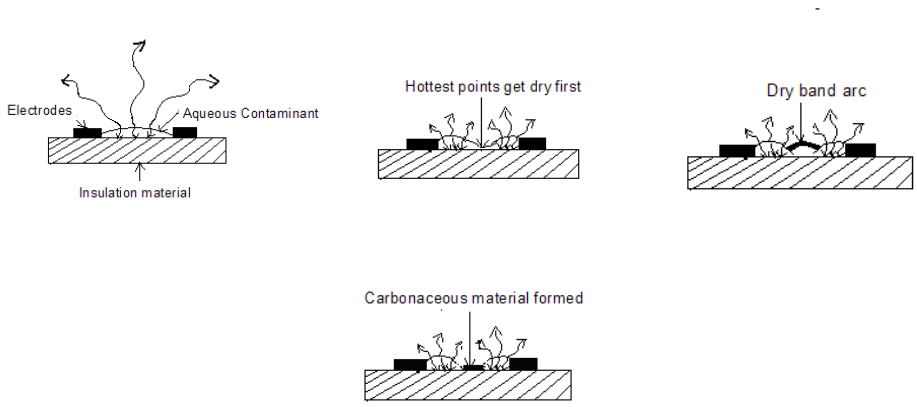

Figure 2.4 – Basic process of tracking across an insulating surface contaminated with an aqueous layer

The breakdown of an insulation gap where gaseous insulation exists in the gap between two

electrodes is determined by Paschen's law. As previously explained, a minimum voltage is therefore required to cause a breakdown in this gap.

In contrast, a surface that is wet sees current flow through the contaminant as previously described. When this current causes evaporation of the liquid, an arc is drawn and damage can be result the underlying surface by this arc. The voltage across the gap that leads to this process taking place depends on the resistance of the liquid layer and the level of current needed to cause evaporation. There is no requirement for a voltage at the level of Paschen's minimum since an arc is being drawn when the liquid layer separates.

Higher voltages are more likely to cause electrical tracking owing to the increased level of heating that can occur in contamination deposited in a given size gap. In addition, having a voltage above Paschen's minimum means that there is a chance of re-ignition of the arc (particularly important in an AC system where it will extinguish every half cycle). However the differentiation between breakdown of an insulation gap such as an air gap leading to Paschen's law and interruption of a current leading to discharge in a wet test at lower voltage is attributed to differences in their mechanism. The former is to breakdown the dielectric strength of gas insulation. And the latter is the due to interrupt a current. The electric arc at atmospheric pressure is familiar in appearance to most of us. It consists of a bright column that is highly visible to the naked eye. At its heart are ionized gases that allow the electric current to flow between two electrodes. The presence of ionised gas correctly suggests that there is a very high temperature at the core of the arc.

In an AC electrical circuit with an existing arc, the arc voltage and arc current are in nature passing through the locations around a voltage/current zero every half cycle. When the arc current is approaching zero, the arc voltage is equal to the system voltage, which results in current zero. When the current is zero, there is no new charge/energy in gases so that the insulation could cool down and the dielectric strength between electrodes could recover. The re-ignition of arc is dependent on the competition between the dielectric recovery rate and system voltage increases. If the former rate is bigger, then re-ignition will not occur.

Hence the frequencies of the voltage applied have impact on the electrical tracking. The higher frequency, the less severe the physical damage would be since the re-ignition is not achieved with very high frequency. But with power frequency, it can be always expected to have re-ignition as long as the voltage is above the Paschen's minimum. While with DC voltages, damages will be very badly since there will be no extinction at all as long as the arc takes place. As liquid boiling points lower with decreasing pressure, larger separations of electrodes become necessary at altitude since more contaminants within larger separation need more heat to dry out. Otherwise systems can be characterized to whether they are located in an environment that will not be subject to ingress of liquids in any form.

In aircraft systems, existing standards deal with the phenomena of arc tracking on cabling including wet arc tracking, dry arc tracking and series arc tracking. Generally, these events take place in locations where the insulation system has been compromised. Discharge activity in the form of an arc then burns surrounding insulation allowing damage to propagate over long distances. More details of these phenomena can be found in [54].

All of these forms of electrical discharge must be considered in the design process to ensure that the electrical system remains functional over its intended lifetime.

2.4. Existing design standards

A range of standards also exist that can support the design of high voltage aerospace systems. However, not all aspects of high voltage design for aerospace environments are yet fully covered by standards and it is likely that this is an area on which the industry will need to focus in the coming years.

IEC 60664 'Insulation Coordination for Equipment within Low Voltage Systems' defines the required clearances for equipment operating at a range of voltages for altitudes of up to 2000 m [55]. This is done for DC, AC and lightning voltages. The use of an altitude correction factor contained in the standard can convert this data for use at higher altitudes

even though the standard is not strictly applicable for aerospace use. The standard does not differentiate the gap size required according to the type of voltage (i.e. steady state DC/AC or lightning), as the breakdown voltage (based on the peak voltage) is the same for all voltage types for small gaps. The standard also contains a useful discussion on the dimensioning of air insulation that is required to withstand high frequency voltage stress (such as would be found in a power electronic converter switching square waves). The voltage withstand capability with increasing frequency arises due to the limited velocity of heavy positive ions [56]. The maximum effect of an increase in frequency above the critical value is to reduce the breakdown voltage of a uniform field gap by around 20%. It would therefore be prudent in an aerospace application to base clearances on a voltage roughly 25% higher than the value expected to account for this effect.

IEC 60664 also provides guidelines for dimensioning creepage distances along surfaces (to prevent tracking). The guidelines are based on empirical data and are not applicable to equipment installed in low pressure environments.

In a similar way IPC 2221 provides information on the distances between tracks on printed circuit boards design [57]. It covers all total aspects of design details using organic materials or organic material in combination with inorganic materials like metal, glass, ceramic, etc., as well as electronic packaging issues.

Aerospace Standard AS50881 [58] provides guidance for choosing conductor and insulation sizes for aerospace wiring. Conductor size is based on an analysis of the required current carrying capability and takes the impact of altitude and the use of conductor bundles into account. Insulation size is determined by examining the required operating voltage, the insulation selected being thick enough to withstand partial discharges.

From the above-mentioned background of design development trends within the aerospace industries, it can be summarized that reduction of weight and volume of the greater number of electronic components on the aircraft is absolutely critical. Due to much better electrical

and mechanical properties, solid insulation, especially those using organic insulation materials, are widely used to save significant insulating space. Higher power supply and voltage level has been applied. Additionally, to employ much higher frequencies, an increasing number of electronic converters and high frequency switch power supplies will be applied. The recent rapid development in electronic component technologies has heightened the need for evaluation of the electrical strength of solid insulation to guarantee the reliability and safety of operation of aircrafts.

2.5. Test techniques for electrical tracking

Since the majority of the work in the thesis is about electrical tracking, the series of test techniques for electrical tracking under wet condition are discussed in this section. At present, there are four major laboratory test methods to evaluate electrical tracking and erosion under surface discharge and dry band arc. A.T.S.M. D495 “High Voltage, Low Current Arc Resistance of Solid Electrical Insulating Materials” [59] specifies dry arc test methods, which are very widely used. IEC 60112: 2003 [60] is a standardized comparative tracking index test to evaluate the performance of organic materials by finding out the comparative tracking index values. However, there is a limitation in that only a 4mm gap can be set, since the dropping system for pollution liquids is particularly defined to that measurement. With a much bigger gap, the inclined plane test specified in IEC 587: 1984 [61] is the most comprehensive test for tracking and erosion. However, since the resistor connected in the electrical circuit of this test simulates the healthy insulation materials that are usually on the insulators and that have very large resistance values, it cannot be applied to printed circuit board failure where short-circuit path usually forms when tracking occurs between the tiny gaps between tracks on the boards. Mist-fog test techniques evaluate the degradation of insulating materials with a test period from a few hours up to 200 hours or even more, which is very time consuming.

2.5.1. A.S.T.M. D 495 “High Voltage, Low Current Arc Resistance of Solid Electrical Insulating Materials” [59]

In this test two 0.094 inch diameter tungsten electrodes with elliptically ground tips are rested on the surface of the sample. The electrodes are spaced 0.25 inch apart, and inclined at 35 degrees to the horizontal. A discharge is struck between the electrodes for a prescribed period, the duration of the discharge period increasing every minute until the material fails by a surface conducting channel. The test thus increases in severity with time, and the failure parameter to track is time. It would be very time consuming to test on a good organic material.

2.5.2. IEC 60112:2003 Comparative Tracking Index Tests

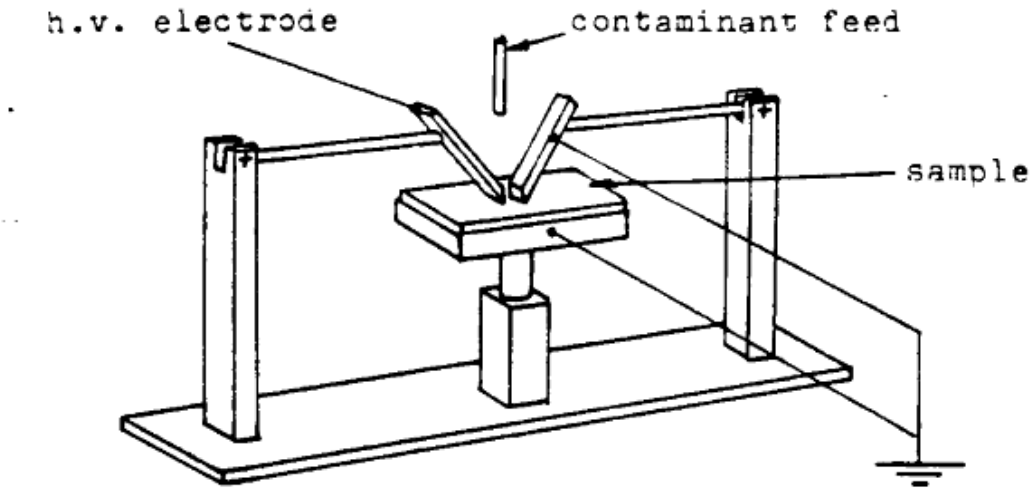

Figure 2.5 IEC 60112 test rig sketch [60]

This standardized method is used to indicate the relative resistance of solid insulation materials to tracking for voltages up to 600 V, when the surface is exposed under electric stress to water with the addition of contaminants. Two chisel shaped electrodes stand in front each other on a tested solid insulation material sample with a gap of 4mm. Around every 30 seconds one drop of the contaminant, which is a 0.1% aqueous solution of NH_4Cl, falls between the gap. Leakage currents flowing through the liquid cause drying

and consequently electrical discharges occur. The voltage that can lead to failure, which should be either leakage current bigger than 0.5 A for 2 seconds or where scintillations continuously occur, determines the comparative tracking index value of the solid insulation material. The comparative tracking index is numerically equal to the failure voltage. Since most CTI values for organic materials result from approximately a 50 drop, IEC have suggested that the CTI values should be defined as the lowest voltage that gives failure in 50 drops, which is approximately 25 minutes based on the specified flow rate. This test is not applied to eroded materials since the testing period is always controlled within half an hour and the maximum voltage that can be applied in tests is limited to 750 V. However, with longer periods of testing at a particular voltage, say 300 V, the mass loss of the eroding material can be obtained. So this test is very feasible so far.

2.5.3. IEC 60587 inclined plane test

This test method was originally established in 1961 as the result of work by Mathes and McGowan. It was later adopted as an A.S.T.M. Tentative Standard, and is now an accepted standard. It is perhaps the most comprehensive test for tracking and erosion, in that its scope covers two tracking procedures and one erosion procedure.

The inclined plane is the sample itself, as shown in Figure 2.6, with dimensions of 5 inches by 2 inches by 0.25 inches thick. A liquid contaminant, the same as used in IEC tests, flows from the filter paper reservoir under an H.V. electrode down the sample face to the lower earth electrode. The rate of flow is tabulated for given applied voltage levels, and is such that continuous scintillations should occur on the sample face immediately above the earth electrode.

Electrostatic forces in the contaminant flow then spread the fluid into a delta shape across the sample width; stable conditions are achieved when scintillations occur across the full width of the sample, between the earth electrode and oncoming contaminant film. For tracking materials it is found that, ultimately, rooting of a single discharge on a “hot spot” on

the sample surface leads to progressive tracking towards the H.V. electrode.

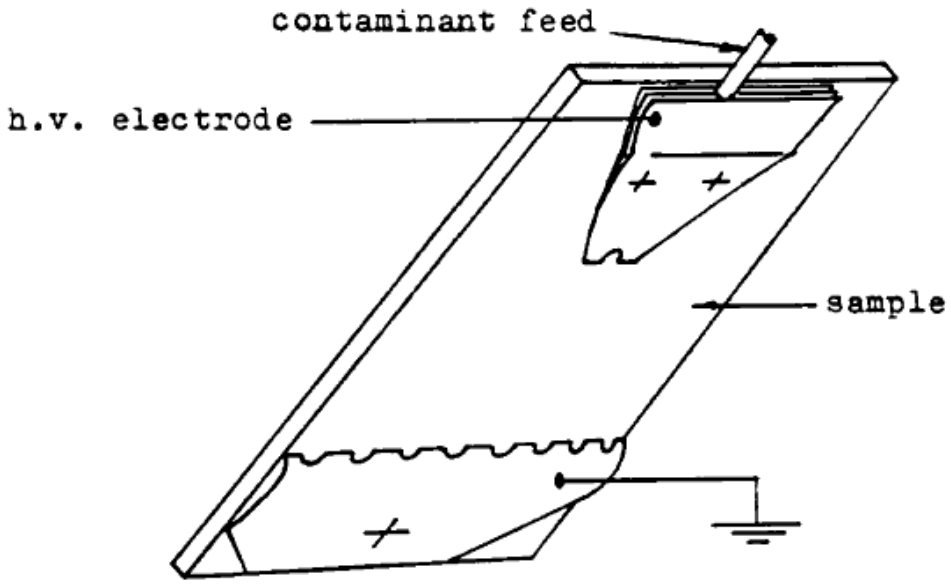

Figure 2.6 Incline plate plan sample and electrodes configurations [61]

Tracking is assessed in two ways: either by the initial tracking voltage, that is the lowest applied voltage at which progressive tracking takes place for a specified 0.5 inches or by the time to track, which the time is taken for tracking to proceed over the specified distance at a given voltage. Mass loss of eroding materials can be measured by continued application of a voltage, below the initial tracking voltage for a specified time. There are also several limitations of this test, such as random discharging, sample surface wetting properties, and degree of difficulty of operation. The voltage applied in the standard, which is provided a 48 Hz to 60 Hz power supply with output varying up to 6 kV with rated current not less than 0.1 A for each specimen, is not appropriate for aircraft applications.

2.5.4. Dust-fog test

This test was first described in 1956 by Allbright and Starr; the dust-fog test is the only test to use a solid pollutant. A.S.T.M. Tentative specification was based on the modified version by Sommerman.

The samples are sheets of 0.0625 inch thick, between 5 inches and 6 inches square, covered

by a dust layer to a uniform depth, 0.02 to 0.035 inch, with the recommended composition by weight of 85% flint dust, 9% clay, 3% salt and 3% paper fibers. The sample is first mounted to the electrodes shown in Figure 2.6 and then coated with the above mentioned pollutant. The whole test rig is put into a chamber, where a discrete water spray or fog can be generated. A dry band arc can occur when a voltage is applied to the electrodes. The surface pollutant is maintained by the continuous wetting of the sample surface at a rate within close limits of the rate of evaporation by the discharge and surface leakage currents in the contaminant film. Initially big discharges occur, but because of the loss of salt from the film, the final applied voltage is specified as 1.5 kV with a discharge current of 10 mA. By applying this method, tracking materials can be categorized to different degrees of resistant to tracking by whether the material can erode or fail, and the time period.

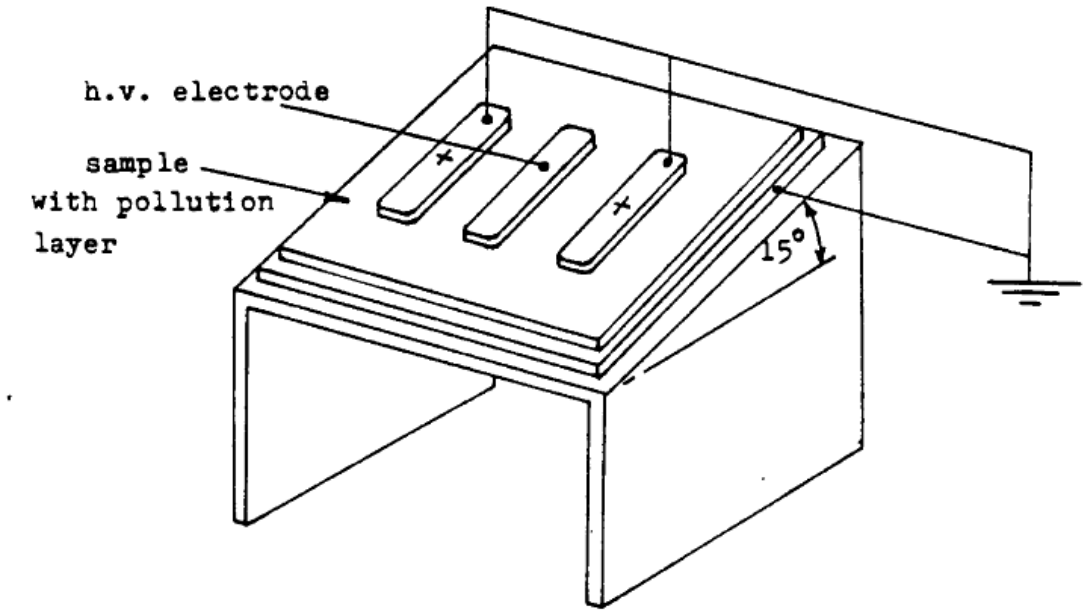

Figure 2.7 Dust-fog test rig sketch [70]

Some materials can be expected to erode after hundreds of hours. During so long a period, the sample has to be re-coated with pollutant. The test is unique in that a sample under voltage is stressed dielectrically between the H.V. electrode and the lower electrodes.

2.5.5. Test methods discussion

At present, many other tests exist to investigate the behaviour of surface discharge or electrical tracking. They all suffer the drawback of a lack of reproducibility and

repeatability of results. We must therefore admit that accelerated laboratory testing under polluted conditions is only successful in determining tracking or erosion materials in those processes.

However, in our research for More Electrical Aircraft applications, the IEC 60112 test method is the most appropriate one to employ. The limit of voltage of 750 V is not a problem at all for both maximum 15/200 VAC 400 Hz conventional commercial systems, 28 V DC or 270 V DC for military usage and a combined 230 V AC 360-800 Hz and +/- 270 V DC (540 V DC) new systems on future large More Electrical Aircraft. The most important reason to employ this method is that it can be used in a environmental chamber where the impact of air pressure can be evaluated.

The first and biggest challenge is how we can control the repeatability and reproducibility to some acceptable extent when we upgrade this method to any creepage distances. The next challenge is how laboratory testing environments can reflect real circumstances.

2.6. Conclusion

This chapter has given not only the fundamental knowledge of different types of electrical discharges but most importantly has shown how the failure types will have an impact on the future electrical system on large More Electrical Aircraft. The existing design rules have also been investigated and their limitations show that we have to re-validate both clearance and creepage distance dimensioning guidelines for much higher pressures with more precise values. It is very straightforward to evaluate clearances by using the IEC 60: 1989 standardized method while different tracking test techniques were discussed. Considering execution and application, IEC 60112's specified method was chosen for my research to investigate mechanisms of electrical tracking at varying air pressures, pollution degrees and even different ambient temperatures.

Chapter 3 Clearances and Creepage Distances to Avoid Dry Flashover

3.1. Introduction

As previously described in Chapter 1, the conventional aircraft electrical power system is a low-voltage system with typical voltage levels of 115/220 V AC and 28V DC. 270 V DC was used by the military to provide further weight savings in the 1980s. The concept of More Electrical Aircraft/All Electrical Aircraft (MEA/AEA) supports the use of higher voltage levels to enhance aircraft performance. Boeing has moved from a 115 AC 200 Hz system to a combined 230 V AC 360-800 Hz and +/- 270 V DC system. At the low voltage (115 V) used in conventional systems, the electric fields between conductors are lower than the critical field strength shown by Paschen's law and as such disruptive and partial discharges cannot take place (although tracking can). However, higher voltages such as 230 VAC and +/- 270 V DC introduce the likelihood of disruptive and partial discharges. Hence it is increasingly important in these high voltage systems to define safe levels of clearances and creepage distances. In IEC 60664, clearance is defined as the shortest distance in air between two conductive parts, while creepage distance is defined as the shortest distance along the surface of the insulating materials between two conductive parts. Figure 3.1 shows the clearance and creepage distance between two electrodes diagrammatically.

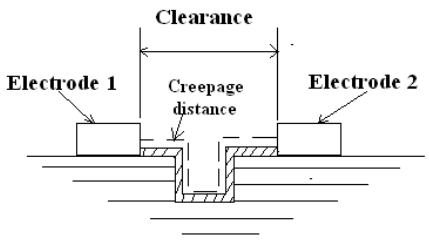

Figure 3.1 Sketch of clearance and creepage distance

A determination of clearance in air can be precisely defined for a certain electrode geometry based on Paschen's law. The fundamentals of Paschen's law have been discussed in section 2.2. It relates the electrical breakdown strength with the pressure and gap distance between electrodes in which a uniform field is present. By considering the density of a gas, Paschen's law can also be used to explain the relationship between the breakdown strength and temperature.

A limitation of Paschen's law is that it is only applicable to disruptive discharges in uniform electrical fields. Should non-uniform fields be present, different dimensions of clearances will be expected in different electric fields to avoid both disruptive and partial discharge. However, it is expected that for the majority of clearances in an aircraft power system where space is limited, short gaps will be common and as a good approximation, the electric fields between these short gaps can be accepted as uniform so that Paschen's law can be applied.

In contrast to determining clearances, determination of creepage distances is more complex and cannot rely on Paschen's law in all cases. When a surface is contaminated, tracking behaviour can take place – creepage distances to avoid this are examined in more detail in Chapters 4, 5 and 6. While tracking over dry surfaces is possible, the nature of a flashover on a dry surface over a short gap will usually be similar to a flashover in air. Some researchers believed that the dry tracking method is more suitable for determing the material properties since there is no artificial environment affecting the behaviors of tracking and the reproducibility of the tests is much better [62]. However, they also admitted that the testing voltage to start tiny discharges from the surfaces of insulators is extremely high. In other word, creepage distances required to avoid flashover in air in dry conditions will generally be much smaller than the distances needed to avoid tracking across the surface when wet, and the evaluation of creepage distances for dry conditions is therefore limited in application to situations where aqueous contamination is not present.

In this chapter, we will review the design rules for clearances and creepage distances under dry conditions as specified in IEC 60664 and IPC 2221. The values stated in both the

standards are compared against experimental test results using both an air gap and printed circuit board samples for different air pressures and varying gap widths.

3.2. Review of IEC 60664-1:2003

3.2.1. Introduction

IEC 60664 deals with the insulation coordination for equipment within low voltage systems. It applies to equipments for up to 2000 m above sea level having a rated voltage up to AC 1000 V with rated frequency up to 30 kHz or rated voltage up to DC 1500 V. The design rules for clearances, creepage distances and solid insulation for equipment based on their performance criteria has been specified.

As the standard is not applicable for equipment used over 2000 m, it is clearly not intended for use in aerospace equipment design. However, air pressure factors are specified in the standard for correction of clearance distances in any design used above 2000 m (with a maximum altitude of 20000 m being described).

3.2.2. Determination of clearance

The flow chart given in Figure 3.2 shows that clearances should be selected by first considering the highest transient voltage that will be applied to the equipment. It should be noted that if the equipment is energized directly to the low-voltage supply mains (obviously not the case for an aerospace system), the rated impulse voltage is given in tables. The impulse voltage is used to derive a clearance distance from a table (such as that shown in Table 4.1). In addition, the steady-state (working) voltage is used to derive a second clearance distance and the largest of these two is selected as the required dimension.

In many systems, impulse voltages will be higher than the steady state rated working

voltage and will therefore define clearance. However, in a well shielded system that is immune from transients such as lightning overvoltages, the steady-state voltage may determine the clearance.

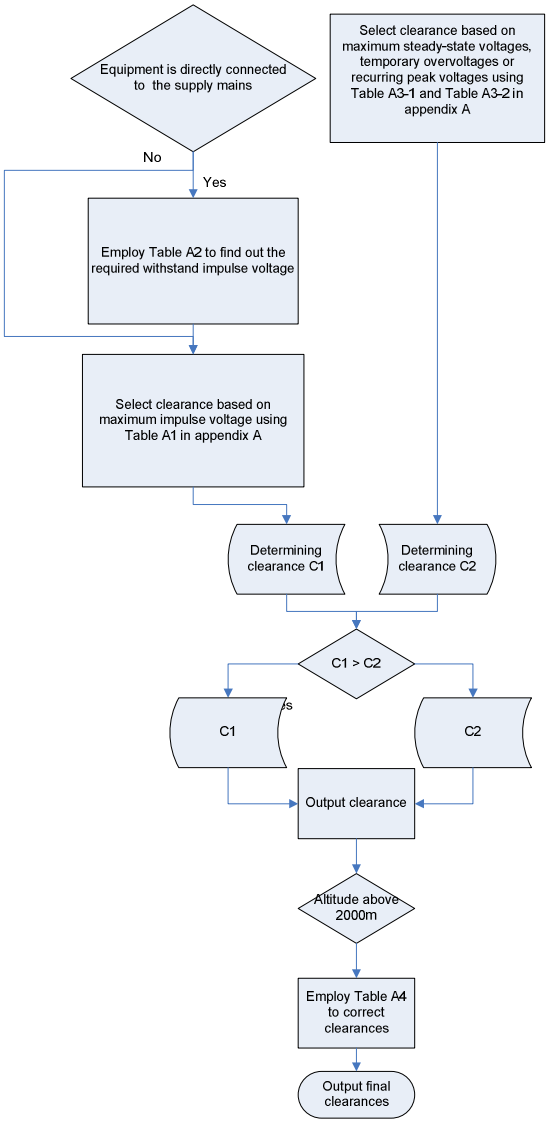

Figure 3.2 Flow chart of dimensioning clearances for the equipments in low-voltage systems

Table 3.1 shows the clearance distances to withstand both impulse and steady state voltages in a homogenous and inhomogeneous field. Under homogenous field conditions, the same values of impulse voltages and steady-state voltages require the same values of clearances. Normally it can be found that the impulse voltage in an electrical system is bigger than the steady-state figure, which will result in impulse voltages normally determining the design dimensions of clearance. In inhomogeneous fields, with a voltage lower than 0.6 kV, no

matter whether the voltages are impulse or steady-state, the same dimensions of clearances are required. However, when the voltages increase to 0.8 kV and above, the same values of steady-state voltages always need larger clearances in comparison to impulse voltages. For instance, there may be a situation when lighting impulse voltage is propagating in an electrical system, whereby the steady-state voltage for an electrical system is 5 kV while the impulse voltage is 6 kV. The design clearance will therefore be determined by steady-state voltage, which will be 5.7 mm, since the clearance to withstand the impulse voltage of 6 kV is only 5.5 mm.

Table 3.1 Clearance distances to withstand impulse and steady state voltages in a homogeneous and inhomogeneous filed.

Required Voltage (kV)	Homogenous Field		Inhomogeneous Field*	
	Impulse Clearance (mm)	Steady-State Clearance (mm)	Impulse Clearance (mm)	Steady-State Clearance (mm)
0.33	0.01	0.01	0.01	0.01
0.4	0.02	0.02	0.02	0.02
0.5	0.04	0.04	0.04	0.04
0.6	0.06	0.06	0.06	0.06
0.8	0.1	0.1	0.1	0.13
1	0.15	0.15	0.15	0.26
1.2	0.2	0.2	0.25	0.42
1.5	0.3	0.3	0.5	0.76
2	0.45	0.45	1	1.27
2.5	0.6	0.6	1.5	1.8
3	0.8	0.8	2	2.4
4.0	1.2	1.2	3	3.8
5	1.5	1.5	4	5.7
6	2	2	5.5	7.9
8	3	3	8	11
10	3.5	3.5	11	15.2

IEC 60664 defines an inhomogeneous field as having a point electrode with a 30 μm radius and a plane with a size of 1m×1m.

Once the appropriate clearance has been defined, the use of altitude correction factors is required. These are used to correct clearances when the altitude goes above 2000 m.

Table 3.2 Altitude correction factors

Altitude (m)	Normal barometric pressure (kPa)	Multiplication factor for clearances
0	101.325	1
2000	80	1
3000	70	1.14
4000	62	1.29
5000	54	1.48
6000	47	1.7
7000	41	1.95
8000	35.5	2.25
9000	30.5	2.62
10000	26.5	3.02
15000	12	6.67
20000	5.5	14.5

Figures 3.3 and 3.4 illustrate the clearances for both uniform electric field conditions (Case B) and non-uniform electric field conditions (Case A) respectively. Values for sea-level, 2000 m, 3000 m and 20000 m have been determined using the altitude correction factors where required. Both figures show that the IEC standard's requirements tend to be conservative when compared to Paschen's law values, especially for those with pressure-distance products larger than 10. Little difference can be found for different altitude values.

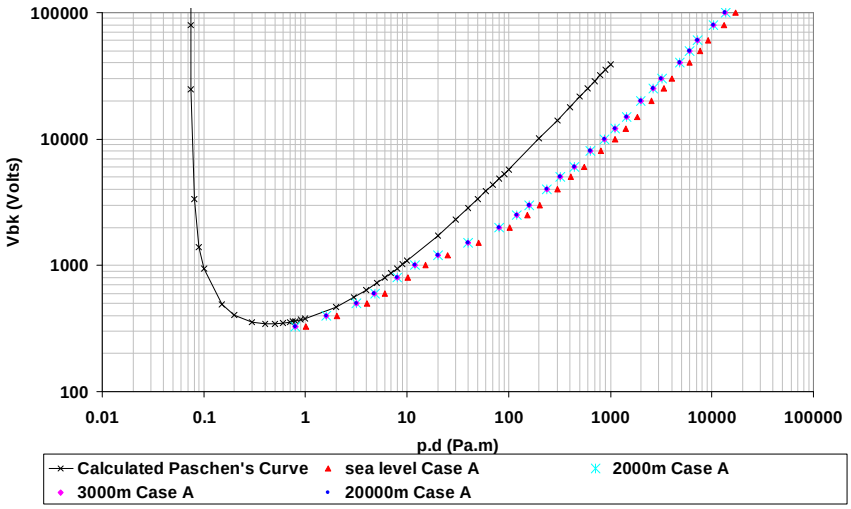

Figure 3.3 Clearances specified in IEC 60664 for varying altitude application under uniform electric field condition

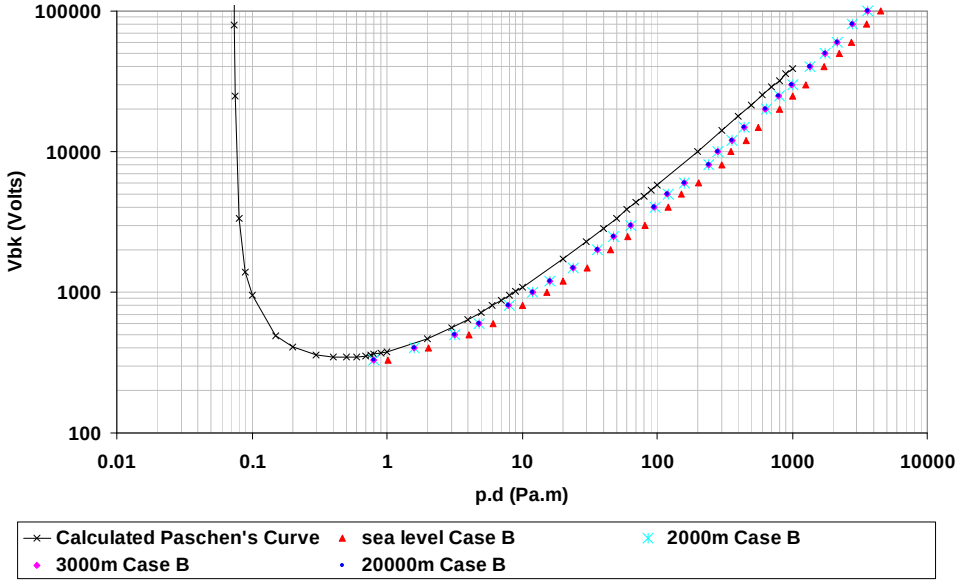

Figure 3.4 Clearances specified in IEC 60664 for varying altitude application under non-uniform electric field condition

3.2.3. Dimensioning of creepage distances

Creepage distances are determined using the steady-state voltage. Transient overvoltages which normally last only a few milliseconds for dimensioning for creepage distances are neglected since they do not influence the tracking phenomenon. Temporary overvoltages have to be considered if their duration and frequency of occurrence has an impact on tracking.

The creepage distance is not just a function of voltage but is also based on the degree of surface pollution and the material group used to make the equipment. The former defines the level of conductivity on the sample surface while the latter defines the response of the material to arcing damage. However, for determination of the creepage distance in dry conditions, the material property is not used. The values of creepage distances to avoid failure in dry conditions are therefore given by the standard as shown in Table 3.3

Table 3.3 Creepage distances to avoid failure due to tracking.

Voltage (V) r.m.s	Minimum creepage distance
	Pollution degree 1
	All material groups (mm)
10	0.08
12.5	0.09
16	0.1
20	0.11
25	0.125

Within the IEC standard, the relationship between voltage and required creepage distance is very non-linear (see Figure 3.22-Figure 3.26). The reason for this appears to be that the creepage distance cannot be lower than the minimum clearance distance. In turn, this minimum clearance distance is based on a value of transient voltage to which low voltage equipment is expected to be exposed. Therefore, for low values of voltage, the creepage distance is not representative of the distance required to avoid tracking but appears to be a distance required to avoid flashover owing to a transient voltage.

A creepage distance cannot be less than the associated clearance so that the shortest creepage distance possible is equal to the required clearance. However, there is no physical relationship, other than this dimensional limitation, between the minimum clearance in air and the minimum acceptable creepage distance (IEC 60664-1:2003). According to dimensioning rules in the standard shown in table 3.1 and 3.3, the creepage distance of 0.1 mm under pure dry condition can only withstand the voltage of 16V while with the same size of the clearance, the value of the withstand impulse voltage is 800 V under inhomogeneous fields, in which the transient voltage is normally the voltage to determine clearance dimensions.

3.3. Review of IPC 2221

3.3.1. Introduction

IPC 2221 “Generic Standard on Printed Boards Design” provides generic requirements for the design of organic printed boards and other forms of components, mounting or interconnecting structures to eliminate the misunderstanding between manufacturers and purchasers, facilitating interchangeability and improvement of products, and assisting the purchaser in selecting and obtaining with minimum delay the proper product for his particular need. To design the physical features and select materials for a printed wiring board, not only should factors such as electrical, mechanical and thermal properties be considered but also reliability of performance, manufacturing and cost, which have to be balanced at the same time.

3.3.2. Electrical clearances

First of all, it should be noted that the term “electrical clearance” in IPC 2221 here designates the different spacing as specified by the same term in IEC 60664. In IPC 2221, clearance standards are given for spacing either between two conductors on an individual layer, between conductive patterns, for layer to layer conductive spaces, and between conductive materials (such as conductive markings or mounting hardware) and conductors. It states that spacing between conductors on an individual layer should be maximized whenever possible. Otherwise, table 3.4 should be applied.

Table 3.4 Electrical Conductor Spacing

Maximum Voltage Between Conductor (DC or AC Peaks) (V)	Minimum Spacing (mm)	
	Bare Board	
	B2	B3
0-15	0.1	0.1
15-30	0.1	0.1
30-50	0.6	0.6
50-100	0.6	1.5
100-150	0.6	3.2
150-170	1.25	3.2
170-250	1.25	6.4
250-300	1.25	12.5
300-500	2.5	12.5
Calculation – see Equation 3.1	0.005 mm/volt	0.025 mm/volt

B2 - External Conductors, uncoated, sea level to 3050 m
B3 - External Conductors, uncoated, over 3050 m(100 mbar)

For voltages greater than 500 V, the table values must be added to 500 V values. The electrical spacing D for a type B2 board with x ($\rangle 500\ V$) is calculated as:

$$D = 2.5 + (x - 500) \times 0.005 \ldots\ldots\ldots\ldots\ldots (3.1)$$

It can be clearly seen that when the maximum voltage between conductors is above 50V, bigger spacings are required at altitudes over 3050m where the air pressure is lower than atmospheric pressure.

Figure 3.5 provides us the comparison between Paschen's curve and electrical spacing specified in IPC 2221. It can be seen that the specification for electrical clearances in IPC 2221 which is actually the creepage distance between two uncoated conductors is very conservative. It can be explained as the creepage distances are always vulnerable to environment conditions. Under wet condition with conductive pollution, the withstand voltage for the same size of gap would be lower than that in dry condition.

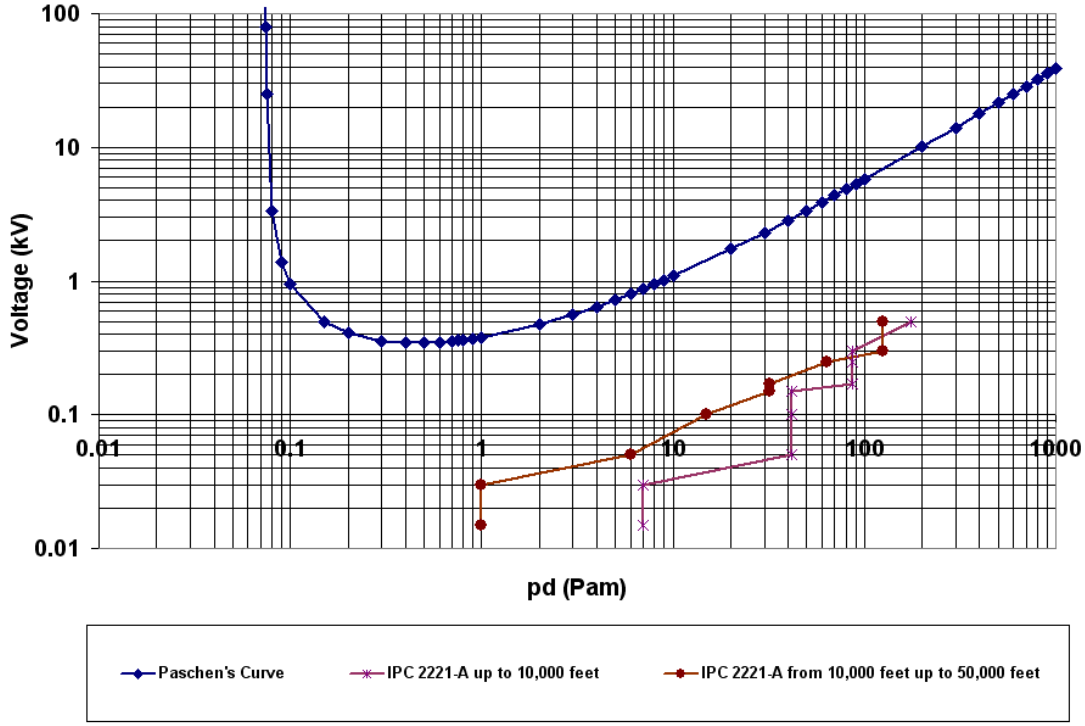

Figure 3.5 Electrical spacing specified in IPC 2221 for varying altitude application

3.4. Uniform field breakdown tests

Over the past century considerable research effort has been made to understand the breakdown of air gaps. Recent developments in microeletronmechinical technology have heightened the need for research on short-gap breakdown including the microscopic description of the phenomena and development of detection methods. The small gaps between conductors refer to those of the order of a few microns or even below. Normally high voltages are applied across such small gaps of the air. Electric breakdown which leads to leakage currents can be detrimental to the operation of electrical systems. Hence, good knowledge of the value of the breakdown voltage and the parameters that affect it will be an important consideration for their design. All of the recent studies [63-66] on small-gap breakdown have drawn a conclusion that Paschen's law, which defines the theory of breakdown mechanism for uniform fields with minimum value for breakdown of 360 V [67], is not applicable for small gaps of a few microns or below. Breakdown voltages are not only determined by gap distance but also other factors such as the type of electric fields and

density of air. In order to find out the mechanism of breakdown for small air gaps, it is necessary to carry out further experimental tests. The aim of this study was to evaluate and validate the values of breakdown voltage for air gaps, especially for small gaps of 0.265, 0.165, 0.07, and 0.43 mm at varying air pressures, to get pressure and distance products of 0.1, 0.25, 0.4, 0.6, 0.8, 1, 2, 5, 10 and 20. The test results have then been compared with both Paschen's law (achieved through Andrew Nelm's Thesis), and IEC 60664 "Insulation coordination for equipment within low-voltage systems". The IEC standard defines the dimensions of clearances, which are the shortest distances between conductors. Further experiments are recommended for their design. However, with regards to bigger gap breakdown, the results show agreement with Paschen's law, considering acceptable errors. Finally, the Normal Distribution treatment with 5% probability specified in IEC 60-1:1989 was used to find out the withstand breakdown voltage values.

3.4.1. Test circuit

The test circuit for breakdown of air gap is shown in Figure 3.6. A DC source with the maximum output voltage of +/- 3 KV was used to apply high voltage to the breakdown air gap. The breakdown voltages were then measured through a voltage divider with a rate of 1:1000. There was also a current limiting resistor with resistance of 100 kΩ before the test gap.

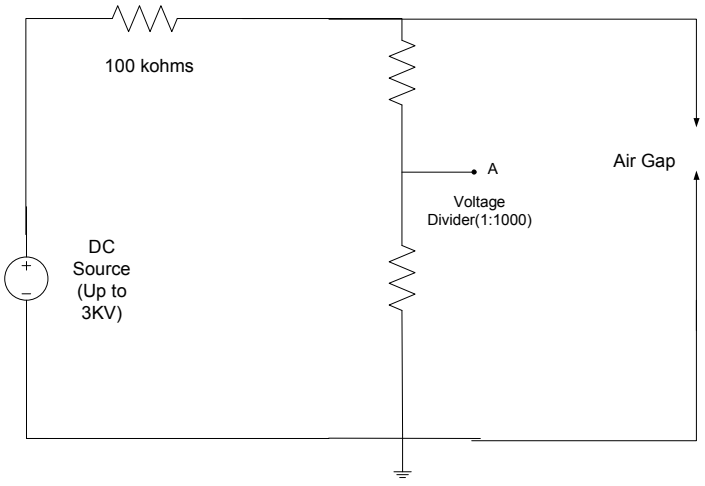

Figure 3.6 Sketch of the test circuit for breakdown of air gap

3.4.2. Test apparatus and procedure

Two brass electrodes with perfect sphere finish were used to provide a uniform field. In order to gain a very precise space between these electrodes, a test rig was established as shown in figure 3.7 with a wood frame and self-calibrating system. This self-calibrating system consists of two dummy end spacers with precise dimensions. In my test setup both were 1.699 inches (43.15 mm). Dummy spacers were used to fix these electrodes to a wooden block. For each gap distance setting, the total height of the block 1, dummy spacer 1 and electrode 1 is measured as h_1. And the total height of block 2, dummy spacer 2 an electrode 2 is measured as h_2. Then the space between two electrodes is $1.699 - h_1 - h_2$. To achieve the gap distance wanted, calibrated polyethylene sheet spacers are added to the gap.

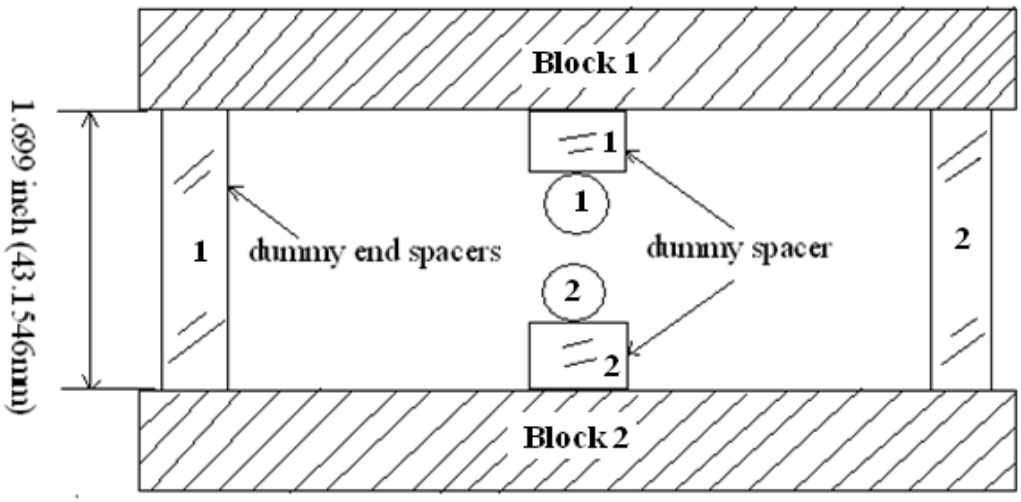

Figure 3.7 Sketch of the test rig for uniform electric field breakdown in air

Tests at distance-pressure products of 0.1, 0.2, 0.4, 0.6, 0.8, 1, 2, 5, 10 and 20 Pam with gaps of 0.002, 0.006, 0.01, and 0.0169 inches (0.05/ 0.15/0.25/0.42 mm) were carried out. However, it should be noted that for some distances not all the product tests could be achieved due to the limitation of the environment chamber where the pressure range can only be set between as low as 8mbar and ambient pressure around 1 bar. All tests were carried out at 20 degrees Celsius.

A DC voltage was applied using a generator with an output of +/- 3 kV. The National Instrument Labview program was used to control the output of the generator with the ramp rate of 10 kV per minute. The breakdown voltage was measured with ten breakdown voltage measurements at each pressure-distance product being carried out.

3.4.3. Test results and discussion

The recorded breakdown voltages are shown in the following figures from Figure 3.8 to Figure 3.11, which all present the results for a different gap distance. These figures are the average of ten measurements. Error bars are also displayed to show the maximum and minimum values at each pressure and distance product. It can be seen that Paschen's minimum appears to be shifted to a lower pressure distance product place. It is known that the breakdown in air not only has the character that Paschen's law describes and also relies on two impact factors which include device geometry and surface roughness of electrodes[68]. Device geometry will determine the shape of electrical fields while surface roughness will lead to amplification of the electrical field at the sharp points. That is why measurements of breakdown tests can have more or less shift from the theoretical values. However, the data ties in with Paschen's law which shows a similar trend to the right hand side of Paschen's law. A probable shift in the minimum location data at low pd values was not collected to confirm this.

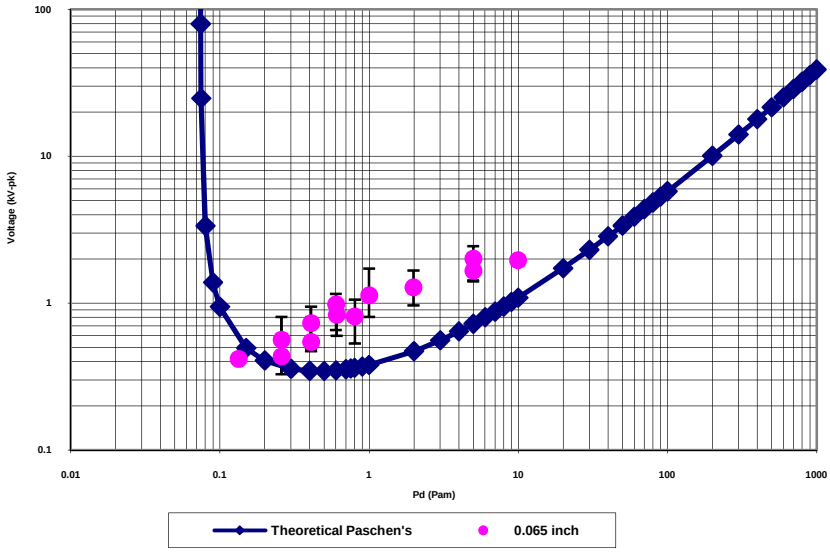

Figure 3.8 Uniform field breakdown test results for 0.065 inch

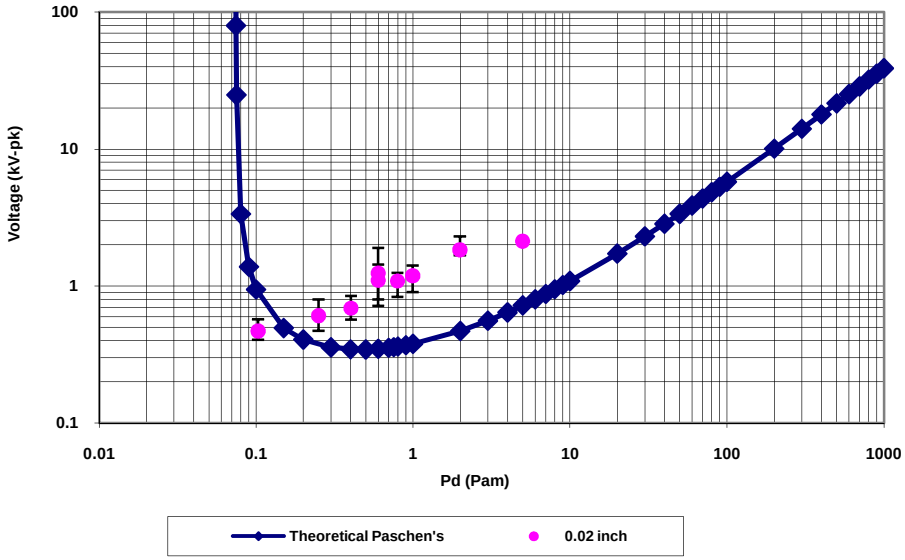

Figure 3.9 Uniform field breakdown test results for 0.02 inch

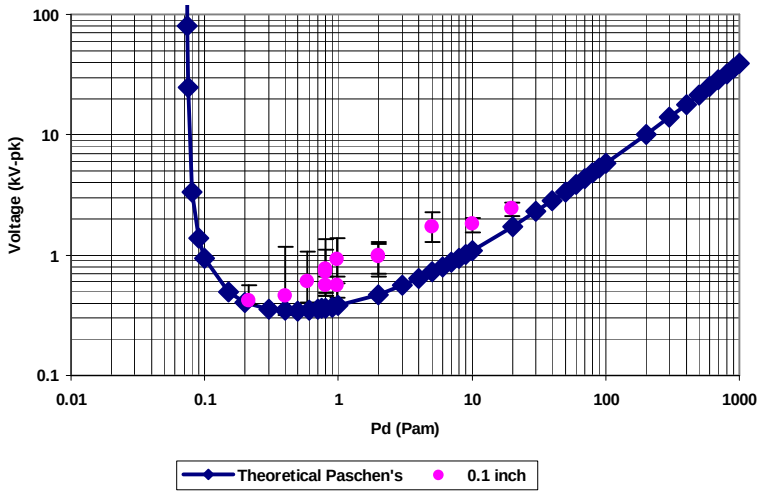

Figure 3.10 Uniform field breakdown test results for 0.1 inch

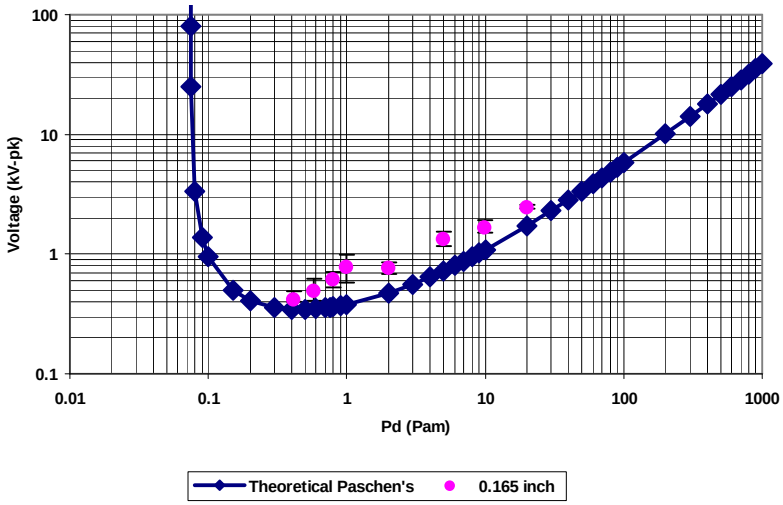

Figure 3.11 Uniform field breakdown test results for 0.1 inch

The test results were then used to determine the withstand voltage at each pressure-distance product as detailed in IEC 60060-1: 1989 High-voltage testing techniques [69]. For a Gaussian (or Normal) distribution, estimates of the parameters U_{50} and z are given by:

$$U_{50}^{*} = \sum U_i / n \quad \text{.....3.1}$$

$$z^{*} = \left[\sum \left(U_i - U_{50}^{*} \right)^2 / (n-1) \right]^{1/2} \quad \text{.....3.2}$$

The confidence limits for Gaussian distributions may be found using the Student's t or

Chi-squared distributions as described in the technical literature.

Normal (or Gaussian) distribution in statistics is the most widely used probability distribution. It is normally used as a first approximation to describe a group of random variables that tend to gather around a single mean value. Its probability density function is "bell" shape with the expression as shown in the equation 3.3.

$$f(x) = \frac{1}{\sqrt{2\pi\sigma^2}} e^{-\frac{(x-\mu)^2}{2\sigma^2}} \quad \ldots\ldots 3.3$$

Where parameter μ is the mean (location of peak) and σ^2 is the variance (the measure of the width of the distribution). In our case, the mean is calculated from all the measurements taken from the tests. The variance is calculated by apply the equation 3.2 above. In my research the 5% chance of flashover for the estimates of U_{05} and z obtained from a test are used to calculate the withstand breakdown voltages shown in following figure. The methods are shown in detail in Appendix B.

The limitation of usage of normal distribution to predict the 5% probable breakdown voltage is that with higher variance of the distribution the values of the calculated value could be close to zero which is not true in reality.

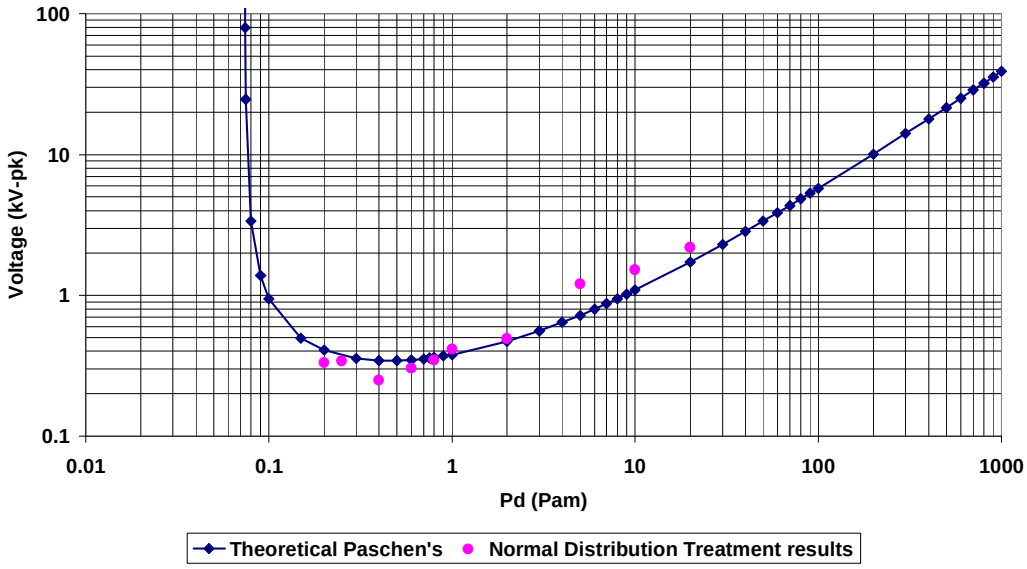

Figure 3.12 Comparison of test results treated by normal distribution specified in IEC 60060-1: 1989 High-voltage testing techniques and Theoretical Paschen's curve.

The withstand voltages for pressure and distance product less than 0.8 is slightly smaller than the Paschen's law values as show in Figure 3.12. For the product of 0.8, 1 and 2, the values suggested by Paschen's law is the as big as the withstand voltages calculated based on the test measurements. However, for those bigger products such as5, 10 and 20, the withstand voltages are bigger by the amount of around a few hundred voltages. To summarize, with given errors produced by use of Gaussian distributions, it can be found that the predicted withstand voltages in conditions of less than 0.8 pd values are smaller than theoretical Paschen's values.

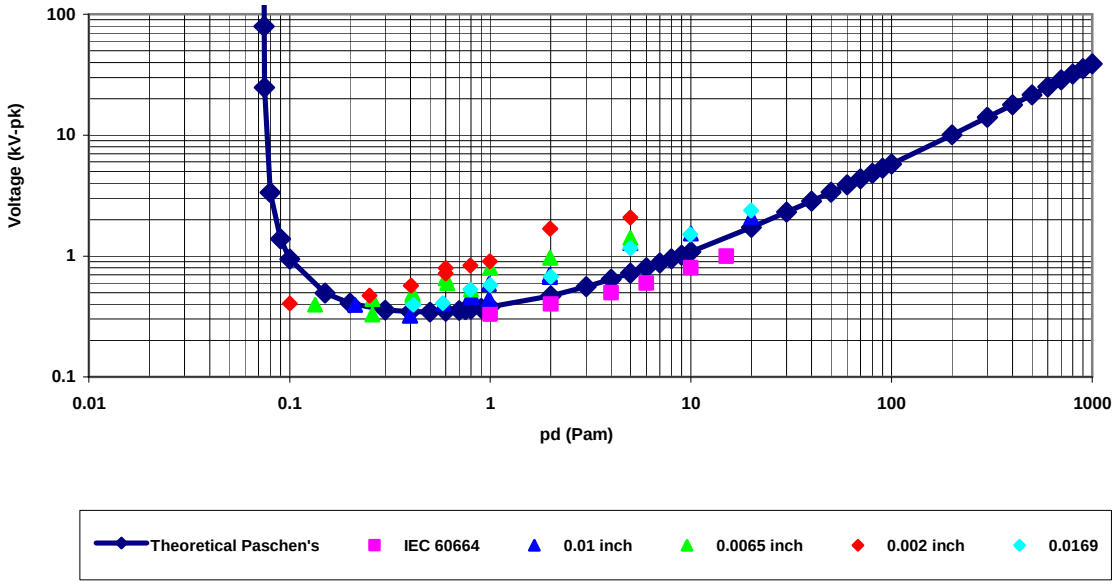

Figure 3.13 Comparison of Normal distribution treatment results and Theoretical Paschen's curve and IEC 60664 clearances requirements.

Figure 3.13 summarizes all the test results and compares these with IEC 60664. We can see that Paschen's law and both tests suggest higher withstand voltages for a certain space. And as a conclusion, applications of IEC standards are very conservative and safe.

3.5. Non-uniform field breakdown tests

The principle limitation of Paschen's law is that it is only valid for uniform field geometries, which has been proven in previous section. The non-uniform field in the IEC standard was derived using the point-plane electrode configuration, which is the worst case scenario with regard to withstand capability. As defined, the point electrode has a 30μm radius and the plane a size of 1m×1m. In a divergent field, partial discharges (corona) become significant.

3.5.1. Test apparatus and procedure

The electrodes used in my research were a point-plate electrode system. The point electrodes used in my tests are conical stainless steel with 0.1mm at points (these are larger than that defined in the IEC standard so should yield a more uniform field). The test circuit is shown in Figure 3.14, and includes an AC voltage amplifier with a rated output voltage of 20kV. Current limit resistors were connected after the output of a voltage amplifier. A 1/1000 voltage divider was used to output the breakdown voltage to the oscilloscope. A blocking capacitor and partial discharge detector were used. The environmental chamber was used to achieve pressure ranging from 1bar to as low as 100 mbar. All the tests were carried out at 20 degrees Celsius.

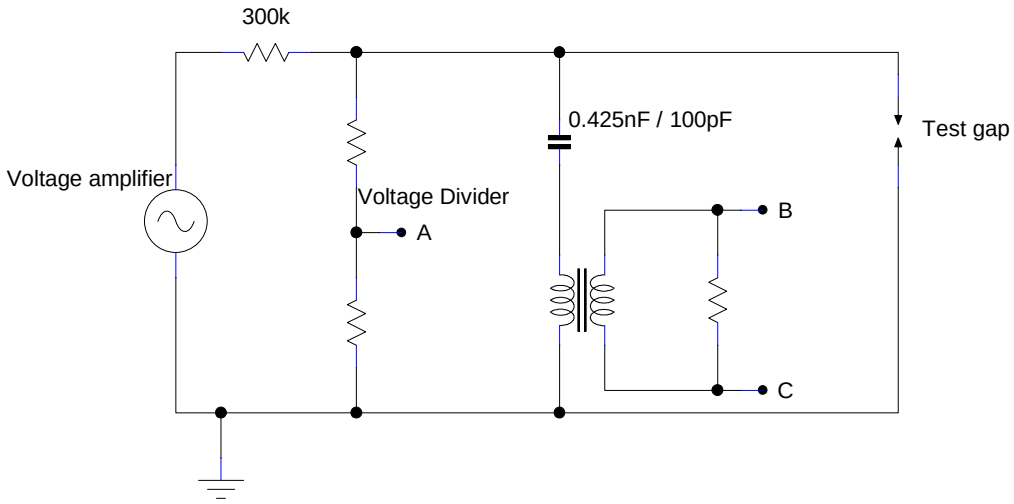

Figure 3.14 Test Circuit for non-uniform electric field breakdown and partial discharge tests

To carry out partial discharges and breakdown tests, the voltage applied to electrodes was increased until partial discharges were found. At this point the voltages were recorded as

inception voltages. The voltages were then lowered to find out the extinction voltage of partial discharge. Finally, the voltages were again raised until the disruptive sparkover occurred. A visual monitor was set up to observe the entire testing process. Three measurements for each of the gap distances have been recorded. In all cases, peak voltages are presented.

3.5.2. Summary of test results

The test results of inception voltages and breakdown voltages are shown in the Figures below. Figure 3.15 shows us that the inception voltages increase with the pressure for all electrode separations. However, there is no strong link between the electrode separation and the inception voltage, suggesting that the partial discharge behavior is dominated by the sharpness of the point electrode and not the gap separation. The experiments were carried out in the order from 50 mm decreasing to 5 mm. For the first three series of tests for gaps of 50 mm, 40 mm, there was no significant difference of the inception voltages. However, owing to the needle point getting blunter as observed under a microscope, the peak fields were reduced and therefore higher inception voltages for partial discharges were found for gaps of 30 mm, 25 mm and 20 mm.

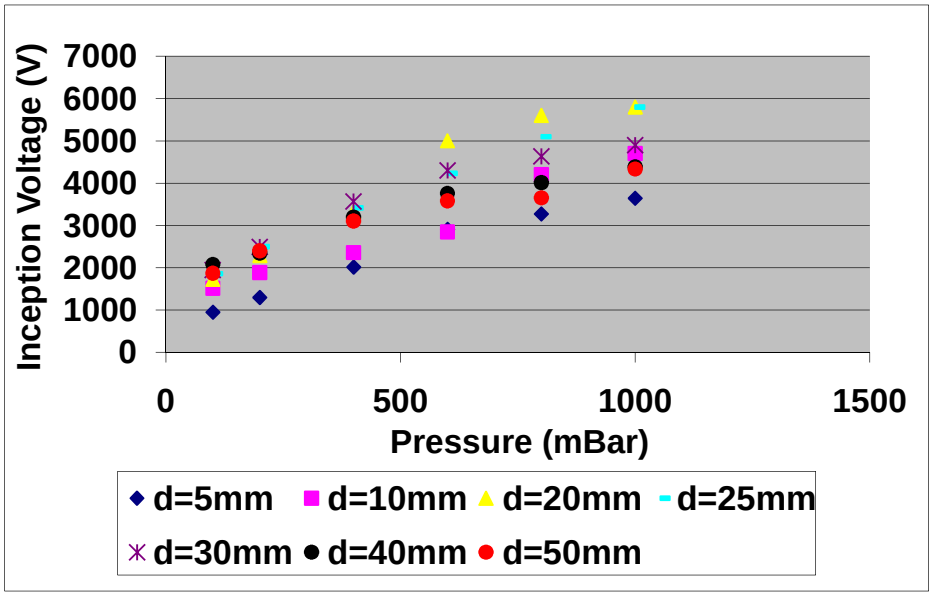

Figure 3.15 The inception voltages measured at the conditions of various pressures for different electrode separations

Figure 3.16 shows that the breakdown voltages increase as a function of pressure for all the different electrode separations. The relationship between gap distance and breakdown voltage appears to be approximately linear in nature (unlike that of the partial discharge inception voltage). A number of points could not be plotted owing to the limited output voltage of the amplifier.

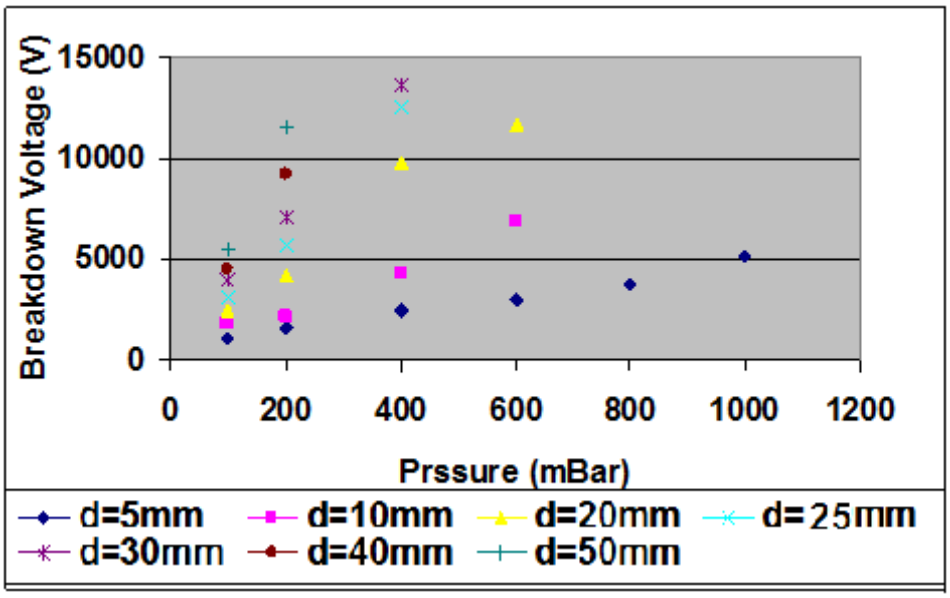

Figure 3.16 Breakdown voltages measured at the conditions of various pressures for different electrode separation

3.5.3. Discussion

In Figure 3.17, the IEC 60664 recommended values of clearance to avoid partial discharge at specific voltages are compared with the test results taken at 1000 mBar. The IEC specified safe voltage at a particular clearance distance is generally conservative apart from at larger gap distances. As explained previously the order in which the experiments was carried out are from 50 mm decreasing to 5mm. Due to the blunter condition of the needle after the 30 mm gap was tested, the higher inception voltages for partial discharges are shown in the figure. This is in agreement with the knowledge that the blunter the needle is, the higher voltage needed to initiate partial discharges.

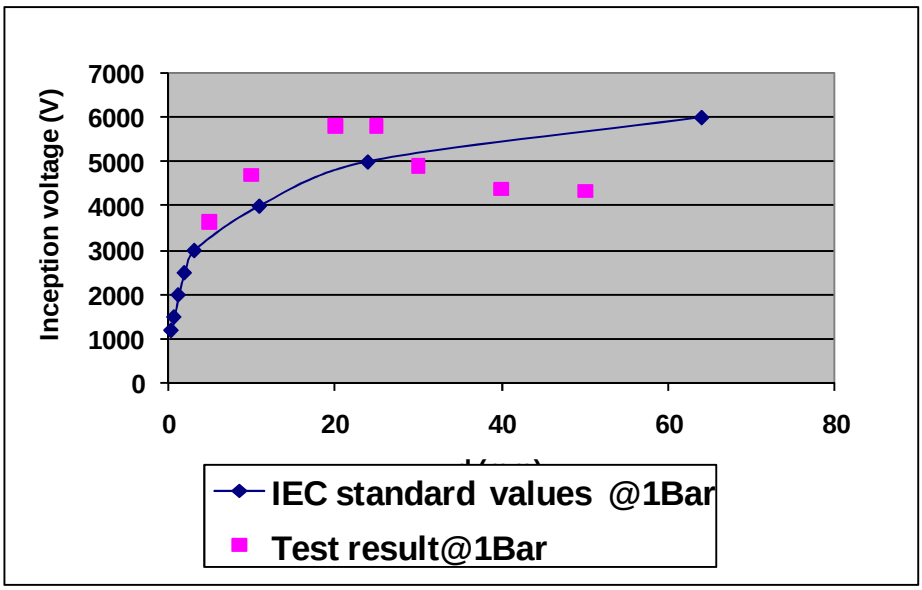

Figure 3.17 Comparison of the IEC values of the inception voltages with the measurements at 1Bar.

Figure 3.18 shows a comparison of IEC recommended values with the measurements at 100 mBar. Altitude correction factors have been used to calculate the IEC values at 100 mBar. In this case, it is clear that the IEC standard suggests higher inception voltages at a specific gap spacing than the test results, which means it would not be advisable for use.

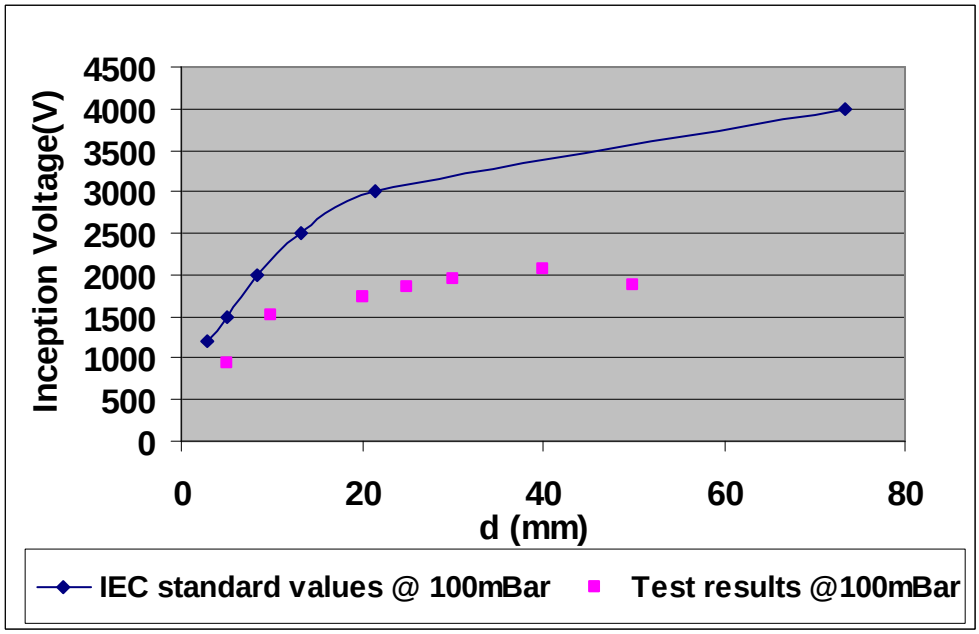

Figure 3.18 Comparison of the IEC values of the inception voltages with the measurements at 100mBar.

In Figure 3.19 the IEC recommended values of breakdown voltage were compared with the

test results at 100mbar. Because of the limitation of output voltage of the voltage supply, only one point was recorded at 1bar. It shows all of the breakdown voltages are lower than the IEC 60664 recommended values at 100 mbar. Use of the standard should therefore be used with caution for aerospace applications.

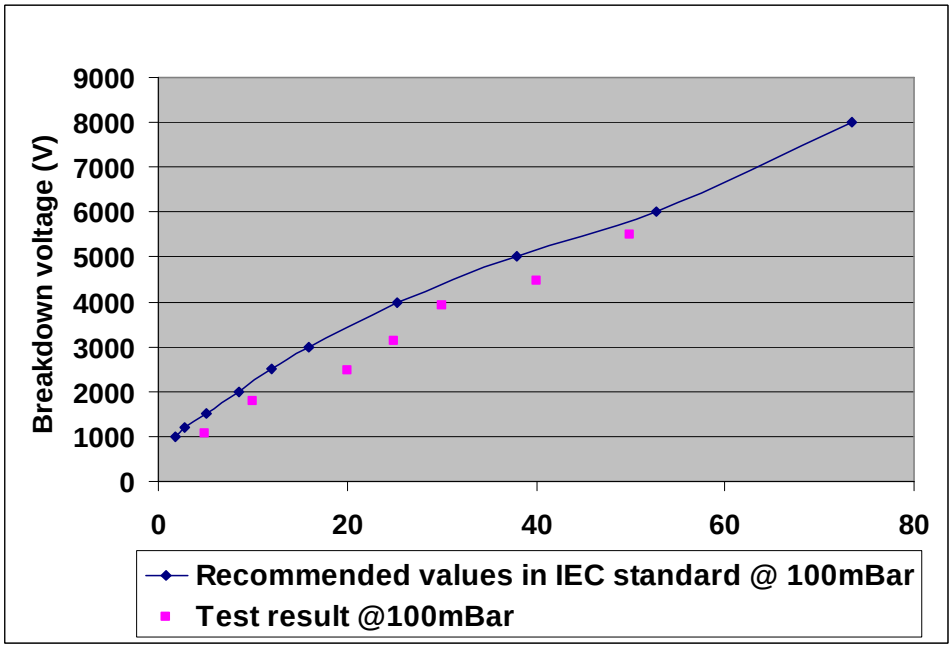

Figure 3.19 Comparison of the IEC values of breakdown voltage with the measurements at 100mBar.

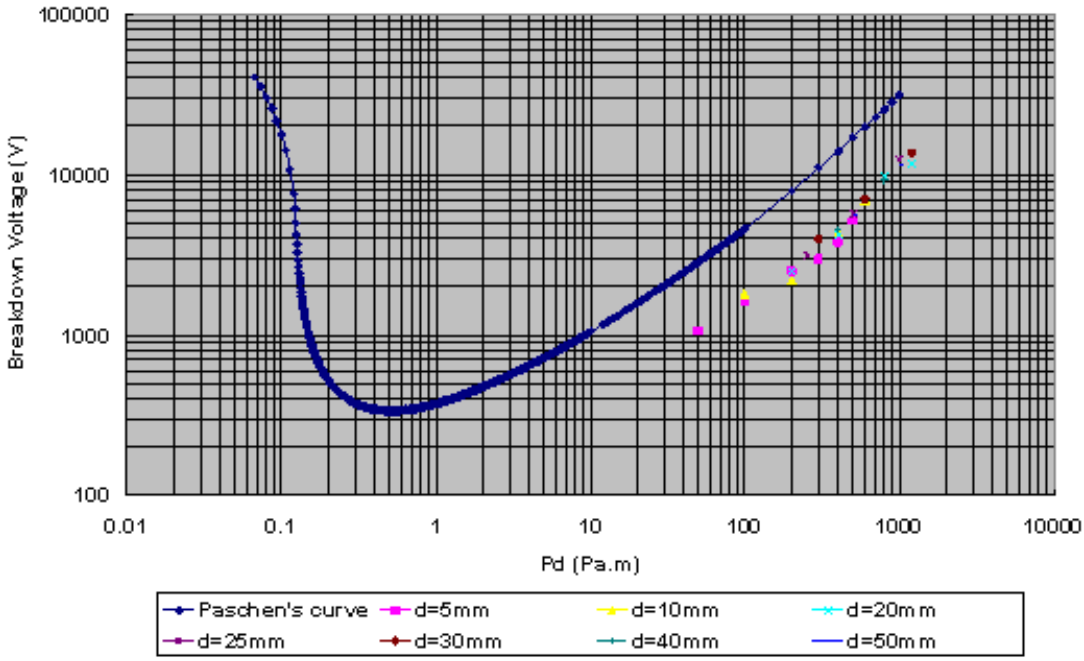

Figure 3.20 Comparison of Paschen's curve of breakdown voltage with the measurements at varying pressures.

To assess the breakdown voltage values under non-uniform fields, Paschen's curve was used as a comparison with the test results, as shown in Figure 3.20. It can be seen that the breakdown voltage values are similar for the same values of pressure-distance products even though tests were carried out separately for different gap distances. However, the breakdown voltages were much lower than Paschen's curve, which applies as well to uniform-field breakdown. It indicates that Paschen's law is not applicable for non-uniform breakdown.

3.6. Flashover on printed circuit boards under dry Conditions

Under dry conditions, it is very difficult for solid insulating materials to undergo tracking unless there is a significant non-uniformity of an electric field. Generally, flashover on the insulating surface can be expected. For design purposes, it is useful to compare the flashover voltages measured on samples in the laboratory with those described in the standards IEC 600664 and IPC 2221. Surface flashover can be affected by field enhancement around the triple junction of the electrodes and the influence of the underlying material on the net-ionization taking place within the gas above the surface.

3.6.1. Test procedure

These tests were also conducted in the environment chamber, where the pressure can be controlled. Test specimens were manufactured by a professional PCB manufacturer. Polyimide was chosen to be the solid insulation with two paralleled brass tracks printed on. The following picture shows one of my specimens with a 0.01 inch gap distance. It can be noticed that the closest parts of tracks are in the middle; this is the 'gap distance', and to the end they move apart. However, in the following discussion of test results, we see that flashover occurred not only in the smallest gap.

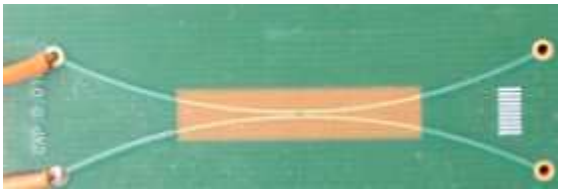

Figure 3.21 Polyimide printed circuit board with 0.01 inch gap

The electrical circuit/measurement system was exactly the same as we used for uniform air breakdown between two sphere electrodes in the air as stated in section 3.4, with the same environmental chamber being used at pressures between 8 mBar and 1Bar, with a temperature of 20 degrees Celsius. Each of the product breakdown tests were repeated three times with fresh new specimens. Gaps of distances 0.01/0.02/0.03/0.04/0.05/0.06/0.07/0.08/0.09/0.1 inch were tested using DC voltage.

3.6.2. Test results and discussion

The recorded breakdown voltages are shown in the following figures. The results show a comparison between the breakdown voltages for different gap distances, Paschen's law and the relevant standards.

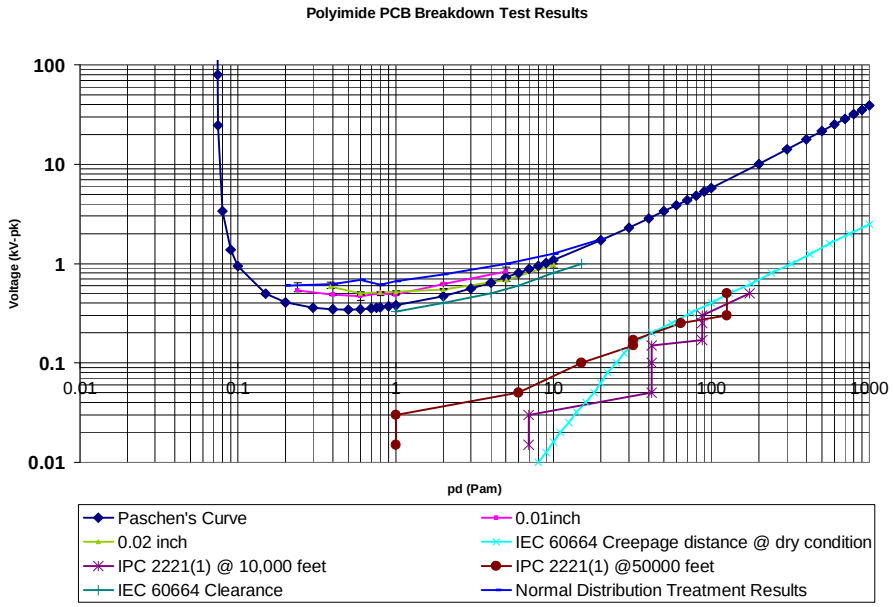

Figure 3.22 Comparison of the IEC/IPC values of breakdown voltage and theoretical Paschen's values with the measurements for 0.01/0.02 inch tests with error bars.

The measured breakdown voltages were higher than the theoretical values produced using Paschen's law. However, the trend lines of each test are similar to the shape of Paschen's law, which suggests that Paschen's law can be applied to circuit boards in dry conditions to establish the suitable clearance distance.

Secondly, it is clear that the standards (IPC 2221 and IEC 60664) overestimate the creepage distance needed in clean, dry conditions by a significant margin. The values of IEC 60664 shown in the plot are creepage distance specifications for all materials group under pure dry condition which is pollution degree 1 based on the definition in the standard. The limitation of this specification is that the air pressure factor is not considered. IPC 2221 has no information environment condition but with rough classification to two categories. With those limitation and uncertainties, existing excessive margins at least can provide safe guidelines. However, use of these standards would result in dimensions being excessive. A similar pattern is shown in the remaining tests, which are detailed below.

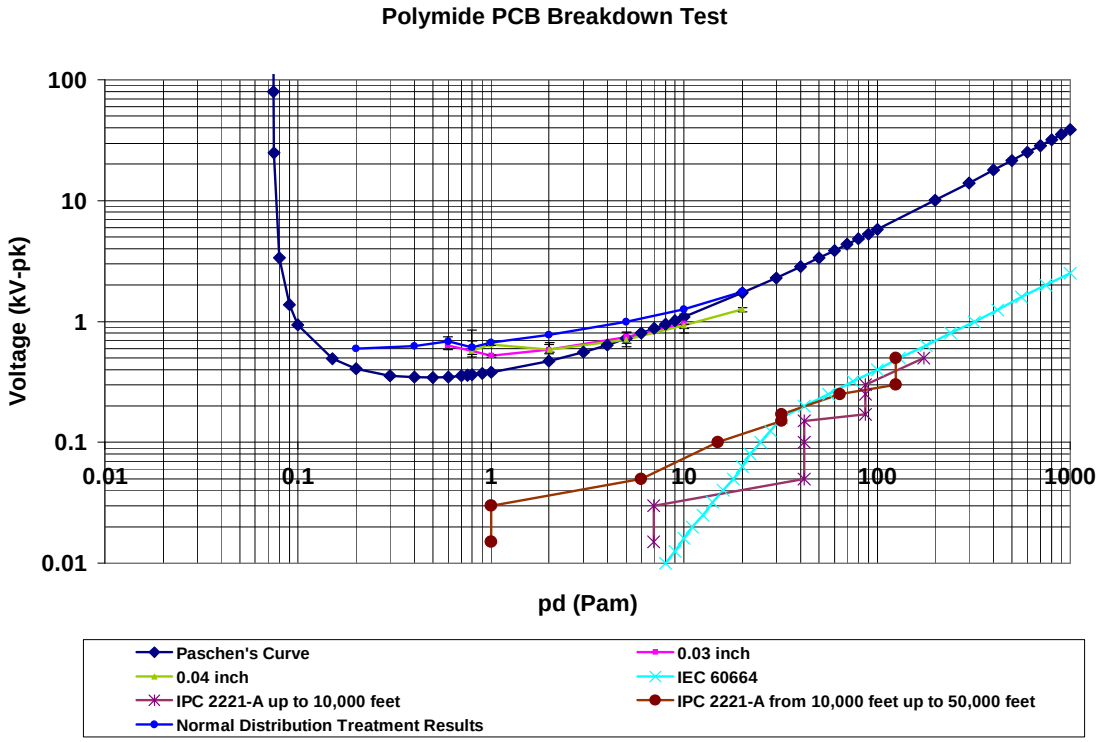

Figure 3.23 Comparison of the IEC/IPC values of breakdown voltage and theoretical Paschen's values with the measurements for 0.03/0.04 inch tests.

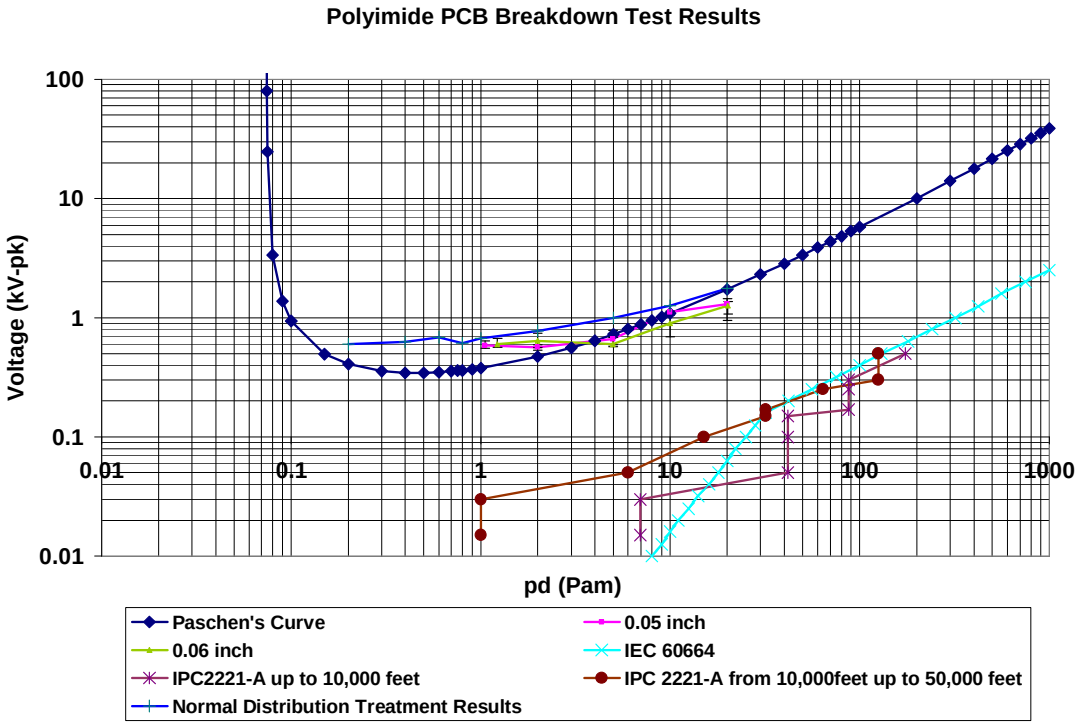

Figure 3.24 Comparison of the IEC/IPC values of breakdown voltage and theoretical Paschen's values with the measurements for 0.05/0.06 inch tests.

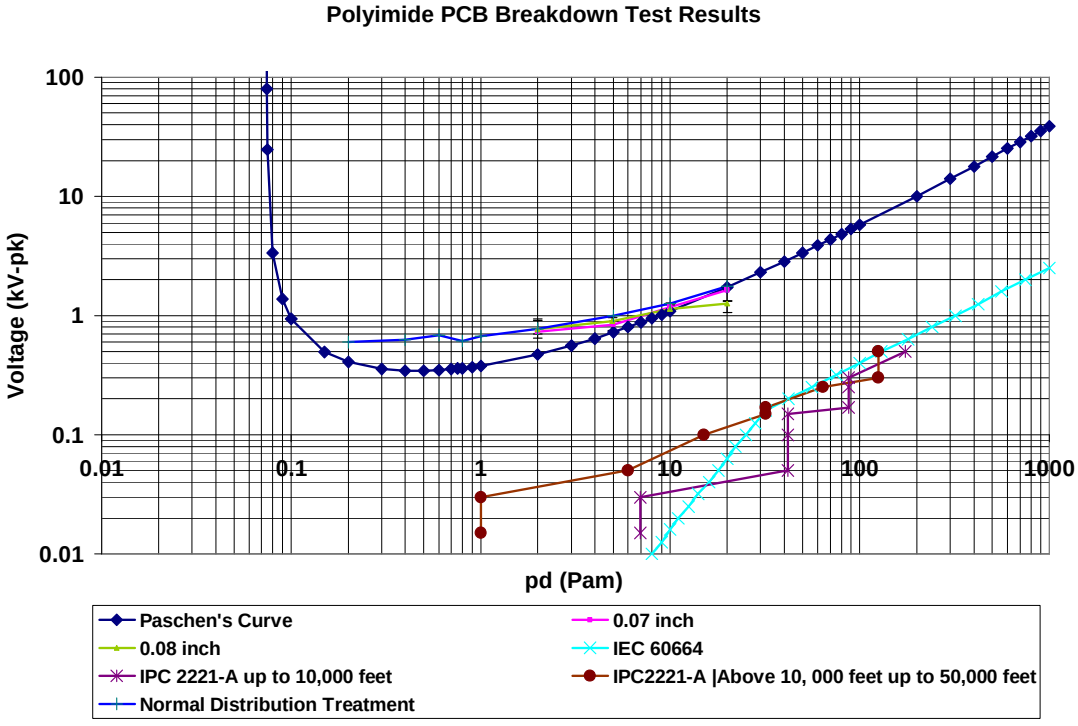

Figure 3.25 Comparison of the IEC/IPC values of breakdown voltage and theoretical Paschen's values with the measurements for 0.07/0.08 inch tests.

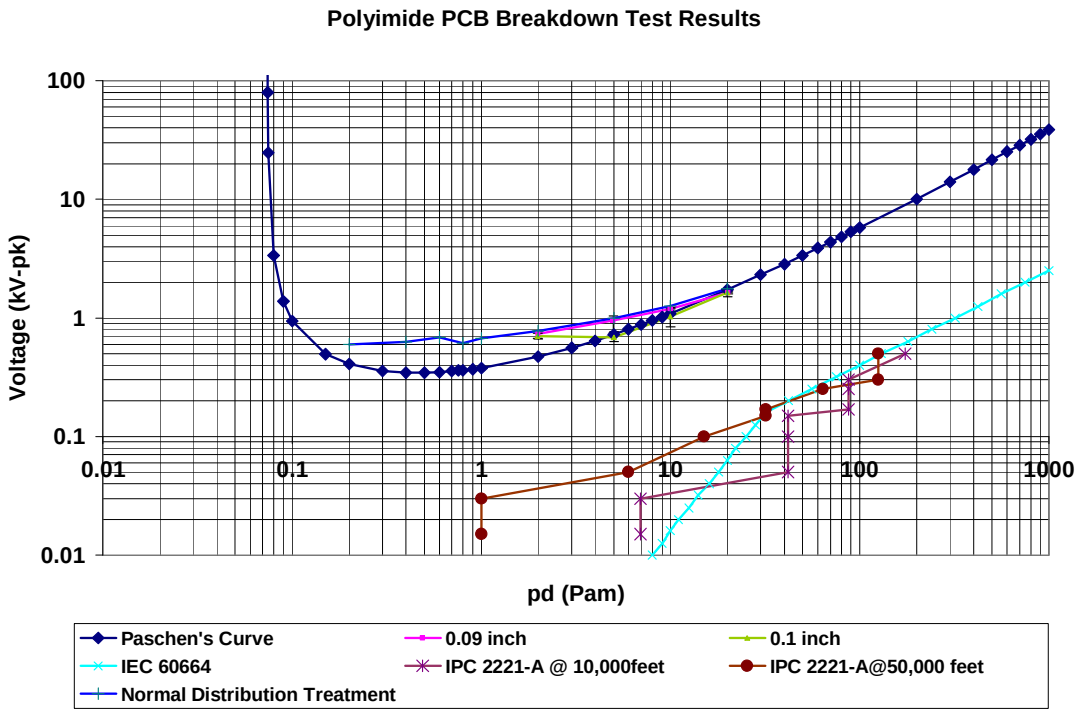

Figure 3.26 Comparison of the IEC/IPC values of breakdown voltage and theoretical Paschen's values with the measurements for 0.09/0.10 inch tests.

3.7. Conclusion

Breakdown tests under uniform fields on right opposite positioning spherical electrodes prove that Paschen's law can be applied with confidence to determine the clearance distances required for a particular voltage in a near uniform field air gap for aerospace application. As Paschen's law appears to be implemented in IEC 60664, this therefore also means that the guidance it provides for dimensioning of clearances is appropriate.

Breakdown tests with sharp point to plane plate to produce non-uniform fields illustrate the use of IEC 60664 does not appear to give results that are totally consistent with experimental tests, but they are a useful approximation for design purposes at atmospheric pressure with a larger deviation at 100mBar pressure. Breakdown voltage measurements show consistency with the IEC 60664 standard at low pressure (although the IEC 60664 standard is not conservative) and no match was possible at atmospheric pressure owing to the limited voltage capability of the test supply.

At last, breakdown tests on Polyimide printed boards show us that under dry conditions, the breakdown voltage is close to that expected using Paschen’s law but also that it far exceeds that predicted using IEC 60664 or IPC 2221. Usage of the standards will lead to big margin for safety but in term of insulating materials size, it is not very economic to apply.

Chapter 4 Modeling of Tracking Process under Wet Conditions

4.1. Introduction

The previous chapter discussed flashover over solid insulating surfaces under dry conditions. Through discussion of the test results and comparison with theoretical Paschen's law values, we concluded that flashovers on dry solid insulating surfaces are consistent with it.

This chapter deals with theoretical modeling of the tracking threat to insulation systems that results from aqueous contamination being deposited on surfaces along which an electric field exists. This aqueous contamination can be from direct water contact (rain, leaking pipework) or can occur in humid conditions where moisture condenses onto a surface. This contamination coupled with a degree of conductivity inherent in the water contaminant itself or through the mixing of water with surface pollution on the board can lead to electrical tracking.

This section first of all looks the mechanism of electrical tracking in wet conditions, especially under conductive aqueous contaminant conditions. A theoretical classical mathematical model is then introduced. This model will in the following chapter be tested and verified in a series of practical tests on solid insulating materials. Inception voltages of electrical tracking are then calculated for certain specific environmental conditions, including air pressure, ambient temperature, conductivity of aqueous contaminant liquid, and even system inherent impedance.

4.2. Electrical tracking under wet conditions

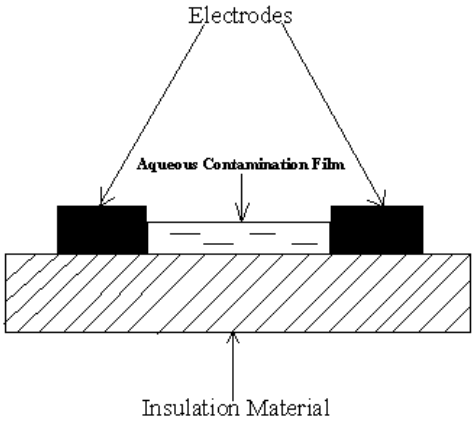

Figure 4.1 Sketch of a typical model for electrical tracking on an insulation material with a film of aqueous contamination

Figure 4.1 illustrates a very simple model in which there is a very thin film of aqueous contamination between two conductors on a layer of insulation material. In reality, there are two ways of formation of water on solid insulation material surface. One is as a thin film of condensation. The other is to form large drops of liquid. In 2005 F.C. Lin and S.M. Rowland [70] investigated the probability of formation of a low current, stable arc between two droplets on the surface of dielectric material with different hydrophobicity, especially on silicone rubber based materials. They found that it is hard to maintain the low current arc between two droplets due to weak hydrophobicity of the surface of the SIR based materials, which leads to those two droplets jointing up under electrostatic forces. As a results, very quickly after initial low current arc occurs, the two droplet always joined together to form a thin film of liquid. Modern processing techniques for FR4 material change the surface from a hydrophobic one to hydrophilic during the etching process [71]. This determines that for vast majority of time the liquid between electrode should be present as a thin film. Hence in my research, the model shown in Figure 4.1 is employed.

The process of electrical tracking can be described as follows. The presence of aqueous contamination on a surface across which an electric field exists will lead to the flow of

leakage current which can be the equivalent to a resistor in series connected in the circuit. The contaminant evaporates after being heated by the leakage current. As it evaporates, an arc is drawn across the dry layer, across which most of the voltage is dropped when the arc eventually extinguishes. The formation of these dry-band arc was first proposed by Obenaus [72]. The relation between the arc voltage and current depends on the arc length, electrode material, and ambient pressure. Typically for an arc, near the peak value of the arc current the voltage necessary to maintain it is relatively low. In contrast, when the current approaches zero, the voltage required to maintain the arc increases. When the voltage across the arc is not high enough, it will be unstable and will become extinguished even before the zero point of the sinusoid of current. When the voltage rises again, re-ignition of the arc can take place should the voltage be sufficiently high. Therefore the arc voltage at the beginning of the half-cycle is considerably higher than that at its end.

Table 4.1 Tracking process sketch with current and voltage waveforms at different stages

Typical tracking process	Sketches	Current and Voltage Waveform
Step 1. A very thin film of aqueous contamination bridges between two electrodes	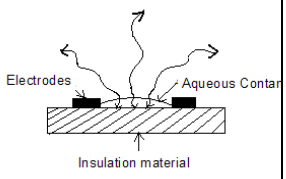	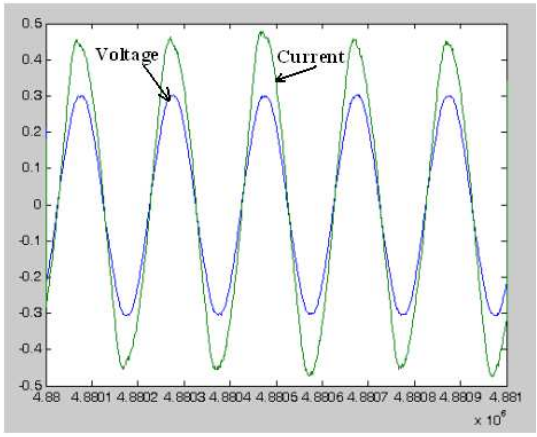
Step 2. The hottest point gets dry firstly due to evaporation	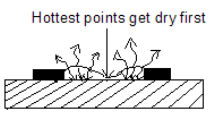	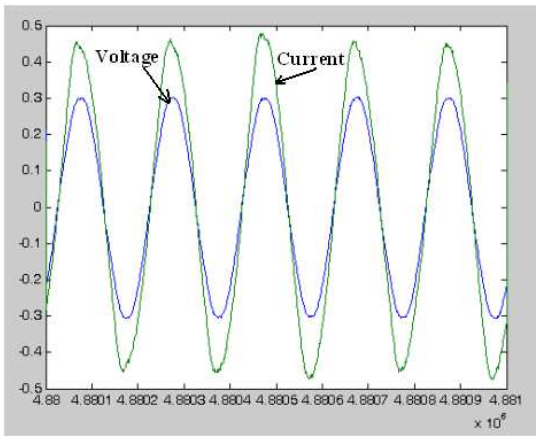

Step 3. Dry band arc occurs	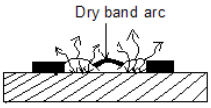	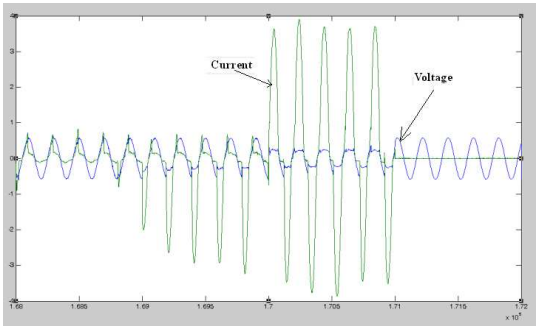
Step 4. Carbonization is formed.	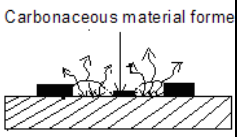	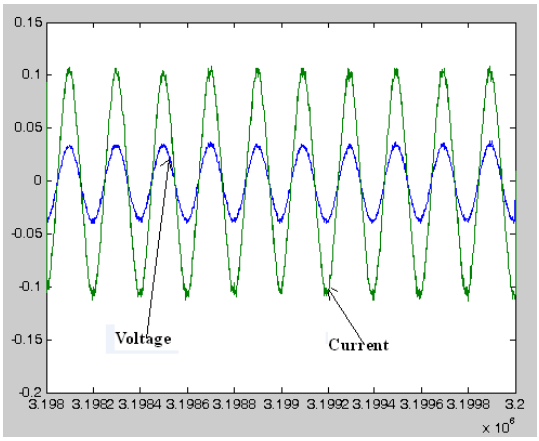

The duration of the arcing event for the model shown in Figure 4.1 will depend on the rate of evaporation across the remaining surface and the magnitude/type (AC/DC) of the system voltage. Should the surface be subject to more moisture deposits, the process can be repeated. Table 4.1 shows that the typical tracking processes described as before with current and voltage waveforms on test samples gained from CTI tests, as is explained later in Chapter 5. It can be seen clearly that at the beginning both waveforms are producing smooth sinusoidal curves, which show that the gaps between electrodes were fully covered by conductive contaminant liquid. When current increases steeply, a very low arc voltage is maintained. However, when the arc current drops to zero, a higher voltage is needed to maintain the arc. Since the arc gap has been very hot at this stage, only very low voltage is needed to maintain the arc.

There is also a period Δt of effectively zero current around the virtual zero point of the sinusoid. The arc column temperature also varies during the AC cycle; the peak temperature lags behind the peak current because of the arc's thermal capacity.

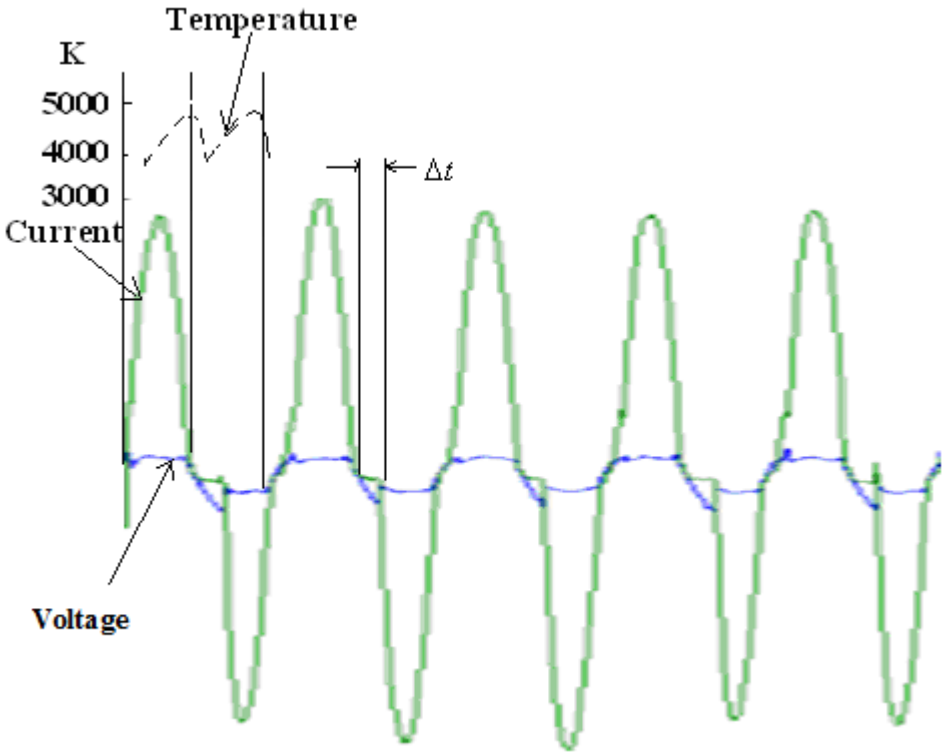

Figure 4.2 Time variations of current and voltage for 4A arc, less than 4mm long, in air between two conductive contamination covered brass electrodes. [73]

The arcs produced during these events can cause significant damage to the insulation surface and if carbonization occurs can lead to eventual failure of the dielectric system. The degree of carbonization is based on the response of the test material to the arc. Materials such as epoxy carbonize when subject to relatively low temperatures while other materials such as silicon rubber ablate when heated.

4.3. Theoretical model of electrical tracking

This section illustrates the development of a simplified model to estimate the impact of the aerospace environment on the likelihood of electrical tracking across insulating surfaces. Before my model was derived, a brief review is provided.

As early as 1966, F. Obenaus [74] introduced his mathematic model of flashover

phenomena influenced by the deposited pollution layer for high voltage insulators. The model was composed of a rectangular recipient that contains a mixture of water and salt.The quantity of the salt dissolved in the water simulates the levels of pollution. This model uses dc current.

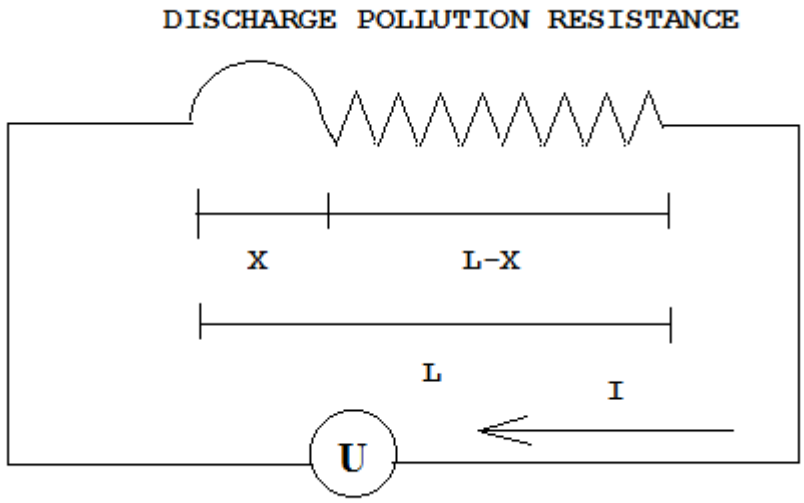

Figure 4.3 - Electrical equivalent circuit of Obenaus' model. [71]

The high voltage of the phenomenon is:

$$U = V_d + V_p \text{ …….. (4.1)}$$

where: U is total voltage; V_d is voltage across the discharge (air gap); and V_p - voltage of the layer pollution. Figure 4.3 shows the electrical circuit of the phenomena.
Hence:

$$U = x \cdot E_a + V_e + V_p \text{ ….. (4.2)}$$

$$V_p = \left\{ (L - x) + \ln \frac{a^2}{4\pi r_d^2} \right\} \bullet \rho \bullet i \quad \text{……. (4.3)}$$

where: x - length of the discharge; E_a - electrical field within the discharge; V_e - voltage of the electrodes; L - longitudinal dimension of the rectangular recipient. a - width of the discharge; r_d - radius of the discharge; ρ - electrical resistibility of the wire mixture; i - discharge current.

In 1995, Oscar Armando Maldonado Astorga and Afonso Jose do Prado [75] presented their results of dynamic behaviour of the flashover phenomenon on the high voltage polluted insulators from a mathematical and an experimental model that introduce the variable thickness influence of the layer pollution deposited on the high voltage insulator surface to the Obenuas model. However, one limitation of Obenaus's model is that air pressure is not a parameter influencing behaviour, while the mathematic model here will consist of the impact of this parameter shown in the following section.

My model is based on one originally developed by Warren [76] This model shown in Figure 4.4 consists of a layer of aqueous contaminant film on a solid insulation surface with electrical fields running through it. Warren focused on the pre-discharge conditions required to evaporate the liquid layer as being an event required for tracking to start; that is the technique adopted in this work.

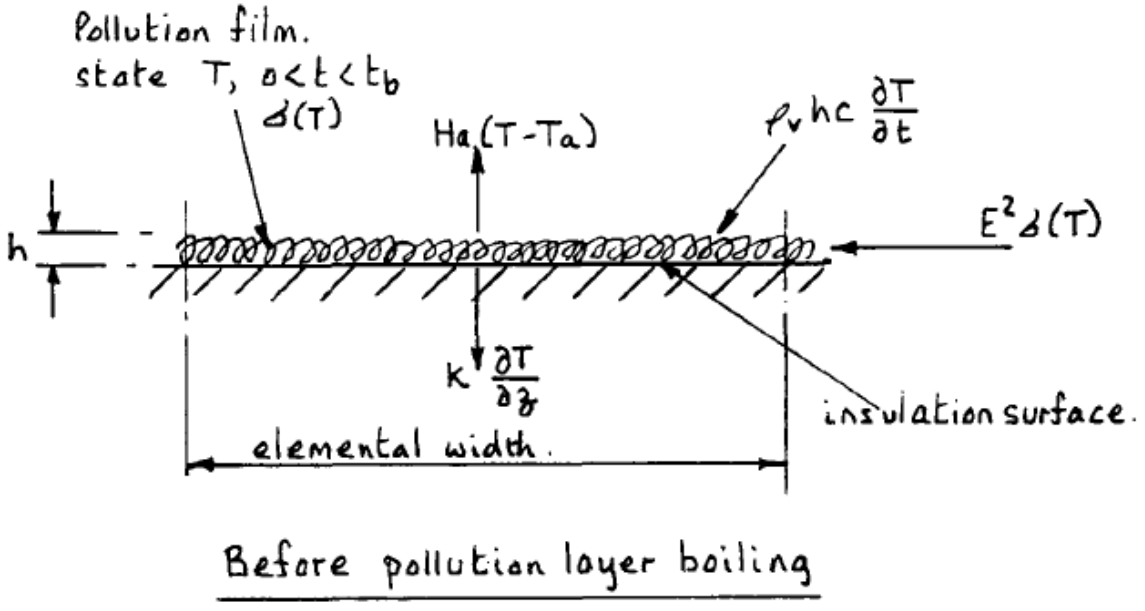

Figure 4.4 the sketch of L. Warren's pre-discharge conditions[76].

As it is seen in Figure 4.4, the aqueous contaminant film with height of h is supposed to be heated up from the existing temperature T until its boiling point t_b before pollution layer is boiling. Underneath the pollution film, the insulating material with elemental width is

also a medium to transfer heat generated by the electrical currents. Surrounding air is another effective heat transfer medium. Then pre-discharge condition can be expressed by input power and output power equilibrium equation as follows.

The heat equilibrium equation is:

$$E^2\sigma(T) = \rho_v h \cdot c\frac{dT}{dt} + k\frac{\partial T}{\partial z} + H_a(T - T_a) \text{ …….. (4.4)}$$

At or after boiling of the contamination, this becomes:

$$E^2\sigma(T_b) = \rho_v \frac{dh}{dt} + k\frac{\partial T}{\partial z} + H_a(T_b - T_a) \text{ ……. (4.5)}$$

The input power $E^2\sigma(T)$ on the left hand side is the electrical power due to the electrical currents through the pollution layer in which E is the voltage applied and $\sigma(T)$ conductance. It can be seen that the conductance is dependent on the existing temperature T of the contamination.

On the right side of the equation 4.1 expresses the output power from the pollution layer. When heat is transferred by a circulation of fluids due to buoyancy from the density changes induced by heating itself, then the process is know as nature convection or free convection. Natural convection occurs when a system becomes unstable and therefore begins to mix by the movement of mass [77]. The convection Ra can be expressed by the following equation 4.6.

$$\text{Ra}=\frac{\rho_0 g\alpha\Delta T L^3}{\kappa\mu} \text{ ……. (4.6)}$$

where L is the characteristic length-scale of convection, and L^3 is the volume of the medium. In the case of L.Warren's pre-discharge situation, it will be the volume of the pollution layer which can expressed as $h \cdot c$. ΔT is the temperature difference across the medium. Since all the items in the equation such as ρ_0 (the reference density, typically picked to the average density of the medium), g (the local gravitational acceleration), α (the coefficient of thermal expansion), κ (a thermal diffusivity) and μ (the dynamic viscosity) are constant, in L.Warren's equation 4.4, they are shorted to a single item ρ_v.

Then the first item on the right hand side of equation 4.1- heat convection of the pollution layer-can be expressed as $\rho_v h \cdot c \frac{dT}{dt}$. The second item is $k \frac{\partial T}{\partial z}$ is the heat transfer to the underlying material (this will be based on the specific heat capacity of the specimen). The last item $H_a(T - T_a)$ is to illustrate the heat conduction to the air where H_a is the heat transfer coefficient of air and $T - T_a$ is the difference between the current temperature of the pollution T and air temperature T_a.

In the following paragraphs, it can be seen that the mathematical model in my research does not include the dynamic behaviour of heat transferred to the underlying material and electrodes and the heat leading to temperature changes.

The model is built based on the geometry illustrated in Figure 4.5, which is based on the test geometry from IEC 60112. Two electrodes are placed on a piece of insulating material. An aqueous contaminant of a specific resistivity falls into place between the two electrodes. To simplify this analysis, the contaminant layer is taken to have uniform thickness and a uniform width across the gap between the two electrodes in a rectangular shape, and contains salt and water to make it conductive. Arc formation will only take place should the contaminant layer be evaporated, i.e. when a dry band develops.

The input power to the aqueous conductive contamination film is the power converted from electrical energy due to leakage current flowing through the equivalent resistance of the film. The film between two electrodes has a dimension of $l \times w \times h$ where l is the length, w is the width and h is the height. The resistance of the film therefore is:

$$R = \rho \frac{l}{wh} \text{ ……. (4.7)}$$

If we consider the system to be uniform and examine the steady state energy balance, then the heat into the system will equal the heat loss as given in Equation 4.8 where 'V' is the voltage across the gap, and '$\rho(T)$' is the resistivity of the contaminant expressed as a function of temperature. According to the power dissipation equation, we can then attain the

equation 4.5 to show the input power to the film:

$$P_{in} = I^2 \cdot R = \frac{V^2}{R} = \frac{V^2 \cdot wh}{\rho(T)l} \text{ ……. (4.8)}$$

The output power consists of heat transferred through the surrounding air, output of the underlying material and even from the electrodes (especially when these are large). As was explained in the previous section, in L. Warren's model, dynamic behaviors of heat transfer to different media should be included to get a full picture of the voltage required for tracking as a function of time. However, in my research the static model ignores the influence of heat capacity, which would only serve to increase the voltage needed for tracking, while the electrodes/specimens act as a heat sink and therefore limit the temperature rise of the contaminant layer. The latent heat, is the energy absorbed during a change of state without a change of temperature, which here is boiling of water or evaporation. The magnitude of the latent heat would on the energy required to evaporate the water drop is 2260 kJ/kg . This magnitude will determine the power required after the contaminant liquid reaches to boiling. As explained before, the phenomena in my research focus on the initiation of discharge for the system. We suppose that as soon as the boiling point is achieved, the dry band appears. [78-82]

Although in my research the static model ignores the influence of heat capacity, a theoretical calculation of the time for the film between electrodes to evaporate can be carried out by considering both heat capacity of the water film and its latent heat. It should be noted that the increase of the amount of water between electrodes in the calculation has been ignored. First of all, the heat energy needed for the liquid with dimension of $5mm \times 4mm \times 1mm$ and weight of 0.02g to be heated up to boiling point can be calculated. It is known that the heat capacity for the liquid is 4183 $J/kg/K$ shown in table 4.2 in chapter 4. Hence the output energy used for the liquid to reach boiling point is calculated as $4183 \times 0.02 \times 10^{-3} \times (373 - 293) = 6.7\ J$. Then output energy for the liquid to evaporate to vapor is calculated as 45.2 J $(= 0.02 \times 2260)$ since the likely magnitude of latent heat for water drop to evaporate is 2260 kJ/kg . As a conclusion, the total output energy is the sum

of the two output energy, which is 51.9 J .

The contaminant liquid used is the solution specified in the section 5.2.4 in chapter 5 and its resistivity at 23 ± 1 °C is 395 ± 5 $\Omega \cdot$cm. Hence the resistance for length of 4 mm film between electrodes is 3160 Ω. So the energy in to the liquid under applied 50 V on the electrodes is $\frac{50^2}{3160} \cdot t \quad J$ where t is the time. Finally the time for 0.02 g of liquid under 50V to reach boiling point is about 73 s. If the applied voltage rises to 70 V, the time for the certain amount of the liquid to evaporate is about 33 s. It can be seen that with a low voltage such as 50V, the liquid will not evaporate within 72 s. In chapter 5, the dropping system specified in the IEC 60112 standard can produce one liquid drop every 30 s, which is much less than 72 s. As a result, it is expected that the amount of liquid will keep increasing during the whole test period. However, when the voltage is raised to 70 V, the evaporation time for the liquid is around 33 s, which is close to the dropping rate. In this case, the evaporation rate and replenishment rate of the liquid reach to equilibrium. The amount of the liquid on the solid insulation material should stay pretty much the same. From the calculation above, it can also be seen that the energy needed for the liquid to reach boiling point compared to the energy for the liquid to change to vapor is relatively low. It will not have big effect on the process. In my research, the arc will occur as soon as the continuity of film is broken. Higher applied voltages will increase the input power to the liquid which will lead to shorter time for the liquid to evaporate. As a result, with higher voltages the first arc will be ready to occur much more quickly. And the time for the next liquid to replenish will be longer. This will eventually lead to arc reignition and more severe tracking damages on the solid insulation.

In the static state the electrodes and specimens have been heated up to their maximum heat capacity (based on the maximum temperature of the liquid). This heat transfer does not need to be modeled but the heat lost through the electrodes and specimen to the air must be accounted for. An equivalent thermal resistance of the film to the surroundings (accounting for conduction, radiation and convection, and including the losses not just from the liquid

but also from the electrodes and the specimen) is introduced as ' R_T '.

The output power can therefore be expressed as in equation 4.9 where ' T ' is the temperature of the liquid or the surroundings as indicated by the subscript.

$$P_{out} = (T - T_{air}) / R_T \text{ ..... (4.9)}$$

R_T is taken to be the equivalent thermal resistance as calculated by equation 4.10 and representing conductive, radiative and convective losses (although it is noted that these will not be linear effects).

$$R_T = \frac{1}{\frac{1}{R_{T_{air}}} + \frac{1}{R_{T_{material}}} + \frac{1}{R_{T_{electrodes}}}} \text{ ..... (4.10)}$$

To begin the tracking process, T_{liquid} must be raised to the boiling point of the liquid. We can therefore achieve equation 4.11, which expresses the thermal equilibrium at boiling state of the static model.

$$\frac{V^2 \cdot wh}{\rho(T) l} = \left(T_{boiling} - T_{ambient}\right) / R_T \text{ .....(4.11)}$$

The equation shows that the tracking process is highly dependent on the ambient temperature. A lower voltage will be required to raise the liquid to a temperature at which it will evaporate when the ambient temperature is high. The current standards such as IEC 60664 and IPC 2221 state one specific requirement for creepage distance and do not vary this as a function of ambient temperature.

The process is also dependent on the boiling point of the liquid. Given that pressure changes the boiling point of a liquid and as the pressure falls the boiling point reduces, it is expected that a lower voltage will be required to evaporate the contaminant at lower pressures.

In reality, a number of other factors exist that mean the exact relationship between the voltage and the boiling point will not be as straightforward as that presented. The resistivity of the contaminant will change as a function of time as it changes temperature (the higher the resistivity of the contaminant, the lower the heat input for a given unit voltage).

As described, there will also be a significant impact of the test sample and the electrodes owing to the heat capacity that they exhibit. The heat flow will therefore change as a function of time as the electrodes and the test specimen heat up. This is discussed in the following section 4.5.

4.4. Theoretical model analysis

The static model expressed in equation 4.11 clearly shows that the significant factors influencing electrical tracking are the applied voltage, resistivity of aqueous contamination, dimensioning of film between electrodes, boiling temperature of the contamination, ambient temperature and equivalent thermal resistance. A number of these factors are inter-dependent, which consequently makes it even more complicated to understand the electrical tracking mechanism and draw Conclusion.

4.4.1. Static thermal analysis

A static thermal analysis was run on the Finite Element Analysis software ‘Vector Field Opera version 11’ to determine the thermal resistance between the liquid layer and the surrounding air while including the effects of heat loss through the electrodes and the specimen (once the system had reached a steady state).

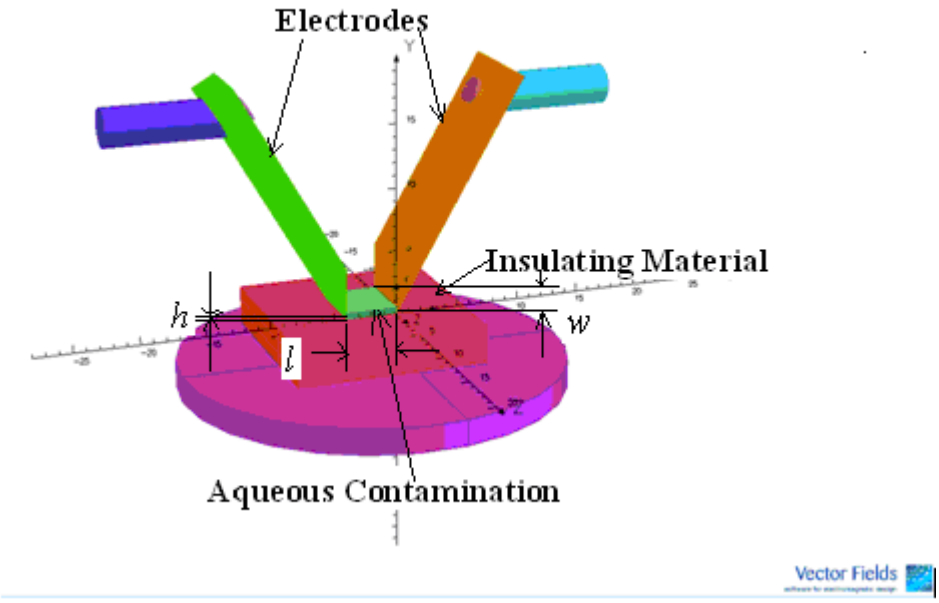

Figure 4.5: Vector Field OPERA static electrical tracking modeller

In the Vector Field Opera software, the 3-dimensional model is built and illustrated in Figure 4.5. The material properties and its thermal properties are listed in Table 4.2, in which specific heat capacity is only employed when dynamic thermal analysis is carried out. The model was surrounded with air with an ambient temperature being set at the boundaries of the model.

Table 4.2: Thermal property of different components used in Opera model

Component	Material	Thermal conductivity ($W/m/K$)	Specific Heat Capacity ($J/kg/K$)	Density (kg/m^3)
Electrodes	Brass	380.0	390.0	8960.0
Contaminant film	Solution	0.6	4183.0	998.3
Specimens	Epoxy Resin	0.3	970.0	1970.0
Air	Air	0.0257	1005.0	1.205

Heat flux boundary conditions are used in nine different blocks uniformly placed within the aqueous contaminant film with values gained from the experimental CTI tests described in

Chapter 5 at 50 V (and using the voltage and current to work out the power input). The following figures show us the model once meshed.

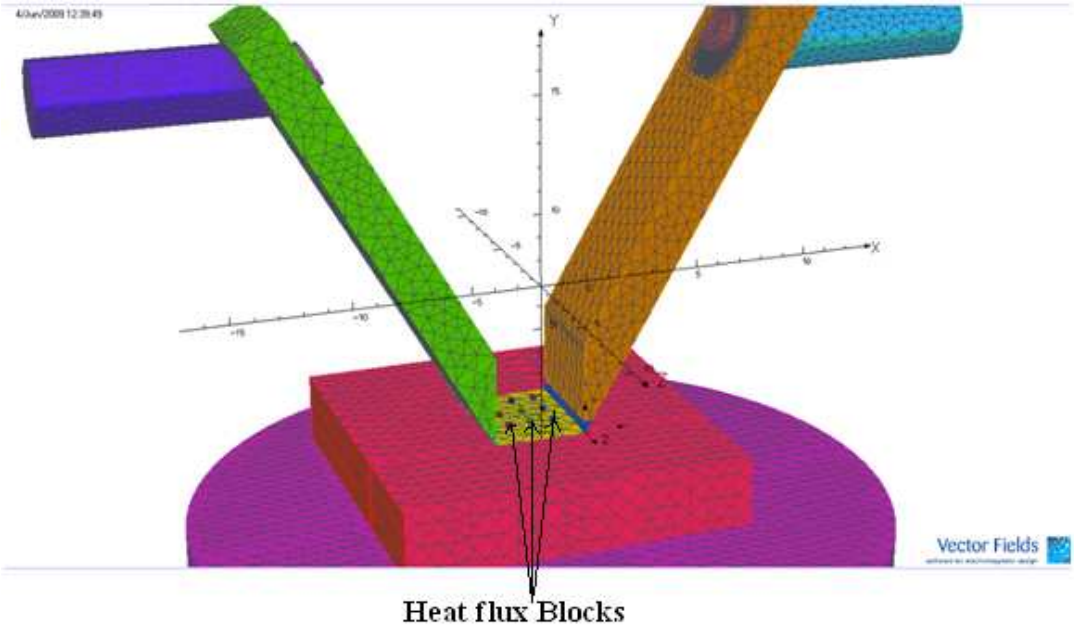

Figure 4.6 a three-dimensional model for research on heat transfer from conductive liquid film on insulation surface under electric stress to surrounding media.

After the model has been meshed, the static thermal analysis called TEMPO is run. In the following Figure 4.7 a 3-dimensional temperature distribution of the model is shown with temperature contour and its value band. It can be seen that the highest temperature around 329 K is found at the middle of the contamination film. With distances further from the middle part of film, the temperatures gradually decrease to 293 K, which is room temperature. The temperature change of electrodes around 20 K indicates that electrodes do have an impact on the voltage required for tracking since they dissipate heat into the surrounding air effectively, which will lower the thermal resistance of the water film to the surroundings.

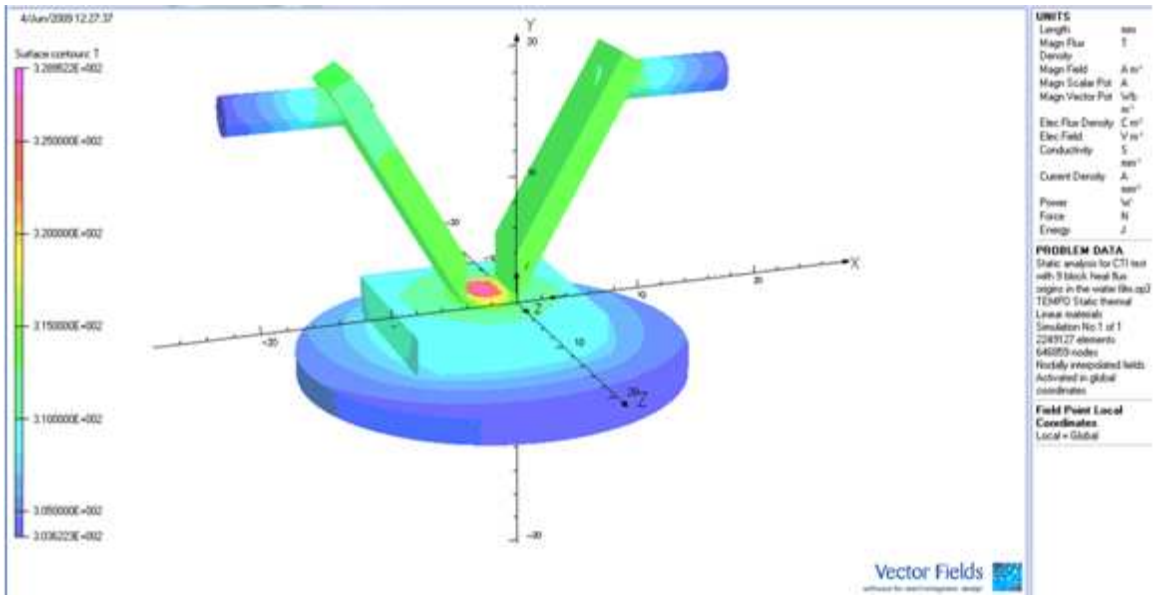

Figure 4.7 three-dimensional displayed temperature distribution of the static model with temperature contour label band.

Using the output of this model, it is possible to compute the thermal resistances from the liquid to the air, the electrodes to the air and the specimen to the air by examining the heat being dissipated off each element. The thermal resistances for different surrounding media are calculated as follows:

- Thermal resistance from liquid to air: 378.79 K/W
- Thermal resistance from specimen to air: 381.67 K/W
- Thermal resistance from electrodes to air: 259.07 K/W

This means that the paralleled resistance calculated using equation 4.11 is 109.6 K/W assuming there is no resistance to heat flow between elements.These values were applied to static mathematic models above so that the following analysis of different impact of external conditions could be achieved.

4.4.2. Application of static thermal simulation results to the environments of varying pressure

The temperature of the liquid described in Equation 4.11 needs to be elevated to the boiling

point for tracking to occur (some liquid needs to be evaporated to allow the boiling point to be reached). The differences between the room temperature and boiling point determine the maximum output power. The boiling point will vary as a function of pressure. Therefore when the influence of air pressure is studied, the varying boiling with air pressure should be carefully looked into. In an aerospace application, the air pressure may reach as low as 1165 Pa at an altitude of 15,255 m (50,000 feet). The relationship of air pressure with altitude is shown in Figure 4.8, which indicates that the air pressure decreases with altitude increasing. For the solution used in the IEC 60112 test described in Chapter 5, the boiling point is 54.3 ºC at 1000 Pa (100 mbar) and 101.5 ºC at 100,000 Pa (1000 mbar) as the measurement result from testing carried by myself. This section shows the pressure impact on withstand voltage for electrical tracking by ignoring conductivity changes of aqueous contamination with temperature.

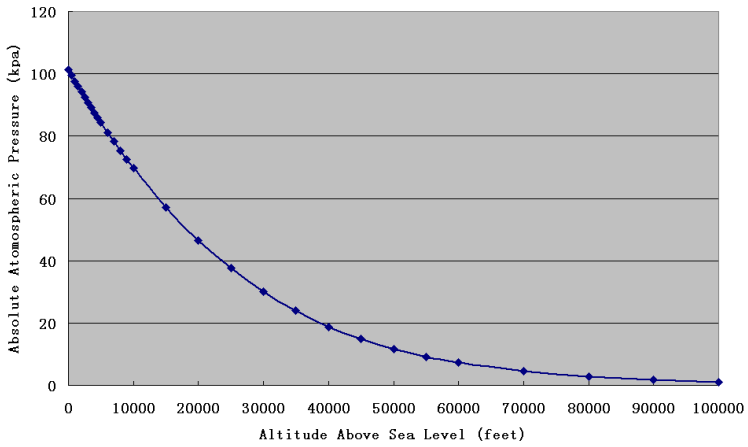

Figure 4.8 the relationship of air pressure with the altitude.

To identify the impact of pressure on the voltage that will instigate electrical tracking, the formula given as Equation 4.11 was used, where the water film is simplified as a cuboids with 4mm of length by 5mm of width by 0.5mm of height, boiling points of deionized water and solution as a function of pressure as shown in Figure 4.9, and ambient temperature is 293 K (20 °C).

To achieve the relationship between the boiling point of two types of liquids including deionized water (0.0008 S/m) and solution A specified in IEC 60112 (0.258 S/m) and

ambient pressure, measurements of the boiling point were taken by conducting tests in the environment chamber, in which the pressure can be controlled from atmospheric pressure to 0.8 kPa. The boiling state is an equilibrium state. Hence when a liquid is boiling, its temperature will keep constant. Our test method takes advantage of this characteristic to have a liquid of 100ml in a glass beaker positioned in the environment chamber. Then the liquid was heated up until the temperature of the liquid measured stays steady for 2 minutes. Tests were conducted under varying pressure from 0.8 kPa to 100 kPa. Three measurements were taken for each pressure, which means each point in Figure 4.8 is the average of three measurements from the tests.

Trendlines and their log formula $y = 22.337Ln(x) - 56.325$ and $y = 21.48Ln(x) - 45.744$ for deionized water and solution A respectively were shown in Figure 4.11 for boiling points against varying pressure.

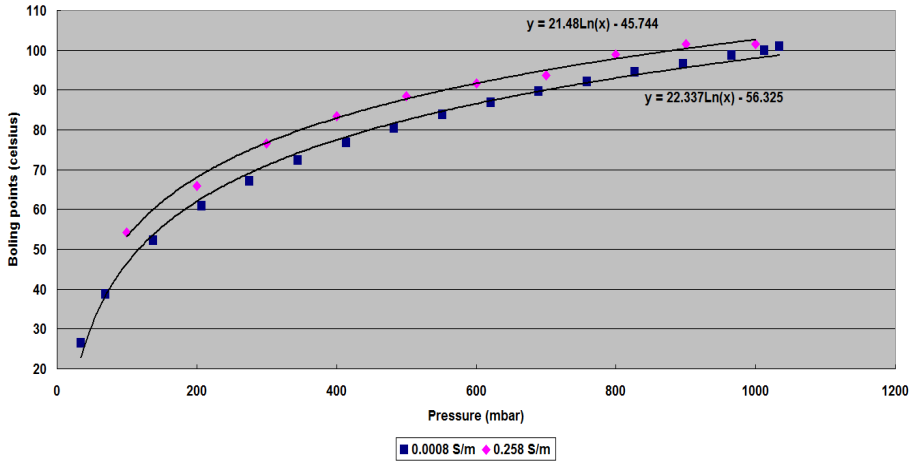

Figure 4.9: The relationship between boiling points and air pressure for deionized water and solution

Figure 4.10 illustrates the relationship between the voltage that will instigate tracking and the air pressure when the aqueous contamination is pure deionized water with conductivity of 0.0008 S/m. In reality, the conductivity of water varies with temperature. However, in this section, this factor is ignored.

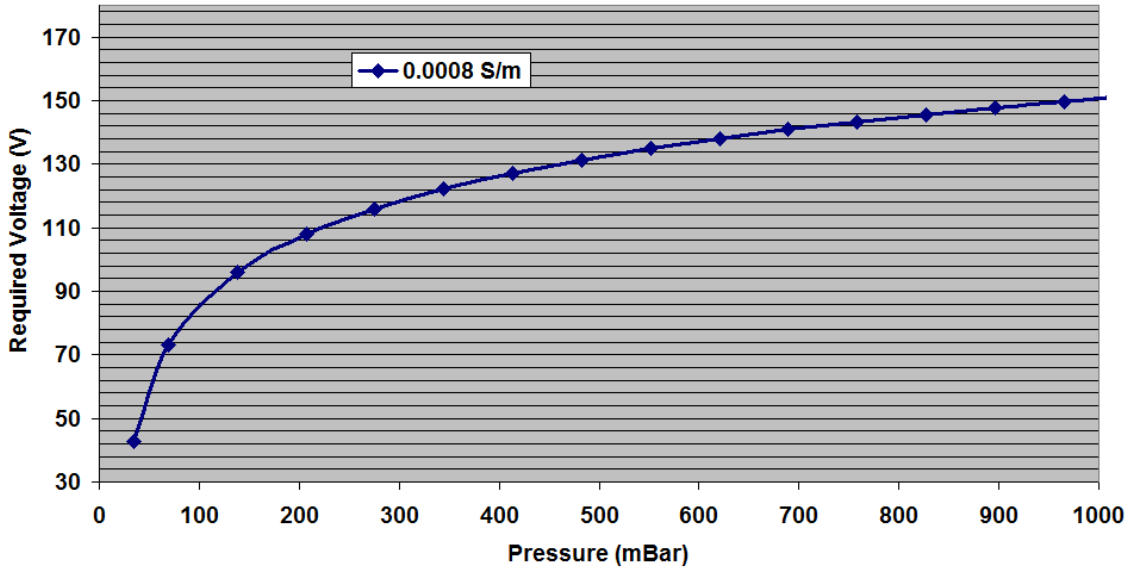

Figure 4.10: The relationship between the voltages required to instigate tracking and air pressure by using pure deionized water.

In Figure 4.10, the required voltage for initiation of electrical tracking at ambient pressure 1000 mbar is around 150 V while at lower pressure 100 mbar it drops to 46 V. The results indicate that the voltage for electrical tracking increases with pressure for pure deionized water contamination.

Figure 4.11 presents the calculation results of required voltage for solution A as specified in IEC 60112 with a resistivity of 0.258 S/m. The voltages are much lower than for the previous case owing to the higher conductivity of the fluid. A reduction in the voltage needed to instigate tracking at low pressure is still seen. The graph highlights the low voltages that may be needed to instigate electrical tracking.

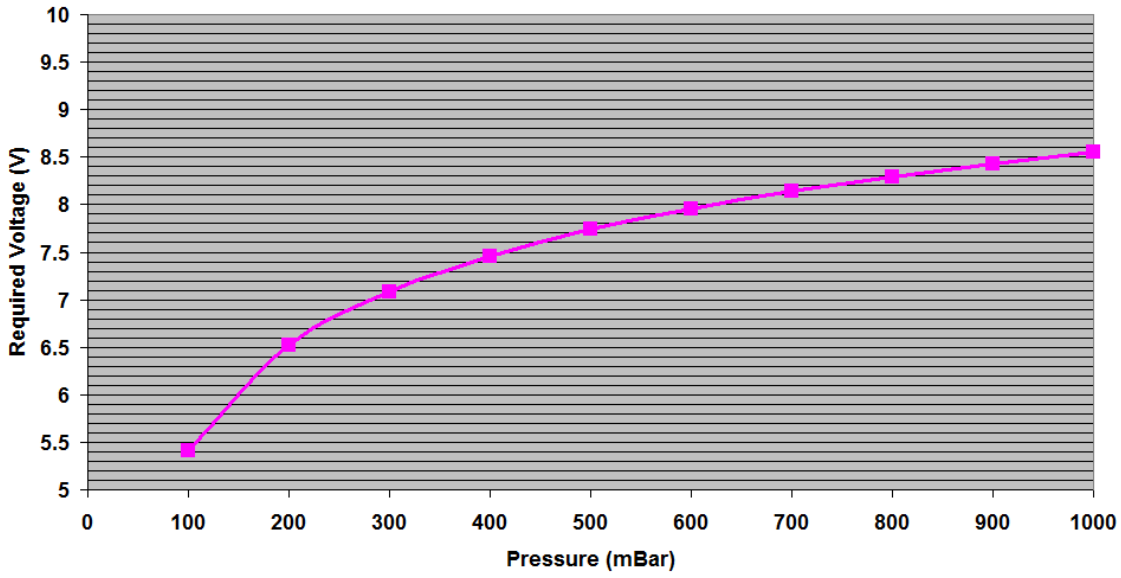

Figure 4.11: The relationship between the voltages required to instigate tracking and air pressure by using solution A defined in IEC 60112.

The results from both pure deionized water and solution A show that the voltage that would be required to cause tracking falls sharply as the air pressure reduces. Such a finding would be significant when applied to equipment designed for use in the aerospace sector. At ambient pressure a voltage fifteen times larger for pure deionized water condition can be found compared with the value under solution A conditions. Even at 100 mbar, the value of the required voltage for pure deionized water is eight times bigger than that under solution A conditions. A similar result is seen for the higher conductivity solution. It should be noted that the equivalent thermal resistance to surrounding media is calculated in a simplistic way and that the static thermal model used in my research above has ignored the heat capacity of the specimen, electrodes and water film, which will introduce certain errors. However, qualitatively my analyses indicate how the pressures influence the required voltages for electrical tracking.

4.4.3. Application of static thermal simulation results to the environments of varying pressure, contaminant resistivity and ambient temperature

When examining equation 4.10, it is clear that the lower the contaminant resistivity, the lower the voltage that will be needed to cause tracking. Similarly, the higher the ambient temperature, the lower the heat input that will be required to raise the temperature of the liquid to the boiling point. Hence in this case, the required voltages are lower.

However, the conductivity of the contaminant actually varies with temperature. In order to find the relationship, measurements of conductivity on both deionized water and solution A as used in IEC 60112 were carried out. The results are shown in Figure 4.12 and 4.13 with trendlines and their equations give us the relationship between the conductivity of the two different contaminations and temperature. It is found that the conductivity increases with temperature, the respective equations for deionized water and solution A being $y = -4E-08x^2 + 3E-05x - 0.0047$ and $y = 0.0092e^{0.0121x}$ respectively, where y is the conductivity and x is temperature.

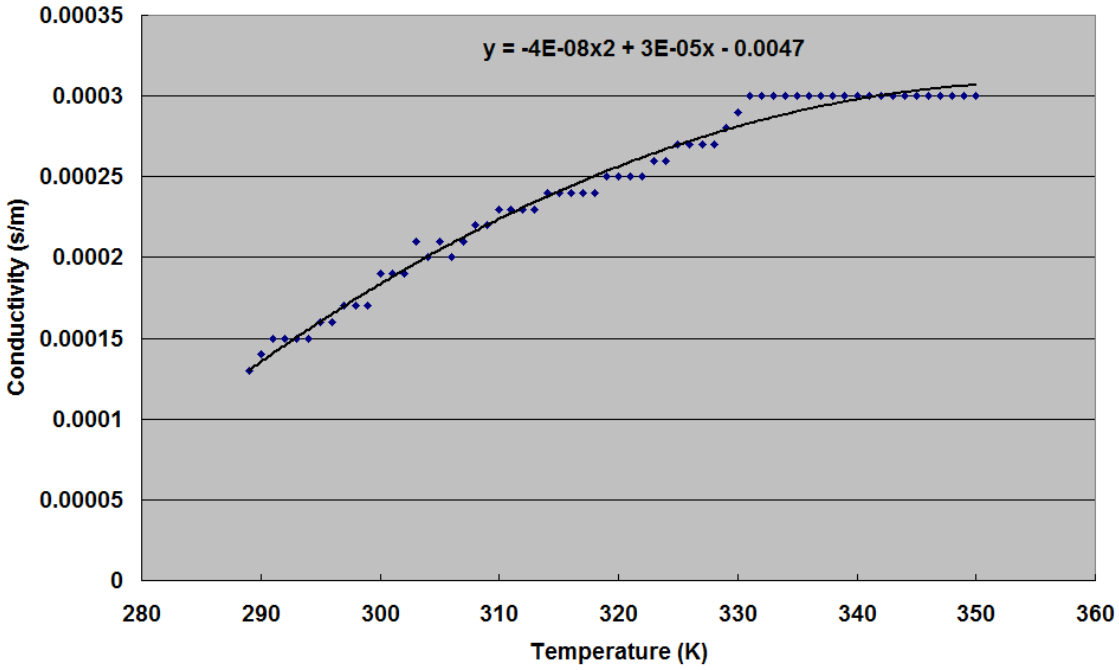

Figure 4.12: The relationship between the conductivity of deionized water and temperature.

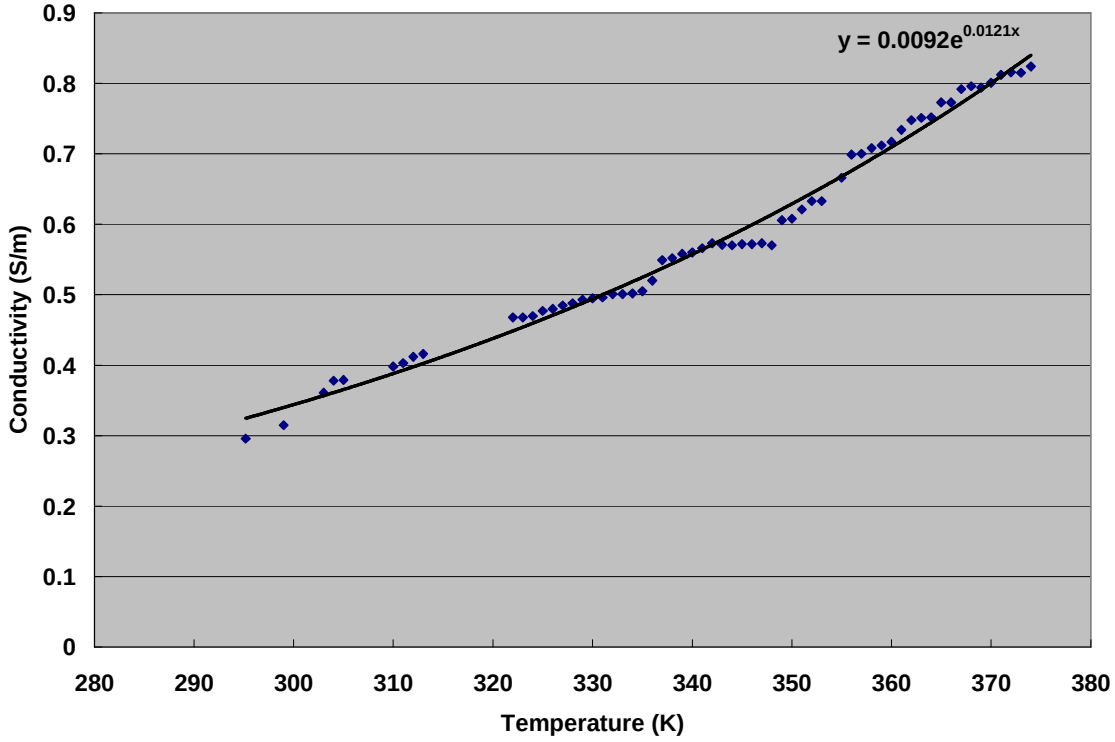

Figure 4.13: The relationship between conductivity of solution A in IEC 60112 and temperature.

This relationship between conductivity and temperature is then included in the static

analysis. Figure 4.14 shows the voltages required to initiate tracking as a function of pressure and ambient temperatures for pure deionized water with a conductivity of 0.0008 S/m. The variation of conductivity with temperature was considered here. The voltages seen are significantly higher than those in the previous static model since the contamination conductivity is higher at the liquid boiling point (in comparison to the value at 20 degrees C used before). For all three different ambient temperatures, the required voltages increase with pressure. The influence of pressure on the voltage to instigate tracking is more pronounced at 323 K. As the ambient temperature increases, the voltage required to instigate tracking also falls (significantly at lower pressures where the ambient temperature nearly reaches the liquid boiling point).

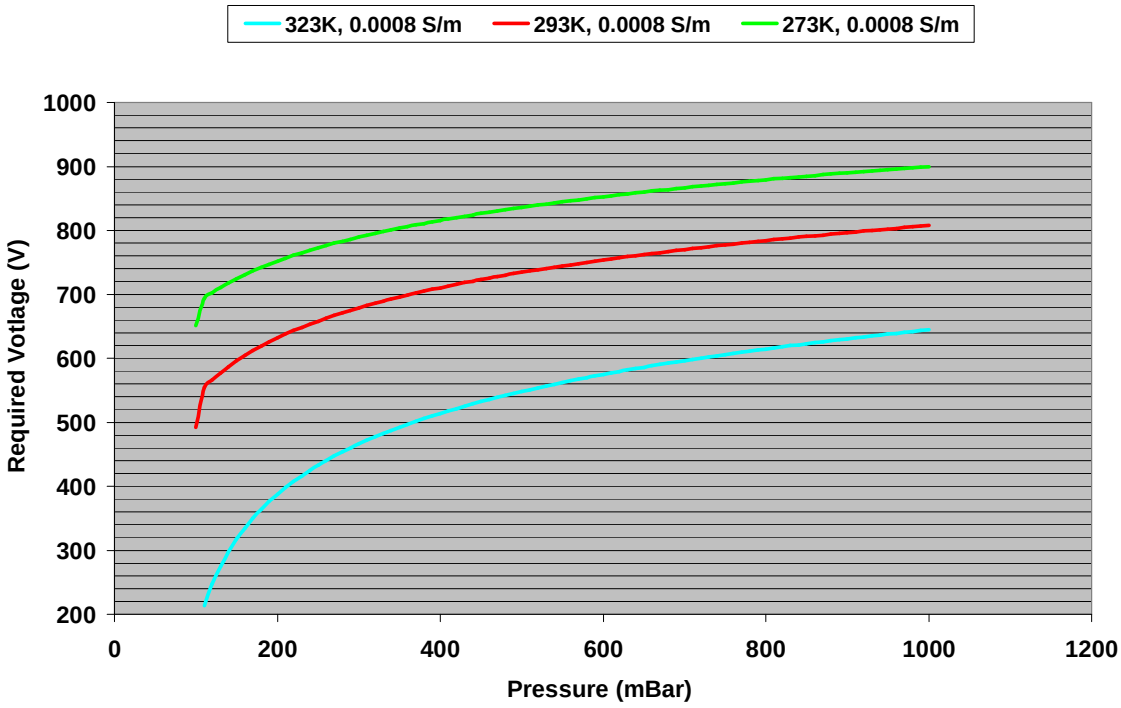

Figure 4.14: Required voltages as a function of pressure at different ambient temperature for deionized water of conductivity of 0.0008 S/m

Figure 4.15 illustrates the voltage required for electrical tracking as a function of pressure and ambient temperature for solution A with a conductivity of 0.258S/m. The similar trend can be found on those voltage curves at 323 K and 293 K, which is that the voltage to initiate electrical tracking increases with pressure. However, required voltages first increased and then at 273 K decrease with pressure with very small magnitudes. These

differences can be explained by equation 4.10. With ambient temperature increasing, the required voltage becomes lower as less heat input into the aqueous contamination needs less electrical power input. However, in the meantime conductivity increases with temperature. In equation 4.10, when conductivity of the contamination goes up, the required voltage should be raised to achieve the same level of power input. These two factors have opposite effects on required voltage. Normally, although the difference between the boiling point and ambient temperature decreases with ambient temperature going up and pressure going down, the increase of conductivity requires a higher voltage. However, this difference can be so small at lower pressure for higher ambient temperatures that only a low voltage has to be applied to evaporate the aqueous contamination even with the influence of conductivity. At higher pressure, the boiling point increases significantly, resulting in a need for higher electrical power input which can be achieved by raising the voltage.

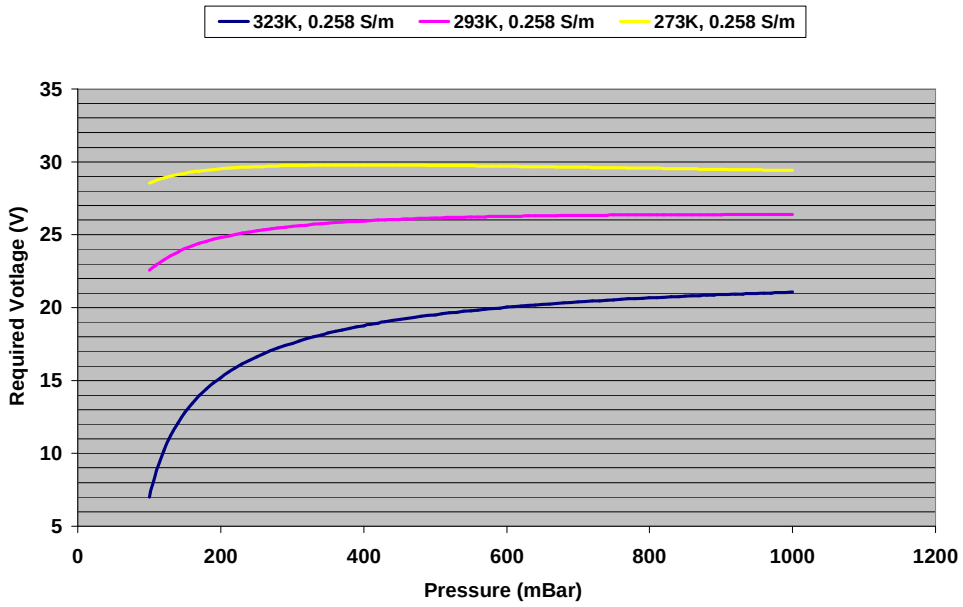

Figure 4.15: Required voltages as function of pressure at different ambient temperatures for solution A with conductivity of 0.258 S/m.

The results of the calculation show us that higher voltages are required for lower conductivity pollution. Ambient temperature is also shown to have a significant effect on the voltage required to instigate tracking. For lower ambient temperatures, there is no significant difference in the voltage required to instigate tracking as a function of pressure

(this being due to the change in conductivity of the contaminant as a function of temperature).

These results suggest that the use of both the standards [44,45] detailed in this paper, which do not account for ambient temperature or contaminant conductivity, must be performed with caution.

4.4.4. Dynamic thermal analysis

In the previous sections of this chapter, the impact factors of various environmental situations have been discussed based on the static model of electrical tracking developed. The static mathematical model shown in Equation 4.11 ignores two dynamic items $\rho_v h \cdot c \frac{dT}{dt}$ and $k \frac{\partial T}{\partial z}$ in contrast to L.Warren's Model. As explained before, the former represents the heat convection of depending on temperature increase, and latter shows the heat transfer to the underlying material. Both of them indicate the control of temperature on the transfer of heat to surrounding heat dissipating media. To find out the influence of these dynamic processes depending on the temperature changes to the required voltages for electrical tracking, the same model in Vector Field software but with more material properties and boundary conditions than in the static thermal simulation shown before.

The dynamic modeling analysis was run on the same Finite Element Analysis software 'Vector Field Opera version 11' since the software has the capability of running both static and dynamic analysis. However, the material properties and boundary conditions have a few differences. Specific heat capacities for surrounding heat transfer media indicated in Table 4.2 are now employed to determine the dynamic processes of heat transfer controlled by their temperature. Heat flux boundary conditions are used in nine different blocks uniformly placed within the aqueous contaminant film with values gained from the experimental CTI tests described in Chapter 5 at 50 V (and using the voltage and current to work out the power input). The simulation time steps were set to 1 s, 2 s, 3 s, 5 s, 15 s, 20 s, 30 s, 60 s, and 120 s. After the model had been meshed both on the surfaces and within

volumes, the dynamic thermal analysis was run.

It is known that initially all the surrounding media were at room temperature. When the leakage current flowed through the aqueous liquid, heat was generated and transferred to the surrounding heat transfer media including air, electrodes and insulating material at the bottom. Heat capacity characterizes the amount of heat that is required to change a body‘s temperature by a given amount. Calculation of this is very complicated due to consideration of more than one state variable or physical property for thermodynamic systems unless a particular infinitesimal path had been defined including the definition of changes of temperature, pressure, volume, number of particles and any other relevant macroscopic variable. If the system has more than just a simple homogenous structure, each part of the system should be defined separately. Therefore to study thermal dynamic heat transfer behaviors which would influence electrical tracking is not straightforward after initial simulation with the software.

4.5. Discussion

The static mathematical model to initiate electrical tracking in this chapter has been developed based on L. Warren’s model by ignoring heat transfer to surrounding heat transfer media depending on temperature. Both the static and dynamic thermal simulations were done in the Finite Element Analysis software ‘Vector Field Opera version 11’. The static simulation was used to find out the equivalent heat transfer resistance while the dynamic simulation was used to help predict the possible changes of required voltages to initiate electrical tracking.

The static mathematical model was then employed to analyze different impact factors of environments. Electrical tracking could happen when the continuity of the conductive path – in this case, the aqueous contamination – is broken. Due to the boiling of the liquid, the conductive path will be pulled apart most probably at the hottest point. It has been proven that the boiling points increase with ambient pressure for both deionized water and

solution A, defined in IEC 60112: 2003. Hence the required voltage to initiate electrical tracking also increases with pressure. The value of voltages at ambient pressure 1000mbar was around 150 V while at lower pressure 100 mbar it dropped to 46 V for deionized water; it was 8.4 V for the highly conductive solution A at 10000mbar and 5.5 V at 100 mbar. This also represents the fact that the more conductive the aqueous contamination, the lower the voltages are that are needed for electrical tracking.

Ambient temperature also plays a very important role in determining the electrical tracking and its required voltages. Theoretical calculation results show that at higher ambient temperatures, less voltage is required to initiate electrical tracking. The most interesting results are those values of voltages required at 273 K for the highly conductive solution A, which shows that the voltage actually decreases with pressure going up. This result can be attributed to the combination of the influence of ambient temperature, pressure and the conductivity of the aqueous contamination. Especially, these impact factors are inter-dependent. This therefore proves that the mathematic model does predict this complicated relationship.

Dynamic thermal analysis was presented to find out the influence of the thermodynamic processes before the thermal equilibrium was reached. The heat capacities of surrounding heat dissipating media are critical properties to consider. Again it is not a simple variable, but varies with temperature, pressure and volume. My initial study according to the simulation results with the software show us that the required voltage to initiate electrical tracking before the surrounding electrodes are heated up is higher than that when all the surrounding media has been at the same high temperature.

Finally, if we compare those calculated withstand voltage at atmospheric pressure to avoid electrical tracking with those specified in IEC 60664, we can find for pollution degree 3 (conductive pollution occurs or dry non-conductive pollution occurs which becomes conductive due to condensation which is to be expected, which is close to the situation of use of solution A in my calculation) and material group III, the withstand voltage in

standard is 250 V (320 V for material group I and bigger than 250 but less than 320 for material group II) while the results from the model is only 25 V. And the withstand voltage under pollution degree 2 (only non-conductive pollution occurs expect that occasionally a temporary conductive caused by condensation is to be expected, which is close to the situation of use of deionized water in my calculation) which is equal to the deionized water pollution situation is 400 V while the calculated voltage is around 780 V. Comparing to the values in Table A6 in appendix A from IPC 2221, it can be seen that without considering any pollution degree difference, the withstand voltage for 4mm gap above sea level up to 3050 m (around 696.4 mbar) is 800 V while my calculated voltage is 25 V for very conductive pollution condition, and around 740 V for deionized water pollution condition. For any case above 3050m, the withstand voltage in the standard is 170 V. All the standard have no consideration of the impact of ambient temperature.

4.6. Conclusion

The computational model developed in my research can predict the inception voltages of discharges for wet condition electrical tracking model considering the impact of air pressure, ambient temperature, and pollution degree (through the conductivity of contaminants). Those environment factors are very important for aerospace application, especially for the MEA concept with higher voltage levels. And boiling point of liquid pollution is a very critical parameter to influence the start electrical discharges and hence electrical tracking. However, one major drawback of this model is that the thermal dynamic processes have been ignored, which are believed to have effect on the initiation of discharge on insulation surfaces between electrodes.

Chapter 5 Experimental Investigation I: Standard CTI Tests on FR-4 and ABS Materials

5.1. Introduction

Experimental verification is highly necessary to prove the results and conclusions gained from the previous computer simulation and computation. Furthermore, it is clearly helpful for promoting understanding of the mechanism of electrical tracking under different micro-environmental conditions. Many factors that affect the behaviour of electrical discharges on organic insulating material surfaces should be identified further by testing.

The various tracking resistance test methods has been developed as described in Chapter 2, It generally can be divided into two classes: wet and dry methods. Dry test is based on the idea that the tracking phenomenon developed from tiny electrical discharges on the solid insulating surfaces. They are repeated until the whole path between the two conductors becomes tracking. The dry method has characteristics of repeatability since the method is very simple. The disadvantage of dry method is that very high applied voltage is needed and time-consuming. The biggest concern of the dry method is that the electrical tracking mechanism is different from electrical tracking under pollution condition in real life.

Wet condition tracking test method obviously has advantage in term of simulating the environment condition in real life closely by utilizing artificial contamination. However, the biggest challenge for wet tracking tests is that the reproducibility of the test results is not acceptable. Therefore the repeatability of the test results will be inspected in this chapter by

repeating the same test for three times for all the tests.

Organic insulation materials are used in a variety of electrical apparatus owing to their lightweight and useful electrical and mechanical properties.The experimental work was carried out on two kinds of organic insulating materials widely used in power electronics equipments on modern aircraft, which are FR-4 and Acrylonitrile butadiene styrene (ABS).

FR-4 is made of woven fiberglass cloth with an epoxy resin binder that is flame resistant. FR-4 glass epoxy is a popular and versatile high pressure thermoset plastic laminate grade with good strength to weight ratios. It is most commonly used as an electrical insulator with near zero water absorption and considerable mechanical strength. All these attributes make it a very good insulation material for printed circuit boards. It is usually used as a substrate with a copper layer. The FR-4 used in PCBs is typically UV stabilized with a tetra-functional epoxy resin system. It is typically a transparent yellowish color - the green, red and sometimes blue color of a finished board comes from the solder mask. FR-4 manufactured strictly as an insulator (without copper cladding) is typically a di-functional epoxy resin system and a greenish color.

ABS is a very commonly used thermoplastic, used to make light, rigid, molded products with different CTI values of greater than 600 from FR-4 with CTI value of between 175 and 249 [83-85]. Hence CTI tests were carried on both materials to find out the mechanism of electrical tracking and also the relation to the material groups.

The experiments were carried out while strictly following the instruction in IEC 60112：2003. The standard provides a method to evaluate the resistance of solid electrical insulating materials to electrical tracking or erosion for voltages up to 600 V when the surface is exposed under electric stress to water with the addition of contaminants. The comparative tracking indices are those values of applied voltages leading to the leakage current flowing through the surfaces above a particular threshold (0.5 A) or scintillation fire. However, my research focused on finding out the mechanism of electrical tracking on

solid electrical insulating materials in different micro-environments, such as different air pressures, degrees of conductive pollution.

The leakage current and voltage waveforms had been recorded from a series of tests on both FR-4 and ABS (Acrylonitrile Butadiene Styrene Plastic) by using National Instrument Company hardware and the software Labview. By analyzing those results and the experimental observations, four modes of electrical tracking mechanism through the whole process have been developed.

5.2. Experimental conditions

5.2.1. Test Circuit

To test a number of samples of insulating materials and as a framework for comparison with the thermal model, the test circuit and technique described in IEC 60112 has been used. However, in this research it is used to examine the tracking mechanism itself but not comparative tracking indices of different materials. Figure 5.1 shows the circuit diagram used for the tests.

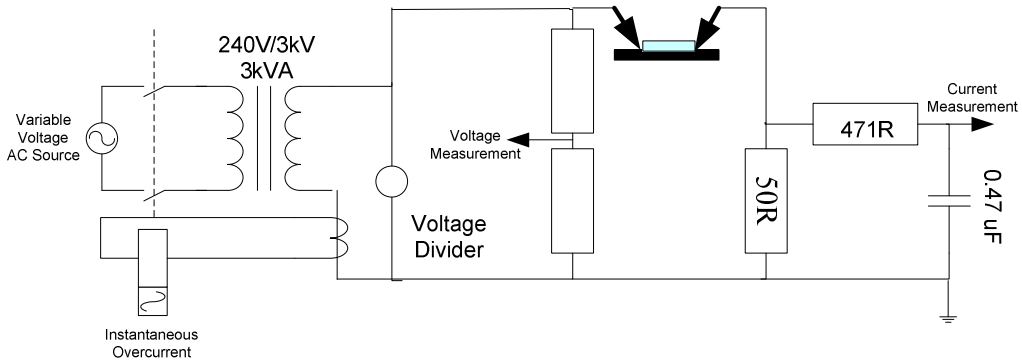

Figure 5.1: Sketch of the test circuit

The power source is provided by a 240/3000 V 3 kVA 50 Hz transformer. This is fed through a resistor that is set to keep the prospective short circuit current across the sample to a value of 1 A (in reality this is low in comparison with the level of current that could be available in many systems). A voltage divider measures the voltage across the test object with a further

measurement being taken to measure the voltage on the feed side of the transformer. A resistive shunt is used to measure the current flowing through the test sample. The output of this is displayed on an oscilloscope following filtering using a first order RC low pass filter set to have a 3 dB frequency of 677 Hz. An overcurrent relay is used to trip the circuit when the current flowing in the circuit is above 0 .5 A for a period of 2 s illustrated in Figure 5.2.

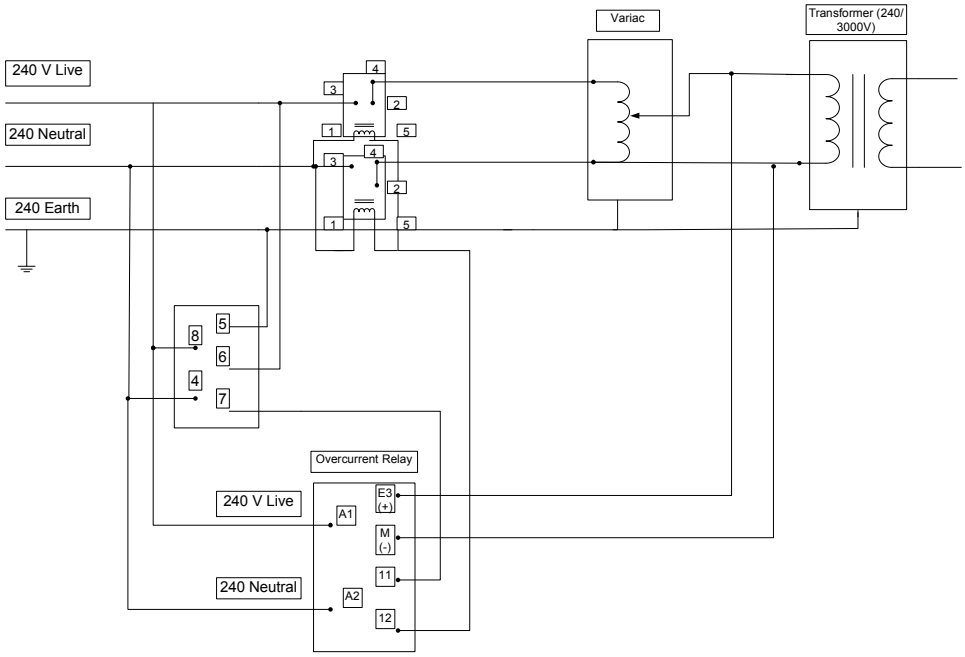

Figure 5.2 Leakage current trip circuit

5.2.2. Test specimens

Flat surfaces of test insulating materials were used of at least 3 mm thick according to the standard widths dimensions of 20 mm by 20 mm so that the area is sufficient to ensure that during the test no liquid flows over the edges of the specimen. The thicknesses of the FR-4 specimens were around 3 mm which was gained by stacking three 1mm thick FR-4 boards together for all the tests. Only two of the ABS boards were needed to achieve the thickness requirements. It has been explained in Chapter 4, the simulation parts results, that electrical tracking is highly determined by the thermal dissipation system around the specimens. A thinner layer of specimen could lead to the heat generated by electrical discharges being removed quickly through the surrounding air, electrodes or even supporting plate.

The surfaces of the test specimen were cleaned by using some cloth if necessary with Fairy wash-up liquid to make sure they were free of dust, dirt, fingerprints, grease, oil, mould release or other contaminants that could influence the test results but not lead to any swelling.

5.2.3. Electrodes

The two copper electrodes with a rectangular cross-section of 5 mm × 2 mm, with one end chisel-edged with an angle of 30° were set to a gap of 4.0 ± 0.1 mm. The electrodes were symmetrically arranged in a vertical plane, the total angle between them being 60°, and with opposing vertical electrode faces. The force exerted by each electrode on the surface was 1 ± 0.05 N. An arrangement for applying the electrodes to the specimen is shown in Figure 5.3. While copper was used for the test electrodes in this paper, platinum is specified in the standard. However, other researchers believe that the use of copper electrodes replicates the conductor-insulation systems in practice more closely[86, 87], since copper and alloys including copper are often used in electrical apparatus. It has also been found that spectrogram-histograms of the elements on the surface of insulation after a CTI test with copper electrodes show the same materials as W. H. Middendorf's results [87]in except that there was no platinum and the concentration of copper was much higher than that of platinum electrodes in[86]. Although the paper[86] states that pure copper is appropriate for the electrodes, it should be noted that there are many kinds of copper due to its mixture species. Even pure copper will inevitably have some impurities. Likewise the platinum cannot be 100% pure. If there is an influence on the results due to the impurities in the copper electrodes, this would also be true if platinum electrodes were used. However, many researchers have also found that the copper does affect the results [88-91]. Therefore to imitate real electrical equipment situation, it is to use copper, which is widely used in electrical apparatus to carry out CTI tests to replicate the conductor-insulation systems in practice more closely.

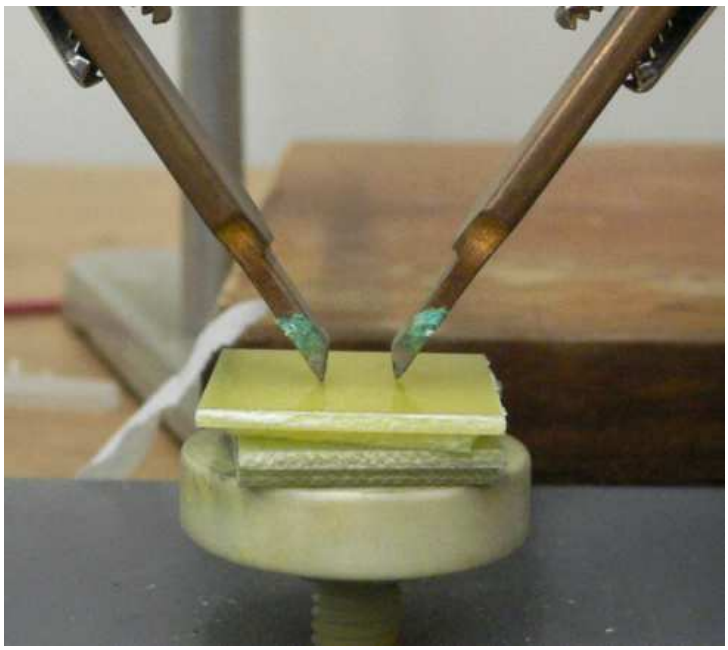

Figure 5.3 Test electrodes setup and direction on the surface of stack of FR-4 specimens

5.2.4. Dropping devices and test solution

The surfaces between the electrodes were wetted with drops of the test solution at intervals of 30 ± 5 s. The drops fell centrally between the electrodes from a height of 30 mm to 40 mm. The size of the drops was $20\,mm^3$. A peristaltic pump with integral drive model with a hypodermic needle was used to meet the abovementioned requirements, as shown in Figure 5.4. The aqueous contamination was contained in a bottle and flowed through a flexible tube inside a circular pump casing. A rotor with a number of roller and shoes attached to the external circumference compressed the flexible tube. When the rotor was turning, the part of tube under compression closed, thus forcing the fluid to be pumped to move through the tube. The output operating speed of the model used in my research was 1-6 rpm which can provide a $40\,mm^3$ per minute flow rate with suitable tubing. Prior to each test, the needle or other outlet for the drops should be cleaned and sufficient drops let out to ensure that the correct concentration of the test solution is used. This solution is mixed by 0.1 ± 0.002 % by mass ammonium chloride (NH4Cl) with deionized water with resistivity at 23 ± 1 °C is 395 ± 5 $\Omega \cdot cm$.

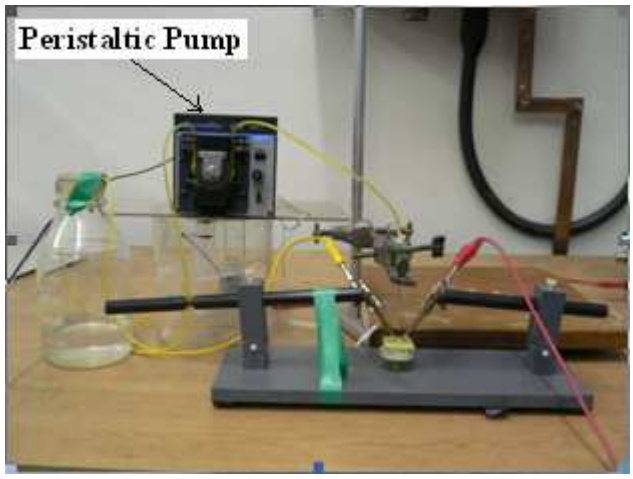

Figure 5.4 Illustration of CTI test dropping system and test rig

5.2.5. Leakage current and voltage recording

During the tests, data were recorded using a NI LabView system. Voltage and current signals were digitized using a 12-bit data acquisition card running at 10 kS/s. stored data included snap shots of the actual voltage and current waveforms and calculated RMS/peak values that were logged every 0.1 s. For selected measurements, the thermal state of the test samples was captured using an infra-red camera using both still images and video footage.

5.2.6. Test procedure

Standardized CTI tests were carried out on both the FR-4 and ABS specimens at varying air pressure. At ambient pressure, the voltage applied ranged from 50 V up to 100 V with a step of 10 V. Above 100 V the voltage steps were increased to 20 V until 300 V for both FR-4 and ABS. The test with same experiment condition were repeated three times to checkout the reproducibility of the test method.

The experimental work was carried out using the following procedures:

1. The resistor connected in series in the circuit was adjusted to the value equal to the test voltage so that the maximum current could only be 1 A even at the worst case that the gap was completely short-circuited. For example, if the voltage to be applied

is 50 V, then the resistance of the slide rheostat should be set to $50\,\Omega$, which is the possible worst case if a short circuit occurs.

2. The three pieces of FR-4 specimens or two pieces of ABS specimens were cleaned by the cloth if necessary; domestic cleanser was used to clean fingerprints, grease or oil off the surfaces.
3. The gap distances were set to 4mm by using the slide caliper. The stack of specimens was then clipped onto the plastic plate with some pressure applied by insulating tape on the electrode extensions.
4. The flow rate of aqueous contaminant was set to one droplet every 30 ± 5 seconds. It was allowed to run for a while until the flow was stable.
5. Using a multimeter to test the applied voltage at the output points of the transformer the value expected before the specimens were wetted by the test solutions was found.
6. Tests were carried out until the leakage current reached the threshold. The circuit was cut off by a control circuit including timer, circuit breaker and overcurrent relay in series. Otherwise when 50 drops of aqueous contamination had fallen, the circuit was cut off based on the timer record.
7. Labview software and hardware were used to record the leakage currents and voltages. Fifty water drops were applied to each specimen with 30 s between each droplet. During the tests, data was recorded using an NI LabView system. Voltage and current signals were digitized using a 12-bit data acquisition card running at 10kS/s. Stored data included snap shots of the actual voltage and current waveforms and calculated RMS/peak values that were logged every 0.1 s.

8. For selected measurements, the thermal state of the test samples was captured using an infra-red camera using both still images and video footage.

5.3. Experimental results and discussion

5.3.1. Behaviour of FR-4 samples at the atmospheric pressure

FR-4 samples were tested at 100,000 Pa and 20 °C using voltages from 50 V upwards until 100 V with steps of 10 V. Then with steps of 20 V the voltage applied was increased up to 300 V. By using National Instrument hardware and the software Labview, summarized voltage and current signal files with testing period were recorded. The raw current and voltage waveforms were also recoded. To verify my theoretical explanation of the electrical tracking mechanism, the infra-red camera was employed for atmospheric testing to obtain the thermal images from tests, from which we can see the temperatures of different part of the CTI test rig, test specimens, and even the aqueous contaminants so that we can further prove my theory stated in Chapter 4.

50 V Testing

For the 50 V case, Figures 5.5 and Figure 5.6 show the voltage across the test gap and the leakage current measured of three times respectively during the test period of 30 minutes. The sample did not fail and no damage was observed on the surface of the sample shown in Table 5.2 in the section 5.4.3.

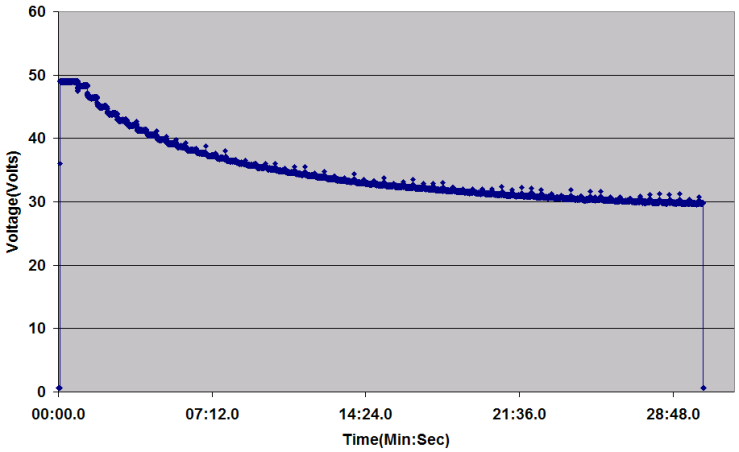

Figure 5.5: Summarized voltage vs. time plot for the test at 50 V and 1000 mbar on FR-4

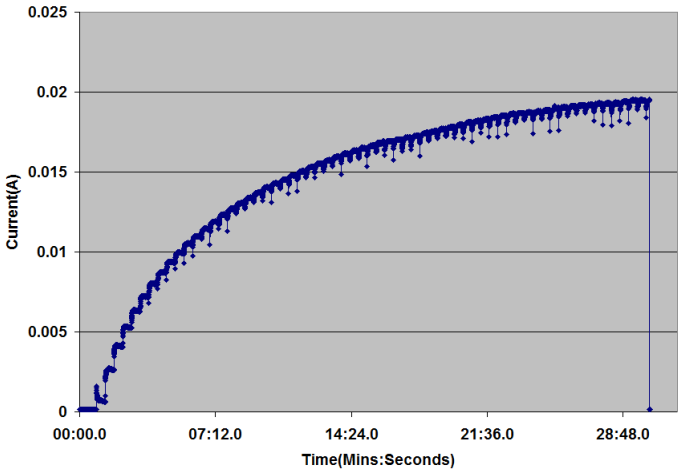

(a) 1st time test result

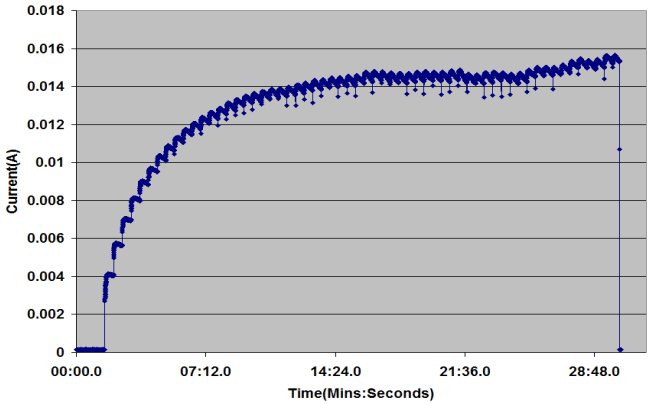

(b) 2nd time test results

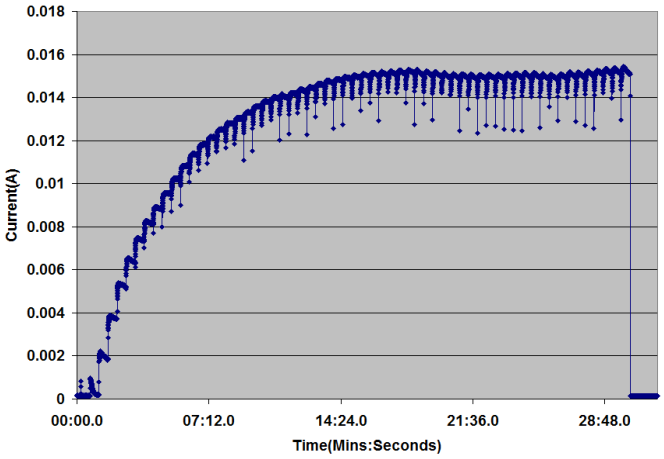

(c) 3rd time test results

Figure 5.6: Summarized current vs. time plots for the three times' test at 50 V and 1000 mbar on FR-4.

In this case, the RMS current was seen to steadily increase during the test period although the applied voltage was decreasing with small magnitudes and ultimately it reached a constant value. This result can be seen to be repeatable from these three times' test results. It should be noted that the voltage value stated as my testing voltage was measured by a multimeter at the secondary output of the transformer before any test specimens were connected. The real transformer inevitably have its' inherent resistance and inductance. Figure 5.7 show us a very typical single phase transformer mathematical equivalent circuit. Normally the short circuit test, in which the high voltage side is applied at the rated current while the low voltage is shorted, gives R_1, X_1, R_2 and X_2. The high voltage side corresponds to the low current side; applying the test current to the low current side is done for safety reasons. In my test, an RLC bridge meter was used to obtain the resistance and inductance of the equivalent circuit. Since the shunt impedances (R_c and X_c) are much larger than series impedances, they are ignored in my considerations. The equivalent impedance then of the transformer in the CTI test is $80.41+j200.134\ \Omega$.

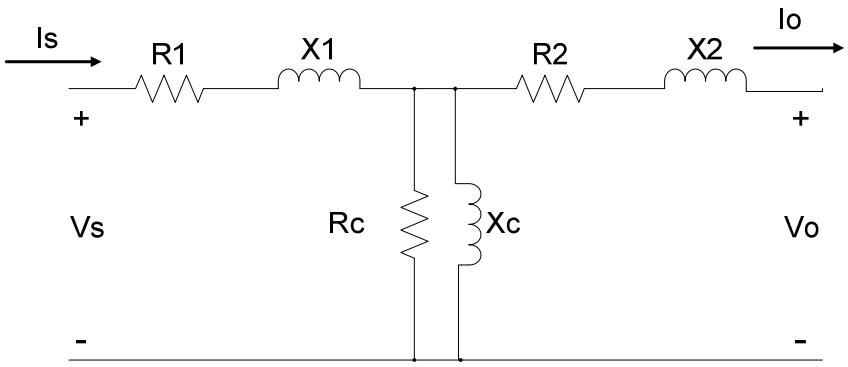

Figure 5.7: Single phase transformer equivalent circuit

After the circuit was connected to the specimen, the voltage drop on the transformer and current limiting resistor should therefore be around 4.8 V eventually as a constant value. The voltage recorded automatically on the data acquisition system should then be 46.2 V. Turning back to the real electrical system, when a transient current impulse occurs, it could be much larger than 1 A which make the total drop of voltage applied to two conductors probably 20 V.

With the contaminant liquid being continually dropped on the FR-4 board, the decreasing voltage and increasing current result shows that the sample exhibits a decreasing resistance between the electrodes. The reason can be analyzed by the combining effect of evaporation and replenishment rates. The rate of liquid deposition exceeds the rate of evaprotion at the low temperatures.In other words, the current flow through the solution is therefore insufficient to cause evaporation (or at least evaporation occurs at a lower rate than the rate at which the contaminant is dropped on the surface). Even though higher currents flow further into the test, the quantity of liquid between the test electrodes has increased. The increase in power dissipation is therefore negated by the increased surface area and heat capacity of the contaminant. This means that the temperature does not reach boiling point at any stage in order to make evaporation occur very quickly.

We can prove the above mentioned explanation by the following evidence. First of all, it was rather obvious that there was always unevaporated liquid left on the specimens for all three identical tests. It is then necessary to look at the raw data of voltage and current waveform. If we can find current waveform kept sinusoidal, then we can say it was totally

conductive between the electrodes.

Figure 5.8 shows us the zoom-in view of a section raw current waveform between 2 and 2.1 seconds. It can be seen that it was of a very clear sinusoidal shape, which proves that there was aqueous contaminant left on the specimen.

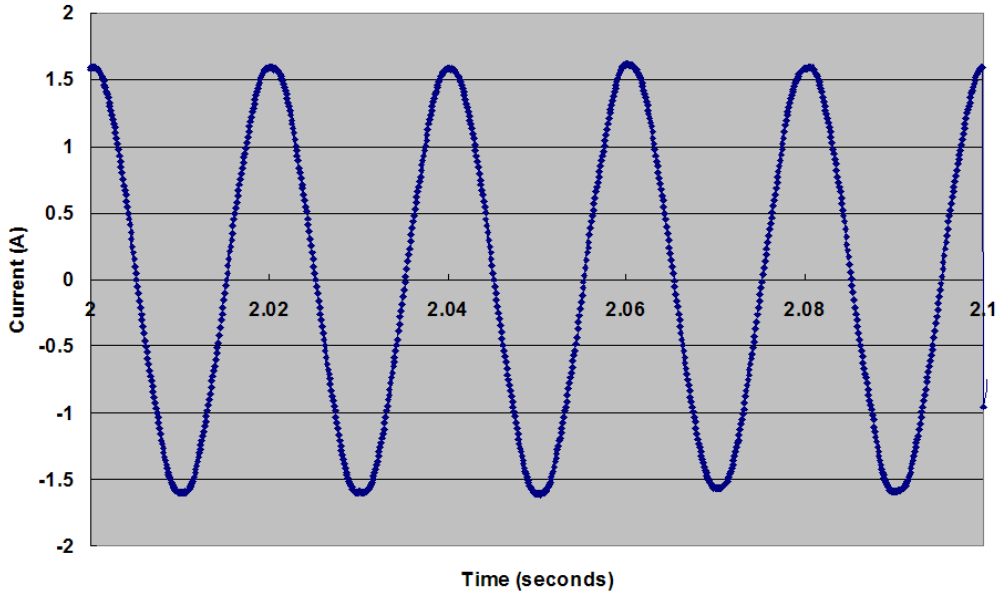

Figure 5.8 Raw current waveform signals vs. time plots for the test at 50V and 1000mbar on FR-4.

The thermal state of the test samples was captured using an infra-red camera using both still images and video footage. Figure 5.9 illustrate one of the infra-red camera still pictures taken with temperature palette scale included. On the following image the hottest point was labeled as 88.5 °C of the solution on the specimens. A bigger area on one of the electrodes close to the specimen was chosen and the maximum, minimum and average temperatures were labeled as 36.8 and 36.3 and 36.5 °C. For any other areas temperatures in the image not labeled can be found on an approximate temperature range by using the palate scale on the left.

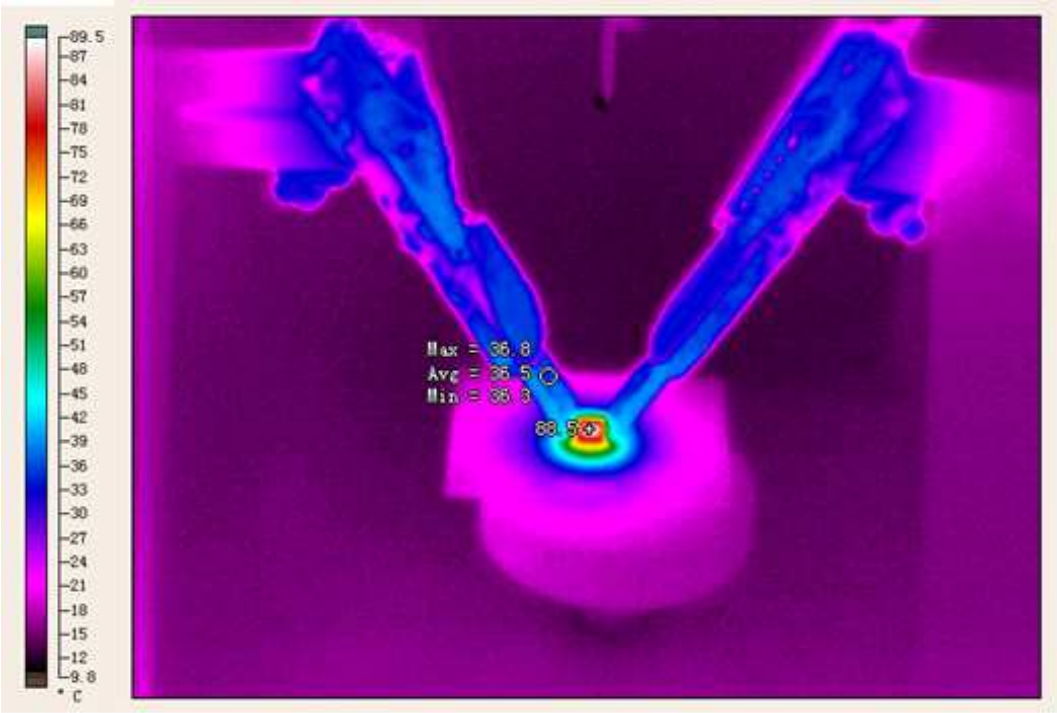

Figure 5.9 Infra-red Camera Image taken during testing at 50V ambient pressure at 08:24 moment.

It should be noted that all the thermal pictures were taken with emissivity of 0.93, which is stated as that of water in[92]. The emissivity of a material is the relative ability of its surface to emit energy by radiation. It is the ratio of energy radiated by a particular material to energy radiated by a black body at the same temperature. Hence the darker a material is, the closer its emissivity is to 1. It depends on factors such as temperature, wavelength, emission angle and even thickness of a material.

In order to find out an accurate number of temperatures for the contaminant liquid used in the tests, a beaker of the solution was heated up to its boiling point with temperature measurements through the whole process, while thermal images were taken with an emissivity of 0.93. Figure 5.10 illustrates the test results in relation to the real solution temperatures based on the thermal meter reading versus the thermal image indicating temperatures. By drawing a trendline, we can then discover that their relation equation is $y = 0.7884x + 2.6754$ where y is the real temperature of the solution and x is the reading from the thermal images with emissivity of 0.93. This will then be used to correct the

thermal image readings of all the test results.

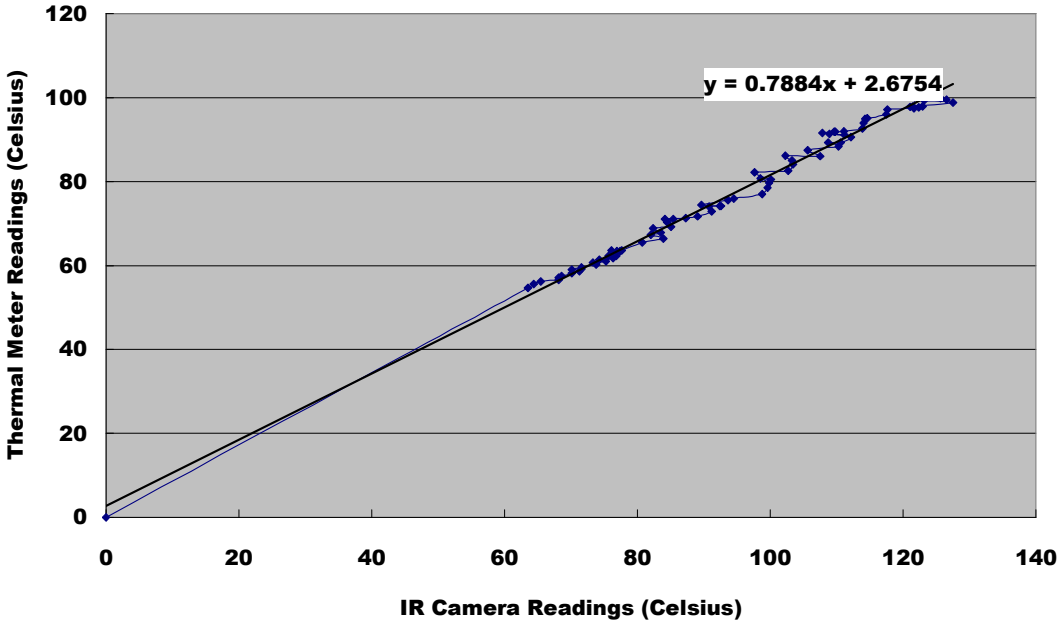

Figure 5.10 Relation between the thermal meter reading and Infra-red camera readings.

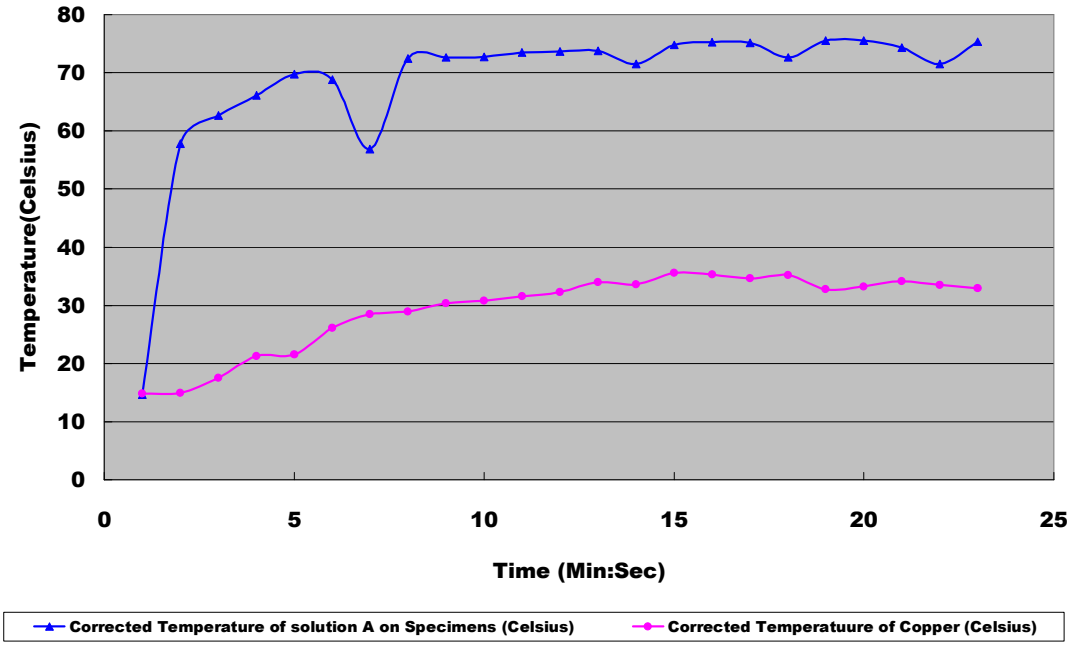

Figure 5.11 Varying Temperature vs Time after correction for 50V CTI test

The plot of the temperature of the liquid between the electrodes from the still thermal images taken is represented in Figure 5.11. Evaporation activity is fiercer since the

temperature of the solution has been raised higher than room temperature ($20^{\circ}C$). The boiling point of the solution used in the CTI tests with resistivity of 395 ± 5 $\Omega \cdot$cm at ambient temperature is $101.5^{\circ}C$. We can see that through the whole testing period, there is no moment at which the temperature of the solution could reach to boiling point. This is because that the function of the conductive solution replenishment is larger than that of evaporation of liquid. With the volume of the liquid increasing, according to the definition of resistance, the bigger the crossing area and the smaller the resistance; consequently, with almost the same applied voltage, the current flow was increasing. However, in terms of power generated to heat up the liquid, the magnitude of the decreased resistance was larger than that of the square increased current, which leads to insufficient power generated to heat up the liquid to boiling before the next drop of fresh liquid arrives. The other interesting phenomenon is that the temperature of the electrode in this case was increasing by quite a big stride from 15 °C to almost 35 °C during 30 minutes' test period.

70 V testing

When the test voltage is increased to 70 V, the RMS current varies as shown in Figure 5.12 including three times' test results which indicate the repeatability of test method. Initially, the current was increasing gradually which indicate the aqueous contamination was collecting on the surface. This also can be proven by the raw current waveform from 0 to 0.01 A with pure sinusoid shape show in Figure 5.13 (a). Then the current reaches a steady state before falling after around 20 minutes, which also have a sinusoid shape of raw current waveform with higher magnitude of almost 0.0 2 A show in Figure 5.13 (b). In this case, the applied voltage is thought to generate a level of heating that evaporates some of the solution, the evaporation rate being roughly equal to the rate of replenishment. This leads to a steady state current flow. However, after a certain period of time, the electrodes start to reach thermal equilibrium and act as less of a heat sink, meaning increased levels of heat can act to evaporate the contaminant resulting in the increased circuit resistance and lower current flow seen after 20 minutes, which is also illustrated in Figure 5.13 (c). No sample damage

was observed at this voltage and the maximum water temperature observed during the final five minutes of the test was 95 ˚C.

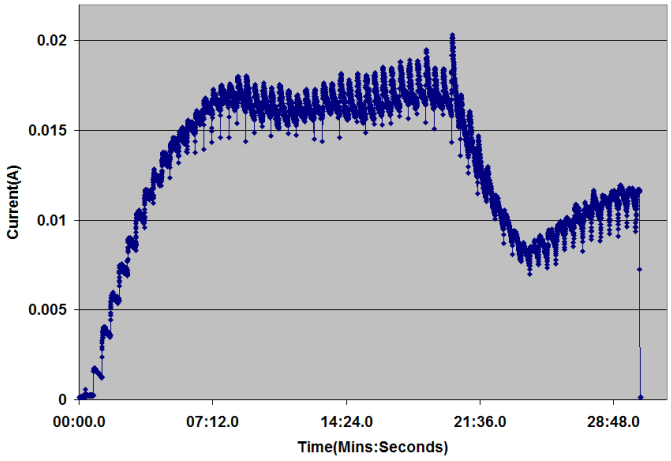

(a) 1st time test result

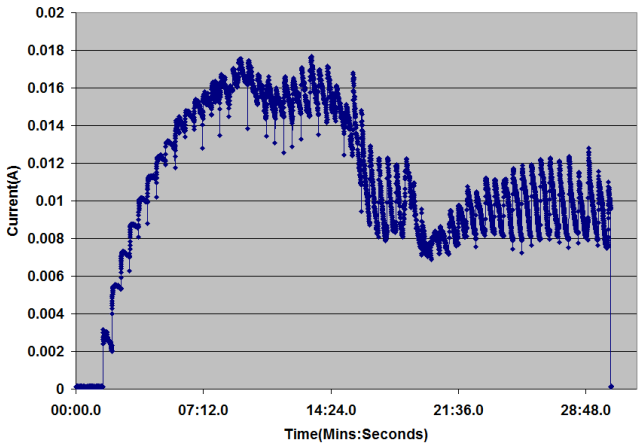

(b) 2nd time test result

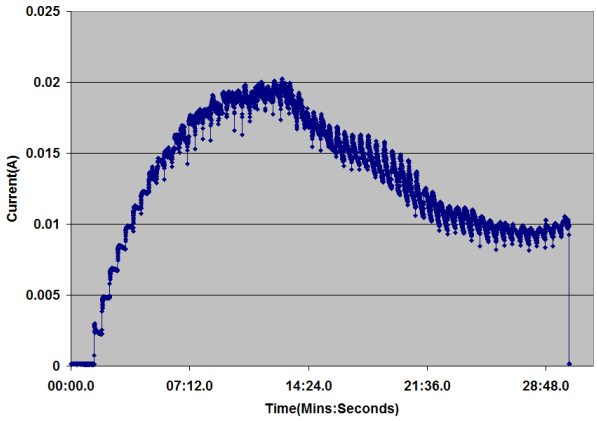

(c) 3rd time test result

Figure 5.12 Summarized current vs. time plots for the three times' test at 70 V and 1000 mbar on FR-4

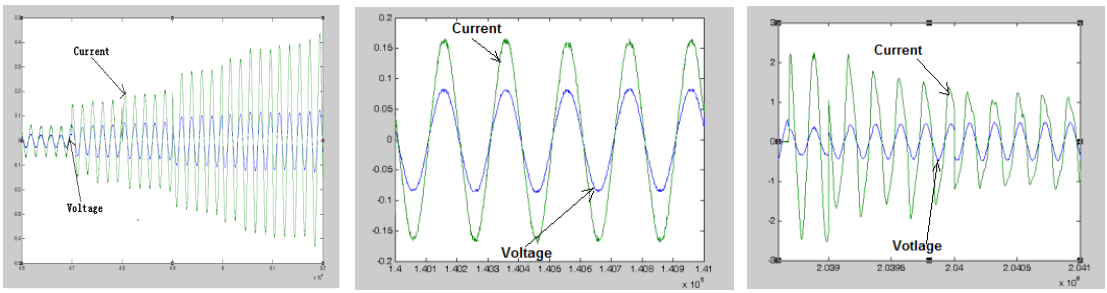

(a) gradually increasing current (b) constant current (c) gradually decreasing current

Figure 5.13 Raw current data vs Time for the test at 70 V, 1000 mbar on FR-4

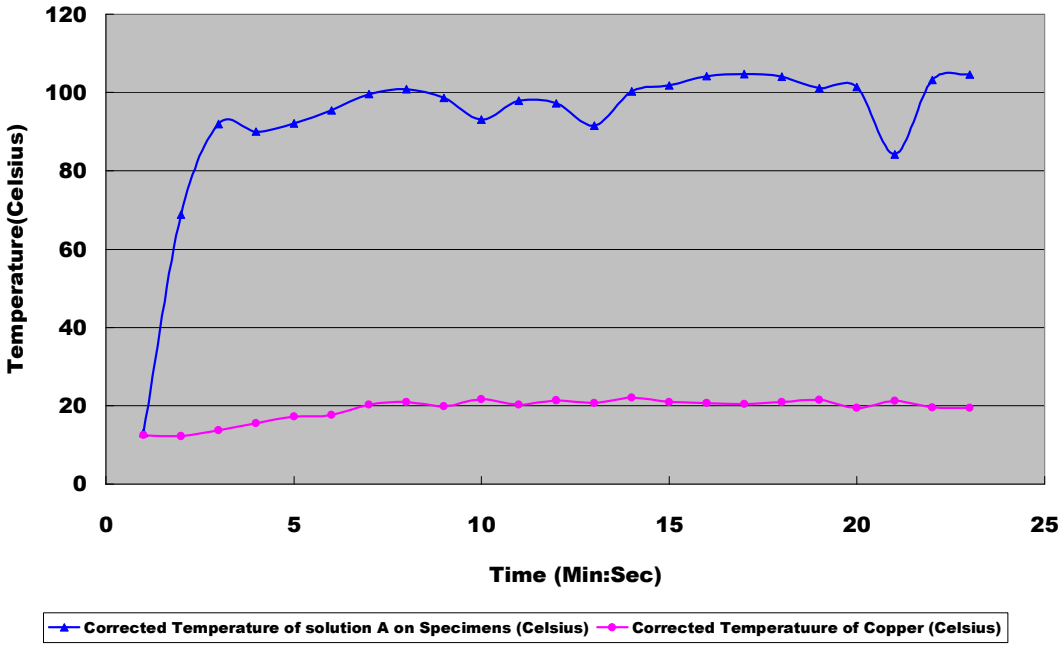

Figure 5.14 Varying Temperature vs Time after correction for the test at 70 V, 1000 mbar on FR-4

The plot of temperature versus testing time above shows us that through the whole testing period the temperature of the contaminant liquid increased to just below 100 °C. A balanced heat transfer system was then reached. During the whole process, the temperature of the electrode only went up from 14 °C to a maximum of 22 °C within smaller time scope (around 8 minutes) comparing to the case (increasing during whole period of test) at 50 V. As we know, the evaporation effect will be intensified with higher temperatures since the molecules of liquid can gain more energy to escape from its surface. At a higher voltage level, Figure 5.14 confirms that the temperature of the solution achieved a higher temperature and the equivalent heat transfer of the solution is bigger,

which leads to a different heat transfer equilibrium compared to that at 50 V. Hence, comparing the temperature change from 15 °C to almost 75 °C for 50 V, a bigger change can be seen for 70 V. And the time range is still very quick at around 2 minutes.

100 V testing

When increasing the voltage further to 90 V or 100 V, spikes of current are observed. In this section, the test results at 100V were illustrated. Summarized current vs. time plot is shown in Figure 5.15, where the repeatability can be validated according to three times' test results. These typical summarized current waveforms with current spikes were reproducible for 90V test. This behavior is characteristic mechanisms that will be likely to cause tracking damage. Contaminant is being evaporated, resulting in the reduction of current from the peak values, and in doing so will allow arcing to take place on the surface of the sample. The maximum temperature observed on the test sample was around 100 ˚C presented in Figure 5.17. Testing at increasing voltages gave similar plots of current with the current spikes reducing in width (since evaporation of the contaminant and the instigation of arcing takes place more rapidly).

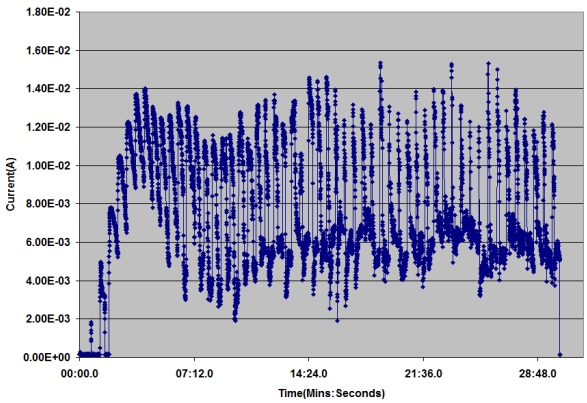

(a) 1st time test result

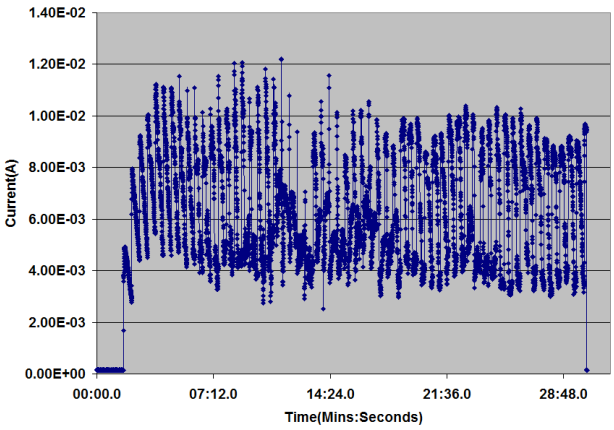

(b) 2st time test result

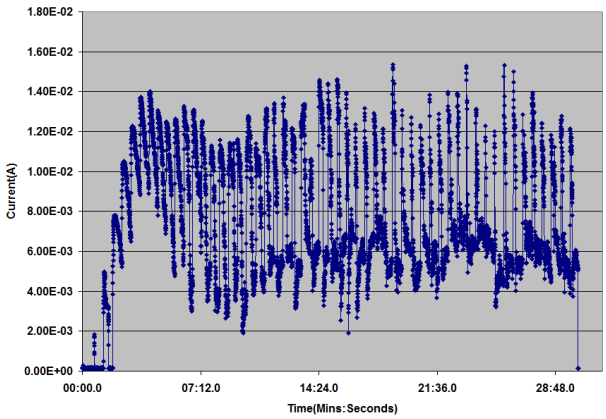

(c) 3st time test result

Figure 5.15 Summarized current vs. time plots for the three times' test at 100 V and 1000 mbar on FR-4

For further explanation of the characteristic arc and tracking mechanism shown in the test, Figure 5.16 presents that the raw current and voltage waveform of the test at 100 V. In the AC circuit, the voltage and current would pass through a zero point naturally every half cycle which provide a opportunity for the electric arc to extinguish. As the arc current was close to zero, the arc voltage becomes equal to the system voltage (if in resistive circuit, plus the inductive voltage) thus resulting in zero current flowing through the circuit. When the current is extinguished, there are no new energy being produced within the gas between the contacts and the need for an increasing arc voltage to reignite the gap. If the dielectric strength of the gap can not recover quickly as the system voltage, reignition of the arc will take place. The higher the system voltage, the more chance there is to achieve arc reignition, and the longer time for the reignition to occur. Hence it can be predicted that

with applied voltage increasing from 100 V to 150 V, 200 V or even more, the period for current at zero will be smaller and smaller. Reignition is much more aggressive and damages on the surfaces of solid insulation should be more severe. The evidence of damages will be shown in the following section 5.4.3.

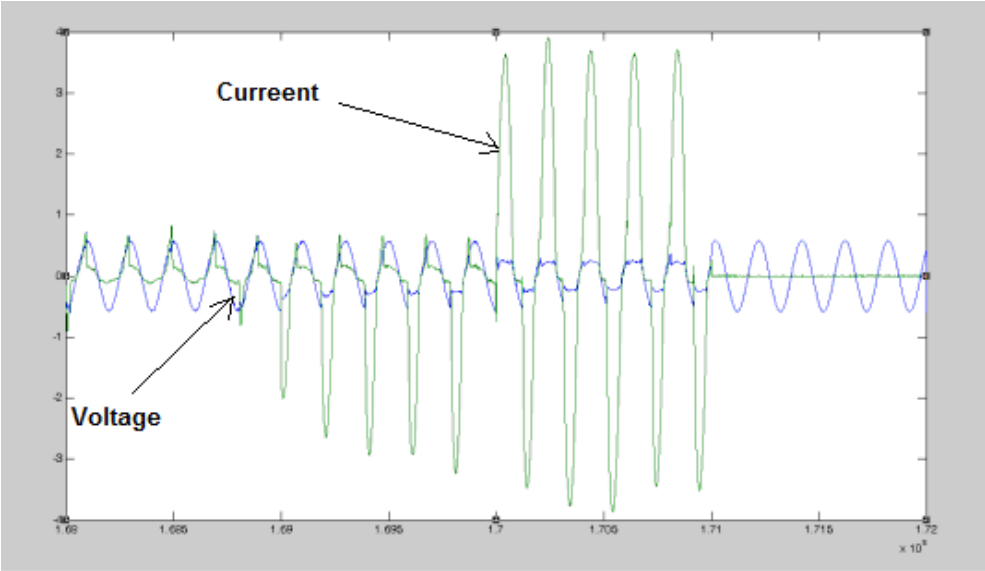

Figure 5.16 A typical raw current waveform for current spikes.

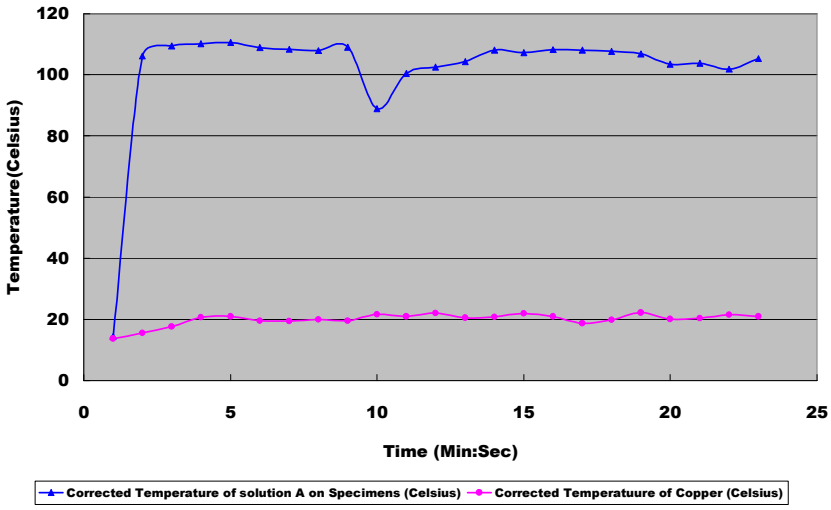

Figure 5.17 Varying Temperature vs Time after correction for the test at 100 V, 1000 mbar on FR-4

The plot of temperature versus testing time in Figure 5.17 shows us that the solution between electrodes under an applied voltage of 100 V was heated up within 1 minute as at other voltages to its boiling point of 101.5 °C (some error exists in the figure). A balanced heat transfer system was then reached for solution A since the boiling points were achieved. However a interesting phenomena is that the electrodes was still being heated up

until around 4 minutes (quicker than previous lower voltage cases, 30 minutes and, 8 minutes respectively for 50 V and 70 V) then it stays at 22 °C. During the whole process, the temperature of the electrode only went up from 14 °C to a maximum of 22 °C. The summarized current waveforms shown in Figure 5.15 to some extent reflect the same time scope as electrode temperature varied by the initial increase of the current with spikes for 4 minutes and then the current spikes level stayed the same for rest of the test period. This proves to us that the surrounding heat sink media definitely have impact on the initiation of discharge and hence electrical tracking. With bulk electrodes, it is expected that more heat dissipates through them and the inception voltage hence is need to be higher.

In order to have a more detailed investigation of impact of the surrounding media on heat transfer, including the impact of brass electrodes, the specimens, and underlying support, the following Table 5.1 is made to present the heat properties of those media including material ABS used as one of our specimens and also the underlying support. And the theoretical calculation of heat capacity of those surrounding media was carried out and those results present in Table 5.2.

Table 5.1: Thermal property of different components of the surrounding heat transfer media

Component	Material	Thermal conductivity ($W/m/K$)	Specific Heat Capacity ($J/kg/K$)	Density (kg/m^3)
Electrodes	Brass	380.0	390.0	8960.0
Contaminant film	Solution	0.6	4183.0	998.3
Specimens	Epoxy Resin	0.3	970.0	1970.0
Air	Air	0.0257	1005.0	1.205
Underlying support/ the 2nd type of specimen	ABS	0.18	1200	1040

Table 5.2 the theoretical calculation results of heat capacity of those surrounding media

Component	Material	Dimensions ($mm \times mm \times mm$)	Energy to lift the temperature of 1K (J/K)
Electrodes	Brass	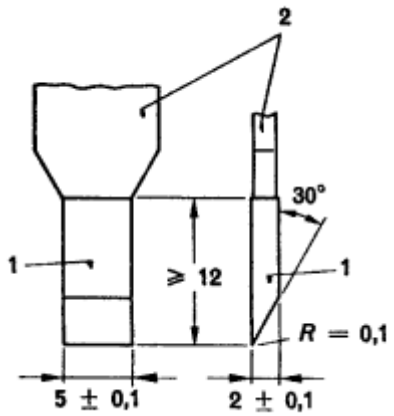 with length of the electrode main part is 50mm	1.8
Contaminant film	Solution	$4mm \times 5mm \times 1mm$	0.08
Specimens	Epoxy Resin	$15mm \times 15mm \times 3mm$	1.28
Air	Air	N/A	N/A
Underlying support	ABS	Cylinder with diameter of 20mm and height of 10mm	3.9
2nd type of Specimens	ABS	$15mm \times 15mm \times 3mm$	0.08

As shown in Table 5.1, the test sample Epoxy resin has the specific heat capacity value of 970.0 $J/kg/K$ with dimension of $15mm \times 15mm \times 1mm$. Three of them are piled up to make the total height of 3mm. Hence the energy needed to lift the temperature by 1K can be calculated as $15 \times 15 \times 3 \times 10^{-9} \times 1970 \times 970 = 1.28$ J/K. By using the same method, it can be found that for the liquid film and underlying support, they are 0.08 J/K, and 3.9 J/K. The theoretical calculation results of heat capacity of those surrounding media have been summarized in Table 5.2 above.

Now it can be found that it is easier for the liquid to be heated up to boiling point for the

epoxy resin specimens while the test sample underneath, the underlying support, and electrodes need bigger amount of energy to be heated up.

Two different situations can be considered. One is the applied voltage is high which lead to high input energy. The liquid will be heated up to its boiling point and evaporate while there is not much time for the surrounding electrodes, epoxy resin specimens which directly contact with the liquid to be heated up. However, if the voltage applied is low, it takes even very long time for the liquid to come to boiling point and evaporates, then the underlying support will dominate the heat transfer with the high value of energy needed to raise the temperature energy. However, it should be noted that the heat transferred to the underlying support flows through the specimens. So the thermal resistance of the specimens will have impact.

As shown in the equation 4.9 $P = \Delta T / R_T$ in Chapter 4, the power conducted to support through specimens can be calculated as $\frac{80}{R_T}$ where $R_T = \frac{1}{0.3} \times \frac{3}{15 \times 15} \times 10^{-3} = 4.4 \times 10^{-5}$ K/w. Hence the power conducted to underlying support should be $1.8\,w$. The input power from the electrical energy under 50V is 0.79 w $(= \frac{50^2}{3160})$. The calculation results indicate that during the period when the liquid has been at boiling state, the power to the underlying support can be very dominant.

It can also be found that the energy to lift the temperature by 1 K is pretty much the same for the ABS specimen and the liquid. This finding indicates that different specimens have different impact on the thermal processes. A higher inception voltage is expected for electrical tracking for ABS since the heat can readily transferred to specimens just as in the liquid.

Other voltage testing

All the other voltage testing results are illustrated in Figure 5.18. It can be summarized that the inception voltage for electrical tracking is 90 V in the specified environmental circumstances in the standard, including the specific pollution degree specified, room temperature and ambient pressure. This also can be proved by the evidence of damages on the specimens show in Table 5.2 in Section 5.4.2 since the test level at 90 V was the first at which damage was seen on the FR-4 sample. We can always see that the current continuously increased during the whole testing period when 60 V was applied. And then as it has been shown in section 5.3.1.2, it was a transient situation when 70 V was applied. It is believed that there are also some voltages just less than 70 V that could make this system reach equilibrium, so that the current went up initially and then as time passed it remained constant at a particular value.

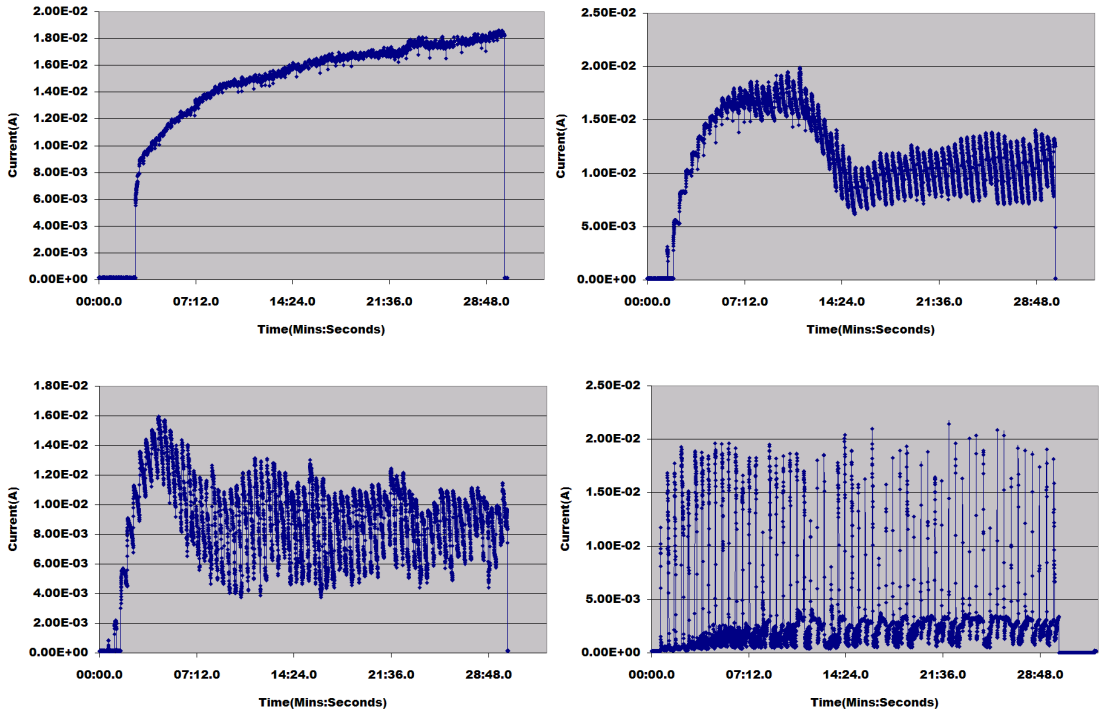

Figure 5.18 RMS current vs. time plot for the tests at 60 V, 80 V, 90 V, 200 V at 1000 mbar on FR-4 (reading from left to right)

For each voltage applied, three measurements were carried out. Although the problem with wet electrical tracking test is that the data of tracking resistance fluctuates greatly, my research shows repeatability, which is reflected in the similarity of the three times' test

results. And the analysis of the thermal dynamic processes is also applicable to 90 V and 200 V test results show above. The heat generated from the electrical losses at 90 V is less than that at 100 V, and from the summarized current waveform it can be seen that it took longer for the system to reach current spikes or initiate discharges. The thermal images also showed temperature could reach the boiling points for the solution. The temperature of electrodes is higher than that for 100 V and took longer time to reach equilibrium.

5.3.2. Behaviour of ABS samples at the atmospheric pressure

The discussion from the mathematical static model developed in Chapter 4 and the test results of tracking on FR-4 boards indicate that the thermal process is the critical factor influencing tracking. However, IEC 112: 2003 is normally used to categorize a material into a certain material group, which is classified based on the measured CTI value of the material. Hence a different material belonging to a different material group from FR-4 was chosen. ABS is a very commonly used thermoplastic used to make light, rigid, molded products with different CTI values of greater than 600 (Material group I based on the definition in IEC 60664), in comparison to FR-4 with CTI values of between 175 and 249 (Material group IIIa based on the definition in IEC 60664).

Similarly, ABS samples were tested at 100,000 Pa and 20 °C using voltages from 50 V upwards until 100 V with steps of 10 V. Steps of 20 V were then applied up to 300 V. Both RMS currents and voltages were recorded.

All test results for ABS are illustrated in the following Figures 5.19-5.24. Not only is the repeatability of the test proven again, but also the most important thing is that the voltage required to initiate electrical discharge for both FR-4 and ABS materials is 90 V. As a conclusion, the material itself has little influence on initiating electrical discharge.

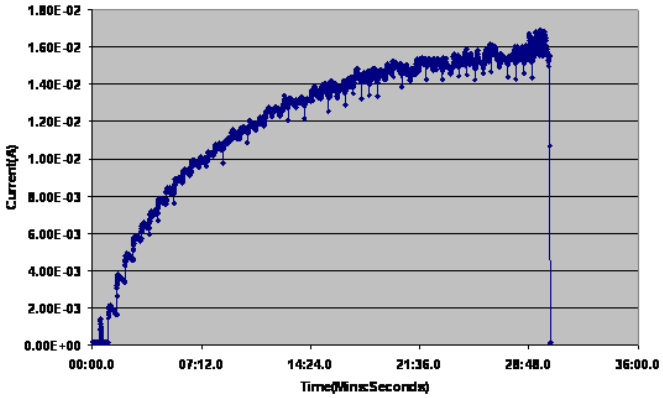

Figure 5.19 Summarized current vs. time plot for the test at 50 V and 1000 mbar on ABS

Figure 5.19 shows us that it follows a similar trend to the FR-4. Within 30 minutes of testing, the leakage current kept increasing, since with the amount of the conductive aqueous contaminant increasing, the conductivity was also increasing. This indicates that a voltage of 50V is not high enough to heat the solution between electrodes to evaporate to boiling point so that electrical tracking could occur. The solution was therefore collecting on the test specimens, which increased the conductivity through the whole testing period.

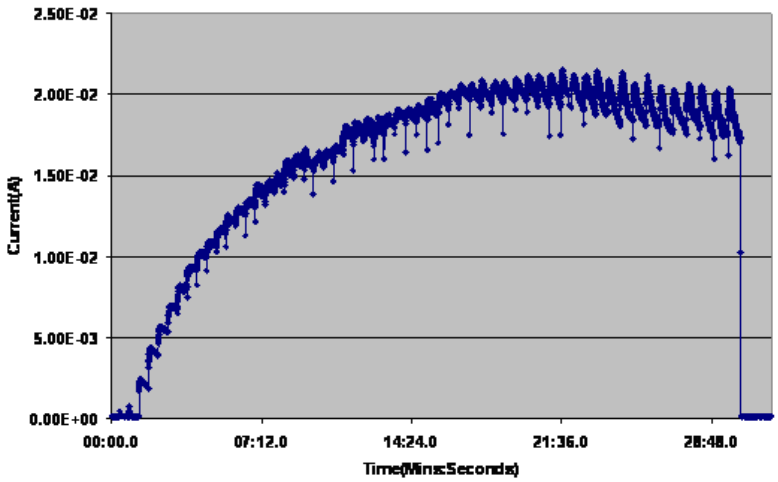

Figure 5.20 Summarized current vs. time plot for the test at 60 V and 1000 mbar on ABS

The plot in Figure 5.20 shows there was equilibrium for current after it initially increased when the voltage of 60 V was applied. The initial increase of current is attributed to the collection of the solution between the electrodes when the heat generated had not yet made the solution evaporate acutely. However, after a few minutes of testing, the current remained constant because power input (electrical power) and power output (dissipating

heat) reached equilibrium. This equilibrium would remain as long as the whole thermal equilibrium was not broken.

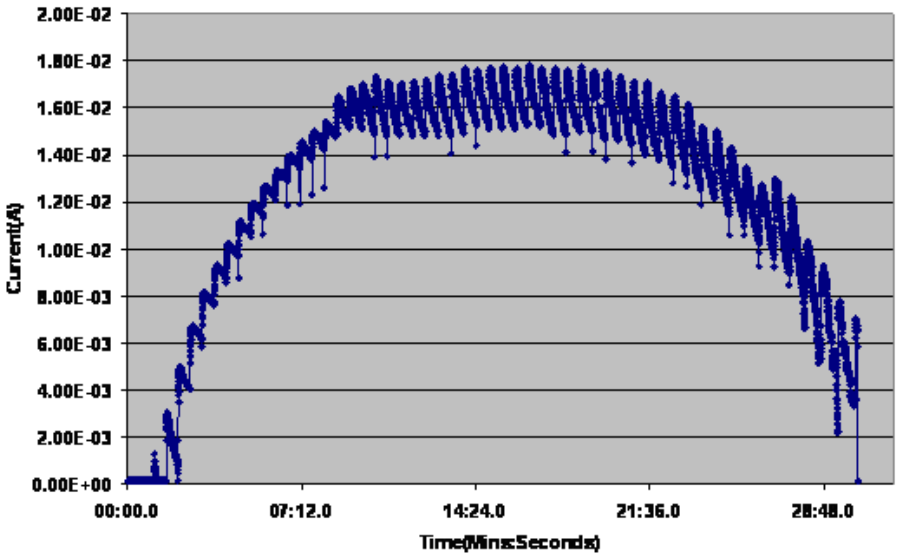

Figure 5.21 Summarized current vs. time plot for the test at 70 V and 1000 mbar on ABS

When the test voltage is increased to 70 V, the current varies, as shown in Figure 5.21. Initially, the current reaches a steady state before falling after around 10 minutes. In this case, the applied voltage is thought to generate a level of heating that evaporates some contaminant, the evaporation rate being roughly equal to the rate of replenishment. This leads to a steady state current flow. However, after a certain period of time, the electrodes start to reach thermal equilibrium and act as less of a heat sink, meaning increased levels of heat can act to evaporate the contaminant thus resulting in the increased circuit resistance and lower current flow seen after twenty minutes. No sample damage was observed at this voltage and the maximum water temperature observed during the final five minutes of the test was 95 ˚C.

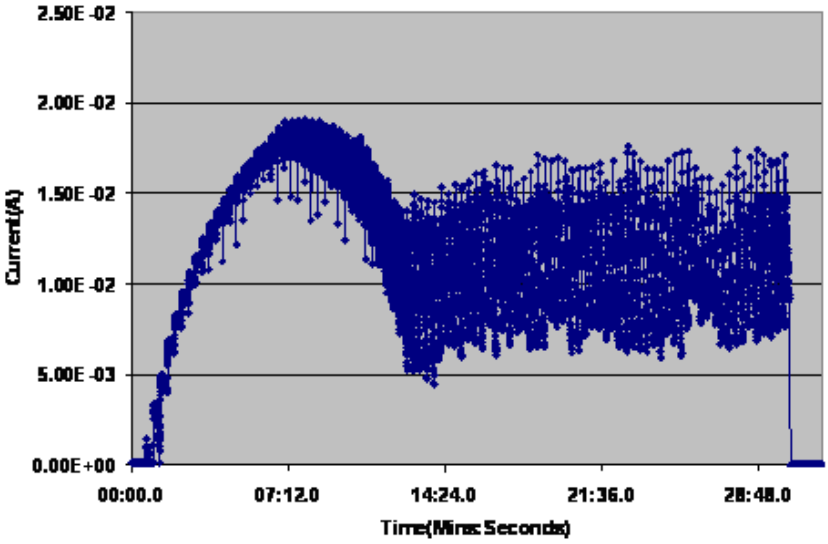

Figure 5.22 Summarized current vs. time plot for the test at 80 V and 1000 mbar on ABS

When the voltage went up to 80 V, the equilibrium process had been shortened to zero, with an initial increase of current, and subsequent decrease, but without current constant between them, the spikes of the leakage current indicating that there were electrical discharges occurring.

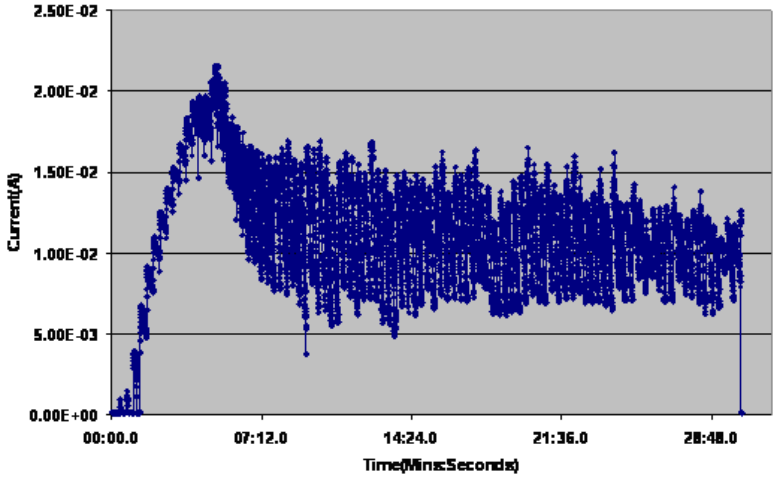

Figure 5.23 Summarized current vs. time plot for the test at 90 V and 1000 mbar on ABS

The abovementioned trend happened more quickly when the voltage applied went up to 90V.

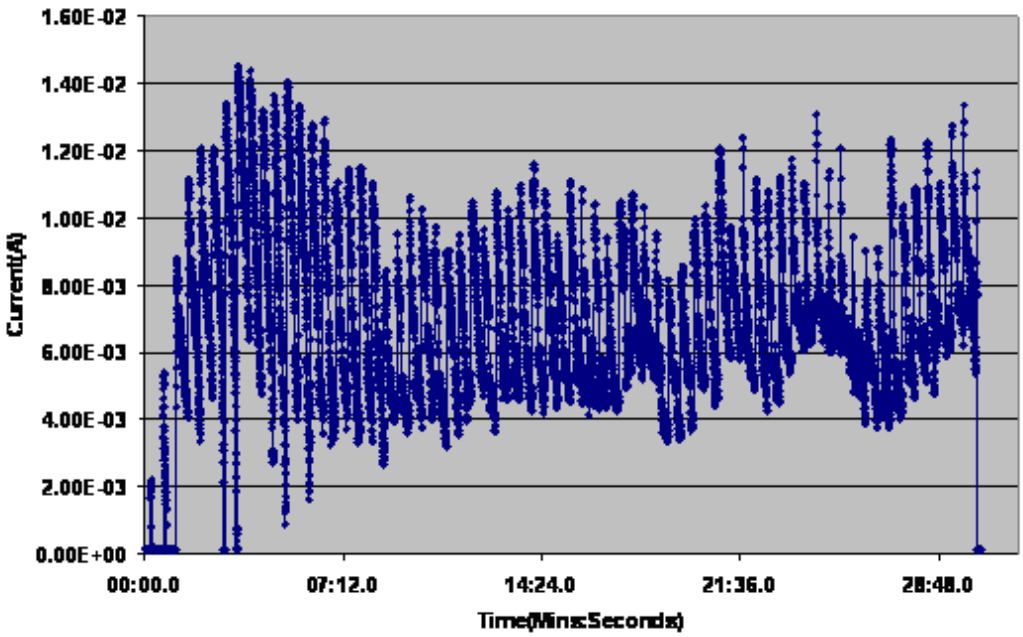

Figure 5.24 Summarized current vs. time plot for the test at 90 V and 1000 mbar on ABS

Eventually spikes of current last for the whole period of testing, which illustrates the electrical discharges occurs acutely. Electrical tracking occurred with damage on the test specimens. All the evidence of damages will be show in the following section 5.4.3.

5.4. Summary of discussion

5.4.1. Four Modes of Electrical Discharges

On the basis of the results described so far and knowledge of tracking processes, it is possible to define the following modes:

- **Mode 1 – Insignificant power:** In this mode, the current flow through the contaminant is too low to heat it sufficiently and cause evaporation. A steady increase in current flow is seen in the gap as the amount of fluid increases. No damage occurs.

- **Mode 2 – Constant current:** At a certain voltage, the current flow causes sufficient heating to evaporate contaminant at the same rate of replenishment leading to a steady state current flow. No damage occurs.
- **Mode 3 – Evaporation, arcing and no re-ignition:** When the contaminant evaporates owing to a high level of heating, an arc occurs in the dry band. Re-ignition does not take place.
- **Mode 4 – Evaporation and significant arcing:** As the voltage is increased further, the system voltage allows re-ignitions of the arc to take place once it has initially been extinguished. Severe damage is seen.

5.4.2. Comparison of the withstand voltages to electrical tracking between the test results and the standards

In IEC 60664, it has been stated that a 4mm gap on a material belonging to material group I under very severe wet conditions would withstand 320 V while for materials in group II, it is less than 320 V and greater than 250 V. Material group IIIa under the same situation would withstand only 250 V. FR-4 and ABS belong to material group IIIa and I respectively. However, their withstand voltage of 90V, which we found in my test, is far lower than those values specified in IEC 60664. The withstand voltage for a 4 mm gap in IPC 2221-A is 800 V at atmospheric pressure for bare boards, which is much higher than my test results. And following table 5.3 provide a comparison of withstand voltages of IEC 60664, IPC 2221 and test results for 4mm gap. It has indicated that the application of these standards with consideration of electrical tracking fault should be cautious.

Table 5.3 Comparison of withstand voltages of IEC 60664, IPC 2221 and test results for 4mm gap at 1000 mbar.

	IEC 60664 (Pollution Degree 3)			IPC 2221	Test Results at 1000 mbar
	Material group I	Material group II	Material group III		
Withstand voltage for 4mm gap	320 V	$250V \leq V \langle 320V$	250 V	800 V	90 V

5.4.3. Visual damages on the specimens

Table 5.4 below clearly demonstrates the damage of electrical tracking on both FR-4 and ABS at atmospheric pressure. The pictures are the physical evidence of a lower voltage being required to initiate tracking.

Table 5.4: Comparison of the damage observed on FR-4 and ABS under atmospheric pressure

Pressure (1000mbar)	30V	50V	70V	90V	100V	300V
FR-4						
ABS						

5.5 Conclusion

The electrical tracking testing method is an accelerating way to find out the tracking resistance within a short time by using much more conductive contaminant than would be found in reality. However, the data of tracking fluctuate greatly, which is the key problem. My research contribution as shown in this chapter is that the repeatability of the test results for both FR-4 and ABS.

A test rig was developed that allowed to apply AC voltage up to 600 V to the contaminated gap on the organic insulating material FR-4 and ABS for certain test period, 30 minutes in my tests. And both raw leakage current/voltage and summarized current data on the test objective were designed to be recorded automatically by the Labview program.

Although different materials belonging to different categories of the material group according to their CTI values were tested by using the standard test methods, we found that the material itself was not the critical factor for initiating electrical tracking. For both FR-4 and ABS, at 50 V the testing showed a gradually increasing leakage current during the testing period. There was no any damage found on the specimens. At around 60 V and 70 V for both materials, due to the equal rate of the replenishment and evaporation, the leakage currents for both cases were presented a constant trend after initial increase for 7 minutes. Then with time going, after 20 minutes' testing the current dropped again. Finally, At 90 V, the summarized current plots illustrated there were spikes which is the characteristic mechanism of electrical arc and the evidence of damages were found for both materials. In this chapter the very typical raw data at 100 V also proved that there was arc taking place. It also should be noted that according to all the three times' repeated test results the reproducibility of the test method has been proven.

When these numbers above mentioned are compared the standard, we see that withstand voltage of 90 V for 4mm gap on both FR-4 and ABS in my tests is much lower that the value of 320 V for material group I and less than 320 V but above 250 for material group II and 250 V for material group IIIa under pollution degree 3 (conductive pollution occurs or dry non-conductive pollution occurs which becomes conductive due to condensation which is to be expected, which is close to the situation of use of solution A in my tests) in IEC 60664 and 800V in IPC 2221.It suggested that the application of the dimensioning of creepage distances in these standards should not be applied.

The comparison also can be done with the calculated withstand voltages in chapter 4. It can be seen that the calculated value under pollution degree3 at atmospheric pressure of 25

V is even lower than test result of 90 V. However, the dynamic thermal processes were not considered in my mathematic model, which could be the reason of this difference.

Finally, it should be emphasized that the reason for electrical tracking on the organic materials is that the conductive pollution layer can lead to electrical current flowing through. With different voltage levels, the pollution layer dried at different rates, and the rate of replenishment is the critical factor. The voltage and replenishment of pollution together have a big effect on the mechanism of initiation of electrical tracking. So as a conclusion the voltage level of any system and potential pollution degree are very important to evaluate whether a system can survive and operate reliably. Then when any dimensioning rules in any standards are employed, these two factors should be evaluated very carefully.

Chapter 6 Experimental Investigation II: CTI tests under the Conditions of Lower Pressure and Varying Conductivity of Contamination

6.1. Introduction

The static mathematical model and computer simulation studies in Chapter 4 show that macro-environmental factors such air pressure, ambient temperature and pollution degree have an impact on electrical tracking formation and hence the values of required voltage. In Chapter 5, the standardized CTI tests have been discussed under atmospheric pressure conditions. It has been proven that the test method used in my research is repeatable, which provides a reliable test method to study further the influences of those environmental factors on electrical tracking.

For aerospace applications, air pressure is a highly critical environmental impact factor. In this chapter we will see a series of CTI tests undertaken in the environment chamber where the surrounding air pressure could vary from atmospheric pressure 1000 mbar (100000 Pa) to as low as 100 mbar (10000 Pa), which is approximately 51,806 feet above sea level. According to the static mathematical model in Equation 4.7 in Chapter 4, the boiling point of aqueous contaminations determine the amount of heat needed to heat the contamination up to boiling point. It is known that air pressure has a big effect on boiling point, as shown in Figure 4.10 in Chapter 4. The lower the pressure, the lower the boiling point would be, and accordingly less heat would be needed to heat the contamination up to boiling. Similarly therefore, under lower pressure less electrical power input is needed for electrical tracking to take place (if we assume both the ambient temperature and pollution degree are constant). By using the same test method as in Chapter 5 but under a lower

pressure, we should expect lower voltages to initiate electrical tracking.

The impact of pollution degree has also been evaluated based on the test results by employing contamination with varying conductivity. These tests were carried out at room temperature and atmospheric pressure. The conductivity of contamination, which is solution A in my research, represents different degrees of pollution. It directly influences the resistance of the electrical conductive path, and consequently would have effect on the value of leakage current flows through it. According to the static model in Equation 4.7 in Chapter 4, the electrical power input would be larger with a more conductive aqueous contamination. Therefore a lower voltage is needed to heat up the contamination to its boiling status, which leads to a higher level of evaporation and consequent formation of electrical tracking. As a conclusion, we should expect lower voltage for higher conductivity solution tests and higher voltages for lower conductivity solution tests compared to standardized CTI test results.

Low pressure experiment conditions and procedures are presented in this chapter first Discussion of the results and comparison with IEC 60664 and IPC 2221 will be provided afterwards. And then the tests employing the contamination of varying conductivities will be then shown with the discussion of test results at last.

6.2. Low pressure CTI tests

To evaluate the impact of air pressure, experimental tests by using the same test methods as explained in Chapter 5 were carried out. In the following section 6.2.1 the differences of experiment conditions from the standardized ones are presented firstly. Then the test results are illustrated and then discussed.

6.2.1. Experiment conditions

Test Circuit

Figure 5.1 in Chapter 5 shows the circuit diagram used for the tests. The test gaps for lower

pressure tests were located in the environment chamber capable of controlling pressure between 100,000 Pa (1000 mbar) to 10,000 Pa (100 mbar) and temperature between -50°C and 20 °C. The chamber has internal dimensions of 0.6 m x 0.6 m x 0.6 m and is equipped with electrical connectors. The details of the electrical circuits are provided in Section 5.2.1, in Chapter 5. Electrodes and the solution used in low pressure tests are the same as those in the standardized CTI tests.

Test Specimens

Only FR-4 material was used. Flat surfaces of test insulating materials were used at least 3mm thick according to the standard, with dimensions of 20 mm x 20 mm so that the area was sufficient to ensure that during the test no liquid flows over the edges of the specimen. To gain FR-4 specimens with a thickness of 3 mm, three 1mm thick FR-4 boards were stacked together for each of the tests.

Dropping Devices and Test Solution

The surfaces between the electrodes were wetted with drops of the test solution at intervals of 30 ± 5 s. The drops fell centrally between the electrodes from a height of 30 mm to 40 mm. The size of the drops was $20\,mm^3$. A medical transfusion dropping system with a hypodermic needle was used to meet the abovementioned requirement. To control the droplet of the contaminants falling on the specimen located in the pressure-tight environment chamber when the test is ready to go, a DC powered motor was used to pull up a very small bottle on top of the specimen which is used to collect the continuously falling down liquid during the vacuuming period. Prior to each test, the needle or other outlet for the drops was cleaned and sufficient drops let out to ensure that the correct concentration of the test solution is used. This solution A is mixed by 0.1 ± 0.002 % of mass ammonium chloride (NH4Cl) with deionized water with resistivity at 23 ± 1 °C is 395 ± 5 $\Omega \cdot cm$.

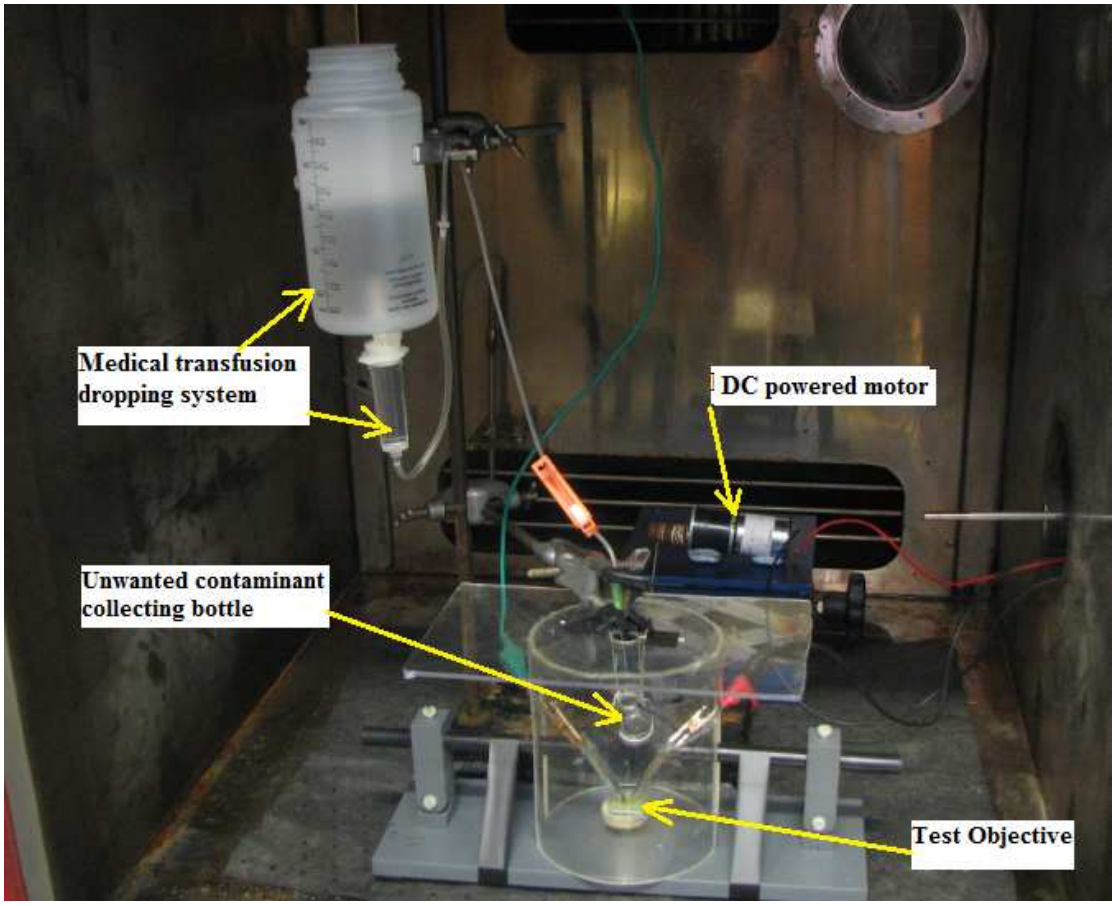

Figure 6.1 Illustration of CTI test dropping system and test rig in the environment chamber for lower air pressure testing.

Test Procedure

CTI tests were carried out on FR-4 specimens at varying air pressure. The voltage applied ranged from 50 V up to 100 V with steps of 10 V. Above 100 V the voltage steps were increased to 20 V until 300 V for both FR-4. For each voltage, the test was carried out three times.

The experimental work was carried out using the following procedures:

1. The resistor connected in series in the circuit was adjusted to the right values so that the maximum current could only be 1 A at the worst situation when the test gap was short-circuited. For example, if the voltage to be applied is 50 V, the resistance of the slide rheostat should be set to 50Ω, which is the possible worst case when the short

circuit occurs.

2. The three pieces of FR-4 specimen were cleaned by the cloth if necessary and domestic cleanser was used to clean fingerprints, grease or oil from the surfaces.
3. The gap distances were set to 4mm by using the slide caliper. The stack of specimens was then clipped onto the plastic plate with some pressure applied by an insulating tap on the electrode extensions.
4. The flow rate of aqueous contaminant was set to one droplet every 30 ± 5 seconds, and was allowed to run for a while until the flow was stable.
5. A multimeter was used to test the applied voltage at the output points of the transformer for the value expected before the specimens were wetted by the test solutions.
6. The pressure set point of the environment chamber was set to a certain low pressure value. This was then switched on until the pressure was constant around the set point.
7. The DC powered motor was switched on to pull up the very small bottle containing the pre-test pollution liquid. Voltage was applied to begin the test.
8. Tests were carried out until the leakage current reached the threshold. The circuit was cut off by a control circuit including timer, circuit breaker and overcurrent relay in series. Otherwise when 50 drops of aqueous contamination had fallen, the circuit was cut off based on the timer record.
9. Labview software and hardware were used to record the leakage currents and voltages. Fifty water drops were applied to each specimen with 30 s between each

droplet. During the tests, data was recorded using an NI LabView system. Voltage and current signals were digitized using a 12-bit data acquisition card running at 10 kS/s. stored data included snap shots of the actual voltage and current waveforms and calculated RMS/peak values that were logged every 0.1 s.

6.2.2. Experimental results for the 100 mbar tests

FR-4 samples were tested at 100, 00 Pa (100 mbar) and 20 °C using voltages from 20 V upwards until 100 V with steps of 10 V. By using National Instrument hardware and software Labview, summarized voltage and current signal files with testing period were recorded. The raw current and voltage waveforms were also recorded.

The following figure 6.2 presents the comparison of summarized current vs. time plots for the test at both 100mbar and 1000 mbar pressure. The test result shown in Figure 6.2 (a) at 20 V, 100 mbar indicates that the electrical discharges and tracking did not take place when the voltage of 20V was applied, since it can be seen that the currents during the 30 minute test period gradually increased. Comparing to the result shown in Figure 6.2(b) at 50 V, 1000mbar, the gradual increasing current plot proves the voltages applied were not big enough to evaporate the contaminant before the next drop of it refilling. Hence the increase amount of contaminant solution kept collecting on the specimens.

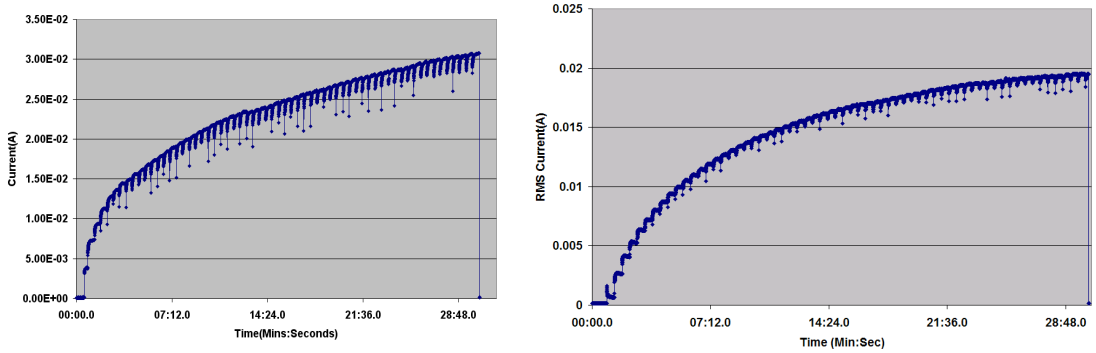

(a) Test result at 20V, 100mbar. (b)Test result at 50V,1000mbar.

Figure 6.2 Comparison of summarized current vs. time plots for the tests at both 20 V, 100 mbar and 50 V, 1000 mbar on FR-4

According to the understanding in Chapter 5, it is expected when the voltage applied increases, at some point there is a state where the equilibrium of the rate of replenishment and evaporation reaches. The current plot during testing should appear constant for a while as show in Figure 6.3 (b) for the test at 70 V, 1000 mbar. However, under lower pressure 100 mbar condition, this process can not be easily found. As it shows in Figure 6.3 (a) where the voltage applied was increased to 40 V, the summarized current plot has already shown the spikes which is the typical characteristic of electrical discharge which will lead to electrical tracking. The evidence of damages on the specimens will be presented in the following section 6.2.3. And at 100mbar the inception voltage of electrical tracking would be 40V.

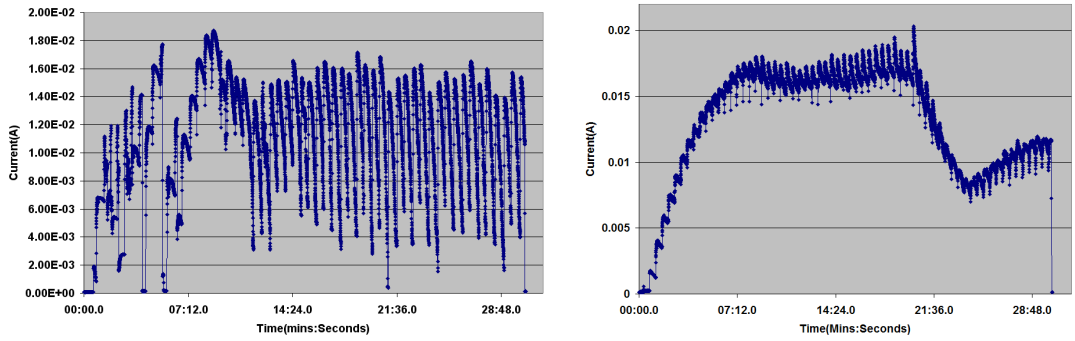

(a) Test result at 30 V, 100 mbar. (b)Test result at 70 V,1000 mbar.

Figure 6.3 Comparison of summarized current vs. time plots for the tests at both 30V, 100mbar and 70 V,1000 mbar on FR-4

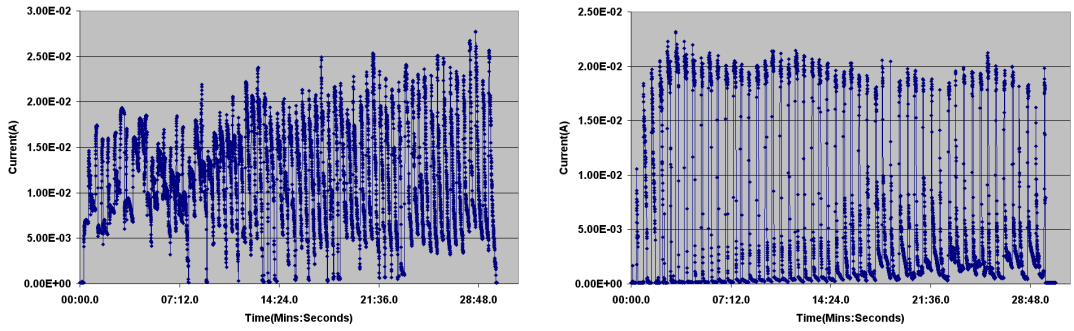

(a) Current vs. Time plot at 40 V and 100 mbar (b) Current vs. Time plot at 80 V and 100 mbar

Figure 6.4 Summarized current vs. time plots for the tests at, 40 V,80 Vand 100 mbar on FR-4

When the voltage was increased further with steps of 10 V, large current spikes were found during the whole testing period, shown in Figure 6.4 (a) and (b). Damage due to electrical tracking on these specimens was observed as progressively worsening. The evident of damages will be show in Section 6.2.3.

6.2.3. Discussion of the results

Work by other authors on the failure of organic insulating material samples exposed to discharges state that they more readily fail at low pressure than when they are at atmospheric pressure [93, 94]. Table 6.1 below clearly demonstrates the influence of lower pressure on tracking on the FR-4 samples. The pictures are the physical evidence of a lower voltage being required to initiate tracking. In addition, damage is more severe at lower pressures, possibly due to the lower latent heat of vaporization of liquids at low pressure and hence the longer time available for arcing.

Table 6.1: Comparison of the damage observed on plain circuit boards (FR-4) at varying pressure

Pressure (mbar)	30 V	40 V	80 V	90 V	100 V	300 V
1000						
100						

From both summarized current plot shown in Figure 6.3 (a) and evidence of damages show in Table 6.1, it can be summarized that the inception voltage of electrical tracking at 100mbar on FR-4 is 40 V which is much lower than 90 V at 1000mbar.

Referring to Table A5 in Appendix A from IEC 60664, it can be found that the standard recommends the withstand voltage is 250 V for a 4 mm creepage distance without any

pressure information at all for material group III, bigger than 250 V but smaller than 320V for material group II, and 320 V for material group IIIa. FR-4 used in the tests belongs to IIIa. However, it can be noticed that Table A4 provides altitude correction factors for clearances but not creepage distances. With the altitude correction factors, which will come up a number of less than 10 V as withstand voltage. IPC 2221, referring to Table A7 Electrical Conductor Spacing in IPC 2221-1 in Appendix A, also specifies the voltage range from 170 V to 250 V for the creepage distance of 4mm for bare board used above 3050 m (696.4 mbar) without mentioning CTI material groups categories at all.

Comparison with IPC 2221A indicates that dimensioning of creepage distance to avoid electrical tracking failure is not safe to be applied for aerospace application. And the classification of the altitude and air pressure condition is too rough for aircraft designers to utilize. And IEC 60664 seems to give a safe number when the altitude correction factors defined for clearances was used to creepage distances. However, IEC 60664 fails to explain why the material groups really have influence on dimensioning of creepage distances. From my research, the material itself will have impact on the thermal dynamic processes of the electrical tracking systems although it is not as critical as the impact of the pollution. Even electrodes including its mass and thermal property need to carefully consider. As a conclusion, it is necessary to conduct testing on the materials designer would employ on aircraft.

6.3. Atmospheric pressure CTI tests with a solution of the half conductivity of the solution A

To evaluate the impact of conductivity, firstly the standardized CTI tests with the solution of half conductivity of solution A defined in IEC 60112:2003 were carried out and their results and discussion are shown in the following sections.

6.3.1. Experiment conditions

All the tests in this section were done by using the same test methods as stated previously in Chapter 5. The only difference was that the solution used was not the solution as defined in IEC 60112. This solution is mixed by 0.02 ± 0.002 % of mass ammonium chloride (NH4Cl) with deionized water with the resistivity at 23 ± 1°C being 790 ± 5 Ω·cm, which is double of original resistivity (resistivity is reciprocal with conductivity, hence it is half of the original conductivity of solution A).

6.3.2. Experimental results

FR-4 samples were tested at 100,000 Pa (1000 mbar) and 20 °C using voltages from 69 V upwards until 198 V. By using National Instrument hardware and software Labview, summarized voltage and current signal files with testing period were recorded. The raw current and voltage waveforms were also recorded.

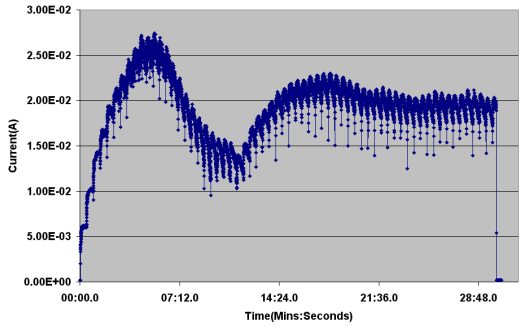

(a) Current vs. Time plot at 99 V and 1000 mbar

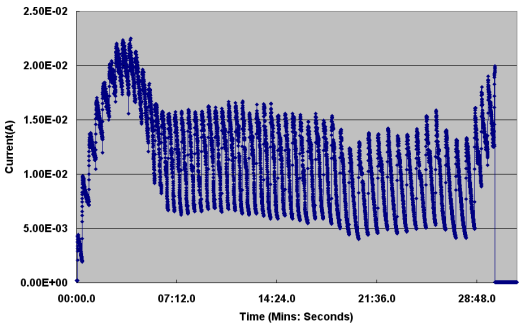

(b) Current vs. Time plot at 113 V and 1000 mbar

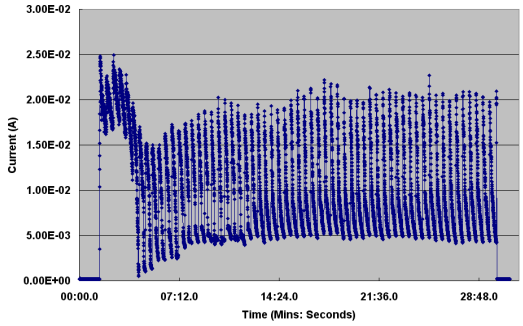

(C)Current vs. Time plot at 141 V and 1000 mbar

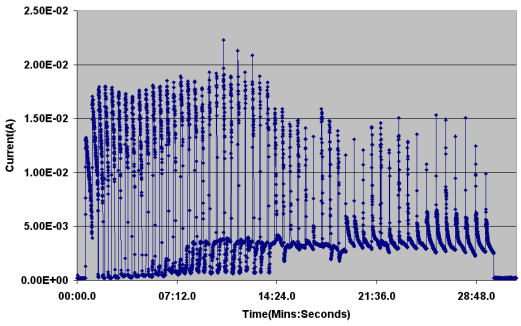

(d) Current vs. Time plot at 198 V and 1000 mbar

Figure 6.5 Summarized current vs. time plot for the test at 99 V(a), 113 V(b), 141 V(c) and 198 V(d) at 1000 mbar on FR-4 with the solution of 790 ± 5 Ω·cm.

When the conductivity of the solution was halved (the resistivity was doubled), leakage current flowing through the conductive path was lower. Therefore higher voltages were needed to heat the same amount of the liquid. It should be noted that conductivity also influenced the boiling points as show in Figure 4.10 in Chapter 4. The test results shown in Figure 6.5(a) indicate that electrical tracking did not even take place when the voltage of 99 V was applied, since there are no large current spikes found. Current first increased to its peak, then dropped for seven minutes and finally reached a constant. From the analysis in Chapter 5, the increase stage is due to increase in the amount of the solution collecting on the specimens. It takes time for the system to reach the final thermal equilibrium, when we can see that the current became constant.

When the voltage was raised to 113 V, the large current spikes indicate that electrical tracking occurred, and it also can be seen that the current increase and drop period was shortened. It took less time for the system to reach thermal equilibrium. However, in this case, the voltage was enough to trigger electrical discharges and hence electrical tracking. With higher and higher voltages applied, figures (c) and (d) clearly show the phenomena explained previously. Damage on specimens also provides evidence of the electrical tracking, as shown in Table 6.2. As a summary, the inception voltage of electrical tracking at atmospheric pressure but with the solution of half conductivity of original one is 113 V.

Table 6.2: Damage observed on plain circuit boards (FR-4) at atmospheric pressure with the solution of 790 ± 5 Ω·cm.

Pressure (mbar)	99 V	113 V	127 V	141 V	198 V
1000		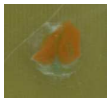			

6.3.3. Discussion of the results

The pictures in Table 6.2 are the physical evidence of a higher voltage (113 V) being

required to initiate tracking with half conductivity solution comparing to the inception voltage of 90 V with original solution. In addition, damage is less severe at lower conductivity.

To compare this with IEC 60664 and IPC 2221 standards, it has been found that IPC 2221 has not defined the pollution degree factor in their dimensioning rules while IEC 60664 only gives very vague description of pollution degrees, as show in Chapter 3. If we assume the Pollution Degree 3 stated as conductive pollution occurs or dry non-conductive pollution occurs that becomes conductive due to condensation, which is to be expected, again 250 V for a 4mm gap distance is far dangerous to apply. It should be noted that IEC 60664 has no dimensioning rule for pollution degrees worse than Pollution Degree 4, stated as continuous conductivity that occurs due to conductive dust, rain or other wet conditions.

6.4. Atmospheric pressure CTI tests with a solution of the double conductivity of the solution A

To evaluate the impact of conductivity, the standardized CTI tests with the solution of double conductivity of solution A defined in IEC 60112: 2003 were carried out and their results and discussions were shown in the following sections.

6.4.1. Experiment conditions

All the tests in this section were done by using the same test methods as stated before in Chapter 5. The only difference was that the solution used was not the solution as defined in IEC 60112. This solution is mixed by 0.005 ± 0.002 % of mass ammonium chloride (NH4Cl) with deionized water with the resistivity at 23 ± 1 °C being 197.5 ± 5 Ω·cm, which is double the original resistivity (resistivity is reciprocal with conductivity hence it is double the original conductivity of solution A).

6.4.2. Experimental results

FR-4 samples were tested at 100,000 Pa (1000 mbar) and 20 °C using voltages from 50 V upwards until 198 V. By using National Instrument hardware and software Labview, summarized voltage and current signal files with testing period were recorded. The raw current and voltage waveforms were also recorded.

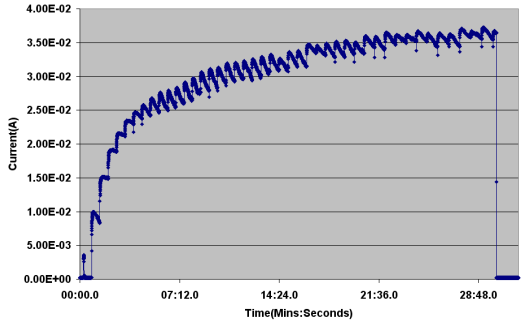

(a) Current vs. Time plot at 56 V and 1000 mbar

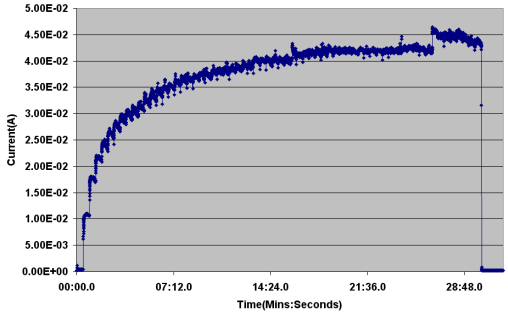

(b) Current vs. Time plot at 70 V and 1000 mbar

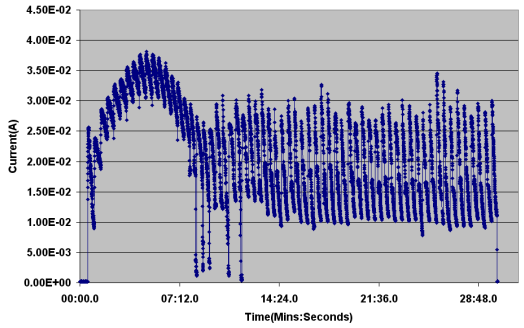

(c) Current vs. Time plot at 84 V and 1000 mbar

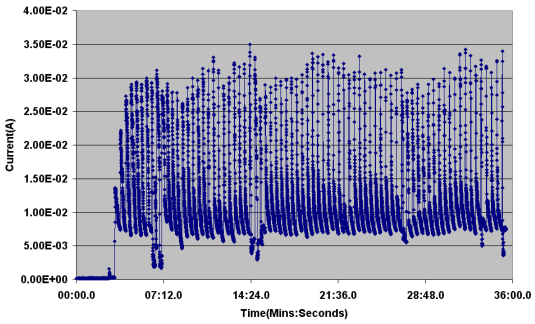

(d) Current vs. Time plot at 99 V and 1000 mbar

Figure 6.6 Summarized current vs. time plot for the tests at 56 V(a), 70 V(b), 84 V(c) and 198 V(d) at 1000 mbar onFR-4 with the solution of 197.5 ± 5 Ω·cm.

When the conductivity of the solution was doubled (the resistivity was halved), leakage current flowing through the conductive path was higher. Therefore lower voltages were needed to heat the same amount of the liquid. It should be noted conductivity also influences the boiling points as show in Figure 4.10 in Chapter 4. It can be seen in Figure 6.6(a) that the current kept increasing during the testing period of 30 minutes, which indicates the collection of the solution on the specimens. The voltage of 56 V was not enough to heat the solution up and evaporate it to trigger arcing and hence the formation of electrical tracking. Figure 6.6(b) shows that when 70 V was applied to the electrodes,

currents increased and reached a constant after 20 minutes. When the voltage continued to be increased to 84 V, after four minutes' rise and another three minutes 'drop with the current plot, there were current spikes indicating arcing and electrical tracking occurred. When 99V was applied, from the very beginning of testing arcing took place and lasted for the whole period of testing. This would lead to severe damage on the specimens, which has been proven in Table 6.3. As a summary, the inception voltage of electrical tracking at atmospheric pressure but with the solution of half conductivity of original one is 84 V.

When the voltage was raised to 99 V, large current spikes indicating electrical tracking were found and it also can be seen that the current increase and drop period was shortened. It took less time for the system to reach thermal equilibrium. However, this time the voltage was enough to trigger electrical flashover and hence electrical tracking. With higher and higher voltages applied, figures (c) and (d) clearly show the phenomena explained previously. Damage on specimens also provide evidence of the electrical tracking in Table 6.3.

Table 6.3: Damage observed on plain circuit boards (FR-4) at atmospheric pressure with the solution of 197.5 ± 5 Ω·cm.

Pressure (mbar)	56 V	70 V	84 V	99 V	127 V	169 V
1000						

6.4.3. Discussion of the results

The pictures in Table 6.3 are the physical evidence of a lower voltage (84 V) being required to initiate tracking with half conductivity solution comparing to the inception voltage of 90 V with original solution.. In addition, damage is more severe compared to those results with

a half conductivity solution due to the longer time available for arcing.

Again there is no any information regarding the pollution degree in IPC 2221. Additionally, IEC 60064's dimensioning rules are based on a very vague description of the pollution degrees. 250 V for a 4mm creepage distance is not applicable when compared with my test results.

6.5. Discussion

The comparison of the inception voltages of electrical tracking at 100mbar with the IEC 60664 and IPC 2221 is presented in Table 6.4. IEC 60064 has no information regarding pressure influence at all in its dimensioning rules of creepage distances. However, it can be noticed that Table A4 provides altitude correction factors for clearances in IEC 60064 but not creepage distances. If employing the altitude correction factors, which will come up a very small number of less than 10 V as withstand voltage comparing to existing numbers show in the table. Then this will show that IEC 60664 would be very conservative in term of definition of withstand voltage of 4mm creepage distances for lower air pressure. Compared with IPC 2221's creepage distance of 4 mm for 3050 m (696.4 mbar), the voltage of 170 V-250 V is much higher than the withstand voltage of 40 V found in my tests. The use of IPC 2221 need to be cautious.

Table 6.4 Comparison of withstand voltages of IEC 60664, IPC 2221 and test results for 4mm gap on FR-4 at both 1000mbar and 100mabar.

	IEC 60664 (Pollution Degree 3)			**IPC 2221**		**Test Results**	
	Material group I	**Material group II**	**Material group III**	**Above sea level up to 3050 m (696.4 mbar)**	**Above 3050 m (696.4 mbar)**	**1000 mbar**	100mbar
Withstand voltage for 4mm gap	320 V	$250V \leq V \langle 320V$	250 V	800 V	170-250 V	90 V	40 V

When conductivity of the solution was doubled (the resistivity was halved), leakage

current flowing through the conductive path was higher. Therefore lower voltages were needed to heat the same amount of the liquid. The reverse is also true. It should be noted that conductivity also influences the boiling points as show in Figure 4.10 in Chapter 4. With a more conductive solution (a more severe pollution situation), physical damage on specimens is also much more severe.

In terms of pollution degrees, the IEC 60664 standard lacks quantified statements. With the rough pollution degree definitions, both half conductivity tests and double conductivity tests were under pollution degree 3, since there is no information for Pollution Degree 4. The withstand voltages for a 4mm creepage distance under Pollution Degree 4 for either half or double conductivity solution were 113 V and 84 V respectively. They are much lower than the 250V specified in IEC 60664 for pollution degree 3, which indicates that the usage of the standard is not acceptable. It also can be seen that the dramatic increase of the withstand voltages for 4mm gap on the material belonging to material group III from 250 V at pollution degree 3 (conductive pollution occurs or dry non-conductive pollution occurs which becomes conductive due to condensation which is to be expected), to 400V at pollution degree 2 (Only non-conductive pollution occurs except that occasionally a temporary conductivity caused by condensation is to be expected) and 1250 V at pollution degree 1 (No pollution or only dry ; Non-conductive pollution occurs. The pollution has no influence). Finally IPC 2221 have no information about pollution degrees, which only provide the withstand voltage of 800 V for 4 mm gap at atmospheric pressure on FR-4.

Table 6.5 Comparison of withstand voltages of IEC 60664, IPC 2221 and test results for 4mm gap on FR-4 at 1000mbar.

	IEC 60664 (Material Group III)			**IPC 2221**	**Test Results**		
	Pollution Degree 3	**Pollution Degree 2**	**Pollution Degree 1**	**Above sea level up to 3050m (696.4 mbar)**	395 Ω · cm	790 ± 5 Ω · cm.	197.5 ± 5 Ω · cm
Withstand voltage for 4mm gap	250 V	400 V	1250 V	800 V	90 V	113 V	84 V

In Chapter 4, The calculated value of withstand voltages at ambient pressure 1000 mbar for 4 mm gap on the solid insulating material surface was around 150 V by using deionized water with the resistivity of 125k Ω·cm. It is a little bigger than the test result of 113 V at 1000 mbar and 125k Ω·cm. And while at lower pressure 100 mbar , it dropped dramatically to 46V for deionized water; it was only 8.4V for the highly conductive solution A at 1000 mbar while it is as big as 90V from testing. and the withstand voltage of 5.5 V at 100 mbar with solution A is achieved from calculation while it was 40 V. This again represents the fact that the more conductive the aqueous contamination, the lower the voltages are that are needed for electrical tracking. The big differences between calculated results and test results could be due to the equation 4.7 only utilize the steady-state calculated thermal parameters to calculated thermal resistances.

Table 6.6 Comparison of withstand voltages of calculated result in Chapter 4 and test results for 4mm gap on FR-4 at both 1000mbar and 100mabar.

	Calculated Results						Test Results		Test Results	
	Deionized water (125k Ω·cm)		Solution A (395 Ω·cm)		790 ± 5 Ω·cm	197.5 ±5 Ω·cm	790 ± 5 Ω·cm.	197.5 ±5 Ω·cm	Solution A 395 Ω·cm	Solution A 395 Ω·cm
	1000 mbar	100 mbar	1000 mbar	100 mbar	1000 mbar	1000 mbar	1000 mbar	1000 mbar	1000 mbar	100 mbar
Withstand voltage for 4mm gap	150 V	46 V	8.4 V	5 V	32.9 V	16.5 V	113 V	84 V	90 V	40 V

6.6. Conclusion

The use of the IEC 60112 test procedure has allowed the examination of the relative tracking performance of FR-4 at reduced pressures such as would be found in an aerospace environment. The work has shown that the change in the boiling point of the liquid has a significant impact on the tracking performance and damage being instigated at a lower voltage and lower pressures. Increased levels of damage have been seen at lower pressure in FR-4. This may be due to different mechanisms of decomposition taking place, but these

processes need to be more clearly understood.

The computational simulation and experimental data confirm that the guidelines for creepage distances in IEC 60664 and IPC 2221 are not applicable for aerospace application considering the environment impact. The calculation results here tend to be lower than those from the standard because dynamic thermal processes have not accounted for in my model.

Chapter 7 Experimental Investigation III: CTI tests Developed for Varying Creepage Distances

7.1. Introduction

The standard CTI tests discussed before were carried out on a limited 4mm gap distance. The reason for that is firstly this test method was designed to indicate the relative resistances of different solid electrical insulating materials to tracking for a voltage up to 600V when the surface is exposed to water mixed with the addition of contaminations under electrical stress, but not to find out withstand voltages for varying creepage distances. Hence, the parameter of the gap distance should be the same for the purpose. Secondly, the flow rate of the dropping solution was also particularly designed for the 4mm gap so that it is just right to allow the liquid film formed between the two electrodes to evaporate at certain voltages applied to initiate electrical tracking under a certain time. By changing the original gap distance to a shorter one, the flow rate used now will be so large that there is no time for the aqueous contaminant to evaporate to initiate electrical tracking, although the voltage needed would be much lower. If the gap was longer than 4mm, the flow rate would be too low to actually form any continuous conductive current path between the electrodes. All the difficulties make it challenging to extend the CTI test method to varying gap distances.

My research developed a way to upgrade the CTI test method to be used for varying gap distances under atmospheric pressure. Two key changes to the original method are with dropping devices and the shape of the specimen. Apart from the successfully developed test technique for varying gaps, a range of possible test techniques were tried to resemble

the real pollution wet condition.

This chapter first presented the section of test techniques for varying creepage distance tracking tests. Their limitation and the reason of failure to application would be discussed. And then a range of test cases were shown consequently. Those test results with the upgraded CTI test method for a 4mm gap were compared with those by using the standardized CTI test method. The repeatability of the test result with the upgraded CTI test method is validated. Two gap distances 2mm and 8mm were tested and their test results were presented and discussed. Finally the test results were discussed and compared with dimensioning rules in IEC 60664 and IPC 2221.

7.2. Selection of a wetting technique for the varying creepage distance tracking test

As explained in introduction section of the chapter, a system to produce the pollution environment with a right flow rate, the same as the rate defined by standardized CTI test in IEC 60112:2003, is needed to design. The key objective is that the pollution should not have orientation, which is different from droplet falling on the solid insulting material surface between two electrodes.

Initially, the idea was simply based on the utilization of a small water pump to make the aqueous contaminant circulating from a container and transferring pipes. Those pipes were equipped with various nozzles with different designs and sizes. It was hoped that the nozzles would provide fine mists to the testing space. However, the first challenge was lack of enough water pressure to make the mists to be really fine. As a result, this simple design of mist system could only give a bundle of big droplets and they normally ejected to a same area with a big diameter.

Then we found a pond mister produced by professional manufacturers. The idea was to produce a mini pond mister system in the aqueous contaminant container. The pond mister

was located underneath the water level in a container. By changing the distance from the mister to the water level, the flow rate of the mist generated can be roughly controlled. And then the test objective which was FR-4 board in my research would be positioned just above the water level submerging in the fog. This time we achieved very fine mist environment. Then the next parameter of the system, the flow rate of the mist, was checkout.

The flow rate of mist was checked by measuring the liquid gathered in a Petri dish (This method was also used for the following humidifier method). It was positioned at the same location where the test objective will be placed. And within certain time the weights of the liquid collected in the Petri dishes were measured. And then the flow rate was calculated with unit of mm^3/minute. As it is known that the flow rate of the standardized CTI test is 40 mm^3/minute. Considering the area of Petri dish was different, so the unit for evaluation of the flow rate was included the per typical specimen area (20 mm×20 mm).

Unfortunately, it was found that it is very difficult to achieve the same flow rate used in the standardized CTI tests. Hence No further research was continued by using this technique. This technique is still a possibility to improve the standardized technique.

Finally, instead of the devices to provide droplets with intermittent time period (every 30 seconds), a domestic humidifier was introduced. It can provide continuous very fine mists. With condensation, we achieved a very uniform flow rate of liquid film between electrodes and also comparative to the original flow rate as specified in IEC 60112: 2003. The most important thing is the mist generated by the humidifier does not have orientation so no matter how big or small the gap would be; the same flow rate should be achieved. However, the surface tension of liquid should be taken into consideration if the two electrodes are very close too each other especially in order a few millimeter or even less. These challenges has been successfully solved by the test technique presented in this chapter later and what is more is that the technique can be applied in environment

chamber where the impact of air pressure can be evaluated.

7.3. Experimental conditions

The standardized CTI test circuits were used as described in IEC 60112, shown in Figure 5.1 in Chapter 5. And the same electrodes arrangements were applied as described before. However, the dropping devices and shape of specimens were different. Figure 7.1 presented the picture of the upgraded CTI test rig with the humidifier.

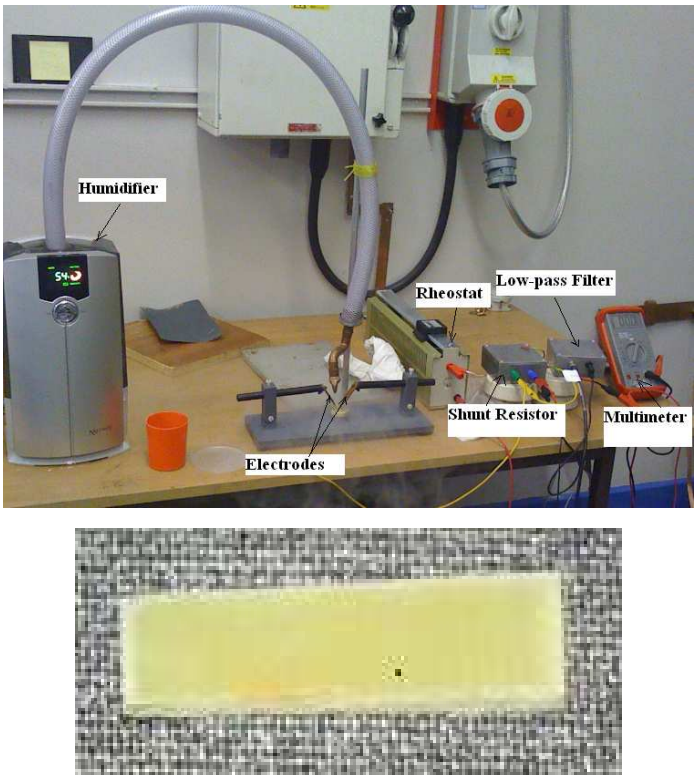

Figure 7.1 Illustration of the CTI test dropping system and test rig and a FR-4 test sample

Only FR-4 material was used. The flat surfaces of test insulating materials were used with dimensions of 20 mm by 5 mm. Since the width of the electrodes was 5 mm, this design can avoid the influence of the surface tension of liquid when two electrodes are too close to each other. The surface with a dimension of $20\text{mm}\times20\text{mm}$ used in the standardized CTI methods had massive extra space beside the space between the electrodes to hold the extra aqueous contaminant. Due to the surface tension of the liquid, especially for those with a very small gap distance (2 mm), those redundant liquid would change the amount of liquid actually supposed to be condensed between electrodes. So, the way to get rid of the extra area of the specimen will prevent those extra liquid from falling on the

specimens. By doing validating tests with the 4mm gap, shown in the following section, it will prove that this design does prevent the variation of the flow rate of the contaminant, and consequently repeatable test results can be gained.

The surfaces of the test specimens were cleaned by using a cloth if necessary with domestic cleanser to make sure they were free of dust, dirt, fingerprints, grease, oil, mould release, or other contaminants which can influence the test results but not lead to any swelling.

The surfaces between the electrodes were wetted with fine mist generated by the humidifier, as shown in Figure 7.1. The humidifier caller NScessity Digital Combination Warm Mist and Humidifier was bought from Argos with the following specifications of 8 hours timer, 3.5 L water tank, warm mist and ultrasonic humidifier. The flow rate was controlled by the humidity setting on the humidifier. However, the difficulty is to generate the continuous flow of mist since the domestic humidifier itself is controlled by the inner sensor which will automatically switch on/off the humidifier due to the humidity of the environment humidity. By using the long tube, as shown in Figure 7.1, the inner-side environment of the humidifier was stable, which would not be changed according to the amount of mist generated. By collecting the condensed solution using a Petri dish, the flow rate was controlled to the same flow rated stated in IEC 60112. The same humidity level was always used. The solution was mixed by 0.1 ± 0.002 % by mass ammonium chloride (NH4Cl) with deionized water with the resistivity at 23 ± 1 °C is 395 ± 5 $\Omega \cdot$cm.

7.4. 4mm gap tracking test at the atmospheric pressure

Similar to the standardized CTI tests, the new test method was employed to carry out the testing on FR-4 specimens with a 4mm gap from 50 V with a voltage step of 10 V until 150 V when electrical tracking can definitely lead to damages on the specimens. Each voltage tests were repeated for three times. All the current and voltage raw data were recorded by the Labview program designed for the previous standard CTI tests. However, we are more interested in the summarized current plot vs. time plot so that they can be

compared to those in chapter 5 by using the standardized test method to validate the upgraded test method and also refer to the different stage discharge modes we explained in Chapter 5.

7.4.1. Experimental results

FR4 samples were tested at 100,000 Pa (1000 mbar) and 20 °C. By using National Instrument Hardware and the software Labview, the summarized voltage and current signal files with a testing period were recorded. The raw current and voltage waveforms were also recoded as well.

50 V Tests Results

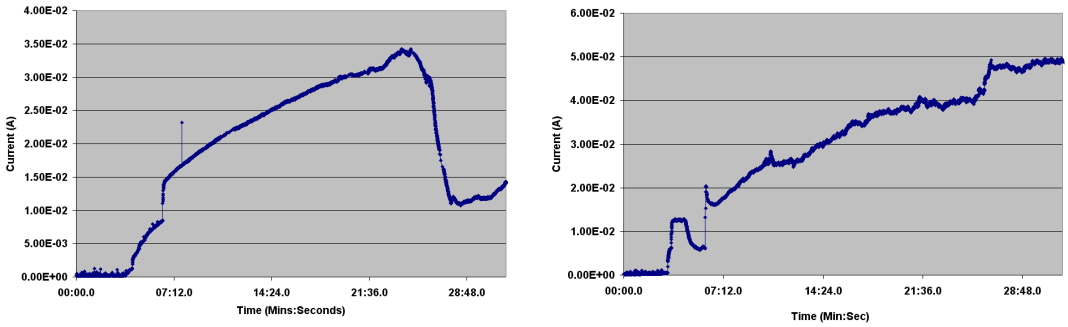

(a) 1st time test result (b) 2nd time test result

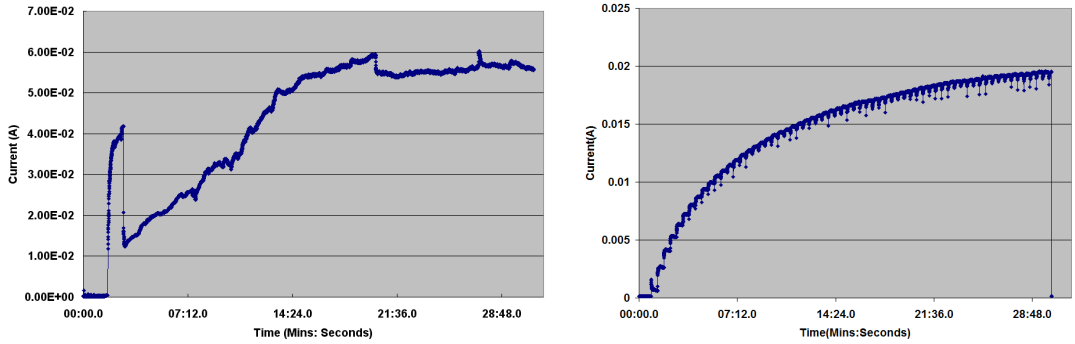

(b) 3nd time test result (d) Standardized CTI test result

Figure 7.2 Comparison of the summarized current vs. time plots for three times' tests at 50V using the new CTI test methods for a 4mm gap and the standardized CTI test at 1000mbar.

The first set of test results, shown in Figure 7.2 (a), (b) and (c), presents the summarized leakage currents vs. time within the 30 minutes' testing period under 50 V. All three times of the repeated tests results were shown. For the 1st time test under 50 V the current was

increasing from 0 to 0.035 A. It was from 0 to 0.05 mA for the second time and up to 0.06mA. It can be seen that the leakage current were raised gradually with time passing when the condensed conductive aqueous contaminants were collected between the electrodes. The bigger the amount of the condensed liquid, the higher the conductance of the path of the leakage currents will be and consequently higher currents. The effect of the evaporation of the liquid is not enough to prevent more and more conductive liquid building up since the voltage applied was only 50 V which can not generate enough electrical energy to accelerate the evaporation. Comparing the test results under 50 V with the standardized CTI test method, this is completely repeatable with confidence. It can be seen in the Figure7.2 (d) that the key difference is the increase of the current using new method was not as smooth comparing to the plot for the CTI tests at 50 V,. It is because the collection of the contaminant was taking longer comparing to the droplet just falling on the solid insulation surface between electrodes.

70 V Tests Results

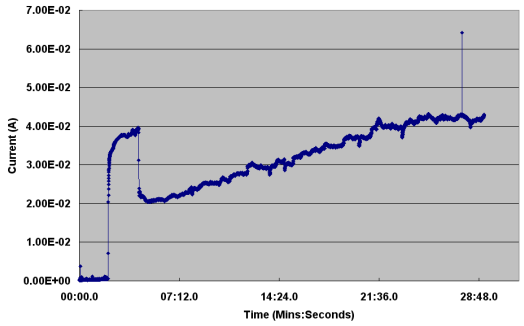

(a) 1st time test result

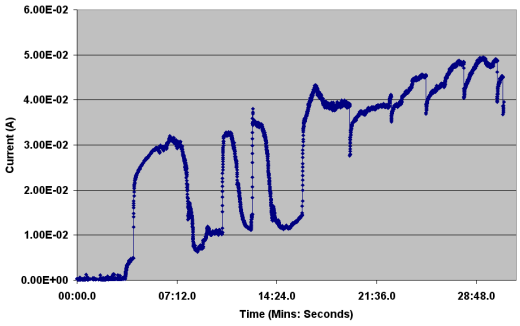

(b) 2nd time test result

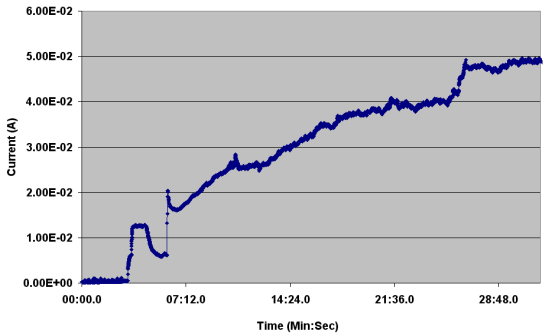

(b) 3rd time test result

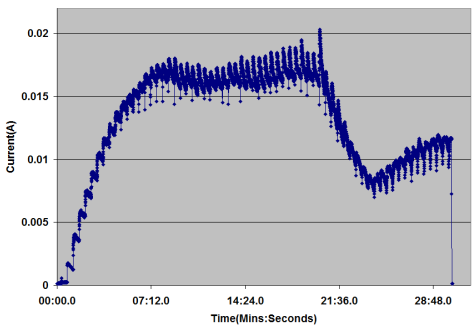

(d) Standardized CTI test result

Figure 7.3 Comparison of the summarized current vs. time plots for three times' tests at 70 V using the new CTI test methods for a 4 mm gap and the standardized CTI test at 1000 mbar.

Figure 7.3 (a), (b) and (c) presents the summarized currents vs. time plots for the three times ‘tests within 30 minutes’ testing period by using new test method. The figure (a) in Figure 7.3 illustrates the current was increasing gradually from 0 to 0.04 A and for the last 7minute the constant values of currents of 0.04 A can be found which indicate that the equilibrium of evaporation and replenishment had been achieved. This also has been found for those results under 70 V with the standardized CTI test method in Chapter 5 shown in Figure 7.3 (d). However, we also see some different current trends in figure (b) in Figure 7.3 as the current had some spikes with the general trend of increase from 0 until 0.05 A. As it is know that from the previous test results in Chapter 5, 70 V is the critical voltage to initiate the electrical tracking since it is an equilibrium point. This equilibrium is very easy to break if there is a tiny change of the flow rate which is inevitable. And for the third time test with the same parameter, we again gained the increased current from 0 to 0.05 A with time, although the constant current at the end is not convinced, which again proves that this equilibrium state is very fragile.

80 V Tests Results

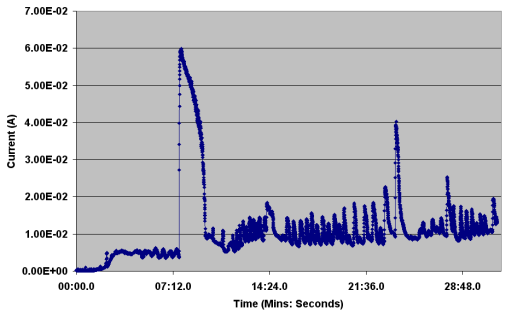

(a) 1st time test result

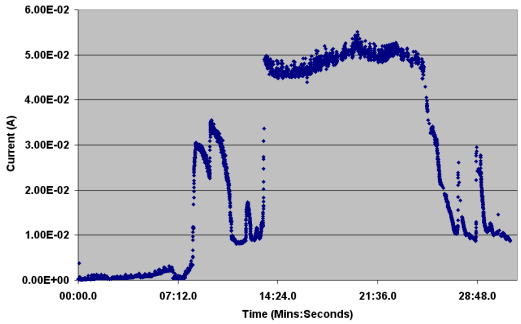

(b) 2nd time test result

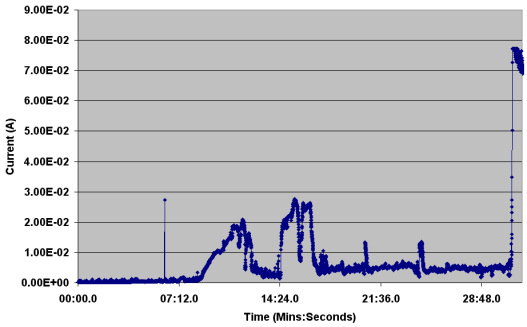

(b) 3rd time test result

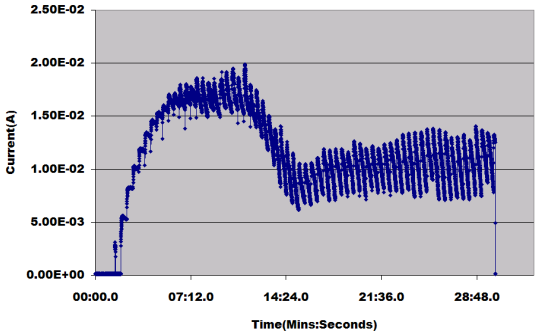

(d) Standardized CTI test result

Figure 7.4 Comparison of the summarized current vs. time plots for three times' tests at 80 V using the new CTI test methods for a 4 mm gap and the standardized CTI test at 1000 mbar.

These test results in Figure 7.4 (a) (b) and (c) show us that the summarized current vs. time plots for the three times' tests within 30 minutes' testing period at 80 V for a 4mm gap by using the new test technique. The 1st figure (a) above in Figure 7.4 presents the current with big current spikes which has been proven to be a sign of electrical tracking occurring. Although Figure (b) and (c) are not typical current spikes plots to indicate the electrical tracking, the physical damages were found for all the three tests. With the upgraded CTI test method, 80 V is the inception voltage of electrical tracking occurring on FR-4 material. Comparing those test results by using the standardized test technique with these results, It can be seen that the after a gradual increase of current and then a little bit drop, the current started fluctuating with smaller magnitudes and without any point crossing zero in Figure 7.4 (d) for the standardized CTI test at 80 V. It has been proved that there is no evidence of damage on the specimen until the voltage was increased to 90

V for standardized CTI test.

100 V Tests Results

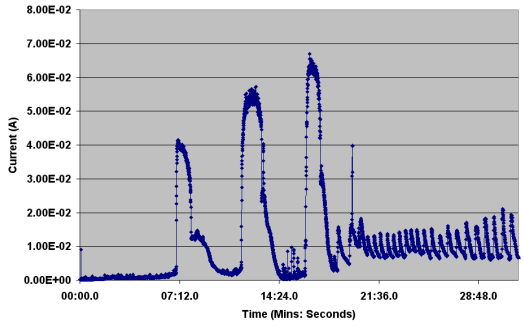

(a) 1st time test result

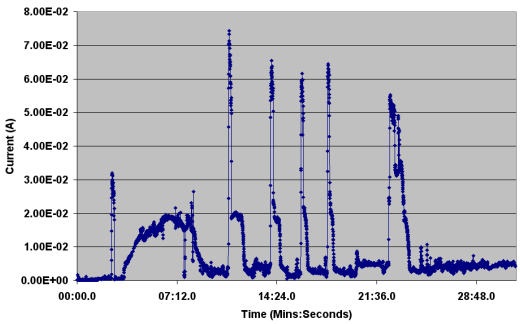

(b) 2nd time test result

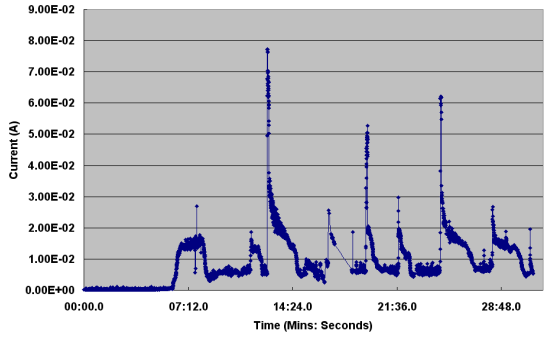

(b) 3rd time test result

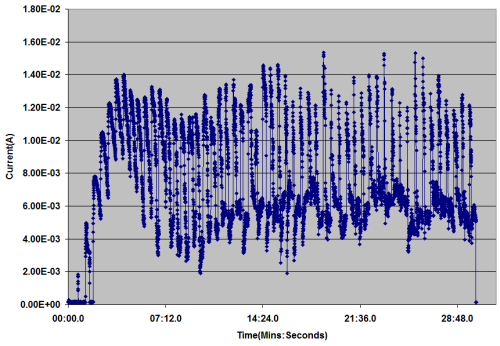

(d) Standardized CTI test result

Figure 7.5 Comparison of the summarized current vs. time plots for three times' tests at 100V using the new CTI test methods for a 4 mm gap and the standardized CTI test at 1000 mbar.

Three times' test results under 100 V were presented in Figure 7.5 (a), (b) and (c) with. The current was fluctuated from 0 and 0.08 A. And very clear and stable current spikes were always found under 100V which means that the voltage of 100 V is big enough to evaporate the condensed conductive aqueous contaminants so that the electrical arc and tracking was triggered. Damages found on the specimens were much worse than those under 80 V. However, if the frequency of the current spikes is looked into carefully by comparing the results from the testing by using the new test technique with those by using the standardized CTI test method show in Figure 7.5 (d), it can be found that the current spikes took palace much more frequent for standardized CTI test results. Again this is due to the difficulty of collection of the contaminant from those fine mists generated by the humidifier. Comparing to the droplets, it takes longer for the specimen surfaces to reach

the same intensity of the flow rate, which is the same as the one used for standardized CTI test specification.

7.4.2. Discussion of the results

Table 7.1 below clearly demonstrates the status of physical damages on specimens by using the upgraded CTI tests at different voltages as evidence of the electrical tracking and my analysis above according to each test result. When the voltages of 50 V and 70 V were applied, electrical discharges and hence tracking was unable to take place due to the continuity of the conductive path between electrodes during the whole testing period. However, when the voltage raised to 80V, electrical energy was high enough to evaporate the contaminant on the surface of the specimens. Therefore the electrical discharges were occurring and then the damages of electrical tracking can be found as show in the table below. Higher voltage resulted in severer damages such as the evidence in the table for 100V.

Table 7.1: Comparison of the damage observed on plain circuit boards (FR4) for 4 mm gap test with the new CTI method

Applied Voltage (V)	50	70	80	100
Damage Status on Specimens	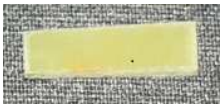			

The most important meaning to repeat the 4mm gap tests with the upgraded CTI test method by using the humidifier and new shape specimen instead of the dropping devices and original specimen in previous Chapter 5 is that to evaluate the feasibility and reliability of the new test method. The summarized currents vs. time plots presented above do provide us an evidence about the four modes of electrical tracking processes. And that the three times' test results can be copied each other confirm that the reliability of the new

test results. Finally, in this section the table of the status of damages on specimens double proves my explanation. As a conclusion, the new test method for electrical tracking has been validated to be not feasible but also reliable when to be applied to varying gap distances.

7.5. 2mm gap tracking test at the atmospheric pressure

The Previous section proves that the test method with the humidifier and new shape specimens can produce repeatable electrical tracking results as the standardized CTI test method does. Therefore, the upgraded CTI test method in this section will be applied to specimens with a 2 mm gap distance between two electrodes. By doing different gap distance tests with the upgraded test methods, it is expected that a general test method can be developed to study the dimensioning rules of creepage distances. Similar to the standardized CTI tests, the new test method was employed to carry out the testing on FR-4 specimens with a 2mm gap from 40V with voltage step of 10 V until 100 V when the electrical tracking can definitely lead to damages on the specimens. Each voltage tests were repeated for three times. All the current and voltage raw data were recorded by the Labview program designed for previous standard CTI tests.

7.5.1. Experimental Results

40V Tests Results

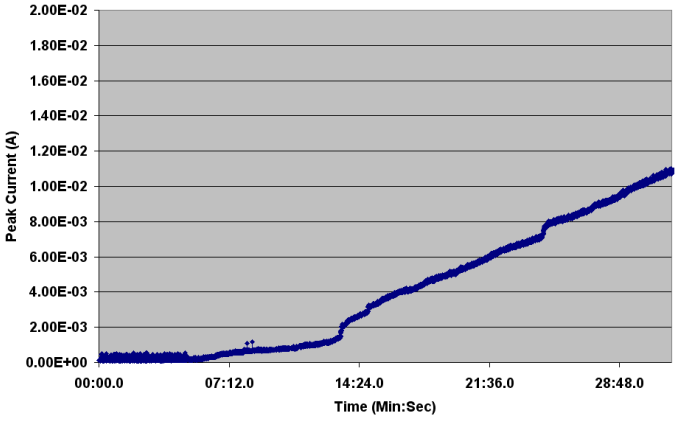

Figure 7.6 The summarized current vs. time plot for the test using the new CTI test methods for a 2 mm gap at 40 V 1000 mbar.

Figure 7.6 provides the summarized currents vs. time plot for the test within 30 minutes' testing period at 40 V by using the new test technique. It was chosen from three similar test results with a very typical leakage current plot under 40 V for a 2 mm gap specimen. It can be seen that the current gradually increased from 0 up to 0.011 mA. There was no arc or damages on the specimens. The bigger the amount of the condensed liquid, the higher the conductance of the path of the leakage currents will be and consequently higher currents. The effect of evaporation of the liquid is not enough to prevent more and more conductive liquid building up since the voltage applied was only 50 V which can not generate enough electrical energy to accelerate the evaporation. Comparing the test results under 50 V with the standardized CTI test method, this is completely repeatable.

50 V Tests Results

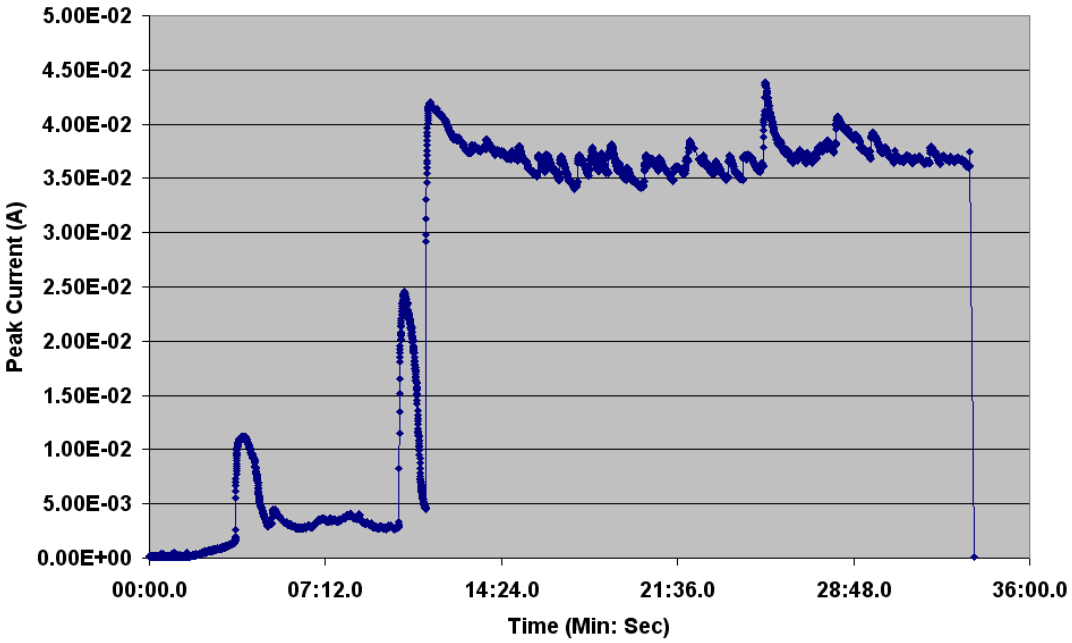

Figure 7.7 The summarized current vs. time plot for the test using the new CTI test methods for a 2 mm gap at 50 V 1000 mbar.

The set of test results under 50 V present the summarized currents vs. time within the 30 minutes' testing period for a 2 mm gap in Figure 7.7. A very typical current plot was shown and the current was increasing gradually from 0 to 0.04 A with two small spikes at the 4^{th} minute and 11^{th} minute respectively. From the 12^{th} minute on t the constant values

of currents of 0.04 A can be found which indicate that the equilibrium of evaporation and replenishment had been achieved. This also has been found for those results under 70 V with the standardized CTI test method in Chapter 5. There was no damage found on specimens under 50 V.

60 V Tests Results

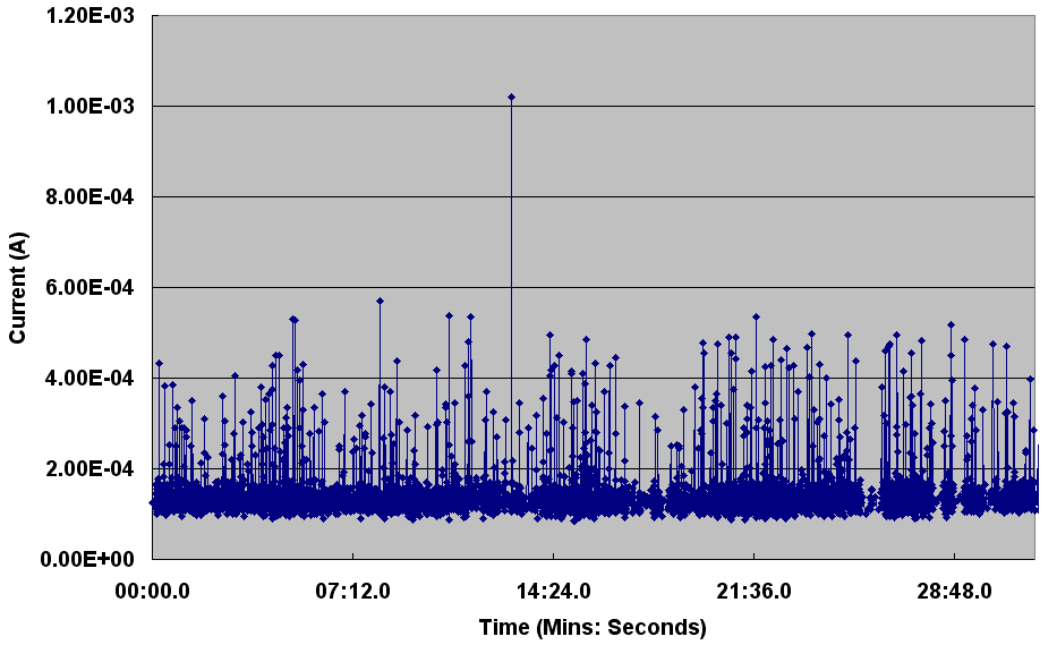

Figure 7.8 The summarized current vs. time plot for the test using the new CTI test methods for a 2 mm gap at 60 V 1000 mbar.

This set of test results show us that the summarized current vs. time within 30 minutes' testing period under 60 V for 2 mm gap. Again the typical current plot was shown here. And it presents the current with big current spikes from 0 to 0.001 A at maximum and damages were found on specimens. With the upgraded CTI test method for 2mm gap, 60 V is the inception voltage of electrical tracking occurring on FR-4 material which will be compared with those figures of creepage distances defined IEC 60664 and IPC 2221 standards.

100 V Tests Results

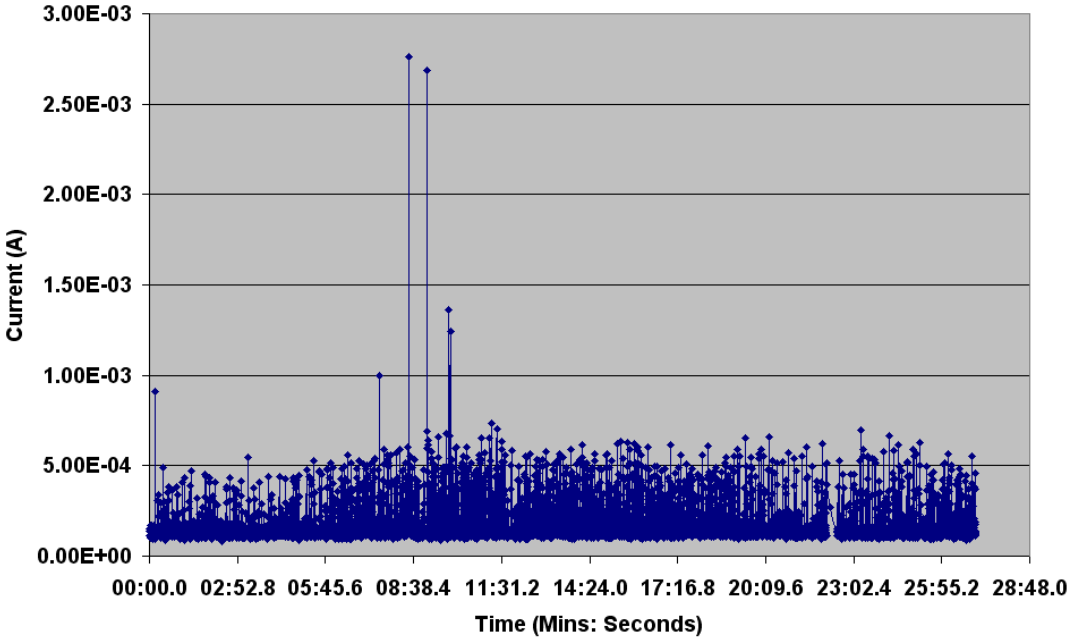

Figure 7.9 The summarized current vs. time plot for the test using the new CTI test methods for a 2 mm gap at 100 V 1000 mbar.

Test results under 100 V were presented in Figure 7.9 for a 2 mm gap with the upgraded CTI test method. The current was fluctuated from 0 and 0.0025 A at a maximum. And very clear and stable current spikes were always found under 100 V which means that the voltage of 100 V is big enough to evaporate the condensed conductive aqueous contaminants so that the electrical arc and tracking was triggered. Damages found on the specimens were much worse than those 4 mm gap tests under 100 V.

7.5.2. Discussion of Results

Again, Table 7.2 below provides us with the damage status of the specimens used in the 2mm gap tests with the upgraded CTI test method. The pictures are the physical evidence of the voltages being required to initiate tracking.

Table 7.2: Comparison of the damage observed on plain circuit boards (FR4) for 2 mm gap test with the new CTI method

Applied Voltage (V)	50	70	80	100
Damage Status on Specimens	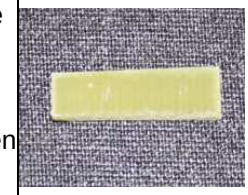			

It has been proven that the inception voltage of electrical tracking under atmospheric pressure conditions for a 2mm gap is 60 V. Referring to Table A5 in Appendix A from IEC 60664, it can be found that the standard recommends that the withstand voltage is 63 V for a 2 mm creepage distance without any pressure information at all for material group III material which FR-4 belongs to due to its CTI value under the environment of pollution degree 3 (conductive pollution occurs or dry non-conductive pollution occurs which becomes conductive due to condensation which is to be expected). This dimensions for design is very close to the value of 60 V we have found for electrical tracking taking place. However, even with this very close specification, it should be applied with caution. Additionally, IEC 60664 never explained why the material groups really have influence on the dimensioning of creepage distances which, based on my research, is not critical.

IPC 2221, referring to Table A7 Electrical Conductor Spacing in IPC 2221 in Appendix A, recommends the voltage range from 300 V to 500 V for the creepage distance of 2 mm for bare board used above sea level and below 3050 m (100 mbar) without CTI material groups categories at all. Dimensioning of the creepage distance to avoid electrical tracking failure in IPC 2221 is dangerous to be applied for aerospace application under very severe pollution conditions because such as conductive pollution may exist.

7.6. 8 mm Gap Tracking Test under Atmospheric Pressure

Similar to the 2 mm gap tests, the new test method was employed to carry out the testing on FR-4 specimens with an 8mm gap from 50 V with voltage step of 10 V until 150 V when electrical tracking can definitely lead to damages on the specimens. Each voltage tests were repeated for three times. All the current and voltage raw data were recorded by the Labview program designed for the previous standard CTI tests.

7.6.1. Experimental Results

For the 8 mm gap tests, instead of 30 minutes' testing, a longer testing period of 40 minutes were employed since it takes time for the longer conductive path between electrodes to have very concentrated leakage currents.

80 V Tests Results

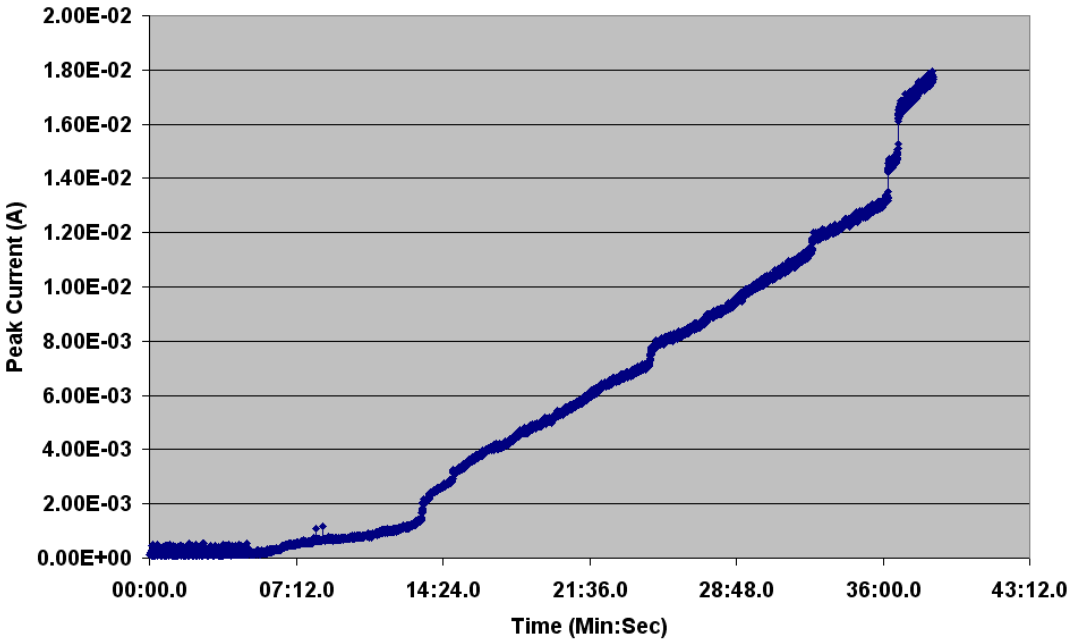

Figure 7.10 The summarized current vs. time plot for the test using the new CTI test methods for an 8mm gap at 80 V 1000 mbar.

Now, the set of test results under 80V present the summarized currents vs. time within the 40 minutes' testing period for an 8mm gap with the new CTI test method in Figure 7.10 and the typical plot is shown here. Under 80 V the input power (transferred from electrical

energy to heat) is not enough to evaporate the aqueous contaminant between electrodes to initiate electrical tracking. And the continuously falling liquid kept collecting between electrodes which made the conductance of the conductive path for the leakage current increase. Therefore, we can find that the current was raised gradually from 0 to 0.018 mA. It should be pointed that when voltages lower than 80 V were applied, the similar current plot vs. time can be seen which reflects the insignificant input power to evaporate the contaminant and initiate an arc and electrical tracking. There was no damage found on the specimens.

90 V Tests Results

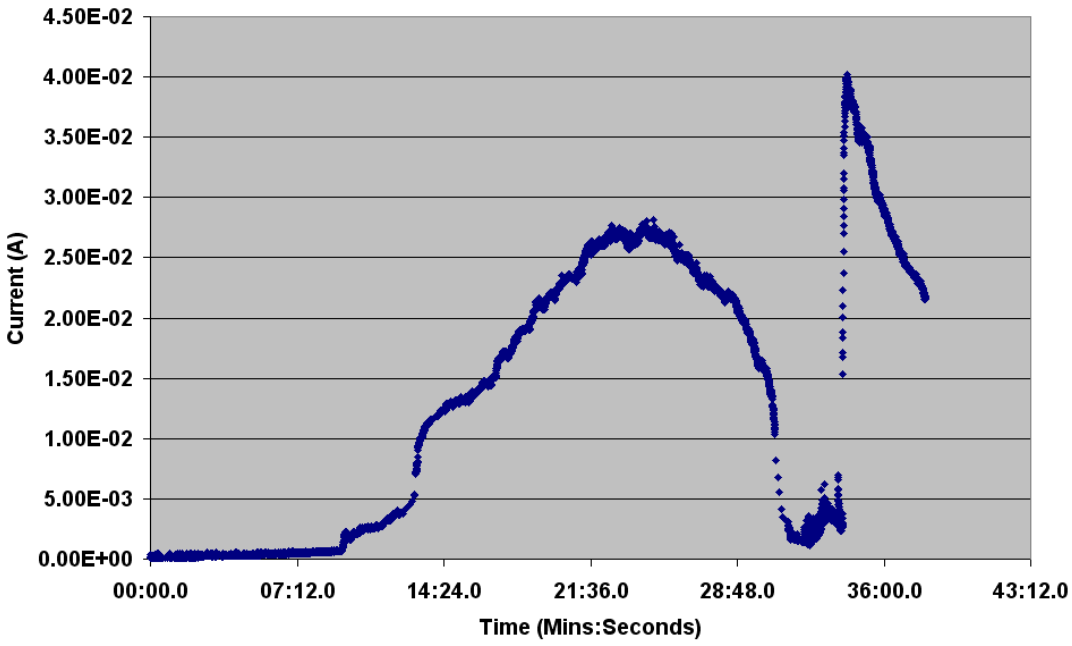

Figure 7.11. The summarized current vs. time plot for the test using the new CTI test methods for an 8 mm gap at 90 V 1000 mbar.

This set of test results show us that the summarized current vs. time within the 40 minutes' testing period for an 8 mm gap with the new CTI test method under 90 V. The current was increasing from 0zero to 0.028 A at first and then at around the 22th minute it experienced a very short time constant and finally started to drip to almost zero. At the beginning with the contaminant collecting between the electrodes, the conductance of the conductive path was going up. Therefore, the leakage current was increasing at first until the rate of

evaporation and replenishment of the contaminant was at the same level when the amount of liquid between the electrodes should stay still. At this moment the current also stays constant. However, apparently the evaporation rate was higher after the 3 minutes' equilibrium period. Then, the amount of the contaminant decreased and consequently the leakage current dropped. Then, around the 35th minute, the current jumped up to the summit of 0.04 mA and again dropped significantly immediately. There was no damage found on specimens.

100 V Tests Results

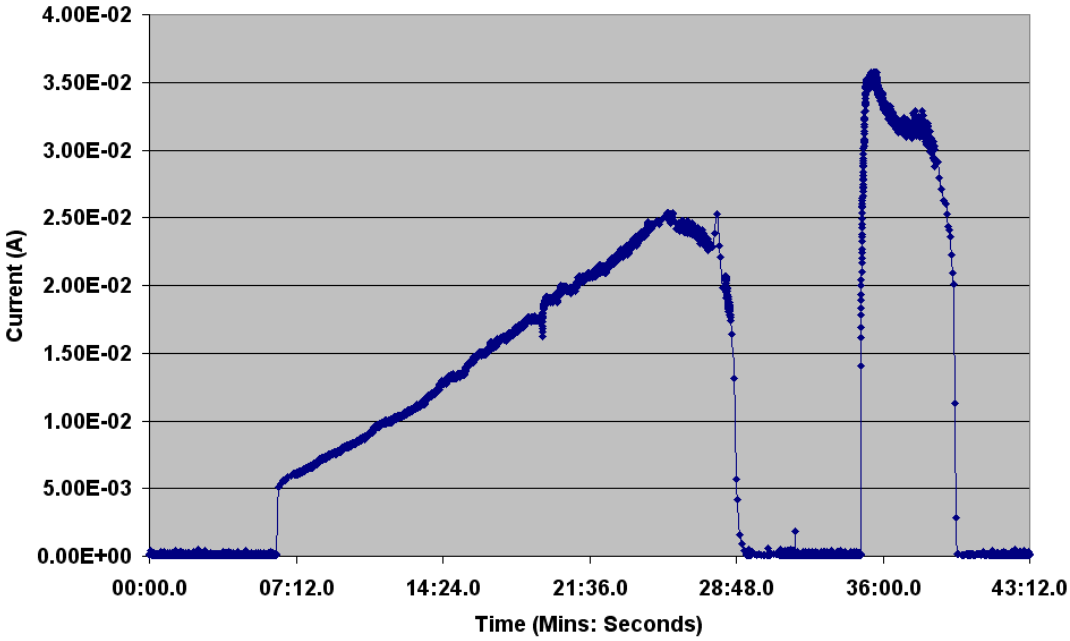

Figure 7.12 The summarized current vs. time plot for the test using the new CTI test methods for an 8 mm gap at 100 V 1000 mbar.

Test results under 100V were presented in Figure 7.12 for an 8 mm gap with the CTI test method. Initially, the current was increasing from 0zero to 0.025 A. And then, all of a sudden, the current was dropped dramatically to zero for 8 minutes and then jumped up to 0.035 A for 3 minutes. And then it dropped to almost zero. Since the current stayed at the summit for a few minutest, damages were found ere formed on the specimens.

150 V Tests Results

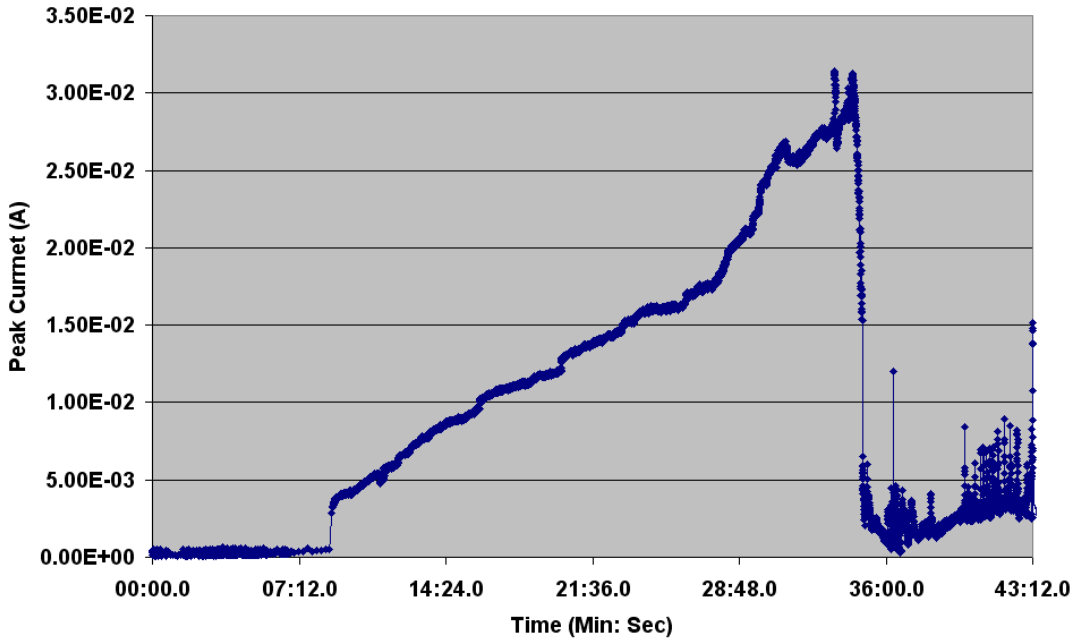

Figure 7.13 The summarized current vs. time plot for the test using the new CTI test methods for an 8 mm gap at 150 V 1000 mbar.

When the voltage applied increased to 150 V, after 35minutes' the current rose from zero to 0.03 A, and very frequent current spikes were seen. This indicates that the input power was very high and the arcs took place due to evaporation and re-ignition. There were damages found on the specimens.

7.6.2. Discussion of Results

Table 7.3 presents the damages status of the specimens tested with the new CTI test method. The pictures are the physical evidence of the voltages being required to initiate tracking for an 8mm gap on FR-4.

.

Table 7.3: Comparison of the damage observed on plain circuit boards (FR4) for the 8 mm gap test with the new CTI method

Applied Voltage (V)	50	70	80	100
Damage Status on Specimens	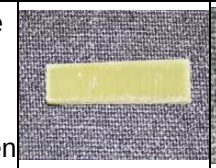			

According to the 40 minutes' tests on FR-4 with the new CTI test method for an 8 mm gap, it can be summarized that the inception voltage of electrical tracking is 100V. Referring to Table A5 in Appendix A from IEC 60664, it can be found that the standard recommends that the withstand voltage is 500 V for an 8mm creepage distance without any pressure information at all for material group III material to which FR-4 belongs. Additionally, IEC 60664 never explained why the material groups really have influence on the dimensioning of creepage distances which, based on my research, is not critical. The dimensioning rule of the standard is dangerous to apply under very severe environment conditions according to the comparison above. So it should be applied with cautions.

And IPC 2221, referring to Table A7 Electrical Conductor Spacing in IPC 2221 in Appendix A, specifies the voltage range from 1600 V for the creepage distance of 8 mm for bare board used above sea level and below 3050 m (100 mbar) without CTI material groups categories at all. Comparing to the inception voltage of 100V in my test during the 40 minutes' test under very conductive pollution conditions, apparently the dimensioning rule should be applied with caution.

7.7. Conclusion

The standardized CTI test method defined the creepage distance is a 4 mm gap and

accordingly the dropping devices and flow rate of the contaminant are particularly designed for this length of gap. An electrical tracking testing method has been developed based on the standardized CTI tests with manipulating the dropping device to a domestic humidifier and the shape of organic insulating material board from 20mm×20mm to 20mm×5mm with which the width of the specimen is as big as the width of the contacting electrode.

The challenge of accelerated electrical tracking tests is always attribute to the big fluctuation of test results. Therefore, not only the feasibility but also reliability of the new CTI test method has been confirmed in the thesis by recognizing the four modes of initiation of discharges on solid insulation material surface. The 4 mm gap tests with the new CTI test method firstly have been shown with comparisons with the test results with those by using the standardized CTI test method. It can clearly be seen that even with the new dropping device and new shape of the specimens, the similar summarized current vs. time plots can be found under the same amount of voltage applied. And four modes of electrical tracking processes can be reflected by the results. The repeatability also has been achieved by comparison of the three times of repeating the tests for each voltage.

Then, the new CTI test method was applied to a 2 mm gap and an 8 mm gap. The test results were used to compare with the specifications defined in IEC 60664 and IPC 2221. The measurement of the inception voltage of electrical tracking for a 2 mm gap is 60 V, which is just around the 63 V defined in IEC 60664 for material group III which FR-4 belongs to under pollution degree conditions without any information on air pressure impact and much lower than 300 V to 500 V, as defined in IPC 2221, for applications above sea level and below 3050 m without the pollution degrees information. And the measurement of the inception voltage of electrical tracking for an 8mm gap is 100 V, which is much smaller than the 500 V defined in IEC 60664 for material group III which FR-4 belongs to under pollution degree conditions without any information on air pressure impact, and is much lower than 1600 V as defined in IPC 2221 for applications above sea level and below 3050 m without the pollution degrees information. As a conclusion, the application of the dimensions of creepage distance in the standards should be considered with the

environment conditions where the electrical apparatus will operate with significant caution. And the best resolution for any specific design is to conduct the accelerated electrical tracking test by using the upgraded CTI test method discussed in the thesis. The comparison of withstand voltages of IEC 60664, IPC 2221 and the test results for 2mm, 4mm and 8mm gaps on FR-4 at 1000mbar was summarized in the Table 7.4.

Table 7.4: Comparison of withstand voltages of IEC 60664, IPC 2221 and the test results for 2 mm, 4 mm and 8 mm gaps on FR-4 at 1000 mbar.

	IEC 60664 (Material Group III)	**IPC 2221**	**Test Results**
	Pollution Degree 3	**Above sea level up to 3050m (696.4 mbar)**	395 $\Omega \cdot$cm
Withstand voltage for 4mm gap	250 V	800 V	90 V
Withstand voltage for 2mm gap	63 V	300-500 V	60 V
Withstand voltage for 8mm gap	500 V	1600 V	100 V

Chapter 8: Conclusion and Future Work

8.1. Summary

8.1.1. Validation of clearances and creepage distances in standards

One of the objectives of the thesis was the evaluation of the reliability of the existing standards for the dimensioning of clearances and creepage distances, including IEC 60664, 'Insulation coordination for equipment within low-voltage systems', and IPC 2221, 'Generic Standard on Printed Circuit Board'. This was carried out in Chapter 3 based on:

A. Interpreting the dimensioning rules specified in IEC 60664 and IPC 2221 for clearance and creepage distances.

B. Measuring the withstand voltages for varying lengths of clearances and creepage distances under varying air pressure under dry conditions for aerospace applications.

C. Comparing the measured data with IEC 60664 and IPC 2221 specifications.

D. Comparing the measured data with Paschen's curve values.

- IEC 60664 deals with the insulation coordination for equipment within low voltage systems. It applies to equipment up to 2000 m above sea level having a rated voltage up to AC 1000 V with a rated frequency up to 30 kHz or rated voltage up to DC 1500 V. As the standard is not applicable for equipment used over 2000 m, it is clearly not intended for use in aerospace equipment design. And Table A5 in Appendix A provides the

dimensions of creepage distances for different material groups' materials under different pollution degrees. Apart from a lack of information on the impact of air pressure for aerospace applications, there is no explanation of the reason why the material groups have an influence on withstand voltages for electrical tracking, which have been proven to be not very relevant in the thesis.

- IPC 2221, 'Generic Standard on Printed Boards Design', provides generic requirements for the design of organic printed boards and other forms of components, mounting or interconnecting structures to eliminate the misunderstanding between manufacturers and purchasers, facilitating the interchangeability and improvement of products, and assisting the purchaser in selecting and obtaining with minimum delay the proper product for a particular need. The dimensions of electrical clearances given in Table A7 in Appendix A provide two categories of situations for below 3050 m and above 3050 m. However, there is no any information on the pollution degrees which is very critical to trigger electrical tracking.
- A determination of clearance in air can be precisely defined for a certain electrode geometry based on Paschen's law for a uniform electrical field. As Paschen's law appears to be implemented in IEC 60664, this therefore also means that the guidance it provides for the dimensioning of clearances is appropriate.
- For non-uniform fields, the use of IEC 60664 to determine clearances does not appear to give results that are totally consistent with experimental tests, but they are a useful approximation for design purposes at atmospheric pressure with a larger deviation at

100mBar pressure. Breakdown voltage measurements show consistency with the IEC 60664 standard at low pressure (although the IEC 60664 standard is not conservative) and no match was possible at atmospheric pressure owing to the limited voltage capability of the test supply.

- However, determining the creepage distances in both standards somehow has its limitations. For creepage distances under dry conditions, the test results on printed circuit board with a polyimide substrate and varying creepage gap printed on show that the breakdown voltage is close to that expected using Paschen's law, but also that it far exceeds that predictions used in IEC 60664 or IPC 2221.

8.1.2. Electrical tracking under wet conditions

The most important objective of the thesis is the exploration and development of the understanding of electrical tracking with the consideration of different environmental conditions, including air pressure, and pollution degrees for aerospace applications. An series of studies have been carried out. The required voltage levels and the mechanism to trigger an arc and electrical tracking and in consequence, discussed in Chapter 4, 5 and 6, are based on:

A. Establishing the mathematical calculation model of initiating electrical tracking with parameters of the pollution degrees, ambient temperature, and ambient pressure. By analysing the influences of different impact parameters, the mechanism of electrical tracking has been understood to have a very close relationship with the heat transfer mechanism.

B. Employing the standardized CTI test method at various air pressures to measure the leakage currents during the testing period to find out the behaviour of electrical

tracking under electrical stresses. Furthermore, the measurements of the inception voltage for electrical tracking can also provide the inception voltage for a 4mm gap under very severe pollution environment conditions. The impact of air pressure can be judged according to the test results.

C. Comparing the measured inception voltage for a 4 mm gap with that calculated using the mathematic formula and IEC 60664 and IPC 2221 so that the dimensioning rules of the standards can be evaluated.

- The development of the mathematic model of initiating electrical tracking indicates that electrical tracking originally starts from a dry-band arc. The first dry-band arc can take place due to the break of the continuous leakage current path. This can occur at very low voltage even under Paschen's minimum. To have this first dry-band arc, the aqueous contaminant film should evaporate until the dry band appears. As it is known, leakage current can lead to energy transferred from electrical energy to heat, which would accelerate the effect of evaporation of the aqueous contaminant. As a result, the electrical tracking, evaporation and electrical input power have been interconnected. Therefore, the model was established based on the mechanism explained which is the equilibrium between the input electrical power and output power of evaporation. My study also has been proven by L. Warren in his paper. By interpreting Warren's model with dynamic heat transfer, a static mathematical model has been developed, as shown in equation 4.7.

$$\frac{V^2 \cdot wh}{\rho(T)l} = \left(T_{boiling} - T_{ambient}\right) / R_T$$

- By analysing the influences of different impact parameters such as the resistivity of the

conductive contaminant $\rho(T)$, the boiling point of the contaminant $T_{boiling}$, ambient temperature, and equivalent thermal resistance R_T, the required voltage needed cannot determined linearly by air pressure, resistivity and the boiling point of the contaminant since the mentioned parameters are inter-dependent to each other. The resistivity of the contaminant increases with the rise of the temperature, while the boiling point is determined by contaminant itself and air pressure. The static simulation done by running the program in the Finite Element Analysis software 'Vector Field Opera version 11' was used to find out the equivalent heat transfer resistance while the dynamic simulation was used to help predict the possible changes of required voltages to initiate electrical tracking.

- The required voltage to initiate electrical tracking increases with pressure according to the mathematical calculation. The value of voltages at ambient pressure 1000 mbar was around 150 V, while at lower pressure 100mbar it dropped to 46 V for deionized water; it was 8.4 V for the highly conductive solution A specified in IEC 60112: 2003 at 10000 mbar and 5.5 V at 100mbar. This also represents the fact that the more conductive the aqueous contamination, the lower the voltages that are needed for electrical tracking. Theoretical calculation results show that at higher ambient temperatures, less voltage is required to initiate electrical tracking. The most interesting results are those values of voltages required at 273 K for the highly conductive solution A, which shows that the voltage actually decreases with pressure going up.
- The electrical tracking testing method specified in IEC 60112 is an accelerating way

to find out the tracing resistance within a short time by using a much more conductive contaminant than would be found in reality. However, the data of the tracking fluctuated greatly, which is the key problem. My research contribution, as shown in this chapter, is the repeatability of the test results for both FR-4 and ABS.

- Comparisons of the values of inception voltage for electrical tracking at various air pressures with the test results with the mathematical calculation results have been discussed.
- Comparison of the values of inception voltage for electrical tracking at various air pressures with the test results with the standard recommended values have been discussed.

8.1.3. Selection of wet condition electrical tracking test techniques

The last objective of the thesis was to provide guidelines for better electrical tracking testing methods for varying creepage distances. The standardized CTI test method defined the creepage distance as a 4mm gap and accordingly the dropping devices and flow rate of the contaminant are particularly designed for this length of gap. A better electrical tracking testing method has been developed based on the standardized CTI tests by manipulating the dropping device to a domestic humidifier and the shape of organic insulating material board from $20\text{mm}\times20\text{mm}$ to $20\text{mm}\times5\text{mm}$ with which the width of the specimens are as big as the width of the contacting electrode.

The challenge of accelerated electrical tracking tests always attribute to the big fluctuation of test results. Therefore, not only the feasibility but also the reliability of the new CTI test method has been confirmed in the thesis. The 4mm gap tests with the new CTI test method

firstly have been shown by a comparison with the test results using the standardized CTI test method. It can clearly be seen that even with the new dropping device and new shape of specimen, the similar summarized current vs. time plots can be found under the same amount of voltage applied. And four modes of electrical tracking processes can be reflected by the results. The repeatability also has been achieved by a comparison of the three repeat tests for each voltage.

Then, the new CTI test method was applied to a 2 mm gap and an 8 mm gap. The test results were used to compare with the specifications defined in IEC 60664 and IPC 2221. The measurement of the inception voltage of electrical tracking for the 2mm gap is 60 V, which is around the 63 V defined in IEC 60664 for material group III which FR-4 belongs to under pollution degree conditions without any information on air pressure impact, and much lower than 300 V to 500 V as defined in IPC 2221 for applications above sea level and below 3050 m without the pollution degree information. And the measurement of the inception voltage of electrical tracking for an 8 mm gap is 100 V, which is much smaller than the 500 V defined in IEC 60664 for material group III which FR-4 belongs to under pollution degree conditions without any information on air pressure impact, and much lower than the 1600 V defined in IPC 2221 for applications above sea level and below 3050 m without the pollution degree information. As a conclusion, the application of dimensions of creepage distance in the standards should be considered as the environment condition where the electrical apparatus will operate with significant caution. And the best resolution for any specific design is to conduct the accelerated electrical tracking test by using the upgraded CTI test method discussed in the thesis.

8.2. Suggestions for Future Work

The insulation coordination of an electrical power system for aerospace applications is comprised of the determining of clearance and creepage distance under varying air pressures. Breakdown tests on air gaps under either uniform or non-uniform electrical fields have been well developed for many years. An exploration of the mechanism and behaviour

of electrical tracking is always a very challenging research area since electrical tracking by its nature is much more complicated.

The research described in this PhD thesis focused on the interpretation of the behaviour of the electrical tracking on organic insulating materials. Further researches on the following points are needed to implement the idea presented in this thesis to wider aerospace applications.

- Further dynamic thermal analyses for the accelerated electrical tracking test rig are required to improve my understanding of the influence of the heat capacity of different surrounding heat dissipating media on the evaporation and the first dry-band arc for real life applications.
- It is necessary to find out the formation and existence of actual pollution on real aircraft.
- More organic material belonging to different material groups is required to be tested with the standardized CTI test method to double check the findings of my research that the insulating material itself has minimal impact on initiating the first dry-band arc and consequent electrical tracking.
- More different lengths of gaps on organic insulating materials are required to be tested to validate the upgraded electrical tracking test method.
- Low pressure electrical tracking test methods for varying gaps on organic insulating materials are required to be developed for aerospace applications.
- At present, more and more power electronics components such as printed circuit boards employ conformal coating to avoid the macro-environment influence on their functioning. However, this protection could be become fatal if there is some

defect occurring, such as a hole at some point in the complete conformal coating film. Therefore, the impact of conformal coating on the insulation coordination of electrical systems on aircraft should be studied further.

- Non-50Hz and non-sinusoid voltages could be applied to find out the impact of the different voltages on breakdown and electrical tracking.

A test technique to determine safe creepage distances for utilization in aerospace applications should be generated with various air pressures.

8.3. Conclusion

This thesis has used theory, simulation and laboratory experiment, to investigate phenomena of the electrical tracking under wet condition for aerospace application. The new mathematical model to express the energy transfer within the contaminant liquid under applied voltage between the two electrodes had been built when the system reaches the static state which means the temperature of electrodes and specimens keep constant after the initial increase. The effects and their relationship of influencing parameters including the applied voltages, the conductivity of the contaminant, air pressure, ambient temperature, contaminant temperature and equivalent heat resistant have been analysed based on the model. Within all the parameters, the equivalent heat resistance were calculated based on the simulation results. We have found that the required voltage to initiate electrical tracking increases with pressure, the more conductive the aqueous contamination, the lower the voltages that are needed for electrical tracking and at higher ambient temperatures, less voltage is required to initiate electrical tracking. The most interesting results are those values of voltages required at 273 K for the highly conductive solution A, which shows that the voltage actually decreases with pressure going up. This result can be attributed to the combination of the influence of ambient temperature, pressure and the conductivity of the aqueous contamination. Especially, these impact factors are inter-dependent. This therefore proves that the mathematical model does predict this complicated relationship.

The limitation of the research is that the dynamic processes before static state has been achieved have been ignored. The heat capacities of surrounding heat dissipating media are critical properties to consider. Again, it is not a simple variable, but varies with temperature, pressure and volume. However, in the case of my model, the volume and pressure are supposed to be constant.

I have presented that selection of the electrical tracking test methods under lower voltage up to 1000 V. The contaminant dropping system has been proven to be the critical part of design. At atmospheric pressure, the dropping system has employed normal peristaltic pump with integral drive model with a hypodermic needle. However, to prevent impact of the circulating air in the environment chamber, it is better to use the medical transfusion dropping system for lower pressure electrical tracking tests.

I have also presented the experimental accelerating tracking test results for 4mm gap including the current and voltage data and also the thermal images to investigate the temperature changes during the testing periods. Four modes of electrical tracking processes can be reflected by the results. The repeatability also has been achieved by a comparison of the three repeat tests for each voltage. It also can be concluded that the lower pressure, the lower voltage required to initiate electrical tracking. Under lower pressure, the damages were seen much more severe. Different conductivity contaminant test results have proved that with higher conductivity, the lower voltages were required to initiate electrical tracking. According the comparison with the mathematic model results, it has been found that our calculation results are much lower than the experimental results. The comparisons with the IEC 60664 and IPC 2221 show that it is not safe to apply the dimensioning rules recommended.

Although different materials belonging to different categories of the material group according to their CTI values were tested by using the standard test methods, we found that the material itself was not the critical factor for initiating electrical tracking. The reason for

electrical tracking on the organic materials is that the conductive pollution layer can lead to electrical current flowing. With different voltage levels, the pollution layer dried at different rates, and the rate of replenishment is the critical factor. The voltage and replenishment of pollution together have a big effect on the mechanism of initiation of electrical tracking. So, as a conclusion the voltage level of any system and potential pollution degree are very important to evaluate whether a system can survive and operate reliably. Then, when any dimensioning rules in any standards are employed, these two factors should be evaluated very carefully.

At last I have shown that the new electrical tracking test method based on the IEC 60112 method but with the humidifier instead of original dropping system to generate approximate uniform fog environment for wider range of gap distances tests. 2mm, and 8mm gap distances test results including current and voltage data has shown that the bigger the gap, the higher voltage needed to initiate the electrical tracking. According to the comparisons with calculated test results, the higher voltages were presented. And the recommended values in both IEC 60664 and IPC 2221 are not applicable.

Reference

[1] R. I. Jones, "The More Electric Aircraft: The Past and the Future," *the Institution of Electrical Engineers*, 1999.

[2] Joseph A. Weimer and Aright Patterson AFB “Past, Present & Future of Aircraft Electrical Power Systems”, Power Division, Propulsion Directorate, Air Force Research Laboratory, AIAA 2001-1147, *39th Aerospace Sciences Meeting & Exhibit*, 8-11 January 2001, Reno, Nevada.

[3] J. A. Weimer, "Electrical Power Technology for the More Electric Aircraft," *Digital Avionics Systems Conferecne, 1993, 12th DASC AIAA/IEEE,25-28th Oct, pp. 445-450.*

[4] J. A. O. J.A. Rosero, E. Aldabas, & L. Romeral, "Moving Towards a More Electric Aircraft," *IEEE A&E SYSTEMS MAGAZINE*, March 2007.

[5] M. D. Kankam, "A Survey of Power Electronics Applications in Aerospace Technologies," *36th Intersociety Energy Conversion Engineering Conference cosponsored by the ASME, IEEE, AIChE, ANS, SAE, and AIAA Savannah*,Georgia, July 29-August 2, 2001.

[6] J. S. Cloyd and W. L. United States Air Force, "Status of United States Air Force's More Electric Aircraft Initiative," *IEEE AES System Magazine, Aptd 1998 17 Authorized*.

[7] J. A. Weimer, "Power Management and Distribution for the More Electric Aircraft," *Proceedings of the 30th Intersociety Energy Conversion Engineering Conference, 1995: 273-277.*

[8] C. Jie, "Outlook of Roles and Necessicities of Power Eelectronics for VF-Power System of Future Large Aircraft," *IEEE*.

[9] A. C. Newton and I. Moir, "Practical Consideration for the More-Electric Aircraft," in *ERA Avionics Systems Conference*, 1998.

[10] I. Moir, "Future Trends in Aircraft Electrical Systems," in *ERA Avionics Conference*. London Heathrow, 19-20th November 1997.

[11] I. Moir, "The Challenges of Now Technologies for Aircraft Electrical Systems," in *New Challenges in Aircraft Maintenance and ENgineering Conference*. Singapore, 1998.

[12] T. Glennon, "Fault Tolerant Generating and Distribution System Architecture," *IEE*, 1998.

[13] I. Moir, "More-Electric Aircraft- System Considerations," *IEE*, 1999.

[14] N. H. M. Bailey, G. Ucerpi, J. A. Hunt, S. Mollov, and A. Forsyth, "Distributed Electrical Power Management Architecture (DEPMA). *Electrical Machines and Systems for the More Electric Aircraft*," *IEE Colloquium*, November 9, 1999*:* 7/1-7/4.

[15] M. Howse, "All Electric Aircraft," *Power Engineer*, vol. 17, pp. 35-37,2003

[16] L. Faleiro, "Initial Research towards a More Electrical Aircraft," in *More Electrical*

Aircraft Conference: Royal Aeroautics Society, April 2004.

[17] M. A. e. a. Maldonado, "Power Management and Distribution System for a More Electric Aircraft (MADMEL) - Program Status," *Intersociety Energy Conversion Engineering Conf., August 1997: 274-279.*

[18] L. F. Faleiro, "Trends towards a More Electrical Aircraft," *Liebherr_Aerospace Lindenberg GmbH and The Royal Aeronautical Society*, 2004.

[19] S. J. Cutts, "Totally Integrated More Electric Systems (TIMES) Refer to: A Collaborative Approach to the More Electric Aircraft," *Power Electronics, Machines and Drives.International Conference*, on 4-7 June 2002: 223-228.

[20] M. Bailey, N. Hale, G. Ucerpi, J. A. Hunt, S. Mollov, and A. Forsyth, "Distributed Electrical Power Management Architecture (DEPMA). Electrical Machines and Systems for the More Electric Aircraft," *IEE Colloquium*, November 9, 1999: 7/1-7/4.

[21] M. G. Friend and D. L. Daggett, "Fuel Cell Demonstrator Airplane," *AIAA/ICAS International Air and Space Symposium and Exposition: Dayton, Ohio.*, 14-17 July 2003.

[22] KOJORI, Hassan, A., "Electrical Energy Management System on a Vehicle E.G. a More Electric Aircraft (MEA)," *HONEYWELL INTERNATIONAL INC. WO 2006/024006 A1. International Application published under the patent cooperation treaty (PCT).* March 2, 2006.

[23] Emadi, K. Ehsani, M., "Aircraft Power Systems:"Technology, State of the Art and Future Trends," *Aerospace and Electronic Systems Magazine, IEEE*, Volume 15, Issue 1,January 2000: 28-32.

[24] Sriram Chandrasekaran, Douglas K. Lindner,, "Subsystem Interaction Analysis in Power Distribution Systems of Next Generation Airlifters," *IEEE Power Electronic Specialist Conference*, September 1999.

[25] R. G. Michalko, "Electrical Starting Generation Conversion and Distribution System Architecture for a More Electric Vehicle," *HONEYWELL INTERNATIONAL INC. US2006/0061213 A1. United States Patent Application Publication*, March 23, 2006.

[26] Cotton, I.; Nelms, A. , "Higher Voltage Aircraft Power Systems," *IEEE Aerospace and Electronics Systems Magazine*, February 2008.

[27] Boeing Commercial Airplanes, “AERO Magazine”, issue QTR-0407

[28] A. Emadi and M. Ehsani, "Aircraft Power Systems: Technology, State of Art and Trends," *IEEE AES Systems Magazine*, January 2000.

[29] Ian Moir and Allan Seabridge, “Aircraft Systems: Mechanical, Electrical and Avionics Subsystems Integration”, *ISBN: 1 86058 289 3*, 2nd edition 2001.

[30] T. M. Bilodeau, W. G. Dunbar, and W. J. SarjeantIEEE, ""High-voltage and partial discharge testing techniques for space power system," *Electrical Insulation Magazine,IEEE*, vol. 5, pp. 12, 1989.

[31] W. G. Dunbar, D. L. Schweickart, J. C. Horwath, and L. C. A. W. L. C. Walko, "High frequency breakdown characteristics of various electrode geometries in air," *Power Modulator Symposium, Conference Record of the 1998 Twenty-Third International*, 1998.

[32] W. Dunbar and A. A. t. h. v. p. s. d. J. A. Rugama, " presented at *Energy Conversion Engineering Conference, 1989. IECEC-89., Proceedings of the 24th Intersociety, 1989., "Applying AVIP to high voltage power supply designs," Energy Conversion Engineering Conference, IECEC-89., Proceedings of the 24th Intersociety,* 1989.

[33] A. Brockschmidt and I. C. I. presented at Electric Machines and Drives, 1999., "Electrical environments in aerospace applications," *Electric Machines and Drives, International Conference IEMD '99,* 1999.

[34] G. G. Karady, M. D. Sirkis, and L. Li, ""Investigation of corona initiation voltage at reduced pressures,"" *Aerospace and Electronic Systems, IEEE Transactions*, vol. 30, pp. 144-150, 1994.

[35] A. N. Hammoud, M. W. Stavnes, J. L. Suthar, W. A. K. W. Khachen, and J. R. A. L. J. R. Leghari, "Testing of cable insulation for aerospace applications",*Conference Record of the 1994 IEEE International Symposium*,1994.

[36] W. Khachen and p. a. E. I. J. R. Laghari, 1990., Conference Record of the 1990 IEEE International Symposium on, 1990., "Polypropylene for high voltage high frequency airborne applications," *Electrical Insulation, Conference Record of the 1990 IEEE International Symposium*, 1990.

[37] W. G. Dunbar Boeing Report D180-15179-1, "High Voltage Design Criteria," *Boeing Report D180-15179-1*, 1972.

[38] E. Kuffel, W. S. Zaengl, and J. Kuffel, High Voltage Engineering: Fundamentals,1984.

[39] J.S. Townsend Electricity in Gases, Oxford Press. 1914.

[40] Andrew J. Nelms "*Electrical discharges in the more electric aircraft" PhD thesis*, University of Manchester, 2006.

[41] J. J. Thomas and G. P. Thomson. Conduction of Electricity through Gases. 2vol. *New York: Dover Publications Inc.* 1969 (Paper Edition)

[42] G. L. Weissler, "Photoeletric emission from solids," *Encyclopedia of Pyhysics*, vol. 16, pp. 342.

[43] M. Y. Saito, IEEE, Taro Hino, Member, IEEE, AND Mai Suzuki, "A Dry Tracking Resistance Test Method Using a Trigger Discharge," *IEEE Tranctions ON Electrical Insulation*, vol. EI-3, NO. 1, Feburary 1968.

[44] B. X. Du, K. Kato, F. Kaneko and S. Kobayashi, "Temperature Effect of Surface Breakdown of Printed Wiring Board", *J. Japan Inst. Electronic Packaging*, Vol.5, No.4, pp.401-404, 2002 (In Japan).

[45] Y. Yamano and Y. Takaoka, "Surge Endurance Characteristics between Foil Conductors on Printed Wiring Board", *Trans. IEE Japan*, Vol.123, No.11, pp.1130-1135, 2003 (In Japan).

[46] B. X. Du and S. Kbayashi, "Effects of Magnetic Field on Surface Dielectric Breakdown of Contaminated Printed Wiring Board", *Trans. IEE Japan*, Vol.123, No.6, pp.562 -567, 2003 [In Japanese].

[47] G. G. Karady, M. D. Sirkis and J .R. Olivva, "Degrading Effect of High-altitude Corona on Electronic Circuit Boards", *IEEE Trans. Electrical Insulation*, Vol.26, pp.1206-1208, 1991.

[48] B. X. Du, K. Kato, F. Kaneko and S. Kobayashi, "Discharge Characteristic of Printed

Wring Board under Decreased Pressure", *J. Japan Inst. Electronic Packaging*, Vol.5, No.6, pp.604-608, 2002 (In Japan).

[49] B. X. Du and S. Kobayashi, "Analysis of Discharge Current in Surface Breakdown of Contaminated Printed Circuit Board", *Trans. IEE Japan*, Vol.117-A, No.7, pp.783-784, 1997 (In Japanese).

[50] B. X. Du and D. S. Dong, "Recurrent Plot Analysis of Discharge Current in Tracking Test of Gamma-ray Irradiated Polymers", *IEEE Trans. Dielectric Electrical Insulation*, Vol.15, pp.974-981, 2008.

[51] B. X. Du, L. Gu, D. S. Dong and X. L. Zheng, "Recurrent Plot Analysis of Discharge Sequences in Tracking Test of Polybutylene Polymers", *J. Phys. D: Appl. Phys.*,

[52] B. X. Du and Y. Yamano, "Effects of Atmospheric Pressure on dc Tracking of Polymer Insulating Materials", *IEEE Trans. Dielectric Electrical Insulation*, Vol.12, pp.1162-1171, 2005.

[53] B. X. Du, Yong Liu and H. J. Liu, "Effects of Low Pressure on Tracking Failure of Printed Circuit Boards", *IEEE Trans. Dielectric Electrical Insulatio*n, Vol.15, pp.1379-1384, 2008. Vol.41, No.19, 195412 (7pp), 2008.

[54] E. A. Brian G.Moffat, Marc P.Y Desmulliez, Dennis Koltsov and Andrew Richardson, "Failure Mechanisms of Legacy Aircraft Wiring and Interconnects," *IEEE Transactions on Dielectrics and Electrical Insulation, Vol. 15, No. 3*, June 2008.

[55] "Insulation coordination for Equipment within low-voltage systems," *IEC Standard 60664*, 2003.

[56] G. W. John, "Wiley Encyclopedia of Electrical and Electronics Engineering," pp. P125, P162, 1999.

[57] "IPC-2221A Generic Standard on Printed Circuit Board," *IPC 2221 Task Group of the Rigid Printed Circuit Board Committee*, 1998.

[58] "SAE AS 50881C Wiring Aerospace Vehicle," Oct 1, 2006.

[59] A.S.T.M D495 “Test method for high voltage low current dry arc resistance of solid electrical insulation”

[60] IEC 60112:2003 “Determining of the comparative and proof tracking indices of solid insulating materials under moist conditions”

[61] IEC 587:1984 “Method for evaluating the resistance to tracking and erosion for solid insulating materials used under severe ambient conditions ”

[62] Y. Saito, T. Hino, and M. Suzuki, "A Dry Tracking Resistance Test Method Using a Trigger Discharge," *IEEE Transactions On Electrical Insualtion*, vol., EI-3, February,1968.

[63] R. T. Lee, H. H. Chung, and Y. C. Chiou, “Arc erosion of silver electric contacts in a single arc discharge across a static gap,” in *Proc. IEE Sci., Meas. Technol.*, vol. 148, no. 1, pp. 8–14, Jan. 2001.

[64] P. G. Slade and E. D. Taylor, “Electrical breakdown in atmospheric air between closely spaced (0.2um-40um) electrical contacts” *Proc. 47th IEEE Holm Conf. Electrical Contacts*, Montreal,2001 Edited by K. Leung, 245-250

[65] J.-M. Torres and R. S. Dhariwal, " Electric field breakdown at micrometre separations", *Nanotechnology 10, 102.* 1999

[66] A. Wallash and L. Levit,"Electrical breakdown and ESD phenomena for devices with nanometer-to-micron gaps" *Proc. SPIE*, Vol 4980, pp. 87, 2003.

[67] J. Dillon, *Gaseous Conductors: Theory and Engineering Applications*, 1958.

[68] E. Hourdakis, B. J. Simonds, and N. M. Zimmerman, "Submicron gap capacitor for measurement of breakdown voltage in air," *Review of Science Instrument 77*, 034702, 24 March 2006.

[69] IEC 60060-1: 1989 High-voltage testing techniques.

[70] F.C. Lin, S. M. Rowland, "Study on Low Current Arcs on Surfaces of Dielectric Materials", *2005 Annual Report Conference on Electrical Insulation and Dielectric Phenomena*,pp 136-139.

[71] Dengke Cai and Andreas Neyer, "Large-Scale Silicone-Rubber-Based Optical Interconnect Packaged with FR4", *Journal of Microelectromechniacal Systems*, Vol. 19, No. 6, December 2010.

[72] F. Obenaus, "The influence of surface deposited on flashover voltage of insulators," vol. 56, pp. 369, 1935.

[73] Ruben D. Garzon "High voltage circuit breakers-Design and applications" Marcel Dekker Inc. New York, 2002

[74]. F. Obenaus, H. Boehme, "Essais de contournement surisolateurs pollues en laboratoire et en lieu de service du point de vue de la conception d'une model d'amorcage par courant rampant", *CIGRE*, 1966.

[75] Oscar Armando Maldonado Astorga and Afonso Jose do Prado "The Flashover Phenomena: An Analysis With Influence of The Thickness of The Lalyer Polluiton of The High Voltage Polluted Insulators" *Conference Record of the 1994 IEEE Intemational Symposium on Electrical Insulation*, Pittsburgh, PA USA, June 5-8, 1994

[76] L.Warren, "Testing for Tracking," *Insulation Diagnostics - Methods for* Determining Quality, Remnant Life and Proof Testing, *IEE Colloquium* on, 25 Mar 1991.

[77] Wikipedia, "Convection," Retrived on 05 August 2010.

[78] Perrot, Pierre (1998). A to Z of Thermodynamics. Oxford University Press. ISBN 0-19-856552-6.

[79] Clark, John, O.E. (2004). The Essential Dictionary of Science. Barnes & Noble Books. ISBN 0-7607-4616-8.

[80] J. P. Joule (1884), The Scientific Paper of James Prescott Joule, The Physical Society of London, p. 274, "I am inclined to believe that both of these hypotheses will be found to hold good,—that in some instances, particularly in the case of sensible heat, or such as is indicated by the thermometer, heat will be found to consist in the living force of the particles of the bodies in which it is induced; whilst in others, particularly in the case of latent heat, the phenomena are produced by the separation of particle from particle, so as to cause them to attract one another through a greater space." , *Lecture on Matter, Living Force*, and Heat. May 5 and 12, 1847

[81] Textbook: Young and Geller College Physics, 8e, Pearson Education

[82] Cubic fit to Table 2.1,p.16, Textbook: R.R.Rogers & M.K. Yau, A Short Course in Cloud Physics, 3e,(1989), Pergamon press

[83] " http://www.taiwan-leader.com/crm_faq.asp retrieved on 26th May 2010."
[84]"<http://www.richter-elektronik.de/en/content/technische-informationen/basismaterial-kennwerte.php?navanchor=1010047> retrived on 26th May 2010."
[85]"http://www.precoplat.com/tec_tpl/technik_tpl.php?cnt=./faqs/faq_texte/faq.php&nav=5&faq=1&faq_b=f retrived on 26th May 2010."
[86] W. H. Middendorf, "The Use of Copper Electrodes for the Comparative Tracking Index Test," *Electrical Insulation, IEEE Transactions on*, Aug. 1986.
[87] W. H. Middendorf, "The use of copper electrodes for eh cooperative tracing index test," *IEEE Transactions on Electrical Insulation*, vol. Vol. EI-20 No.3, June 1985.
[88] S. Takeda and Y. Saito, "The Infulence of Electrodes Materials to Tracking Resistance," *IEEJ Tookyo Convention*, pp. 117, 1966.
[89] T. R. o. I. o. Japan, "Tracking Phenomena and Sate of the Art on Test Methods of tracking Resistance," *Technical Report (I)*, 1968.
[90] T. r. o. I. Japan, "Testing Method for Tracking Resistance of Insulating Materials Based on IEC Pub1.112," *Technical Report (II)*, 1981.
[91] J. S. o. P. Technology, " Interim report on study in the Testing Method for Tracking Resistance of Plastics Insulating Materials," 1985.
[92]"http://www.coleparmer.com/techinfo/techinfo.asp?htmlfile=Emissivity.htm&ID=254#anchor73 retrieved on 20th Nov 2009."

[93] G. G. Karady, M. D. Sirkis, and J. R. Oliva, "Degrading Effect of High altitude Corona on Electronic Circuit Boards," *IEEE Transactions on Electrical insulation*, vol. 26, December1991.
[94] R. Bartnikas and E. J. MacMahon, "Corona Measurements and Interpretation," *Engineering Dielectrics*, ASTM STP669, Vol. I, 1979

Appendix A

Table A1: Clearances to withstand transient voltages

Required impulse withstand voltage 1) 5) (kV)	Minimum clearances in air up to 2000m above sea level (mm)					
	Case A Inhomogeneous field			Case B Homogeneous fields		
	Pollution degree			Pollution degree		
	1	2	3	1	2	3
0.33 2)	0.01	0.2 3) 4)	0.8 4)	0.01	0.2 3)4)	0.8 4)
0.4	0.02			0.02		
0.5 2)	0.04			0.04		
0.6	0.06			0.06		
0.8 2)	0.1			0.1		
1	0.15			0.15		
1.2	0.25	0.25		0.2		
1.5 2)	0.5	0.5		0.3	0.3	
2	1	1	1	0.45	0.45	
2.5 2)	1.5	1.5	1.5	0.6	0.6	
3	2	2	2	0.8	0.8	
4.0 2)	3	3	3	1.2	1.2	1.2
5	4	4	4	1.5	1.5	1.5
6	5.5	5.5	5.5	2	2	2
8	8	8	8	3	3	3
10	11	11	11	3.5	3.5	3.5
12 2)	14	14	14	4.5	4.5	4.5
15	18	18	18	5.5	5.5	5.5

20	25	25	25	8	8	8
25	33	33	33	10	10	10
30	40	40	40	12.5	12.5	12.5
40	60	60	60	17	17	17
50	75	75	75	22	22	22
60	90	90	90	27	27	27
80	130	130	130	35	35	35
100	170	170	170	45	45	45

1) This voltage is

– for functional insulation, the maximum impulse voltage expected to occur across the clearance (see 3.1.4),

– for basic insulation directly exposed to or significantly influenced by transient overvoltages from the low-voltage mains (see 2.2.2.2, 2.2.2.3.1 and 3.1.5), the rated impulse voltage of the equipment,

– for other basic insulation (see 2.2.2.3.2), the highest impulse voltage that can occur in the circuit.

For reinforced insulation see 3.1.5.

2) Preferred values as specified in 2.1.1.2.

3) For printed wiring material, the values for pollution degree 1 apply except that the value shall not be less than 0,04 mm, as specified in table 4.

4) The minimum clearances given for pollution degrees 2 and 3 are based on the reduced withstand characteristics of the associated creepage distance under humidity conditions (see IEC 60664-5).

5) For parts or circuits within equipment subject to impulse voltages according to 2.2.2.3.2, interpolation of values is allowed. However, standardization is achieved by using the preferred series of impulse voltage values in 2.1.1.2.

6) The dimensions for pollution degree 4 are as specified for pollution degree 3, except that the minimum clearance is 1,6 mm.

Table A2. Rated impulse voltage for equipment energized directly

from the low-voltage mains

Nominal voltage of Rated impulse voltage 2) the supply system 1) based on IEC 60038 3)		**Voltage line to neutral derived from nominal voltages a.c. or d.c. up to and including**	**Rated impulse voltage 2)**			
			Overvoltage category 4)			
Three phase	**Single phase**	V	**I**	**II**	**III**	**IV**
230/400	120-240	50	330	500	800	1 500
277/480		100	500	800	1 500	2 500
400/690		150	800	1 500	2 500	4 000
1 000		300	1 500	2 500	4 000	6 000
		600	2 500	4 000	6 000	8 000
		1 000	4 000	6 000	8 000	12 000

1) See annex B for application to existing different low-voltage mains and their nominal voltages.

2) Equipment with these rated impulse voltages can be used in installations in accordance with IEC 60364-4-443.

3) The / mark indicates a four-wire three-phase distribution system. The lower value is the voltage line-toneutral, while the higher value is the voltage line-to-line. Where only one value is indicated, it refers to three-wire, three-phase systems and specifies the value line-to-line.

4) See 2.2.2.1.1 for an explanation of the overvoltage categories.

Table A3-1 Clearance to withstand steady-state voltages, temporary overvoltages or recurring peak voltages

Voltage (Peak value)(kV)	Minimum clearance in air up to 2000m above the sea level	
	Case A Inhomogeneous field conditions (mm)	Case B Homogenous fields conditions (mm)
0.33	0.01	0.01
0.4	0.02	0.02
0.5	0.04	0.04
0.6	0.06	0.06

0.8	0.13	0.1
1	0.26	0.15
1.2	0.42	0.2
1.5	0.76	0.3
2	1.27	0.45
2.5	1.8	0.6
3	2.4	0.8
4	3.8	1.2
5	5.7	1.5
6	7.9	2
8	11	3
10	15.2	3.5
12	19	4.5
15	25	5.5
20	34	8
25	44	10
30	55	12.5
40	77	17
50	100	22
60		27
80		35
100		45

Table A3-2 Clearance to withstand steady-state voltages, temporary overvoltages or recurring peak voltages

Additional information concerning the dimensioning of clearances to avoid partial discharge

		Minimum clearance in air up to 2000m above the sea level
Voltage (Peak value)(kV)	Voltage (peak value)(V)	Case A Inhomogeneous field conditions

		(mm)
0.33	330	0.01
0.4	400	0.02
0.5	500	0.04
0.6	600	0.06
0.8	800	0.13
1	1000	0.26
1.2	1200	0.42
1.5	1500	0.76
2	2000	1.27
2.5	2500	2
3	3000	3.2
4	4000	11
5	5000	24
6	6000	64
8	8000	184
10	10000	290
12	12000	320
15	15000	Dimensioning without partial discharge is not possible under inhomogeneous field conditions
20	20000	
25	25000	
30	30000	
40	40000	
50	50000	
60	60000	
80	80000	
100	100000	

Table A4 Altitude correction factors

Altitude (m)	Normal barometric pressure (kPa)	Multiplication factor for clearances
0	101.325	1
2000	80	1
3000	70	1.14
4000	62	1.29
5000	54	1.48
6000	47	1.7
7000	41	1.95
8000	35.5	2.25
9000	30.5	2.62
10000	26.5	3.02
15000	12	6.67
20000	5.5	14.5

A5 Creepage distances to avoid failure due to tracking

	Minimum creepage distance								
	Printed wiring material Pollution degree		Pollution degree	Pollution degree			Pollution degree		
	1	2	1	2			3		
Voltage r.m.s(1)	All material groups (mm)	All material groups except IIIb (mm)	All material groups (mm)	|Material group I (mm)	Material group II (mm)	Material groups III (mm)	|Material group I (mm)	Material group II (mm)	Material groups III (mm)(2)
10	0.025	0.04	0.08	0.4	0.4	0.4	1	1	1

12.5	0.025	0.04	0.09	0.42	0.42	0.42	1.05	1.05	1.05
16	0.025	0.04	0.1	0.45	0.45	0.45	1.1	1.1	1.1
20	0.025	0.04	0.11	0.48	0.48	0.48	1.2	1.2	1.2
25	0.025	0.04	0.125	0.5	0.5	0.5	1.25	1.25	1.25
32	0.025	0.04	0.14	0.53	0.53	0.53	1.3	1.3	1.3
40	0.025	0.04	0.16	0.56	0.8	1.1	1.4	1.6	1.8
50	0.025	0.04	0.18	0.6	0.85	1.2	1.5	1.7	1.9
63	0.04	0.063	0.2	0.63	0.9	1.25	1.6	1.8	2
80	0.063	0.1	0.22	0.67	0.95	1.3	1.7	1.9	2.1
100	0.1	0.16	0.25	0.71	1	1.4	1.8	2	2.2
125	0.16	0.25	0.28	0.75	1.05	1.5	1.9	2.1	2.4
160	0.25	0.4	0.32	0.8	1.1	1.6	2	2.2	2.5
200	0.4	0.63	0.42	1	1.4	2	2.5	2.8	3.2
250	0.56	1	0.56	1.25	1.8	2.5	3.2	3.6	4
320	0.75	1.6	0.75	1.6	2.2	3.2	4	4.5	5
400	1	2	1	2	2.8	4	5	5.6	6.3
500	1.3	2.5	1.3	2.5	3.6	5	6.3	7.1	8
630	1.8	3.2	1.8	3.2	4.5	6.3	8	9	10
800	2.4	4	2.4	4	5.6	8	10	11	12.5
1000	3.2	5	3.2	5	7.1	10	12.5	14	16
1250			4.2	6.3	9	12.5	16	18	20
1600			5.6	8	11	16	20	22	25
2000			7.5	10	14	20	25	28	32
2500			10	12.5	18	25	32	36	40
3200			12.5	16	22	32	40	45	50
4000			16	20	28	40	50	56	63
5000			20	25	36	50	63	71	80
6300			25	32	45	63	80	90	100
8000			32	40	56	80	100	110	125

10000			40	50	71	100	125	140	160
125000			50	63	90	125			
16000			63	80	110	160			
20000			80	100	140	200			
25000			100(3)	125(3)	180(3)	250(3)			
3200			125(3)	160(3)	220(3)	320(3)			
40000			160(3)	200(3)	280(3)	400(3)			
50000			200(3)	250(3)	360(3)	500(3)			
630000			250(3)	320(3)	450(3)	600(3)			

1)The voltage is for the functional insulation, the working voltage; for the basic and supplementary insulation of the circuit energized directly form the supply mains, the voltage rationalized through table 3a or table 3b, based on the rated voltage of the equipment , or the rated insulation voltage For basic and supplementary insulation of systems , equipment and internal circuit not energized directly form the mains, the highest r.m.s voltage which can occur in the system, equipment or internal circuit when supplied at rated voltage and under the most onerous combination of conditions of opinion within equipment rating.
2) Material group IIIb is not recommended for application in pollution degree 3 above 630V
3) Provisional data based on extrapolation. Technical committees who have other information based on experience may use their dimensions.

Table A6-1 a Single-phase three or two-wire a.c. or d.c. systems

	Voltage rationalized for table 4	
	For insulation line to line (1)	For insulation line to earth (1)
Nominal voltage of the supply system (V)*	All systems (V)	Three-wire systems mid-point earthed (V)

12.5	12.5	
24,25	25	
30	32	
42,48,50**	50	
60	63	
30-60	63	32
100**	100	
110,120	125	
150**	160	
220	250	
110-220,120-240	250	125
300**	320	
220-240	500	250
600**	630	
480-960	1000	500
1000**	1000	

Table A6-2 a Three-phase four or three wire a.c. or d.c. systems

For insulation line-to-line	For insulation line-to-earth	
All systems(V)	Three phase four wire systems neutral-earthed(2) (V)	Three phase three wire systems unearthed or corner-earthed*(V)
63	32	63
125	80	125
160	-	160
200	125	200
250	160	250

320	-	320
400	250	400
500	250	500
500	320	500
630	400	630
630	-	630
630	400	630
800	500	800
1000	630	1000
1000	-	1000

Table A7 Electrical Conductor Spacing in IPC 2221

Maximum Voltage Between Conductor (DC or AC Peaks)(V)	Minimum Spacing (mm)						
	Bare Board				Assembly		
	B1	B2	B3	B4	A5	A6	A7
0-15	0.05	0.1	0.1	0.05	0.13	0.13	0.13
15-30	0.05	0.1	0.1	0.05	0.13	0.25	0.13
30-50	0.1	0.6	0.6	0.13	0.13	0.4	0.13
50-100	0.1	0.6	1.5	0.13	0.13	0.5	0.13
100-150	0.2	0.6	3.2	0.4	0.4	0.8	0.4
150-170	0.2	1.25	3.2	0.4	0.4	0.8	0.4
170-250	0.2	1.25	6.4	0.4	0.4	0.8	0.4
250-300	0.2	1.25	12.5	0.4	0.4	0.8	0.8
300-500	0.25	2.5	12.5	0.8	0.8	1.5	0.8
Calculation see	0.0025 mm/vol	0.005 mm/vol	0.025 mm/vol	0.00305	0.00305	0.00305	0.00305

Equation 3.1	t	t	t	mm/volt	mm/volt	mm/volt	mm/volt

B1 – Internal Conductors
B2 – External Conductors, uncoated, sea level to 3050 m
B3 – External Conductors, uncoated, over 3050 m(696.4 mbar)
B4 – External Conductors, with permanent polymer coating (any elevation)
A5 – External Conductors, with conformal coating over assembly (any elevation)
A6 – External Component lead/termination, uncoated
A7 – External Component lead termination, with conformal coating (any elevation)

Appendix B

Disruptive discharges test procedures can be divided into three classes for the purpose of statistical evaluation.

Class 1: multi-level tests

m_i Substantially equal voltage stresses (e.g. lighting impulses) are applied at each of n voltage levels U_i. While this procedure is usually employed with impulse voltages, some tests with alternating and direct voltage also fall into this class.

Class 2: Up-and-down tests

N groups of m substantially equal voltage stresses are applied at voltage levels U_i. The voltage level for each succeeding group of stresses is increased or decreased by a small amount ΔU according to the result of the previous group of stresses.

Class 3: Successive Discharge Tests

A procedure leading to a disruptive discharge on the test object is applied n times. The Test voltage may be increased continuously until a disruptive discharge occurs or held constant at some level until a disruptive discharge is observed.

Statistical Behaviour of Disruptive Discharge

When p, the probability of a disruptive discharge during a given test procedure, depends only on the test voltage, U, the behaviour of the test object can be characterized by a function p(U) determined by the processes of discharge development. In practice, this function, the disruptive discharge probability function, can be represented mathematically by expressions depending on at least two parameters U50 and z. U50 is the 50 % discharge voltage for which p(U) = 0,5 and z is the conventional deviation; z = U50 – U16 where U16 is the voltage for which p(U) = 0,16.

NOTE 1 Examples of p(U) can be derived from the Gaussian (or Normal), the Weibull or the

Gumbel probability distribution functions. Experience shows that for 0,15 < p < 0,85 most theoretical distributions can be considered equivalent. Special Weibull or Gumbel distributions are acceptable approximations to a Gaussian distribution having given U50 and z for p lying between 0,02 and 0,98. Beyond these limits little information is available.

NOTE 2 Sometimes p is a function of two or more parameters, e.g., U and dU/dt. In such cases no simple function can be used to describe p. Details of such cases may be found in the technical literature. The function p(U) and the parameters U50 and z can be found from tests with very large numbers of voltage applications, provided that the characteristics of the test object remain constant throughout the tests. In practice the number of voltage applications is usually limited and the estimates of U50 and z based on an assumed form of p(U) will be subject to statistical uncertainties.

Confidence limits and statistical error

If a parameter y is estimated from n test results, upper and lower confidence limits yU and yL can be defined, with the probability C that the true value of y is within these limits. C is termed the confidence level and the half width er = (yU – yL)/2 of the confidence band is called the statistical error. Usually C is taken as 0,95 (or 0,90) and the corresponding limits are called the 95 % (or 90 %) confidence limits. The statistical errorer depends on both n and the value of the conventional deviation z. The conventional deviation z should be estimated when possible from tests made under realistic conditions. In general, the larger the number of tests made, the better will be the estimate of z. It should, however, be remembered that during a protracted test series, ambient conditions may change to an extent which offsets the gain in accuracy from the increased number of tests.Since accurate estimation of z from a limited series of tests is not possible, values estimated from the pooled results of many tests are often given by the relevant Technical Committees. The statistical error er may be combined with estimates of other errors (e.g., measuring errors) to define the overall error limits for the determination of a particular parameter.

Treatment of Results from Class 3 Tests

The result of a Class 3 test is usually a series of n voltages Ui from which parameters U50 and z of a disruptive discharge probability function are to be determined. For a Gaussian (or Normal) distribution, estimates of the parameters U50 and z are given by:

$$U_{50}^{*} = \sum U_i / n$$

$$z^{*} = \left[\sum \left(U_i - U_{50}^{*} \right)^2 / (n-1) \right]^{1/2}$$

For other distributions likelihood methods can be employed to estimate U50 and z (see A.4). The same expressions and methods apply in cases where times to the occurrence of a disruptive discharge ti are to be analyzed.

The confidence limits for Gaussian distributions may be found using the Student's t or Chi-squared distributions as described in the technical literature.
As an example, in the case of a Gaussian distribution, the 95% confidence limits for the estimates of U50 and z obtained from a test with n = 20 are: and 0,76 z* # z # 1,46 z*

A.4 Application of likelihood methods

Likelihood methods may be used for the analysis of the results of all of the above classes of tests. These methods permit estimation of U50 and z and hence Up once a discharge probability distribution function
p (U ; U50, z) is selected.

Furthermore, it is possible to use all the results obtained and the confidence limits corresponding to any desired confidence level C can be found.